WSRC-SA-6
Rev 37
November 2018

FINAL SAFETY ANALYSIS REPORT

SAVANNAH RIVER SITE

DEFENSE WASTE PROCESSING FACILITY

VOLUME 2

NOVEMBER 2018

DISCLAIMER

This document was prepared by AECOM N&E Technical Services, LLC (N&E TS) under contract with Savannah River Remediation, LLC (SRR), subject to the warranty and other obligations of that contract and in furtherance of SRR's contract with the United States Department of Energy (DOE). N&E TS' findings represent its reasonable judgments within the time and budget context of its commission and utilizing the information available to it at the time. This document was prepared solely for the DOE for Contract DE-AC09-09SR22505.

Release to and Use by Third Parties. As it pertains to releases of this document to third parties, and the use of or reference to this document by such third parties in whole or in part, neither N&E TS, SRR, DOE, nor their respective officers, directors, employees, agents, consultants, or personal services contractors (i) make any warranty, expressed or implied, (ii) assume any legal liability or responsibility for the accuracy, completeness, or usefulness, of any information, apparatus, product or process disclosed herein or (iii) represent that use of the same will not infringe privately owned rights. Reference herein to any specific commercial product, process, or service by trademark, name, manufacture or otherwise, does not necessarily constitute or imply endorsement, recommendation, or favoring of the same by N&E TS, SRR, DOE, or their respective officers, directors, employees, agents, consultants or personal services contractors. The views and opinions of the authors expressed herein do not necessarily state or reflect those of the United States Government or any agency thereof.

WSRC-SA-6
Rev 37
November 2018

FINAL SAFETY ANALYSIS REPORT
SAVANNAH RIVER SITE
DEFENSE WASTE PROCESSING FACILITY

CHAPTER 3

SITE CHARACTERISTICS

November 2018

CONTENTS

Page

3.0 SITE CHARACTERISTICS 3.1-1

3.1 INTRODUCTION 3.1-1

3.1.1 Objective 3.1-1

3.1.2 Scope 3.1-1

3.2 REQUIREMENTS 3.2-1

3.3 SITE DESCRIPTION 3.3-1

3.3.1 Geography 3.3-1

3.3.1.1 Location 3.3-1

3.3.1.2 Exclusion Area 3.3-1

3.3.2 Demography 3.3-2

3.3.2.1 Permanent Population and Distribution 3.3-2

3.3.2.2 Transient Population Variations 3.3-2

3.3.3 Uses of Nearby Land and Waters 3.3-3

3.3.3.1 Land Use 3.3-3

3.3.3.2 Water Use 3.3-4

3.3.3.2.1 General Uses of the Savannah River 3.3-4

3.3.3.2.2 Fisheries 3.3-4

3.3.3.2.3 Recreation 3.3-4

3.3.3.2.4 Agricultural Water Use 3.3-5

CONTENTS (Continued)

Page

3.3.3.2.5 Municipal Use of Local Surface Water 3.3-5

3.3.3.2.6 Groundwater Use 3.3-5

3.4 ENVIRONMENTAL DESCRIPTION 3.4-1

3.4.1 Meteorology 3.4-1

3.4.2 Hydrology 3.4-1

3.4.2.1 Surface Hydrology 3.4-1

3.4.2.1.1 Probable Maximum Flood on Streams and Rivers 3.4-3

3.4.2.2 Subsurface Hydrology 3.4-5

3.4.2.2.1 Regional Characteristics 3.4-5

3.4.2.2.2 Geohydrologic Zones at DWPF 3.4-6

3.4.2.2.3 Site Characteristics 3.4-8

3.4.2.2.4 Contaminant Transport Analysis 3.4-9

3.4.3 GEOLOGY AND SEISMOLOGY 3.4-15

3.4.3.1 Basic Geologic and Seismic Information 3.4-15

3.4.3.1.1 Regional Geology 3.4-16

3.4.3.1.2 Site Geology 3.4-16

3.4.3.2 Vibratory Ground Motion 3.4-16

3.4.3.2.1 Geologic Conditions of SRS 3.4-16

CONTENTS (Continued)

Page

3.4.3.2.2 Underlying Tectonic Structures - General Site 3.4-17

3.4.3.2.3 Behavior During Previous Earthquakes 3.4-17

3.4.3.2.4 Engineering Properties of Materials Underlying the Site 3.4-17

3.4.3.2.5 Earthquake History 3.4-17

3.4.3.2.6 Modern Stress Regime 3.4-17

3.4.3.2.7 Correlation to Epicenters with Geological Structures 3.4-17

3.4.3.2.8 Identification of Active Faults 3.4-17

3.4.3.2.9 Description of Capable Faults 3.4-17

3.4.3.2.10 Maximum Earthquakes 3.4-17

3.4.3.2.11 Safe Shutdown Earthquake 3.4-18

3.4.3.2.12 Probabilistic Assessment of Peak Ground Acceleration 3.4-18

3.4.3.2.13 Design Response Spectra 3.4-19

3.4.3.3 Surface Faulting 3.4-19

3.4.3.3.1 Geologic Conditions of the Site 3.4-19

3.4.3.4 Stability of Subsurface Materials 3.4-19

3.4.3.4.1 Geologic Characteristics 3.4-19

3.4.3.4.2 Plot Plans 3.4-21

CONTENTS (Continued)

Page

3.4.3.4.3 Soil and Rock Characteristics 3.4-22

3.4.3.4.4 Properties of Underlying Materials..... 3.4-27

3.4.3.4.5 Excavation and Backfill..... 3.4-39

3.4.3.4.6 Groundwater Conditions..... 3.4-40

3.4.3.4.7 Static Foundation Behavior..... 3.4-41

3.4.3.4.8 Response of Soil and Rock to Dynamic Loading 3.4-44

3.4.3.4.9 Techniques to Improve Subsurface Conditions 3.4-58

3.4.3.4.10 Criteria and Design Method..... 3.4-60

3.4.3.4.11 Recent Evaluations..... 3.4-61

3.5 NATURAL PHENOMENA THREATS 3.5-1

3.5.1 Floods..... 3.5-1

3.5.2 Earthquakes..... 3.5-1

3.5.3 Tornadoes..... 3.5-1

3.6 EXTERNAL MAN-MADE THREATS 3.6-1

3.6.1 Transportation 3.6-1

3.6.2 Missile and Blast Effects 3.6-1

3.7 NEARBY FACILITIES..... 3.7-1

3.8 VALIDITY OF EXISTING ENVIRONMENTAL ANALYSES 3.8-1

CONTENTS (Continued)

Page

3.9 REFERENCES 3.9-1

3.10 TABLES 3.10-1

3.11 FIGURES……3.11-1

TABLES

Page

3.4-1 Elevations of Piezometers Used in the Preliminary Investigation at the DWPF Site 3.10-1

3.4-2 Results of Ground-Water Monitoring for the DWPF Site 3.10-2

3.4-3 Flow Velocities and Travel Times of Ground Water Along Flow Path 3.10-13

3.4-4 Radionuclide Concentrations at Postulated Leak and at Groundwater Outcrop 3.10-14

3.4-5 Sedimentary Stratigraphy at the DWPF Site Based on Subsurface Exploration 3.10-17

3.4-6 Summary of Borehole Groutings 3.10-18

3.4-7 Summary of Borings with Indications of Voids or Leached Zones 3.10-21

3.4-8 Summary of Static and Dynamic Laboratory Testing Program 3.10-23

3.4-9 Summary of Generalized Static Soil Properties 3.10-25

3.4-10 Summary of CU Triaxial Test Results 3.10-26

3.4-11 Summary of Consolidation Test Results for Silts and Clays 3.10-27

3.4-12 Laboratory Determination of Shear Moduli of Backfill at Large Strains 3.10-28

3.4-13 Allowable Bearing Capacities of Mat Foundations for Category I Structures 3.10-29

3.4-14 Soil Design Parameters 3.10-30

3.4-15 Summary of G_{max} Values for Category I Structures 3.10-31

3.4-16 Strong Motion Accelerograms Used for Analysis of Liquefaction Potential 3.10-32

FIGURES

Page

3.3-1 Savannah River Site Map 3.11-1

3.3-2 SRS Map Showing Key Facilities 3.11-2

3.4-1 Streams, Watersheds, and Topography of the DWPF Site Area 3.11-3

3.4-2 River and Stream Cross Sections Near the DWPF Site 3.11-4

3.4-3 Hydrostratographic Nomenclature 3.11-5

3.4-4 Plan View for Piezometric and Monitoring Wells 3.11-6

3.4-5 Zone 7c, Piezometric Contours 3.11-7

3.4-6 Zone 6, Piezometric Contours 3.11-8

3.4-7 Zone 5, Piezometric Contours 3.11-9

3.4-8 Zone 4, Piezometric Contours 3.11-10

3.4-9 SBG Well Locations 3.11-11

3.4-10 Flow Path 3.11-12

3.4-11 Strontium K_d 3.11-13

3.4-12 Cesium K_d 3.11-14

3.4-13 Plutonium K_d 3.11-15

3.4-14 Ruthenium K_d 3.11-16

3.4-15 Response Spectra 3.11-17

3.4-16 Site Location Plan 3.11-18

3.4-17 Plan View of Borings 3.11-19

FIGURES (Continued)

Page

3.4-18 Plan View of Borings 3.11-20

3.4-19 D'Appolonia Section AA 3.11-21

3.4-20 D'Appolonia Section BB 3.11-22

3.4-21 D'Appolonia Section CC 3.11-23

3.4-22 D'Appolonia Section DD 3.11-24

3.4-23 D'Appolonia Section EE 3.11-25

3.4-24 D'Appolonia Section FF 3.11-26

3.4-25 D'Appolonia Section GG 3.11-27

3.4-26 D'Appolonia Section HH 3.11-28

3.4-27 D'Appolonia Section JJ and KK 3.11-29

3.4-28 D'Appolonia Section LL and MM 3.11-30

3.4-29 DWPF Boring Location Plan 3.11-31

3.4-30 Mueser Section AA 3.11-32

3.4-31 Mueser Section BB 3.11-33

3.4-32 Mueser Section CC 3.11-34

3.4-33 Mueser Section DD and EE 3.11-35

3.4-34 Mueser Section FF 3.11-36

3.4-35 Piezometric Heads 3.11-37

3.4-36 Piezometric Heads 3.11-38

FIGURES (Continued)

Page

3.4-37 Piezometric Heads 3.11-39

3.4-38 Piezometric Heads 3.11-40

3.4-39 Plan View of Crosshole Tests, Downhole Tests and Seismic Lines..... 3.11-41

3.4-40 Seismic Line S-8 ..... 3.11-42

3.4-41 Simplified Dynamic Soil Properties 3.11-43

3.4-42 Stratigraphic Nomenclature 3.11-44

3.4-43 Reference Standards..... 3.11-45

3.4-44 Soil Properties Profile 3.11-46

3.4-45 Soil Properties Profile 3.11-47

3.4-46 Soil Properties Profile 3.11-48

3.4-47 Soil Properties Profile 3.11-49

3.4-48 Settlement Summary for S250, S292, and S294..... 3.11-50

3.4-49 Settlement Summary for S221 ..... 3.11-51

3.4-50 Estimated and Actual Settlements for Vitrification Building 3.11-52

3.4-51 G/Gmax and Damping versus Shear Strength 3.11-53

3.4-52 Boring Groups..... 3.11-54

3.4-53 SPT Profiles 3.11-55

3.4-54 Grain Size Distribution 3.11-56

3.4-55 Grain Size Distribution 3.11-57

FIGURES (Continued)

Page

3.4-56 Grain Size Distribution 3.11-58

3.4-57 SHAKE Analysis Input Time Histories 3.11-59

3.4-58 SHAKE Analysis Input Time Histories 3.11-60

3.4-59 SHAKE Analysis Input Time Histories 3.11-61

3.4-60 SHAKE Analysis Input Time Histories 3.11-62

3.4-61 Summary Liquefaction Analysis 3.11-63

3.4-62 Standard Penetration Resistance Versus Ground Failure 3.11-64

3.4-63 Ground Failure Criteria 3.11-65

3.4-64 Cyclic Stress Ration Versus Modified Penetration Resistance 3.11-66

3.4-65 Liquefaction Potential State Diagram 3.11-67

3.4-66 Undrained Cyclic Test Results 3.11-68

3.4-67 Cyclic Mobility Analysis 3.11-69

3.4-68 Grouting Summary 3.11-70

3.4-69 Grout Hole Location Plan for S221 ..... 3.11-71

3.4-70 Grout Hole Location Plan for S250, S294 and S292 ..... 3.11-72

3.0 SITE CHARACTERISTICS

3.1 INTRODUCTION

3.1.1 OBJECTIVE

The purpose of this chapter is to provide information that satisfies the requirements of Code of Federal Regulations 10 CFR 830 Subpart B for a Documented Safety Analysis (Ref. 1, 2).

3.1.2 SCOPE

This chapter provides a description of site characteristics necessary for understanding the Defense Waste Processing Facility (DWPF) facility environs important to the safety basis. Products of this chapter, as applicable based on the graded approach, include:

- Description of the location of the site, the location of DWPF within the site, and DWPF's proximity to the public and to other facilities.
- Specification of population sheltering, population location and density, and other aspects of the surrounding area to the site that relate to assessment of the protection of the health and safety of the public.
- Determination of the historical basis for site characteristics in meteorology, hydrology, geology, seismology, and other natural phenomena to the extent needed for hazard and accident analysis.
- Identification of design basis natural phenomena.
- Identification of external man-made threats.
- Identification of nearby facilities impacting, or impacted by, the DWPF.
- Validation of site characteristics assumptions common to safety analysis that were used in prior DWPF environmental analysis and impact statements.

The information provided in this chapter is to a large degree a summary of the detailed site characteristic information contained in SRNS-IM-2013-00019, Site Information and Program Description (Ref. 3). In many sections of this chapter, reference is made to the DSA Support Document Chapter 1 for additional details on information that is general to the site and is not specific to the DWPF.

3.2 REQUIREMENTS

The Savannah River Site (SRS) is required to comply with Department of Energy (DOE) Orders, as well as codes, standards, and regulations that govern policies and programs. The SRR Standards/Requirements Identification Document (S/RID) states the codes, standards, and regulations governing the operation of the SRS (Ref. 63). Programmatic compliance assessments are performed against the S/RID and documented as specified in the Compliance Assurance Manual 8B (Ref. 64). The Standards Management/Compliance Section maintains records of the programmatic compliance assessments.

3.3 SITE DESCRIPTION

3.3.1 GEOGRAPHY

3.3.1.1 Location

The Savannah River Site (SRS) is owned by the US Department of Energy (DOE) and is operated by the SRS contractors. SRS is an approximately circular tract of 310 square miles (198,344 acres) within Aiken, Barnwell and Allendale counties in southwestern South Carolina (SC). The site is centered approximately 25 miles southeast to the closest edge of the city limits of Augusta, Georgia (GA), 100 miles from the Atlantic Coast, about 110 miles from the North Carolina (NC) border to the north-northwest, and is bounded on the southwest by the Savannah River. Figure 3.3-1 shows the location of specific site areas along with rivers and lakes as well as a schematic of the site relative to SC, GA and the Atlantic Ocean. As shown in this figure, the DWPF site is located in Aiken County.

3.3.1.2 Exclusion Area

SRS terrain ranges from virtually flat to slopes of forty degrees. The vast majority of land is managed as pine plantation with fields, hardwood forests, ponds, marshes and Carolina bays making up about one-third of the total area. The SRS facilities occupy about seven percent of the total land area. There are six principal tributaries leading to the Savannah River from SRS.

SRS has an extensive road system, and an onsite rail system that connects with tracks owned by the CSX rail system. The electrical grid on SRS operates at 115 kV and draws power from two transmission lines on separate rights-of-way from South Carolina Electric and Gas (SCE&G) Urquhart Station and a third line from the 230-kV tie-line between the Summer and Canadys stations of SCE&G. SRS also has a tie-in line to Vogtle Electrical Generating Plant (VEGP).

The outer perimeter fenceline of SRS (i.e., the site boundary) is the point where offsite radiological evaluation guidelines are applied. The site is not open to the public except for guided tours, controlled deer hunts, authorized environmental studies, through-traffic along the CSX Railroad, and open traffic along SC Route 125 (SRS Road A), US Route 278, and SRS Road 1 at the northern edge of the reservation. The outer perimeter is fenced and access is controlled by the security contractor such that access by the public can be restricted as the need arises. The roads that pass through or near the perimeter can be blocked by protective forces personnel or with the assistance of local law enforcement personnel.

For additional information regarding the site location and site description including detailed maps, see SRNS-IM-2013-00019, Site Information and Program Description (Ref. 3).

3.3.2 DEMOGRAPHY

3.3.2.1 Permanent Population and Distribution

Within a 50-mile radius of the SRS center is a total resident population of approximately 730,000. One major urban center, Augusta, GA (1990 estimated city population of 45,000), lies about 25 miles west-northwest of the site. Four other cities within the 50-mile radius had 1990 populations greater than 13,000: Aiken, SC, about 20 miles north-northwest; Orangeburg, SC, 48 miles east-northeast; North Augusta, SC, 23 miles northwest; and Evans, GA, about 35 miles west-northwest of the site. All other cities and towns have populations less than 7,000, the largest being Belvedere, SC, followed by Red Bank, SC, Waynesboro, GA, and Barnwell, SC.

Fort Gordon, located 9 miles southwest of Augusta, GA, is the nearest military facility, with a population exceeding 18,000. Upon the transfer of all communications electronics to Fort Gordon in 1976, it became the Army's single entity for Signal Corps training. More than 54,000 officers, enlisted students, Army Reserve and National Guard troops are trained at the Signal Center each year.

The existing public school population within 5 miles of the site boundary consists of students and school personnel associated with 11 public schools located in New Ellenton, Jackson, Williston, and Barnwell, SC. Total enrollment in the 11 schools was 6895 during the 1992-93 school year. There are no Georgia public schools located within 5 miles of the site boundary nor are there any private schools or colleges in the 5-mile vicinity.

The total onsite employment at SRS during the day shift of a weekday was approximately 8,300 as of November 2014 (Ref. 3).

The principal changes expected in each of the plant areas through the year 2000 are described in the Site Development and Facility Utilization Plan, Vol. II, Savannah River Site. New facilities at SRS, including those which became operable in 1989 and those expected before 2000, will involve the addition of approximately 1900 personnel. The Fuel Materials Facility located in F-Area began operations in 1988, but DOE directed that the facility be placed on cold standby in 1989. The F/H Effluent Treatment Facility began operation in November 1988. The Saltstone Facility (Z-Area) began operating in June 1990. The Defense Waste Processing Facility (DWPF) began water runs in late 1990.

3.3.2.2 Transient Population Variations

Transient population variations for the general SRS are addressed for the area within approximately 5 miles of the SRS boundary. Any transient population variations beyond this limit are not relevant to a SAR. The transient population components investigated are industrial, school, recreational, health care, and casual. There are no military reservations or correctional institutions located within 5 miles of the site boundary.

The transient population consists of all persons traveling through the vicinity of an area. A 5-mile radius is considered when discussing the transient population. The 5-mile area for DWPF falls entirely within the SRS boundary. Therefore, the transient population for S-Area consists of employees, badged visitors, and vendors making deliveries at site locations within the area.

For additional details refer to SRNS-IM-2013-00019, Site Information and Program Description (Ref. 3).

3.3.3 USES OF NEARBY LAND AND WATERS

3.3.3.1 Land Use

Land use within approximately 5 miles of the SRS boundary is discussed in this subsection. The total area investigated is approximately 800 square miles. Of these 800 square miles, 300 are used for industrial purposes associated with the operation of SRS and for commercial and non-commercial timber management. The land that forms a buffer zone around the production facilities is managed by DOE. The countryside surrounding SRS is predominantly forested. Farming in this area is diversified. The main crops are soybeans, corn, wheat, cotton, peaches, peanuts, and various vegetable crops. Land within a 5-mile radius of DWPF lies completely within SRS and is used either for industrial purposes associated with SRS or as forest land. Forested areas are managed by the Savannah River Forestry Service (SRFS), an administrative unit of the United States Forestry Service (USFS). Through an interagency agreement between DOE and USFS, SRFS provides timber management, research support, soil and water protection, wildlife management, secondary road management, and fire management.

The major facilities at SRS include the 100 Area Reactor (R, C, P, L and K-Area) facilities, the 200 Area Separations (F and H-Area) facilities, the 200 Area Tritium facilities including the Replacement Tritium Facility (H-Area), the 200 Area Waste Management Operations facilities (F and H-Area), the 200 Area Defense Waste Processing (S and Z-Area) facilities, the Consolidated Incinerator Facility (H-Area), the Solid Waste Storage (E-Area) facilities, the 300 Area Reactor Materials (M-Area) facilities, the 400 Area Heavy Water (D-Area) facilities, the Construction Central Shops (N-Area) facilities and the 700 Area Administrative (A-Area) facilities. The contractor for security services at SRS has facilities located in 700-B (B-Area).

All facilities scattered throughout SRS but outside the fenced production areas of SRS are designated with a 600 identification "building" number. In Figure 3.3-2, the major areas of SRS (as described above) including the key facilities in each area are identified. The 700-A Area consists of DOE and Westinghouse (now called Washington) Administration, Savannah River National Laboratory (SRNL), and the Savannah River Ecology Lab (SREL). SREL (operated by the University of Georgia) conducts ecological studies on SRS, which was designated a National Environmental Research Park in 1972. In addition, 891 acres are set aside in 10 separate reserve areas for special studies.

The largest single industrial land use is the VEGP in Burke County, GA. Currently, two nuclear reactor units are operating. Other industries in the area with relatively large land use near SRS include Allied General Nuclear Services (no longer operating), Chem Nuclear Systems, Inc., Carolina Metals, Environmental and Chemical Sciences, and Sandoz Chemicals.

3.3.3.2 Water Use

The major rivers near SRS include the Savannah, Salkehatchie, and South Fork Edisto Rivers. The Savannah River bounds the SRS for 17 miles on the southwest side of the site.

3.3.3.2.1 GENERAL USES OF THE SAVANNAH RIVER

The Savannah River forms the boundary between Georgia and South Carolina. Downstream from Augusta, GA, the Savannah River is classified as Class B waters suitable for domestic supply after treatment, for propagation of fish, and for industrial and agricultural uses. The river supplies water for Augusta, GA, North Augusta, SC, Beaufort and Jasper counties in SC, and supplements the water supply of Savannah, GA. It also receives domestic and industrial wastes from Augusta, GA; North Augusta, SC; and Horse Creek Valley in Aiken County, SC.

The production reactors at SRS were, prior to shutdown, cooled with water pumped from the river. Coal-fired power plants on the site are still cooled with river water. Effluents and waste water from SRS are discharged into the Savannah River tributaries which flow across SRS.

Recreational uses of the Savannah River include sport fishing but only limited contact activities such as swimming and water skiing. American shad is the principal fish taken commercially from the river.

3.3.3.2.2 FISHERIES

There are commercial fisheries along the Savannah River. Rivers and streams near and downstream from SRS are fished mainly by local residents for recreation and food.

3.3.3.2.3 RECREATION

Over 95% of South Carolina's impounded waters are contained in large reservoirs. Most have multipurpose recreational uses such as swimming, water skiing, boating, and fishing. Par

Pond, which was previously used for reactor cooling water, is not accessible to the public. Thurmond Lake (Clarks Hill Reservoir), Hartwell Reservoir, and Russell Dam are used for hydroelectric power generation, flood control, and water supply as well as for recreation.

Boat use on the Savannah River can only be estimated. In 1987, there were 21,399 registered boats in South Carolina counties bordering the Savannah River south of Augusta. Most of the boats for this section of the Savannah River were registered near Augusta and Thurmond Lake and in Aiken County.

3.3.3.2.4 AGRICULTURAL WATER USE

Water for agricultural use in Aiken, Barnwell, and Allendale counties is obtained primarily from lakes and ponds. Corn, peanuts, soybeans, and truck crops are the crops for which irrigation is economically feasible.

3.3.3.2.5 MUNICIPAL USE OF LOCAL SURFACE WATER

The Savannah River and its reservoirs are the sources of water for 64 municipal and industrial users. Total withdrawals amount to approximately one billion gallons per day. The largest water user is VEGP.

The larger communities in Aiken, Richmond, and Burke counties use surface water supplies as well as ground water. None of these surface water supplies are impacted by liquid discharges from operations at SRS.

In Aiken County, the city of Aiken uses water from Shaws Creek. The city of North Augusta draws about 2.78 million gallons per day (mgd) from the Savannah River. The Augusta city water system draws its water supply, averaging about 24 mgd, from the Savannah River more than 25 miles upstream from SRS. Columbia County has a surface water plant along Georgia Route 50 to withdraw water from Thurmond Lake.

3.3.3.2.6 GROUNDWATER USE

The coastal plain sediments that underlie SRS are an important hydrologic resource since the formations are sources for drinking water, industrial process and cooling water, and water used for agricultural purposes. Fifty-six municipalities and industries identified near the site use this ground water.

3.4 ENVIRONMENTAL DESCRIPTION

3.4.1 METEOROLOGY

The climate of the area is classified as humid subtropical, and is characterized by short, mild winters and long, warm, humid summers. Average annual precipitation for SRS is 48 inches. The major factor affecting summer weather is the "Bermuda high" pressure system. Frequent thunderstorms are prevalent, accounting for about 16 inches of the annual rainfall. Fog, creating a visibility of 1/4 mile or less occurs on an average of 28 days per year. Autumn weather generally brings cool, clear mornings, and mild, sunny afternoons. Autumn rainfalls account for about 9 inches of the annual rainfall. Winters alternate between warm, moist weather, and dry, cool weather with an occasional Arctic air mass influence. Ice and snow accumulations in excess of 1 inch are rare. Extreme air pollution episodes in the region are rare.

SRS is subject to tornadoes and severe thunderstorms with a low frequency of point strike recurrence. The hurricane frequency average is about one every eight years; highest hurricane winds observed on-site is 75 mph, and occurred in 1959.

Sources of data describing local climatology include an onsite meteorological tower network, an instrumented television tower 8.5 miles northwest of SRS, and the National Weather Service at Bush Field in Augusta, GA, approximately 12 miles west-northwest of SRS. Data from the H-Area tower (one of eight SRS towers with wind, temperature, and dewpoint sensors located at 200 feet above ground) are the most representative for characterizing the dispersion climatology of DWPF.

Since there are no pronounced topographic features within 19.3 miles of the site, the local terrain has little effect on wind and stability climatology at SRS. During stable atmospheric conditions, some channeling or air flow stagnation could occur in some of the more pronounced valleys. However, any terrain-induced increases in pollutant concentrations would be very localized and short-lived.

For additional details on regional climatology, local meteorology and the onsite meteorological measurements program, see SRNS-IM-2013-00019, Site Information and Program Description (Ref. 3). Short-term (i.e., accident) relative diffusion factors (χ/Qs) are calculated. Various computer codes are used in calculating the diffusion factors and consequences. These are identified in FSAR Section 9.4. A description of the methodology is given in the Environmental Dose Assessment Manual (Ref. 4).

3.4.2 HYDROLOGY

3.4.2.1 Surface Hydrology

The Savannah River basin is located in three physiographic provinces, the Blue Ridge, the Piedmont, and the Coastal Plain. The Piedmont contains about 50% of the Savannah River drainage basin, and the Coastal Plain contains about 31% of the drainage basin.

SRS is located entirely on the Coastal Plain. Much of it is located on the Aiken Plateau, and surface water eventually drains into the Savannah River via several streams. The Savannah River was the principal water source for SRS when the nuclear reactors were operating, and is at a substantially lower elevation than SRS. Par Pond, an artificial lake, is the largest impoundment on the site. Water is retained in numerous lakes and Carolina bays. Most of the SRS water comes from aquifers.

Flooding of the Savannah River has been controlled by a series of dams and reservoirs, Thurmond being the largest. The record historical flood at Augusta, GA occurred in 1796, with an estimated discharge of 360,000 cfs; the peak flow (350,000 cfs) recorded by the U.S. Geological Survey occurred on October 3, 1929. Since Strom Thurmond Dam was constructed, no major flood has occurred at Augusta, GA.

For the 30-year period from 1921 to 1950, before construction of Strom Thurmond Dam, the mean annual maximum flow of the Savannah River was 92,600 cfs, the 10-year maximum flow was 211,000 cfs, and the estimated 50-year maximum flow was 362,000 cfs. For the 30-year period from 1956 to 1985, after construction of Strom Thurmond Dam, the mean annual maximum flow was 35,600 cfs, the 10-year maximum flow was 58,000 cfs, and the estimated 50-year maximum flow was 80,500 cfs. The nearest surface stream to DWPF is Upper Three Runs Creek (UTRC) which is approximately 1 mile north of DWPF. No dams are located in the Upper Three Runs Creek watershed.

All structures where nuclear activities are conducted at SRS are located on topographic high points, resulting in no safety threat due to high water from the Savannah River or any of the nearby streams on site. Specifically, DWPF is located as a local topographic high part (minimum grade level 275 feet mean sea level [msl]) and is within the Savannah River drainage basin at the divide between Crouch Branch and McQueen's Branch watersheds. McQueen's Branch drains into Tinker Creek near its junction with UTRC, and Crouch Branch drains directly into UTRC. All streams in the area are at substantially lower elevations than the DWPF. Because flooding of DWPF is not a credible safety hazard, safety equipment and systems to protect structures against adverse hydrologic consequences are unwarranted.

3.4.2.1.1 PROBABLE MAXIMUM FLOOD ON STREAMS AND RIVERS

The Probable Maximum Flood (PMF) values for the Savannah River and for UTRC were determined using Regulatory Guide 1.59 (Ref. 5). The PMF of 1,001,000 cfs for the Savannah River at VEGP and thus at SRS, reported in Appendix B of the Regulatory Guide, is slightly greater than the PMF flood discharge of 895,000 cfs determined by Southern Company Services (Ref. 6) in the VEGP Final Safety Analysis Report (FSAR). Procedures outlined in the Regulatory Guide were used to verify the PMF for the Savannah River and to estimate the PMF for UTRC.

The PMF for McQueen's Branch was calculated by first determining the Probable Maximum Precipitation (PMP). National Weather Service Hydrometeorological Reports No. 51 (Ref. 7) and No. 52 (Ref. 8) were used to develop PMP envelopes for SRS and the Savannah River drainage basin upstream of the site. The runoff hydrograph was developed using methods developed by the Bureau of Reclamation (Ref. 9).

Figure 3.4-1 shows cross sections of the stream valleys and the peak water-level stages under PMF conditions. The figure shows that the peak flood level for each case is well below the DWPF site and poses no hazard for safety facilities at the site.

3.4.2.1.1.1 Probable Maximum Precipitation (PMP)

PMP envelopes for the Savannah River Basin upstream of VEGP were developed for the VEGP FSAR (Ref. 6) following the techniques presented by the National Weather Service (Ref. 8). These elliptic envelopes were spatially distributed to cover the Savannah River Basin and its drainage. For each drainage area, the PMPs at 6-hr intervals were arranged in critical sequence to develop the flood hydrograph.

The 1-hr and 6-hr PMPs for the small watershed adjacent to the site (McQueen's Branch) were determined from Hydrometeorological Report No. 51 (Ref. 7). The values for rainfall at a point were used because of the small size of the watershed above the site (approximately 0.75 mi^2). Using a technique given in a publication by the Bureau of Reclamation (Ref. 9), rainfall increments for additional 1-hr periods were designed to maximize conservative PMF estimates.

Precipitation Losses

Precipitation losses were conservatively assumed to be zero when developing the PMF evaluation from the PMP for the small watershed near the site.

Runoff Model

Using runoff and flood routing routines developed by the US Army Corps of Engineers (including HEC-1), the PMF for the Savannah River at VEGP was determined to be 895,000 cfs, assuming no valley storage effect. Because the VEGP runoff model PMF is about 10% less than the PMF of 1,001,000 cfs for the Savannah River reported in Regulatory Guide 1.59

(Ref. 5), and because the DWPF site elevation is much greater than the VEGP site elevation, the larger PMF was used in this analysis.

The PMF flood peak for UTRC was calculated using the simplified method in Regulatory Guide 1.59. The PMF was plotted using the figures in Appendix B of the guide for drainage areas ranging from 100 to 20,000 mi.^{2}; then interpolation of the logarithmic plot provided the PMF for the 163 mi^2 watershed of UTRC. This method provided a conservative value of 150,000 cfs for UTRC at its closest approach to the DWPF site.

A one-hr synthetic unit hydrograph was developed for the McQueen's Branch watershed (0.75 mi^2) using methods described in "Design of Small Dams" (Ref. 9). Because part of the DWPF site and part of H-Area are in the watershed, the synthetic hydrograph data for urban basins and the point PMP of 19 inches in 1 hr and 31 inches in 6 hr were used to develop a conservative estimate of PMF in McQueen's Branch (Ref. 7). Infiltration was neglected, and the unit hydrographs were compared to determine the peak discharge.

3.4.2.1.1.2 Probable Maximum Flood Flow

The PMF discharge was calculated to be 11,000 cfs for McQueen's Branch just above Road F and adjacent to the DWPF site. This cfs value corresponds to an elevation of 224.5 feet msl at the closest approach of the stream to the site (Figure 3.4-1). The PMF discharge is 15,000 cfs for UTRC at a point just downstream from where it is joined by Tinker Creek, corresponding to a flood stage elevation of 173 feet msl, respectively.

The flood stages are considerably lower in elevation than minimum plant grade at the DWPF site; therefore, coincident wind-generated waves do not pose a threat to site safety.

3.4.2.1.1.3 Water Level Determinations

Because the flood flows calculated are clearly not a threat to the site, conservative estimates of stage were calculated. The Manning equation was used to relate flood stage to the flood discharge. Stream cross sections and channel slopes were taken from topographic maps, and a conservative Manning's "n" value of 0.02 was used. The PMF flood stage elevation is 224.5 feet msl for McQueen's Branch, located approximately 2,200 feet from the DWPF site, and 173 feet. msl for UTRC at its closest approach to the DWPF site.

For the Savannah River, the PMF stage of 140 feet msl computed for this analysis was compared to the PMF stages generated in the VEGP FSAR (Ref. 6) and found to be conservative. Figure 3.4-2 shows the cross section at each location where stage was computed and the maximum stage during PMF.

The flood stages associated with the PMF discharge estimates are well below the DWPF minimum plant grade for a safety structure (274 feet msl).

3.4.2.2 Subsurface Hydrology

3.4.2.2.1 REGIONAL CHARACTERISTICS

Two distinct hydrologic regimes underlie SRS. The first of these systems is comprised of Paleozoic metamorphic and igneous basement rocks and Triassic-aged lithified mudstone, sandstone, and conglomerate within the Dunbarton Basin. The second regime consists of unconsolidated Coastal Plain sediments of Late Cretaceous and Tertiary age. The geologies of these two regimes are described further in Subsection 3.4.3.

The Paleozoic rocks are dominantly gneisses and schists with lesser amounts of quartzite. These metamorphic rocks are intruded by somewhat younger Paleozoic granitic plutons. Similar Paleozoic metamorphic and igneous rocks crop out in the Piedmont Province north of the Fall Line, which is approximately 20 miles northwest of SRS.

Triassic-age sediments lie within the Dunbarton Basin. The Dunbarton Basin is a graben structure within the Paleozoic metamorphic basement. It lies beneath about 1200 feet of Coastal Plain sediments in the southeast part of SRS. The Triassic sediments consist of poorly sorted, consolidated gravel, sand, silt, and clay. Coarser material is found near the northwest margin of the basin where fanglomerate is abundant. Similar to other East Coast Triassic basins in the Atlantic Coastal plain, sand, silt, and clay predominate near the center of the basin. Sorting in the Triassic rocks is extremely poor, resulting in very low primary permeability. The lithology of the clasts in the sedimentary rock indicates that they were derived from crystalline metamorphic rock immediately to the northwest of the Dunbarton basin. Many of the sands are arkosic, indicating little transport and/or rapid burial.

The Coastal Plain sediments comprise a clastic wedge that thickens and dips toward the southeast. Near the mouth of the Savannah River, this wedge is 4000 feet thick and thins northwest towards the Fall Line where it pinches out completely. Coastal Plain sediments are Late Cretaceous to Holocene in age. Coastal Plain sediments in the vicinity of SRS consist of sandy clays and clayey sands, although occasional beds of clean sand or clay also occur.

Both the Paleozoic and Triassic rocks were leveled by erosion and are unconformably overlain by unconsolidated to semiconsolidated Coastal Plain sediments. Two clay-rich zones form an effective seal that separates ground water in the Coastal Plain sediments from ground water in the underlying crystalline Paleozoic bedrock and the Triassic Basin.

The hydrology of the buried Paleozoic and Triassic basement hydrologic system was studied intensively to assess the safety and feasibility of storing radioactive waste in these rocks. Water injection and withdrawal tests on sections of rock isolated by packing off indicate that two kinds of fractures exist in the Paleozoic bedrock. The first consists of minute fractures that pervade the entire rock mass but transmit water slowly. Rocks containing this kind of fracture are called “virtually impermeable rocks.” The second kind of fractures have larger openings that transmit water more quickly. They are vertically restricted but can be traced laterally. Rocks containing these kinds of fractures are called “hydraulically transmissive rocks.”

Groundwater in the Paleozoic bedrock is not pumped at SRS except for testing programs because of the large amount of groundwater in the prolific aquifers of the Coastal Plain sediments. As such, the Paleozoic bedrock will probably not be used as a water source at SRS. The hydrologic regime of the metamorphic and igneous basement rocks at SRS, therefore, is unlikely to change appreciably for many decades. Immediately south of the Fall Line and to the north of it in the Piedmont province, the Paleozoic metamorphic and igneous rocks are domestic aquifers.

In the Dunbarton Triassic Basin, groundwater is present in the primary and secondary porosity of clastic rocks. However, the hydraulic conductivity is extremely low, and water movement is almost nonexistent. Water is not pumped from rocks in the Dunbarton Triassic Basin, nor is there likely to be any pumped in the future because of the poor water quality and low permeability of the rocks.

The Coastal Plain sediments constitute a multilayered hydrologic system that is comprised of low-permeability stratigraphic zones, which retard groundwater flow (confining units), interbedded with permeable zones that readily transmit groundwater (aquifers). In general, the transmissive zones consist of sands while the low permeable zones have high silt and clay content. Groundwater resides primarily in the pore spaces of the unconsolidated sands. Groundwater flow paths and flow velocities for each of these units are governed by the hydraulic properties and geometry of the particular unit, and by the distribution of recharge and discharge areas.

In the SRS region, Coastal Plain sediments are subdivided into two confining systems and two aquifer systems. The basal hydrostratigraphic system in the Coastal Plain sediments is designated as the Appleton Confining System (formerly Confining System I). This is overlain by the Dublin-Midville Aquifer System (formerly Aquifer System I), the Myers Branch Confining System (Confining System I-II), and the Floridan Aquifer System (Aquifer System II). The systems are further subdivided into aquifer and confining units. Several hydrostratigraphic nomenclatures have been used at SRS. Figure 3.4-3 compares some of the hydrostratigraphic nomenclatures that have been used at SRS.

For details of the geohydrology of the confining and aquifer systems including hydraulic conductivity, porosity and permeability data, and for a discussion of water quality at SRS, and use of area groundwater, see SRNS-IM-2013-00019, Site Information and Program Description (Ref. 3).

3.4.2.2.2 GEOHYDROLOGIC ZONES AT DWPF

In the vicinity of DWPF, the comparison of hydrostratigraphy nomenclature by Price in 1988, shown in Figure 3.4-3, describes the hydrostratigraphy beneath DWPF. The Price nomenclature breaks regional systems and larger aquifer units into hydrostratigraphic zones 1 through 8. Some zones are subdivided; for example, zone 5 consists of an aquifer (zone 5a) and a confining zone or aquitard (zone 5b). Other units are not subdivided; for example, zone 1 is an aquitard consisting of clay and clayey, silty sand. Some aquitards (e.g., zone 1) are effective seals throughout the SRS area. However, because of lateral and vertical changes in

permeability, other beds referred to as aquitards inhibit the vertical flow of water between aquifers in some places but allow its passage in others.

Zone 1, an aquitard, corresponds to the Appleton Confining System and consists of clay layers and semiconsolidated, clayes, and silty sands.

Zone 2 comprises three subzones: 2a, 2b, and 2c. Zones 2a and 2b are aquifers which make up the larger McQueen Branch Aquifer, and zone 2c corresponds to the McQueen Branch confining unit. Zone 2a corresponds to the Middendorf Formation, which consists predominantly of dirty-to-clean, fine-to-coarse sands. Clay layers occur within zone 2a. These beds appear to have lateral continuity, but they are only locally impervious. Thus, zone 2a is connected to the overlying lower Black Creek sand (zone 2b). Zone 2c (McQueen Branch Confining Unit) is a clay layer that is fissile in places. It is a confining layer in some parts of SRS, but it does not form an effective seal in other places.

Zone 3 consists of a lower sand aquifer (zone 3a) and an aquitard (zone 3b). Zone 3a corresponds to the Crouch Branch Aquifer. The sand aquifer includes the upper part of the Black Creek Formation and most of the Peedee Formation. Zone 3b is the uppermost part of the Peedee. It is an effective aquitard in many places at SRS, but at other places it allows upward or downward flow of groundwater to the basal, sandy portion of zone 4. Zone 3b is part of the Myers Branch Confining System.

Zone 4 consists of the Rhems and Williamsburg formations of the Paleocene Black Mingo Group. This zone contains lignitic clay interbedded with sand layers. The sand at the base of zone 4 may be water bearing, but it is only a minor portion of the section. Most of the section consists of virtually impermeable material; therefore, zone 4 is considered an aquitard. Zone 4 is a part of the Myers Branch Confining System.

Zone 5 consists of the clastic sediments of the Congaree Formation (zone 5a) and the glauconite bearing sands and clays of the lowermost Santee Formation (zone 5b). Zone 5a corresponds to the Gordon Aquifer consisting predominantly of fine-to-coarse quartz sand. Clay laminae occur throughout the section, but they are too thin and discontinuous to be effective aquitards. Zone 5b, often called the “green clay” or Gordon Confining Unit, is characterized by rapid facies changes. At the DWPF site, it consists of dirty-to-clean sands that enclose clay lenses, which attain a maximum thickness of 10 ft. Thus, the permeability of the “green clay” varies greatly, causing it to act as a confining to semiconfining layer in some places and a moderately transmissive layer in other places. However, the “green clay” is an effective confining unit at the DWPF site.

Zone 6 is the lower portion of the McBean Aquifer which lies within the larger Upper Three Runs Aquifer. At the DWPF site, zone 6 corresponds to the calcareous to noncalcareous sands of the Santee Formation. The hydraulic conductivity of the zone is moderately low at the DWPF site, but elsewhere at SRS it attains a moderate to moderately high hydraulic conductivity. Groundwater leaks into this zone from the overlying Dry Branch Formation.

The saturated zone at the DWPF site begins in zone 7. Zone 7, like zone 6, lies within the Upper Three Runs Aquifer. At the DWPF site zone 7 includes the Dry Branch and the Tobacco Road formations. The three hydrological subdivisions of zone 7 are as follows: zone 7a is the upper portion of the McBean Aquifer corresponding to the lower part of the Dry Branch formation; zone 7b, the "tan clay" horizon within the Dry Branch; and zone 7c, the Barnwell Aquifer corresponding to the upper part of the Dry Branch Formation and the Tobacco Road Formation. The Dry Branch and Tobacco Road formations are predominantly fine-to-coarse sand, but clay laminae are fairly common. The "tan clay" (zone 7b) is a local aquitard only, and zones 7a and 7c are hydrologically connected in some places at the DWPF site. Groundwater occurs under unconfined to semiconfined conditions in zone 7a. In zone 7c, groundwater occurs under unconfined conditions at most places at the DWPF site.

Zone 8 corresponds to the "Upland unit." Dirty to moderately clean, cross-bedded sands are dominant in this unit, but clay bodies are common. Conspicuous quartz pebbles are common locally, and large-to-small clay balls occur sporadically. Nearly all of the sands within zone 8 are unsaturated, but perched water occurs above some of the clay bodies.

3.4.2.2.3 SITE CHARACTERISTICS

D'Appolonia Consulting Engineers installed 23 temporary piezometers during the DWPF site investigation. These piezometers along with 11 others already existing in the area were used for the initial groundwater investigation. The plan location of these piezometers is shown in Figure 3.4-4 and elevation data for these wells are listed in Table 3.4-1. Contours of piezometric head at the DWPF site for zones 7c, 6, 5 and 4 for data collected between October and December of 1981 are shown in Figures 3.4-5 through 3.4-8.

Fourteen monitoring wells (Figure 3.4-4) have been installed at S Area. Wells SCA 1, 1A, 2, and 2A were installed in 1986 to monitor the groundwater beneath the vitrification building. In addition, SCA 3, 3A, 4, 4A, 5, and 6 were drilled in January 1990. These wells have been monitored since construction was completed. Wells SBG1 through 6 (Figure 3.4-9) were installed to monitor the groundwater at the perimeter of the site. The SBG wells were installed in September 1985 except for SBG 5, which was installed in January 1987. In November 1988, wells SLP 1 and 2 were installed in the DWPF low point pump pit, and wells ZDT 1 and 2 were installed in the nearby Z-Area drain tank.

The observed water levels indicate that at the DWPF site zones 7c and 6 flow toward McQueen Branch, zone 5 flows toward UTRC, and zone 4 flows toward the Savannah River. There is a net downward movement of water to zone 5. Zone 5b, the "green clay" which separates zones 5 and 6 appears to be an effective aquitard, as there is almost a 70 ft difference in head across the layer, and piezometric fluctuations in zone 5 are much smaller than in zone 6.

Groundwater from the SBG wells has been monitored since March 1986 (Table 3.4-2). Well SBG 5 has elevated pH, calcium, and conductivity levels, indicating that the water from this well is either being chemically influenced by the well grout or by a calcareous zone in the underlying formations. Mercury (up to 0.001 mg/L) above background levels has been

detected in well SBG 1. Elevated levels of total organic halogens, trichloroethylene, trans-1,2-dichloroethene, and tetrachloroethylene have been detected in well SBG 4. The source of the mercury and organics in the groundwater is unknown. Tritium activities (up to 23.2 pCi/mL) above background levels have been detected in several wells. This tritium probably was released into the air at the nearby separations area and was deposited in rainfall. Elevated lead concentrations (up to 0.062 mg/L) were detected in several wells. The lead in the groundwater is probably due to leaching of naturally occurring lead in the soils.

Two water supply wells, designed with a capacity of 1,000 gpm each, were constructed at the DWPF site during 1985 and 1986. The wells draw water from the Cretaceous-age Lumbee Group, zone 2 and 3, at elevations of 220 to 550 ft below mean sea level. The water from these wells are available for fire fighting, domestic water, and process water.

The DWPF site is within the groundwater recharge areas for zones 5, 6, and 7. The presence of the DWPF site will increase the surface runoff in the area, decreasing the infiltration into the groundwater. This decreased infiltration may cause minor long-term lowering of the water levels in zones 6 and 7. Because no water is used from these zones, and the zones drain into the nearby creeks, lowering the water level will not affect the safety of the site.

3.4.2.2.4 CONTAMINANT TRANSPORT ANALYSIS

In the unlikely event of a leak of radioactive material during DWPF operations, contaminants would move vertically downward to the water table and then through the saturated zone to points of surface discharge. Movement is controlled by the rate and direction of groundwater flow, hydrodynamic dispersion, and the absorptive capabilities of the soils. During the period of travel, the concentration of radioactive materials would be reduced by radioactive decay and soil sorption.

3.4.2.2.4.1 Estimation of Travel Time

Figure 3.4-10 is an potentiometric surface map of the water table underlying DWPF. Shallow ground water beneath the site moves generally to the east toward a small tributary of Upper Three Runs Creek. The water table underlying DWPF occurs in the Barnwell Formation.

A postulated leak (darkened circle) occurring along the waste transfer lines from H-Area to the DWPF canyon building would have a shorter path to a surface discharge than any other point on the site where waste will be handled or stored. The flow path shown from the darkened circle to the surface discharge point is approximately that which would be taken by leakage form the waste transfer lines, assuming that the waste moves along the water table surface*. [*The location of DWPF facilities as shown in Figure 3.4-10 have changed due to later design modifications.] In reality, recharge from precipitation reaching the water table would force the transported wastes deeper, causing the wastes to follow a curvilinear path from point of leakage to surface discharge. As this path would be longer and the travel time consequently greater, considering flow along the water-table surface is conservative.

The transfer lines are buried at some distance above the water table and are underlain by some depth of unsaturated material. Flow velocities in the unsaturated zone are on the order of 7 ft/yr (2.1 m/yr)(Ref. 10). This velocity applies to unsaturated flow; it is assumed that a leak would not be of such magnitude as to produce saturated conditions beneath the transfer line break. The elevation of the transfer line at the hypothetical leak point is 268 feet (81 meters) above mean sea level (Ref. 11). The water-table elevation is about 252 feet (77 meters) above mean sea level and capillary water is assumed to extend 5 feet (1.5 meters) above the water table. The unsaturated zone flow path is therefore assumed to be 11 feet (3.4 meters). The travel time for ground water flow through the unsaturated zone about 1.6 years.

The flow path in the saturated zone begins at the point where the waste, moving vertically downward, encounters the water table. The flow path length in the saturated zone is approximately 1,690 feet (515 meters), and all flow occurs in the Barnwell Formation. The flow path was divided into five segments, and the travel time along each segment of the flow path was calculated using the following relationship (Ref. 12):

$$V_W = \frac{K\,\Delta h}{\varepsilon\,\Delta L} \qquad (1)$$

where:

Vw	=	velocity of groundwater (units of length/time)
K	=	hydraulic conductivity (units of length/time)
ε	=	effective porosity (dimensionless)
Δh	=	change in hydraulic head (units of length)
ΔL	=	change in distance (units of length)

Pumping tests at the DWPF site (Ref. 13) provided a value for transmissivity in the Barnwell Formation of 3,140 gpd/ft (39 m^2/day). At the location of the aquifer test, the saturated thickness of the Barnwell Formation was 33 feet (10 meters), resulting in a hydraulic conductivity of 12.7 ft/day (3.9 m/day). The effective porosity was estimated to be 25%. The gradient of hydraulic head was determined from the water table potentiometric surface map (Figure 3.4-10). Results of the flow rate calculations are provided in Table 3.4-3. The groundwater flow time along the saturated flow path is about 5.8 years. Therefore, the total time for ground water flow from the hypothetical leak point to the nearest surface discharge is 7.4 years. This would also be the travel time for the center of mass of the contaminant plume.

3.4.2.2.4.2 Radionuclides Concentrations at the Groundwater Outcrop

Radionuclides transferred to the DWPF site include the waste tank sludge and supernate, processed to remove selected radionuclides. Typically, the sludge stream contains higher concentrations of radionuclides (Ref. 14 and 15); however, ^{3}H and ^{135}Cs are higher in the

supernate. Only the higher of the two concentrations is listed and used for these calculations* (Table 3.4-4, columns 2 and 3). [* The reference process for supernate treatment is not settled; therefore, this radionuclide inventory may be subject to change.]

The waste transfer lines consist of an inner steel pipe within an outer steel pipe to provide containment. Detection devices for possible leaks are at well-marked field locations, making massive leaks unlikely. Because a waste leak is unlikely, the contaminant transport analysis was done for a 1-gallon volume of waste, which can be ratioed to any postulated volume of leakage.

Table 3.4-4 (column 5) lists the concentration guides for areas with uncontrolled access to protect individuals from exposure to radiation and radioactive material (Ref. 16). Guide values are not available for some isotopes; however calculated concentrations of most of these at the groundwater outcrop are below 10^{-15} Ci/gal.

The three major controls on radionuclide concentration are decay, ion exchange, and hydrodynamic dispersion. Radionuclides with concentrations less than 10^{-15} Ci/gal are not considered further.

The concentration of each radionuclide after 7.4 yr of travel (1.6 yr in the unsaturated zone and 5.8 yr in the saturated zone) is given in Table 3.4-4 (column 6). No ion exchange or dispersion was considered when generating the results in this column. Decay half lives were obtained from standard Tables (Ref. 17). The short half-lives of several isotopes (column 4) cause them to decay to negligible concentrations during the 7.4-year travel time. However, the concentration of most radionuclides remains higher than the concentration guides; therefore, further controls on concentration were considered.

The presence of mica and kaolinitic clays in the subsurface makes ion exchange a significant factor in controlling the rate of contaminant movement. The distribution coefficient (K_d), which determines the amount of radionuclide adsorbed, is influenced by many factors such as pH, solution concentration of the radionuclide, and, for some isotopes, the valence state. Data are available for some distribution coefficients at SRS (Ref. 18). Values for typical SRS soil (80% sand and 20% clay) are shown in Figure 3.4-11 for strontium and in Figure 3.4-12 for cesium.

The pH and concentrations of strontium and cesium in a leak must be known to determine the distribution coefficients (K_d). The strontium concentration in the sludge transfer line is 1.1×10^{-3}M. The highest concentration curve on Figure 3.4-11 is 5×10^{-4}M; however, the concentration will be lowered by mixing with the groundwater. Thus, the curve for 5×10^{-4}M is used in Figure 3.4-11. The cesium concentration is 6.5×10^{-5}M. The pH of the leaking material could range from 5.5 to 9.7 (Ref. 19). Using Figures 3.4-11 and 3.4-12, the following distribution coefficients were estimated: for strontium, K_d - 6; for cesium, K_d - 60 (pH = 5.5 was used for both radionuclides). Figures 3.4-11 and 3.4-12 show that the K_d increases as the radionuclide concentration declines, as it will during transport under the influence of dispersion and dilution. Thus, using the distribution coefficients from the initial leak concentration is a conservative assumption. Competing ion effects are not considered in

this analysis due to their complexity. It is expected that this effect will reduce the K_d to a slight degree. Also, complexing with other agents, which generally reduces the K_d (David Hayes, Savannah River Laboratory, personal communication, January 1989), has not been taken into account.

Some K_d information from SRS is also available for plutonium and ruthenium and is shown in Figures 3.4-13 and 3.4-14, respectively (Ref. 18). Information on K_d versus radionuclide concentration is not available. For plutonium, the more mobile valence state [Pu(VI)] was assumed and the K_d determined to be about 20. A K_d of 100 was determined for ruthenium.

Distribution coefficients (K_d) for most radionuclides have not been determined at SRS. K_d values for many of the remaining radionuclides were obtained from the literature. All K_d values used are listed in Table 3.4-4 (column 7), and their sources are indicated.

The flow rate and travel time for each radionuclide was adjusted for K_d by using the approximation (Ref. 20):

$$\frac{V_c}{V_w} = \frac{1}{1 + K_d R} \qquad (2)$$

where:

V_c = average contaminant velocity (units of length/time)

V_w = groundwater velocity (units of length/time)

K_d = distribution coefficient (units of length^3/mass)

R = ρ / ε (units of mass/length^3)

where ρ = bulk density of the soil (units of mass/length^3)

ε = effective porosity (dimensionless)

R is about 7.5g/cm^3 for SRS soil (ρ about 1.5g/cm^3 and ε about 0.25).

This relationship was used to calculate the radionuclide concentrations given in Table 3.4-4 (column 8). The same K_d value was applied to movement through the unsaturated and saturated zones. If a K_d value was not readily found in the literature for a particular radionuclide, adsorption was assumed not to occur, and the concentration in column 6 was carried forward unchanged to column 8.

Most radionuclides considered are greatly reduced in concentration due to ion exchange. Many remain above concentration guides, and hydrodynamic dispersion was calculated to provide a further control of the radionuclide concentrations.

Contaminants transported by groundwater are subject to hydrodynamic dispersion due to the variation in the grain size of porous media and the tortuosity of microscopic flow paths. The presence of clay layers and the anisotropy of hydraulic conductivity cause dispersion on a macroscopic scale. The result is a distribution of the contaminant around the center of mass of contamination. Hence, some radionuclides arrive at the outcrop ahead of the majority; however, their concentration is lower because of dilution.

Dispersion, which varies spatially because of the variability of subsurface materials, is difficult to evaluate quantitatively. If a simple hydrogeologic setting is assumed, an approximation of the migration rate and pattern can be made using the following relationship (Ref. 20):

$$C(x,y,z,t) = \frac{M}{8(\pi \cdot t)^{3/2}\sqrt{D_X \cdot D_Y \cdot D_Z}} \cdot \exp\left(-\frac{X^2}{4D_X \cdot t} - \frac{Y^2}{4D_Y \cdot t} - \frac{Z^2}{4D_Z \cdot t}\right) \qquad (3)$$

where:

C = concentration distribution of the contaminant mass at time t

t = time

M = mass of a contaminant introduced at a point source

D_X, D_Y, D_Z = coefficients of dispersion in the x, y, and z directions, respectively

X, Y, Z = distances in the x, y, and z directions from the center of gravity of the contaminant mass

This equation assumes that the flow velocity is constant and that the contaminant begins as an instantaneous point source. Although the source is a point, it is assumed to have mass determined as the product of the radionuclide concentration in the leak and the volume of the leak.

Dispersion is assumed to vary only with direction and is directly proportional to flow velocity. The proportionality constant between the velocity and the coefficient of dispersion is the dispersivity. Based on estimates (Ref. 21), a dispersivity of 1 ft longitudinally was used. Flow velocities in the transverse directions are negligible, but dispersion will occur due to diffusion. A value of 0.1 was chosen for the coefficient of horizontal transverse dispersion and 0.05 for the coefficient of vertical transverse dispersion. Dispersion was neglected in the unsaturated zone because of the low flow velocity (7 ft/yr) and the short flow path (11 ft). For this calculation the groundwater velocity in the saturated zone was assumed to average 350 ft/yr based on calculated values ranging from 130 to 365 ft/yr.

At the center of mass (the point of peak concentration), the terms X, Y, and Z will be zero. Therefore, the maximum concentration is given by (Ref. 20):

$$C_{\max} = \frac{M}{8(\pi \cdot t)^{3/2}\sqrt{D_X \cdot D_Y \cdot D_Z}} \qquad (4)$$

where all terms are defined above.

Substituting values of

M = 1 Ci

t = 5.8 yr

D_X = 350 ft^2/yr

D_Y = 35 ft^2/yr

D_Z = 17.5 ft^2/yr

$$C_{\max} = \frac{1}{8(\pi \cdot 5.8)^{3/2}\sqrt{350 \cdot 35 \cdot 17.5}}$$

$$= 3.5 \times 10^{-6} \text{ Ci}$$

Thus, the concentration is reduced at the center of mass of the contaminant plume by about 5.5 orders of magnitude.

Dispersion of the contaminant implies that radionuclides are distributed around the center of mass, with concentrations decreasing from the center toward the edges of the plume. A leading edge exists that will allow some radionuclides to outcrop at a surface discharge ahead of the center of mass, having traveled at a greater velocity than the center. The zone in which 99.7% of the contaminant mass occurs will have an elliptical shape with dimensions, measured from the center of mass, of

$$3\sigma_x = \sqrt{2D_X \cdot t}$$

$$3\sigma_y = \sqrt{2D_Y \cdot t}$$

$$3\sigma_y = \sqrt{2D_Z \cdot t}$$

where σ equals the standard deviation of the concentration distribution (Ref. 20). Considering the x direction only, the leading edge of the plume will be about 60 ft. ahead of the center of the mass as the plume approaches the groundwater outcrop. The arrival time of the leading edge will be about 5.6 yr. Therefore, although the radionuclides at the leading edge arrive sooner than those at the center of mass, they will have decayed by almost the same amount. In this case, earlier arrival time does not mean significantly greater concentration.

The concentration at the leading edge will be greatly reduced due to dilution. If the leading edge is 60 ft. ahead of the center of mass, then X = 60 ft. Along the center line of the plume, y = z = 0.

$$C = \frac{1}{8(\pi \cdot 5.6)^{3/2}\sqrt{350 \cdot 35 \cdot 17.5}} \cdot \exp\left(-\frac{60^2}{4 \cdot 350 \cdot 5.6}\right)$$

$$= 2.3 \times 10^{-6} \text{ Ci}$$

Thus, the concentration at the leading edge of the plume is reduced by nearly six orders of magnitude.

Dispersion is assumed to occur in the system; therefore, the concentration in Table 3.4-4 (column 9) are reduced by a factor of 3.5×10^{-6}. Column 9 lists the concentrations at the center of mass of the plume as that center reaches the surface discharge of groundwater. Almost all radionuclide concentrations are reduced to below the concentration guides due to the combined effects of radioactive decay, ion exchange, and hydrodynamic dispersion. Three radionuclide concentrations remain above the available concentration guides: ^{90}Sr, ^{239}Pu, and ^{240}Pu (by about 43 times, 2.3 times, and 1.3 times, respectively). These concentrations are unlikely because the distribution coefficients assumed for these radionuclides were conservatively low values representing the leak concentrations. As dispersion of the contaminant occurs, the concentration is reduced and the K_d increases. For example, from Figure 3.4-11 it is seen that a two-order magnitude decrease in concentration (i.e., mixing 1 gal of waste with 100 gal of groundwater) will increase the ^{90}Sr / K_d at pH 5.5 from the value of 6 used in the analysis to about K_d equal to 90. This would, in turn, reduce the effective ^{90}Sr velocity from 6.4 ft/yr in the saturated zone to 0.43 ft/yr and increase the travel time to over 3,000 yr, which is adequate time for the ^{90}Sr concentration to decay to a negligible amount.

3.4.2.2.4.3 Possible Contamination of Deep Aquifers

The vertical hydraulic gradient is downward between zones 7 and 6. A potential contaminant reaching the bottom of zone 7 could be transported into zone 6 and then laterally toward UTRC (Figure 3.4-3). A downward hydraulic gradient also exists between zones 6 and 5. However, between zones 5 and 4, the vertical hydraulic gradient is upward. Thus, potential contaminants that reach zone 5 are restricted to this formation and are channeled toward UTRC. The vertical hydraulic gradients for zones 2 and 3 underlying zone 4 are all upward.

Additional constraints on the vertical movement of a potential contaminant are the clay layers underlying the DWPF site. Within zone 7 are several layers of clay, sandy clay, and clayey sands that serve as confining or semiconfining units. These are known as the "tan clay" or Twiggs Clay lithology. At the base of zone 6 is a clay or sandy clay layer known as the "green clay." Besides greatly reducing the vertical velocity of fluid movement, the clays provide additional ion exchange sites for adsorption of potential contaminants.

3.4.3 GEOLOGY AND SEISMOLOGY

3.4.3.1 Basic Geologic and Seismic Information

The site region, defined as the area within a 200 mile radius of the center of SRS, includes parts of the Atlantic Coastal Plain, Piedmont, Blue Ridge, and Valley and Ridge

physiographic provinces. SRS is located on the upper Atlantic Coastal Plain in the Aiken Plateau. The crystalline basement beneath SRS consists of Precambrian/Paleozoic metamorphic and igneous rocks similar to those found in the Piedmont.

3.4.3.1.1 REGIONAL GEOLOGY

For a detailed discussion of the basic geologic and seismic information for the site region, see SRNS-IM-2013-00019, Site Information and Program Description (Ref. 3), which includes the following topics:

- Physiography
- Geologic History
- Blue Ridge Stratigraphy, Lithology, and Structure
- Piedmont Stratigraphy, Lithology, and Structure
- Atlantic Coastal Plain Stratigraphy, Lithology, and Structure
- Tectonics
- Potential Ground Disturbances

3.4.3.1.2 SITE GEOLOGY

Most information pertinent to the geology and seismology of SRS also applies to DWPF. For details of geological features in the immediate vicinity of H-, S- and Z-Areas, see SRNS-IM-2013-00019, Site Information and Program Description (Ref. 3).

3.4.3.2 Vibratory Ground Motion

3.4.3.2.1 GEOLOGIC CONDITIONS OF SRS

The Coastal Plain section at SRS consists of a south-easterly thickening wedge of Cretaceous and younger sediments. The thickness of the sediments range from about 600 feet thick near the northwestern boundary of SRS to about 1200 feet thick near the southern boundary. Beneath this section is a pre-Cretaceous unconformity that developed on a basement consisting of two geologic terranes: 1) the Triassic-Jurassic Dunbarton basin, crystalline terrain of metamorphosed sedimentary and igneous rock that may range in age from Precambrian to late Paleozoic; and 2) crystalline terrain of metamorphosed sedimentary and igneous rock that may range in age from Precambrian to late Paleozoic (Ref. 29).

For additional details refer to SRNS-IM-2013-00019, Site Information and Program Description (Ref. 3).

3.4.3.2.2 UNDERLYING TECTONIC STRUCTURES - GENERAL SITE

The major tectonic structures underlying the SRS consists of basement faults, some of which have propagated upward into post-Cretaceous sediments. For additional details refer to SRNS-IM-2013-00019, Site Information and Program Description (Ref. 3).

3.4.3.2.3 BEHAVIOR DURING PREVIOUS EARTHQUAKES

Refer to SRNS-IM-2013-00019, Site Information and Program Description (Ref. 3).

3.4.3.2.4 ENGINEERING PROPERTIES OF MATERIALS UNDERLYING THE SITE

Refer to Subsection 3.4.3.4.2 below.

3.4.3.2.5 EARTHQUAKE HISTORY

Refer to SRNS-IM-2013-00019, Site Information and Program Description (Ref. 3).

3.4.3.2.6 MODERN STRESS REGIME

Refer to SRNS-IM-2013-00019, Site Information and Program Description (Ref. 3).

3.4.3.2.7 CORRELATION TO EPICENTERS WITH GEOLOGICAL STRUCTURES

Refer to SRNS-IM-2013-00019, Site Information and Program Description (Ref. 3).

3.4.3.2.8 IDENTIFICATION OF ACTIVE FAULTS

Refer to SRNS-IM-2013-00019, Site Information and Program Description (Ref. 3).

3.4.3.2.9 DESCRIPTION OF CAPABLE FAULTS

Refer to SRNS-IM-2013-00019, Site Information and Program Description (Ref. 3).

3.4.3.2.10 MAXIMUM EARTHQUAKES

Investigations of historical seismicity, together with detailed seismic monitoring and geologic studies, have resulted in three hypothetical earthquakes, two of which control the seismic hazard at SRS. One of these two earthquakes is a local event comparable in magnitude and intensity to the Union County (SC) earthquake of 1913 but occurring within a distance of about 25 km of the site. The other is an earthquake representing a potential repeat (similar magnitude and location) of the 1886 Charleston earthquake.

Except for clusters of seismicity in Bowman and Middleton Place, sporadic and apparently random low-level seismicity is prevalent in the Coastal Plain and Piedmont geologic provinces. Regulatory guidance (10CFR100, App. A) prescribes a design basis local event to occur at a random location within a specified radius of the site. Recent geologic investigations conducted to determine and limit the age of deformation of known basement

faults at SRS indicate no post Eocene faulting. Consequently, deterministic analyses have assumed source properties for a random local event with on-site faults considered not capable.

Although more recent seismic hazard characterization information is now available, the URS/Blume (1982) (Ref. 30) was used for seismic characterization of the site (and DWPF) in the early 1980s.

The recommended site acceleration and spectra in the Blume analysis were based on conservative assumptions on the occurrence of specific earthquakes. Two hypothetical earthquakes consistent in size with earthquakes that have occurred in similar geologic environments were found to control SRS spectra and peak ground motion: a hypothesized local earthquake causing an estimated site peak ground acceleration (PGA) of 0.10g, and a hypothetical distant earthquake (1886 Charleston-type) causing an estimated site PGA of <0.1g. For added conservatism, the site PGA was doubled to 0.2g. Local and distant earthquake response spectral shapes were derived from statistical analyses of primarily Western U. S. earthquake data and scaled to the 0.2g PGA.

From this study, URS/Blume completed deterministic estimates of ground motion for SRS facilities including DWPF (Ref. 30).

Refer to SRNS-IM-2013-00019, Site Information and Program Description (Ref. 3) for additional details.

3.4.3.2.11 SAFE SHUTDOWN EARTHQUAKE

The URS/Blume report defined the Safe Shutdown Earthquake (SSE) as the maximum postulated earthquake producing the greatest peak ground acceleration. The SSE for SRS and thus for the DWPF structures was established as 0.20g horizontal acceleration based on the spectral shape given in the Blume analysis (Ref. 30).

The SSE discussed above was redefined as the Design Basis Earthquake (DBE) for the SRS site including the DWPF structures. The DBE for the SRS has a free field horizontal peak ground acceleration of 0.20g. The free-field peak ground acceleration in the vertical direction is two-thirds the horizontal or 0.13g.

For the geotechnical liquefaction analyses, other design earthquake spectra were used (see Section 3.4.3.4.9).

3.4.3.2.12 PROBABILISTIC ASSESSMENT OF PEAK GROUND ACCELERATION

As part of the Blume report (Ref. 30), a probabilistic analysis was performed to assess the recurrence of the peak ground acceleration at SRS. The analysis used the geographic distribution of earthquakes and their recurrence rates as a function of epicentral intensity, the variation of intensity with epicentral distance, and the peak ground acceleration as a function of intensity. Three source regions, following the tectonic province definition above, were used with the Charleston seismic zone having two configurations. The mean annual rates

equal to or exceeding peak, free-field accelerations of 0.10 g and 0.20 g were, respectively, 2 x 10^{-3} and 2 x 10^{-4}. Probabilities of exceeding accelerations of 0.10 g and 0.20 g in any interval of 50 years were 10 % and 1 %, respectively.

3.4.3.2.13 DESIGN RESPONSE SPECTRA

Response spectra were derived (Ref. 30) from statistical analyses of selected sets of strong-motion accelerograph data recorded in California and then related to the SRS site as resulting from a Charleston-type event and a local event. The DBE response spectra envelope both of these controlling events. The shapes of the DBE response spectra are given in Figure 3.4-15 and is normalized to a zero period acceleration of 1.0 g. For structural design purposes, these spectra should be appropriately scaled to 0.20 g in the horizontal direction and 0.13 g in the vertical direction. For the geotechnical liquefaction analysis, other design spectra were used.

3.4.3.3 Surface Faulting

No surface faults have been identified at SRS as discussed in SRNS-IM-2013-00019, Site Information and Program Description (Ref. 3).

3.4.3.3.1 GEOLOGIC CONDITIONS OF THE SITE

Refer to SRNS-IM-2013-00019, Site Information and Program Description (Ref. 3).

3.4.3.4 Stability of Subsurface Materials

3.4.3.4.1 GEOLOGIC CHARACTERISTICS

The complex sequence of marine and terrestrial sediments that underlie SRS produces significant local variations in the stability of subsurface materials. Numerous geotechnical and geological investigations have been performed at DWPF to characterize the in-situ static and dynamic properties of the soils. These investigations have led to conclusions concerning the stability of foundation soils in terms of liquefaction potential and structure settlement. Details of geotechnical considerations considered in the design and construction of the DWPF can be found in Ref. 28 (1984). Mueser, Rutledge, Johnston & DeSimone, Consulting Engineers (Ref. 28), compiled this report from reports, drawings, soil samples, and other materials supplied for the DWPF by D'Appolonia Consulting Engineers; Bechtel National Inc.; Geotechnical Engineers Inc.; URS Blume & Associates.

Details of geotechnical considerations considered in the design and construction of the Glass Waste Storage Building #2 (GWSB#2) can be found in Ref. 66. GWSB#2 was constructed as a PC-2 structure (Ref. 67), whereas GWSB#1 was constructed as a Category 1 structure. The following sections detail the design considerations for Category 1 structures and therefore addresses only GWSB #1.

Geologic features which may affect the stability of soils and rock beneath the DWPF foundations during the vibratory motion associated with earthquake design criteria are discussed in the following subsections.

3.4.3.4.1.1 Subsidence, Uplift, and Collapse

Based on a review of soil boring logs and drilling records, Mueser, Rutledge, Johnston & DeSimone conclude that some dissolution of the calcareous sands has occurred at depths of approximately 100 to 150 feet, resulting in possible voids or leached zones. A grouting program was deemed necessary for all Category I structures, and was accomplished as detailed in Ref. 33.

Subsidence due to removal of groundwater has not occurred at the Savannah River Site (SRS). No large-scale underground pumping is included with the permanent facilities; therefore, it is anticipated that subsidence due to groundwater withdrawal will not occur during the life of the facility. No extensive excavation below the permanent groundwater level was required during construction operations for the DWPF facilities.

Within 5 miles of the site, excavation has been limited to construction of other facilities or borrow areas for construction. The borrow areas are local and shallow and do not pose a hazard to the site. No economically significant mineral deposits exist near or beneath the site, and no future mining activity is expected in the site area.

3.4.3.4.1.2 Deformational Zones

No joints or faults were found at the DWPF site, although faults have been found within the boundaries of the SRS (see Reference 3, SRNS-IM-2013-00019, Site Information and Program Description). These faults are not considered capable, as discussed in detail in Section 3.4.3.2. Faults inferred from the seismic reflection survey were determined not to be capable, and these are discussed in Subsection 3.4.3.4.3.

A pervasive joint or fracture within SRS is suggested by angular drainage patterns and aligned sinks.

No evidence of large-scale shearing or folding has been found at DWPF.

3.4.3.4.1.3 Zones of Alteration and Structural Weakness

The occurrence of soft or underconsolidated zones and rod drops has been described in numerous drilling reports throughout the central portion of SRS (Ref. 34). The prevailing assumption for the cause of these zones has been the dissolutioning of carbonate rich sediments, resulting in vugular porosity where drill rods meet little penetration resistance. Frequently associated with these soft zones are localized beds of silica-cemented sand or indurated limestone where drilling becomes much harder. For example, during drilling in the General Separations Area (E-, F-, H-Areas), drillers reported rod drops immediately after drilling through a well cemented siliceous or calcareous bed or beds (Ref. 34).

The silica cemented horizons are generally noted at, or near, the top of the Santee Formation at, or near, an unconformity that separates the Santee Formation from the overlying Dry Branch Formation (Ref. 34). These cemented horizons at SRS appears to be similar to

cemented zones found in modern coastal environments where rapid lateral and vertical movement of fresh to saline ground water occurs, causing a high variability in cementation (Ref. 34). Thus, it is possible that the upper stiffer horizons and the underlying soft zones, may have developed during the unconformity at the end of Santee times. In fact, the hard zones may act as a resistant cap for the underlying soft zones, allowing them to persist as pockets of underconsolidated material through geologic time (Ref. 34).

Three dimensional mapping of soft zones at H-Area, indicate that low penetration resistances tend to occur in the Santee Formation in a fine to medium-grained, silty or clayey quartz sand having varying amounts of shell fragments and cementation. At H-Area, this sandy facies appears to flank a more competent limestone body in a band that is 100 to 200-feet wide. Although the soft zones shadow the limestone in a relatively wide band, individual penetration resistances within this band are highly variable. The soft material appears to occur as pockets or stringers of calcareous material that are laterally discontinuous. For example, at H-Area, no lateral continuity in standard penetration tests (SPT) N-values and cone penetration tests (CPT) penetration resistances were found that exceeds a few tens of feet. This high degree of variability is probably attributable to either rapid lateral and vertical changes in the amount of carbonate originally deposited or to subsequent changes in the diagenetic history of the sediments, or both (Ref. 34).

3.4.3.4.1.4 Residual Stresses in Bedrock

The site is not directly affected by unrelieved residual stresses in bedrock, because the top of bedrock lies approximately 900 feet beneath the surface.

3.4.3.4.1.5 Unstable Soils and Rocks

Engineering investigations indicated that subsurface materials generally consist of sands and clayey sands to a depth of approximately 70 feet below ground surface (bgs) (210 feet mean sea level [msl]) and interbedded sands and clays to greater depths. The sands above 210 feet msl are typically medium dense based on SPTs resistance (SPT blowcounts of 10 to 30), with a few SPT values below and above this range. Below 210 feet msl the sands are denser on average than those above 210 feet msl and are typically very dense below 135 feet msl. Clays and silts generally vary in consistency from stiff to very stiff.

The sands and clayey sands throughout the subgrade will not experience liquefaction (significant strength loss leading to bearing capacity failures) and will not develop cyclic mobility (significant cyclic or accumulated deformations) under the earthquakes analyzed with a peak horizontal ground surface acceleration of 0.20 g (Subsection 3.4.3.4.8).

3.4.3.4.2 PLOT PLANS

The S-Area is shown in relation to other site features in Fig. 3.4-16. The plan locations (D'Appolonia) of all borings drilled for the site investigation are presented in Figures 3.4-17 and 3.4-18. The locations of 23 piezometers installed to monitor groundwater levels in the four aquifers penetrated by the site geotechnical borings are also shown in the figures.

Existing site monitoring wells are shown in plan in Figure 3.4-4. All other piezometer wells and borings have been cemented and closed and casings pulled. The drawings also show the outlines of all DWPF structures, including the following Category I structures: vitrification building, sand filter, fan house, and glass waste storage building #1. The tunnels that connect the structures listed above are Category I up to the emergency exhaust port between the fan house and the stack.

Boring locations were selected to provide overall coverage of the site and to provide optimum coverage of Category I structures. The logs from the borings have been used to develop subsurface cross sections, which show in detail the stratigraphy underlying the site. The plan locations of the (D'Appolonia) sections are shown in Figure 3.4-17 and Figure 3.4-18. The corresponding D'Appolonia cross sections (a-a through m-m) are shown in Figures 3.4-19 through 3.4-28. Additionally, the plan location of Mueser sections is shown on Figure 3.4-29, with the corresponding cross sections given on Figures 3.4-30 through 3.4-34.

Piezometric heads recorded in the various piezometers are provided in Figures 3.4-35 through 3.4-38.

3.4.3.4.3 SOIL AND ROCK CHARACTERISTICS

3.4.3.4.3.1 Field Explorations

Field explorations consisting of drilling, sampling, in situ testing, and geophysical testing were conducted in three phases between January 1978 and August 1981 at the DWPF site. The last phase, which was conducted in 1981, was necessitated by a relocation of major structures at the site. All drilling, sampling, in situ testing, and piezometer installations were performed using standard specifications and procedures and a quality assurance program developed for subsurface exploration. Audits of the drilling equipment, soil and geophysical testing equipment, soil sampling and sample-handling procedures, and logging of borings and samples were conducted to assure that the field exploration program complied with the requirements of Appendix A to 10 CFR 100 (Ref. 36). Logs of the individual borings are presented in Reference 35.

Approximately 140 borings, including cross-hole and piezometer borings, were drilled for the field investigation. The boring locations are shown in plan (D'Appolonia) in Figures 3.4-17 and 3.4-18 along with the proposed plant layout, existing site contours, and the locations where SPT borings were performed in accordance with the American Society for Testing and Materials (ASTM) designation D1586. The sampling intervals for the SPT borings were generally performed at 2.5 feet intervals between 15 and 150 feet, at 10 feet intervals from 150 to 300 feet, and as necessary to define changes in the materials penetrated.

3.4.3.4.3.2 Soil Sampling

Immediately upon removal from the boring, the split-barrel sampler was carefully disassembled and a visual classification of the sample was made. The most representative and least disturbed portion of the sample, approximately 5 inches in length, was immediately

placed in a glass jar. The jar samples were sealed and labeled in accordance with the quality assurance requirements of D'Appolonia Consulting Engineers, Inc., and subsequently shipped to the soils laboratory for classification and index testing.

Undisturbed soil or sediment samples were obtained by means of , 1) conventional thin-walled tubes, in accordance with ASTM D1587, 2) pitcher barrels, and 3) Osterberg samplers. Undisturbed samples were taken for determining in situ substrate properties and for obtaining design parameters for settlement, bearing capacity, and liquefaction analyses. Approximately 200 undisturbed samples were obtained at the DWPF site. The samples were labeled in accordance with quality assurance requirements and shipped to the soils laboratory. Prior to shipment, the undisturbed samples were x-rayed at the SRS. All of the samples subjected to strength of compressibility testing were also x-rayed after arrival at their destination to check for disturbance in transit.

3.4.3.4.3.3 Cone Penetration Tests

Using a mechanical friction-cone penetrometer, CPT soundings of the "Upland unit" and Tobacco Road and Dry Branch Formations was conducted at six locations in accordance with ASTM D3441. The purpose of the soundings was to provide a more continuous penetration profile than that provided from SPT results and to develop correlations between CPT data and other field and laboratory test data. CPTs were conducted for borings BH 17, BH 21, BH 43, BH 46, BH 70, and BH 86 at an offset of approximately 15 feet from previously completed SPT boring locations. The depth of penetration ranged from approximately 59.7 feet in boring BH 70 to 98.4 feet in boring BH 43.

CPT results are presented with other boring log data and show profiles of cone resistance (q_c) and friction ratio (R_f) that reflect the variation of cone and friction sleeve resistance with depth. In general, q_c is used as an indirect measure of material strength and compressibility, while R_f is used as an indirect identifier of soil composition (e.g., predominantly sandy or clayey). This data for borings BH 17, BH 21, BH 43, BH 46, BH 70, and BH 86 is presented in Reference 35.

3.4.3.4.3.4 Pressuremeter Tests

Pressuremeter tests were performed at boring locations BH 63, BH 86, and BH 90 at the DWPF site. Most of the actual testing was performed in cross-hole seismic survey listing borings BH 63L21, BH 86L2, BH 86L1, and BH 90L2, although two tests were conducted in boring BH 90. The pressuremeter tests were performed to provide representative modulus values for use in foundation analyses. Boring BH 86 is located at the Glass Waste Storage Building #1, and boring BH 90 is located at the Vitrification Building.

Thirty-six pressuremeter tests were conducted at the DWPF site at depths below ground surface ranging from 9.4 to 281.7 feet. The results of each test are plotted in Reference 35. Although in practice three volume readings are made for any particular pressure increment (15, 30, and 60 sec after a pressure increment is applied), only the volume at 60 sec is plotted

against the applied pressure. Generally, the deformation is time dependent, and the volume reading at 30 sec will differ from the volume measured 60 sec after the pressure has been increased. The difference in volume between the 30- and 60-sec readings is termed the creep volume. The creep volume is also shown in the test plots.

The pressure and volume readings obtained in the field were corrected for volume change, pressuremeter inertia, and pressure head before the plots were constructed. Elastic moduli were determined from the corrected pressuremeter test results using a procedure developed (Ref. 52) to reconstruct the elastic portion of the in situ stress-strain curve. The pseudo-elastic portion of each pressure-volume curve (represented by the linear part of each pressure-volume curve following the initial upward curve) was used for this purpose. Values of the in situ elastic modulus for each test are indicated on each pressure-volume curve (Ref. 37). They range from 234 ksf at 76.7 feet deep in boring BH 63L2 to 1,700 ksf at 261.7 feet deep in boring BH 63L2. In general, the results of these tests indicate an in situ elastic modulus of approximately 400 to 500 ksf at elevation 240 feet msl, a gradual decrease in modulus to 250 to 400 ksf at an approximate elevation of 180 feet msl to 150 feet msl, and then a gradual increase to a value of 1,500 to 1,700 ksf at an approximate elevation of 80 feet msl to 50 feet msl. Below these elevations, the results are somewhat scattered (Ref. 35).

3.4.3.4.3.5 <u>Piezometer Installations</u>

Twenty-three piezometers were installed at the locations shown in Figure 3.4-4. Piezometers BH 3, BH 4, BH 6, BH 6B, and BH 15 were, in general, installed by casing the drilled boring with 4-inch diameter steel casing, cleaning the cased borehole, installing a slotted polyvinyl chloride (PVC) pipe and PVC riser pipe in the boring to the desired depth, and simultaneously removing the 4 inches-diameter casing while placing the gravel packing, sand, and bentonite balls. Following placement of the bentonite balls, grout (two parts sand and one part cement) was pumped into the casing, and the casing was retrieved.

Piezometers BH 17A, BH 21A, BH 23A, BH 48B, BH 50A, BH 62A, BH 75A, BH 82, and BH 98A were installed by advancing the uncased borings to the desired zone, installing a slotted PVC well point and PVC riser pipe in the boring, and placing the gravel pack, sand, and bentonite-ball seal in the annular space between the wall of the boring and the PVC standpipe. Following placement of the bentonite-ball seal, grout was pumped into the annular space from the top of the bentonite-ball seal to the ground surface.

Piezometers at borings BH 2, BH 8, BH 9, BH 13, BH 20, BH 20, BH 64A, BH 69A, and BH 86 were installed using an alternate procedure, which was adopted because of problems encountered in retrieving 4-inches-diameter casing from the borings at depths greater than 200 feet. In general, the alternate procedure consisted of placing a 4 inches (outside diameter) PVC pipe (with the bottom end sealed with a pipe cap) in the uncased boring, grouting and annulus between the PVC pipe and boring wall, allowing the grout to set, drilling through the PVC seal, and installing the piezometer components as described above. Sensitivity testing was performed on all piezometers after the piezometric heads had stabilized. Results of these tests indicated that all piezometers responded to applied changes in piezometric heads and thus were properly installed.

3.4.3.4.3.6 Seismic Surveys

A seismic reflection survey was conducted at the DWPF site to provide contours of bedrock surface and other significant reflecting horizons and also to determine the presence and extent of any subsurface faulting. Seismic line coverage of the site included the areas where Category I buildings were to be constructed and additional lines to tie in with an existing survey conducted prior to the DWPF site investigation. The seismic reflection survey is described below.

Seismic Reflection Survey

A seismic reflection survey was conducted at the DWPF site to determine the configuration of the crystalline bedrock surface and overlying sediments and to delineate any faulting (Ref. 35).

A plan view of seismic coverage over the site area is presented in Figure 3.4-39. Lines S-1, S-2, and S-3 run site north-south, and lines S-4, S-5, S-6, and S-7 run site east-west and tie the north-south lines together. Lines S-1 and S-6 intersect at the Vitrification Building. In addition, line S-4 extends to the west across Road 4 to intersect line S-8. Line S-8 (Figure 3.4-40) parallels Road 4 and intersects existing seismic coverage near deep rock boring 7 (DRB 7). Total linear coverage is approximately 27,000 feet.

In general, three reflecting horizons of good to excellent quality have been mapped across and tied into all seismic lines (Ref. 35):

- Yellow horizon corresponding to the crystalline bedrock surface or to the unweathered crystalline rock surface, ranging in time from 210 to 250 milliseconds (ms) or in elevations from -680 to -800 feet (msl).
- Blue horizon corresponding to a Cretaceous sedimentary interface above the bedrock surface and ranging in time from 170 to 190 ms or in elevation from -560 to -620 feet(msl). Further identification cannot be made due to a lack of boring control.
- Red horizon corresponding to an Upper Cretaceous sedimentary interface above the blue horizon and ranging in time from 130 to 150 ms or in elevation from -440 to -500 feet(msl). Further identification would require additional boring control.

The site is characterized by an southeast dipping crystalline bedrock surface or unweathered bedrock surface with ranges in elevation from -680 to -800 feet(msl). Reverse faulting of the bedrock surface occurs in three places, as documented in Reference 35.

Cross-Hole Seismic Survey

A cross-hole seismic survey was conducted at the DWPF to determine in situ seismic compressional (P) and shear (S) wave velocities in the subsurface. This survey provides detailed seismic velocity information at close vertical intervals of 5 feet from the surface to a depth of 300 feet. Cross-hole surveys were conducted in borings BH 38, BH 63, BH 86, and

BH 90. Boring BH 86 lies under the Glass Waste Storage Building #1, and boring BH 90 lies under the Vitrification Building.

The P- and S-wave velocities were used to determine the elastic parameters of the site subsurface materials, which is essential for evaluating structure and foundation behavior under seismic excitation.

Wave velocities and a stratigraphic log for borings BH 38, BH 63, BH 86, and BH 90 are shown in Reference 35. A review of this data revealed that the trends in both P-wave and S-wave velocities were statistically similar among the four test locations.

In order to characterize the subsurface in terms of S-wave velocities, all of the data from the four locations were evaluated together. Trends in S-wave velocity versus elevation were defined by linear regression analyses. Based on this analysis, the subsurface was divided into eight layers, with a representative shear wave velocity for each layer. The relationship of the typical subsurface profile to S-wave velocities is shown in Figure 3.4-41. At shallow depths, where the S-wave velocities vary significantly and where the impact of shear moduli values is most important for design, layer thicknesses were small (10 to 15 feet). At deeper elevations, larger layer thicknesses (25 to 105 feet) were used to characterize the S-wave velocities.

P-wave velocities showed marked increases to values in the range of 5,000 to 6,000 feet/sec at approximately elevations 235 feet msl to 245 feet msl. This increase indicates the approximate elevation of the groundwater level. An increase in material stiffness, represented by the increase in S-wave velocity at a depth of approximately 130 feet, (elevation 160 feet msl) corresponds to the much denser material found near the top of the Congaree Formation.

Down-Hole Seismic Survey

As a supplement to the cross-hole survey a down-hole survey was performed at the site. This work was done to determine if significant vertical anisotropy exists in the elastic properties of the materials at the test locations. The survey was performed at the same boring locations as the cross-hole survey: BH 38, BH 63, BH 86, and BH 90.

The geometry of the down-hole test results in a practically vertical travel path from the impact source to the down-hole geophone (Ref. 35). Average shear wave velocities are determined for the path between the source and the receiver by accurately measuring shear wave transit times.

The down-hole technique is limited to sampling the volume of material in the immediate vicinity of the borehole; but, due to the nature of the vertical travel path, it is insensitive to refraction effects and therefore can delineate thin, low-velocity layers. Also, measurement of velocity in a vertical sense of propagation supplies a field measure of vertical to horizontal anisotropy when compared with results of the cross-hole test at the same elevation. However, the depth of investigation of the down-hole technique is limited, because of the ever-increasing separation of the seismic source (generally a sledge hammer blow to a mass in contact with the ground) and the down-hole geophone.

Data obtained from BH 96 were not as high quality as data from the other test locations. Interpretation of the data was difficult and yielded inconsistent results thus, these data are not presented.

Measured S-wave velocities using the down-hole technique are in close agreement with the values obtained using the cross-hole technique (Ref. 35). This implies that, for small strains, no significant vertical anisotropy exists in the vicinity of borings BH 38, BH 63, and BH 90. Note that the down-hole S-wave velocities have been three-point averaged to remove the inherent data scatter of interval measurements. The amplitude of the P-waves was too small to give repeatable results, so no P-wave data are presented. S-wave data were obtained to a depth of 60 feet. Below this depth, the S-wave amplitude became too small to allow determination of wave arrivals.

3.4.3.4.3.7 Geophysical Borehole Logging

Geophysical borehole logging was performed immediately following completion of coring. Four types of logs were obtained: natural gamma radiation, spontaneous potential, single-point resistance, and caliper. Caliper logs were not obtained in every boring logged. The geophysical logs are extremely sensitive to subsurface lithology, and the data obtained have been used in conjunction with the boring logs to provide a more accurate engineering and lithological definition of the subsurface stratigraphy. The geophysical logs are documented in Reference 35.

3.4.3.4.4 PROPERTIES OF UNDERLYING MATERIALS

3.4.3.4.4.1 Soil Stratigraphy

Soils at DWPF consist of coastal plain sediments that are about 900 feet thick. These sediments range in age from late Cretaceous (about 65 million years ago) to Holocene. The Coastal Plain sediments are predominantly clastic and overlie a sequence of folded and faulted metamorphic rocks of Precambrian/Paleozoic age (up to 570 million years old) (Ref. 35). The sedimentary sequence at DWPF consists mainly of interbedded, clayey sand, sand, silt, and silty clay with some thin carbonate units. The structural properties of the various distinguishable lithologic horizons are discussed in terms of *stratum* that are delineated by elevation, thickness and unique characteristics (physical, chemical and mineralogical composition).

Five shallow, geologic formations were identified by the initial seismic and geophysical surveys performed at DWPF (Ref. 35). These formations were drilled and sampled during subsequent foundation explorations. In descending order, they are: Hawthorne, Barnwell, McBean, Congaree, and Ellenton Formations. New nomenclature has evolved for the various strata and are presented in Figure 3.4-42. Table 3.4-5 illustrates the relative positions of these strata at the DWPF site. The strata of major concern in foundation design for the proposed structures are the sand and clay layers within the “Upland Unit,” the Barnwell Group, and the Santee Limestone. The stresses imposed by the DWPF structures are relatively insignificant at depths greater than 150 feet below ground surface (bgs), the approximate depth of the base

of the Santee Formation. The consistently high penetration resistances encountered in the underlying Congaree and Black Mingo strata indicate these are incompressible for practical purposes.

Strata above elevation 110 feet msl, which extend to depths approximately 170 feet bgs, have been grouped into nine general strata based on SPT testing, as presented in the cross sections. The locations of Category I foundations are shown in the cross sections. The stratification shown on these sections is intended to depict relative depths and thicknesses of the general strata and is not an attempt to define actual interbedding, which is undoubtedly more complex. The change from one stratum to another is also more gradual than shown on the sections. Figure 3.4-43 defines terminology used for the stratum descriptions. The term "compact" is synonymous with the term "dense" used elsewhere in Subsection 3.4.3.5. These terms are accepted engineering designations used to describe the relative compactness of granular, nonplastic unconsolidated sediments and soils. The general strata are summarized below in the typical order of sequence with depth.

Stratum S1--Clayey Sand: Medium compact to compact red-brown and yellow clayey fine to coarse sand, trace gravel, to fine to coarse sand, some clay; occasionally interbedded with sandy clay and sandy silt. Stratum S1 extends from the ground surface to depths of 20 to 45 feet bgs (260 feet msl to 235 feet msl). Organic silt lenses exist at the ground surface and are up to 2 feet thick in topographic depressions such as encountered in boring 65. The clay content of the stratum appears to decrease below depths of approximately 20 feet bgs (260 feet msl). SPT values typically range from 10 to 50 blows/feet averaging approximately 20 blows/feet. Occasional SPT values less than 10 blows/feet were measured in the upper 5 feet. SPT values greater than 50 blows/feet were occasionally measured throughout the deposit; these high blowcounts are probably indicative of the presence of gravel. Natural water contents typically vary from 15 to 25%.

Stratum S2a--Sand, Trace Silt: Medium compact to compact brown, red, and yellow fine to medium sand with trace silt and gravel, occasional clay lenses. Layers of this predominantly clean sand were found underlying and interbedded within the clayey sand of stratum S1. Below stratum S1, between elevations 200 feet msl and 240 feet msl, continuous layers of clean sand vary from 5 to 35 feet thick; discontinuous interbedded layers of this stratum are typically 5 feet thick. SPT values range from 4 to 50 blows/feet but are typically on the order of 20 to 25 blows/feet. Approximately 5% of the SPT results recorded within this stratum are less than 10 blows/feet; however, no continuous loose layers were encountered. Natural water contents range from 11 to 26%, averaging approximately 22%.

Stratum C-2--Stiff Silty Clay: Stiff tan and white silty clay to clayey silt with trace fine sand. Stratum C-2 consists of discontinuous clay layers below strata S2a and S2b between elevations 200 feet msl and 210 feet msl. Within site limits, the deposit ranges from 2 to 10 feet thick; the range in thickness under Category I structures is approximately 2 to 5 feet. SPT values vary from 9 to 27 blows/feet. Natural water contents average 53%.

Stratum S3a--Sand, Some Clay: Medium compact to very compact brown and yellow fine to medium sand, some clay, trace calcareous shell fragments; occasionally interbedded with silty

clay and sandy silt. The surface of stratum S3a is between elevations 195 feet msl and 215 feet msl. This 5- to 50-feet-thick deposit is interlayered with strata S3b and S3c. In Dry Branch Formation, stratum S3a is medium compact to compact with SPT values from 10 to 40 blows/feet. Natural water contents of the upper layers typically vary from 20 to 30%, averaging approximately 23%. In the Santee Formation, SPT values typically range from 10 to 60 blows/feet. Occasional penetration resistances as low as 2 blows/feet were recorded. However, samples with low blowcounts are isolated occurrences. Occasional interbedding with silty clay and sandy silt as well as traces of calcareous shell fragments occur within stratum S3a in the middle and lower portions of the Santee Formation. In borings 84 and 62P, four and six samples, respectively, reacted positively to dilute HCl, indicating the presence of calcium carbonate. Natural water contents in the middle and lower portions of the formation range from 25 to 35% with an average of approximately 30%.

Stratum S3b--Sand, Trace Clay, and Silt: Medium compact to very compact brown and yellow fine to medium sand, trace clay and silt with trace interbedded sandy clay, clay, and silt. Relatively clean sands of stratum S3b are interlayered with the strata S3a and S3c. Layer thicknesses vary from 5 to 40 feet; the thickest layers appear to be near the top of the Santee Formation. SPT values typically vary from 15 to greater than 100 blows/feet, averaging approximately 35 blows/feet. Isolated instances of SPT values less than 10 blows/feet occur; however, continuous layers of loose material do not appear to be present. Natural water contents range from 20 to 30% with an average of approximately 25%.

Stratum S3c--Sand, Some Silt: Compact yellow-brown sand with some silt, trace clay. Stratum S3c occurs in lenses 5 to 10 feet thick. SPT values vary from 12 to 110 blows/feet, averaging approximately 40 blows/feet. Natural water contents range from 22 to 28% and average 25%.

Stratum M1--Silt: Compact to very compact gray and tan silt with trace fine sand and clay. Stratum M1 was encountered from elevations 130 feet msl to 140 feet msl. This deposit is discontinuous and appears in lenses 5 to 10 feet thick. SPT values vary from 20 to 40 blowcounts/feet with an average of 35 blows/feet. Natural water contents range from 25 to 40% with an average of approximately 30%.

Stratum S4--Sand: Very compact brown and yellow silty fine to medium sand, to fine to medium sand, trace silt. The surface of stratum S4 was encountered from elevations 125 feet msl to 135 feet msl. The stratum is approximately 100 feet thick. SPT values vary from 40 to greater than 100 blows/feet with an average of greater than 100 blows/feet. Natural water contents range from 18 to 30% with an average of approximately 25%. Stratum S4 corresponds to the Congaree Formation.

3.4.3.4.4.2 Borehole Grouting

A review of the results of the exploratory boring program indicates that some possible voids of limited lateral extent may exist between elevations 130 feet msl and 180 feet msl. This zone occurs primarily in strata S3a, S3b, S3c, with minor amounts in M1 and S4. The zone of possible voids was disclosed in the borings by grout “takes” larger than the theoretical

borehole volumes, low resistance to penetration of the sampling tools, loss of drilling mud, and positive reaction of some samples upon application of dilute HCl.

Tables 3.4-6 and 3.4-7 summarize the borehole grouting data. Table 3.4-6 includes the grouted depth, the theoretical borehole volume, number of bags of cement used to grout the borehole, the calculated grout take, and the grout take ratio. The calculated grout take was determined assuming one bag of cement yielded 2.12 cubic feet of grout. This average grout yield per cement bag was confirmed by Girdler Exploration and Foundation, Inc. Grout take ratios greater than six indicate the presence of voids or leached zones, grout take ratios between three and six suggest the possible presence of thin zones of leached materials, and grout take ratios up to three can be attributed to boring diameters enlarged during the drilling process and wasted grout due to surface overflow. Table 3.4-7 summarizes the additional indications of voids including rod drops, loose zones noted during drilling, low sat blowcounts, loss of drilling fluid, positive reaction to dilute HCl, and references to calcareous materials on field logs.

Because the Vitrification Building imposes a large net area load on its supporting earth materials, as do the other Category I structures to a lesser extent, there may be some compression of the substrata resulting in differential building settlement at some time during the facility's useful life. Because limited zones of void, and/or soft soil were encountered underneath the Category I structures, a grouting program was completed (Ref. 33). See Section 3.4.3.4.9.

Boreholes with greater grout takes occurred at the northeast end of the site in the vicinity of the road intersection north of the Service Building. Because this area was generally outside the development, a foundation grouting program was not required.

3.4.3.4.4.3 Laboratory Tests

Introduction

Laboratory testing of disturbed and undisturbed samples included the establishment of index properties, i.e., water content, grain-size analysis and classification, Atterberg limits, specific gravity, and unit weight. Static testing of undisturbed samples included consolidation testing of cohesive sediment and soils, one-dimensional compression testing of cohesionless materials, and consolidated-undrained triaxial tests with pore pressure measurements. One-dimensional compression testing of compacted sandy materials from the “Upland unit” and Tobacco Road sand was also conducted to characterize the compressibility of potential compacted backfill. Static test data have been used to establish the material properties relevant to the analysis of foundation bearing capacity and the short-term and long-term stability of excavations. Consolidation and one-dimensional compression test data have been used in foundation settlement analyses.

Dynamic testing of undisturbed samples include resonant column tests on cohesionless and cohesive material and both cyclic triaxial and cyclic torsional tests on sand samples. Resonant column tests were also conducted on compacted Barnwell Group material. The

resonant column test data were used to determine the shear modulus and the material damping ratio as functions of the shear strain. This information was subsequently used with the results of the cross-hole tests to describe the elastic properties of the building substrata under postulated seismic excitation. Cyclic triaxial and cyclic torsional test data were used to calculate the liquefaction potential for cohesionless materials.

Standard and modified Proctor compaction tests were conducted using sample trimmings. Sampled material originating from depths of 10 to 70 feet below grade surface were blended and tested to provide data for establishing backfill compaction control criteria. A summary of the static and dynamic testing is presented in Table 3.4-8.

A summary of the individual static and dynamic testing is given below.

Index Properties and Classification

The natural water content (ASTM D2216) was determined for all split-barrel samples, and each undisturbed sample was subjected to testing. These data, together with the Atterberg limits, provide a qualitative measure of the consistency of subsurface strata. Natural water content data for the disturbed samples are presented graphically on the boring logs, while water contents for undisturbed samples are presented with the specific test results (Ref. 35).

Grain-size analyses were conducted on both disturbed and undisturbed samples. These tests were performed in accordance with ASTM D422, and the results are shown in Reference 35. The results are grouped by geologic formation. One hundred twelve grain-size analyses were conducted on which 30 included a determination of the minus 200 sieve size distribution using the hydrometer method. This number does not include 12 grain-size analyses conducted for resonant column and one-dimensional compression testing of compacted soil samples. These grain-size analyses are presented in Reference 35. Additional analyses (not shown) were conducted using ASTM D1140 to ascertain the percentage of fines passing a No. 200 sieve for classification by the Unified Soil Classification System (USCS).

The liquid and plastic limits (ASTM D423 and D424), together with the resulting plasticity index, were determined for selected cohesive samples. Fifty-five tests were conducted on samples taken from 29 different borings to determine the Atterberg limits and classification of cohesive materials. These data are grouped by boring and geologic formation. Field determinations of formations for these figures may not be entirely consistent with the stratigraphic picks used in Subsection 3.4.3.5. The plasticity charts are shown in Reference 35. The tested samples display a wide range of plasticity characteristics. In general, the plasticity index is less than 50% while the liquid limit, with four exceptions, is less than 80%.

Specific gravity tests were conducted on 25 samples from 10 borings. The specific gravities ranged from 2.64 to 2.82. On the basis of these data, a representative value of 2.70 may be used for all samples.

Average unit weights (Table 3.4-9) were estimated for each stratum to the bottom of the Santee Formation on the basis of the laboratory classification data.

Available extruded sections of 39 undisturbed samples retrieved from boring 24 by D'Appolonia, were reviewed in 1983 by MRJD (Mueser, Rutledge, Johnston, and DeSimone Consulting Engineers). The undisturbed samples were recovered in June 1981 and subsequently extruded in the laboratory. After selection of specific samples for testing, the remaining extruded sections were wrapped in cloth and sealed with paraffin. Although these samples were dry when reviewed in 1983, they were suitable for visual classification and index tests.

Individual sample descriptions, unified soil classifications, and sample elevations, as well as the profile of boring 24 from cross section C-C (Figure 3.4-32), are shown in Reference 35. Reviewed portions of the samples are noted on the profile. Eight Atterberg limits tests and nine gradation analyses were performed on representative samples. The results of these tests are shown in Reference 35. Dilute HCl was applied to all samples during our review; no reactions were observed.

The variable USCS types of the upper 70 feet below ground surface as shown in the cross sections demonstrate that this system of sample description is not generally useful for subsurface mapping of geologic strata. Stratigraphic cross sections are given in Figures 3.4-19 through 3.4-28 (D'Appolonia) and Figures 3.4-30 through 3.4-34 (Mueser). Samples 1S through 5S, between elevations 275 feet msl and 265 feet msl, consist of clayey sand with layers of sandy clay less than 1 feet thick, while samples 6S and 14S consist of sand with a trace clay. Occasional layers of red silty clay less than 0.5 inches thick, pockets of brown clay less than 0.25 in thick, and partings of gray fine sandy clay less than 0.06 inches thick were also observed in the stratum S1 samples from the upper 30 feet of the soil profile.

The reviewed samples from strata S2a and S2b, between elevations 210 feet msl and 240 feet msl, are fine to medium sand with some to trace silt. Although these strata appear to be less complexly interbedded than stratum S1, trace partings and pockets of white fine sand with some clay were observed in all samples within strata S2a and S2b.

A section from sample 36S was the only available material from stratum C2. This sample is interbedded silty clay and clayey fine sand. The plasticity indices of the silty clay are high, as discussed in Reference 35.

The reviewed samples retrieved from elevations 130 feet msl to 200 feet msl demonstrate that the Santee Limestone includes more sand layers and fewer clay layers than the overlying strata.

Samples 11P through 13P of the Congaree Formation consist of silty fine sand to sand, some silt. The upper samples within stratum S4 are fairly consistent with little or no interbedding.

Static Triaxial Tests

Consolidated-undrained (CU) triaxial tests with pore pressure measurements were conducted to determine the effective shear strength parameters and moduli of selected undisturbed samples. The results of the 18 CU triaxial test series are summarized in Table 3.4-10 and are

presented in detail in Reference 35. The tested samples are from the generalized layers within approximately 150 feet of ground surface at the site.

The strength properties of the upper clayey sand and sand, trace clay or silt were determined from static triaxial tests on eight samples from the depths between 17 and 42 feet bgs (263 feet msl to 238 feet msl) (Table 3.4-10). An average effective friction angle of 34° with no cohesion is representative of these medium compact to compact materials.

The strength properties for the undifferentiated silty clay to clayey silt layer separating the Barnwell Group and Santee Formation occurring between elevations 200 feet msl and 210 feet msl were determined from tests on ST-5 from boring 3. The results indicate an effective friction angle of 34° with no cohesion. However, occasional low SPT blowcounts and consolidation test results indicate some weaker zones may occur within this layer. Therefore, a conservative effective friction angle of 31° with no cohesion is appropriate for use in static bearing capacity analyses.

Two series of triaxial tests were performed on a blend of sand and some clay from samples retrieved from boring 24, representing typical backfill at the site. Prior to testing, samples were compacted to 95 and 100% of maximum modified Proctor dry density; test results indicate effective friction angles of 35° and 40°, respectively. These test results are presented in Reference 35 and summarized in Table 3.4-9. Based on these tests, an effective friction angle of 34° is indicated for use in static analyses for typical site backfill compacted to 95% of modified Proctor maximum density.

Consolidation Tests

A total of 42 consolidation tests (ASTM D2435-70) were performed on 39 undisturbed samples recovered from 13 borings. Individual plots of the void ratio versus log pressure curves are shown in Reference 35.

Results of consolidation tests on undisturbed samples recovered during six previous subsurface investigations at H-Area were reviewed and correlated with the S-Area data. The six projects (Figure 3.4-16) are 1,000 to 3,000 feet southwest of the edge of S-Area in H-Area. Void ratio versus log pressure curves for H-Area and S-Area consolidation tests are grouped and discussed in Reference 35. The grouping was based on the Unified Soil Classification System, water content, initial void ratio, and general shape of the void ratio versus log of pressure curve.

An S-Area consolidation test summary for samples recovered from the “Upland unit” and Barnwell Group and Santee Formations is presented in Table 3.4-11. Preconsolidation pressures, compression, and recompression indices were determined using the Casagrande method. Consolidation tests were performed on three basic USCS types: clayey sands, clean sands (sand, trace clay, or silt), and silty clays.

Consolidation curves for plastic materials exhibit a characteristic break in slope at the maximum past pressure (preconsolidation stress). Predominantly nonplastic sandy materials

do not exhibit a similar break in slope. Therefore, preconsolidation stress was estimated only for the plastic soils.

All S-Area consolidation tests were rebounded at a test pressure approximately equal to existing overburden stresses. The average slope of the rebounding and reloading cycle for each test is termed the swelling index (Cs), which is used to estimate settlements at stresses less than the preconsolidation value. Average Cs values and initial void ratios for each stratum to the bottom of the Santee Formation are shown in Table 3.4-9.

The material properties profile for H-Area with the S-Area consolidation test data on plastic material superimposed is presented in Reference 35. The typical S-Area soil, as well as the average existing overburden stress and proposed increase in stresses below the center of the Vitrification Building, are also shown.

The general USCS profiles in H-Area and S-Area are similar. Ground surface elevations in H-Area are somewhat higher, varying between elevations 295 feet msl and 325 feet msl. Where general site fill is not present in H-Area, the uppermost layer, probably of the "Upland unit," consists of still silty and sandy clay with layers of clayey sand. Beneath the clay stratum, interbedded sands, clayey sands, and sandy clays extend down to between approximately elevations 180 feet msl and 190 feet msl and are the Tobacco Road Formation. In four of the H-Area projects, at approximately elevation 190 feet msl, a highly plastic clay layer was found underlying the Tobacco Road sands. While the surface of this lower clay layer is approximately 20 feet lower in H-Area than in S-Area, the soil index characteristics are similar. Where present in H-Area, the clay stratum is 5 to 30 feet thick. Beneath the clay, clayey sands of the Dry Branch Formation were sampled.

Consolidation tests performed for H-Area investigations on clays and clayey sands recovered above elevation 190 feet msl from both the "Upland unit" and Barnwell Group generally showed preconsolidation pressures of 3 to 9 tsf above existing overburden pressures. Water contents of the materials above 190 feet msl generally varied between 20 and 30%. Below elevation 190 feet msl, in stratum C2 and the lower Santee clayey sands, occasional zones of low penetration resistances were encountered. Consolidation tests on undisturbed samples recovered from these zones indicated preconsolidation pressures close to existing overburden stresses. Tests on clayey samples below elevation 190 feet msl, and not within low penetration zones, indicated preconsolidation pressures of 3 to 7 tsf greater than existing overburden pressures. Natural water contents of plastic samples below elevation 190 feet msl generally ranged from 30 to 80%. Triaxial shear tests performed on samples from zones of low penetration resistance showed lower strengths than tests performed on the overconsolidated materials.

All of the H-Area samples exhibiting low preconsolidation pressures and shear strengths were recovered below the Tobacco Road in stratum C2 and the underlying Dry Branch clayey sands. Occasional sandy split spoon samples from the Santee reacted with a weak HCl solution, indicating the presence of calcareous materials that may be subject to leaching. None of the clayey materials exhibiting low preconsolidation stresses reacted with the acid. It is believed that calcareous material may have existed within stratum C2; however, this

material may have been leached by the downward flow of groundwater. This loss of material has increased the void space within stratum C2 and reduced its ability to support vertical load, thereby lowering the apparent preconsolidation stress. The zones are characterized by low preconsolidation and shear strength generally found as pockets rather than as continuous layers.

Most of the S-Area tests on clays, like the H-Area tests, exhibited preconsolidation stresses well in excess of the existing overburden. Two tests, however, indicate the possibility that portions of stratum C2 do not exhibit significant preconsolidation. One of these tests (sample ST-6 of boring 10) had a high seating load of 3.5 tsf. Interpretation of this test indicates the preconsolidation stress is not greater than 3.7 tsf, which is slightly less than the existing overburden pressure at that boring. Interpretation of the second test (sample ST-5 of boring 47) indicates a preconsolidation pressure of 4.5 tsf, which is approximately 0.5 tsf greater than the overburden pressure.

The results of tests performed on stratum C2 samples from S-Area are similar to results of tests on plastic clays encountered at slightly lower elevations in H-Area.

Compaction Tests

To determine the optimum water content and maximum dry densities for the materials that were ultimately be used as compacted backfill, one standard Proctor (ASTM D698) and 12 modified Proctor (ASTM D1557) tests were conducted on nine combined samples and three undisturbed samples. These samples, consisting primarily of silty to clayey, fine to medium sands, were prepared by combining trimmings from undisturbed samples, from combinations of undisturbed samples, or from previously tested undisturbed samples. The combined samples were constructed by blending materials from several depths between 10 and 68 feet and typifying those "Upland unit" and Tobacco Road Formation materials proposed for use as compacted backfill. The results of the Proctor tests and the grain-size distributions for the combined materials are shown in Reference 35. In general, the optimum water content ranges from 10 to 12% for modified compaction and is about 12% for standard Proctor. The maximum dry densities range from approximately 118 pcf for the standard Proctor effort to a maximum of 128 pcf for the modified Proctor. With the exception of one test, all of the moisture-density relationships fall between dry densities of 118 and 128 pcf. The single instance of a much different relationship (BH 24, blend 6) was for a clean, medium-fine sand. One standard Proctor test was conducted and resulted in a maximum dry density of 118 pcf (Ref. 35).

A total of eight consolidation tests were performed on six material blends and two combined samples compacted from 93 to 100% of maximum dry density. Individual void ratio versus log pressure curves for these tests are presented in Reference 35. From a comparison of initial and final water contents, it appears that the samples were wetted as initial loads were applied.

Since backfill used in S-Area is similar to backfill previously placed in H-Area, the S-Area test results on compacted fill were compared with the previous results from H-Area. Atterberg limits and mechanical analyses were performed on over 20 samples of clayey fine

to medium sand fill in H-Area. The properties of a typical sample from a former spoil pile were 38% passing the No. 200 sieve, liquid limit of 56, and plasticity index of 34. Index properties are plotted in Reference 20 for comparison with S-Area materials. A modified Proctor compaction test on the H-Area spoil pile samples resulted in a maximum dry density of 121 pcf and optimum water content of 13% (Ref. 35). The shape of the compaction curve is similar to S-Area test results at similar fines content.

A total of 23 consolidation tests were performed on H-Area samples of fill material compacted in the laboratory to densities ranging from approximately 90 to 120 pcf. Generalized consolidation curves developed from these 23 tests are presented in Reference 35 together with S-Area tests. Results of H-Area samples tested at their natural water content are shown as solid lines; the effects of wetting are shown as dashed lines. Curves are presented for dry densities of 110, 115, and 120 pcf, representing 91, 95, and 99% of maximum dry density, respectively. The vertical distance between H-Area curves from tests at natural water content and the wetted condition for equivalent densities represents the volume change that occurs as the sample is allowed to saturate at a constant load. On the basis of the generalized consolidation curves, 95% of maximum dry density is required to prevent significant strain due to eventual saturation for the clayey sand fill.

The index test and compaction results for the clayey sand samples from H-Area and S-Area are similar. The maximum dry density, optimum moisture content, and shape of the compaction curve of the H-Area sample corresponds to the results of compaction tests on the S-Area blends with more than 16% fines. These similarities indicate that the data from H-Area can be applied directly to evaluate the characteristics of the potential clayey sand fill at S-Area.

Comparing consolidation curves of S-Area blends and generalized consolidation H-Area curves, it is evident that the S-Area data do not have the change in slope at increasing pressure shown by the H-Area data. The difference in curvature may occur because of the difference in the time of wetting test samples.

Generalized H-Area curves show that for a constant fines content of 38% the denser samples are less compressible. The S-Area blends represent a range of materials with respect to both fines content and density. The loading and subsequent saturation sequence used in the H-Area consolidation tests more closely follows field conditions than the immediate saturation procedure used in the S-Area tests. Also, the typical backfill in S-Area consists of clayey sands similar to the H-Area samples. Therefore, H-Area curve 2 (Ref. 35), which represents consolidation of a sample compacted to 95% of maximum dry density, is recommended for use in estimating settlements of shallow footings on compacted clayey fill.

Resonant Column Tests

Shear wave velocities derived from cross-hole measurements reflect the elastic response of material to small shear strains (~ 10^{-4}%). However, these strains are substantially smaller than strain levels experienced during an earthquake. Moreover, materials behave in a nonlinear manner under seismic loading. The shear modulus (G) decreases with increasing strain

amplitude (l) from the maximum shear modulus at small strain (G_{max}). G_{max} is measured at the relatively small strain levels associated with a cross-hole investigation. Also, as shear strain increases, the material damping (D) increases, reflecting the nonlinear hysteretic nature of unconsolidated materials responding to cyclic loading.

To obtain the strain-dependent characteristics of G and D, the resonant column test was performed in general accordance with a procedure developed (Ref. 38). Twenty-one resonant column tests were conducted on undisturbed, trimmed samples of sand having various densities and percentages of fine-grained constituents. In addition, three resonant column tests were conducted using sand samples compacted to near maximum dry density at optimum moisture content using a modified Proctor compaction effort. The samples tested, which were recovered between depths of 31.5 and 94.0 feet, are listed in Table 3.4-12. The test results in terms of shear modulus reduction (G/G_{max}) and damping versus shear strain are shown in Reference 35. Generally, three effective confining pressures (1, 2, and 4 kg/cm^2 or 2, 4, and 5 kg/cm^2) were used in testing each specimen. The compacted samples tested are also listed in Table 3.4-12, and the results are presented in Reference 35. Three effective confining pressures (0.70, 1.41, and 2.81 kg/cm^2) were used for BH 55, ST-1, and BH 90, ST-2.

The plots of (G/G_{max}) for undisturbed sands with some or no clay indicate that these materials tend to soften somewhat less for higher confining pressures (σ_c); however, this trend is not strong. Generally, in the range of σ_c between 1 and 5 kg/cm^2, G lies between 75 and 90% of G_{max} at peak to peak shear strain (γ) equal to 10^{-2}%. The material damping (D) is nearly independent of confining pressure and generally is less than 2% of the critical value over the approximate shear strain range of 5 x 10^{-5} to 5 x 10^{-3}%. For γ equal to 10^{-2}%, D is generally less than 3%.

The clayey sand recovered from boring BH 38 at depths near 73.5 and 94 feet exhibits somewhat less shear modulus reduction and greater damping as a function of shear strain and confining pressures than do the cleaner sands. At γ equal to 10^{-2}%, for example, G/G_{max} ranges from approximately 90 to 95% depending on the confining pressure. Also, at γ equal to 10^{-2}%, D ranges between 4 and 5%.

The plots of G/G_{max} for compacted sands show a more pronounced softening trend with increasing σ_c than was observed for the undisturbed sands. Generally, in the range of σ_c between 1 and 5 kg/cm^2, G lies between 80 and 95% of at γ equal to 10^{-3}%. Using a curve fitting procedure similar to that suggested (Ref. 39), values of G corresponding to strains at γ equal to 10^{-2}% were found to range from 45 to 75% of G_{max} . The compacted material exhibited an overall stiffer response than did the in situ material, as a substantially higher load was required to achieve comparable levels of γ. The material damping (D) is generally constant, at approximately 5%, for γ less than 10^{-4}% and for all confining pressures used during testing. For γ levels above 10^{-3}%, D increases and the influence of σ_c becomes more pronounced.

Cyclic Triaxial Tests on Sand

Liquefaction of saturated sand has been defined as the phenomenon by which the sand undergoes such a substantial reduction in shear strength due to a dynamic load. One of the widely accepted laboratory tests to investigate liquefaction is the constant volume cyclic triaxial test whereby a cyclic deviator stress (s_d) of equal magnitude in compression and tension is applied to a saturated sand specimen(undrained) under initial mean effective confining pressure (σ_o). The constant frequency-constant amplitude cyclic deviator stress is intended to simulate the stress conditions induced in the field.

A total of 19 cyclic triaxial tests were conducted on sand specimens trimmed from undisturbed samples. The samples were recovered from depths between 32 and 57 feet in borings BH 38, BH 47, BH 55, and BH 81. All samples tested were fine to medium sands, most of which possessed between 14 and 19% of material passing the No. 200 sieve. Four samples were classified as clean sands; these had 5 to 6% of fines and uniformity coefficients (Cu) ranging from 2.6 to 3.9. Total unit weights ranged from approximately 121 to 130 pcf, and water contents were between approximately 14 and 26%.

The borehole locations of undisturbed triaxial shear testing were selected and drilled when earlier DWPF configurations were under consideration. No new undisturbed sampling for triaxial shear testing was done after final site configuration. Thus no triaxial samples were obtained directly under the present location of Building 221-S. However, borehole 81 is in the immediate vicinity, and other undisturbed sampling (i.e., shelby tube) and boreholes (i.e., SPT and CPT) are located under the structure.

The cyclic triaxial test data are presented in Reference 35. For each sample, plots are presented for pore pressure (u) versus axial strain (e), stress ratio ($s_d/2s_o$) versus, and u versus time. These data are used to determine the relationship between the shear stress ratio and the number of cycles required to cause liquefaction (cyclic deformations equal to 5% peak to peak strain) for a given sample. These data are summarized in Subsection 3.4.3.4.8.

Cyclic Torsional Tests on Sand

Cyclic torsional tests were performed on hollow, thick-walled cylindrical samples subjected to a prescribed cyclic torsional shear stress.

The sample is a hollow cylinder having inside and outside diameters of 1.4 inches and 2.8 inches, respectively. The sample height varies linearly from 1.0 inches to 2.0 inches from inside to outside. This shape permits uniform shear strains to develop in the sample when it is subjected to a torsional rotation. The sample can be saturated under either an isotropic confining condition (i.e., horizontal confining stress [σ_h] equal to vertical stress [σ_v]) or an anisotropic condition (i.e., σ_h not equal to σ_v). During the test, the shear stress is applied independently from the normal stresses. In contrast to the cyclic triaxial stress conditions, the octahedral normal stress remains constant in the torsional simple shear test.

A total of five trimmed samples were tested. The results are shown in Reference 35. The results are summarized with the cyclic triaxial test results in Subsection 3.4.3.4.8.

In addition to the cyclic torsional testing of undisturbed material, a cyclic torsional test was also conducted to obtain data relative to the behavior of the compacted backfill materials. The test was performed using a representative laboratory compacted sample from boring BH 24 at depths between 40 and 50 feet (blend 4). The test was conducted at a mean effective normal stress equal to 1 kg/cm^2. The results of the cyclic torsional test at two shear strain levels are shown in Table 3.4-12, and they demonstrate the reduction of shear modulus with increasing strain. Also included in Table 3.4-12 are data obtained from a static triaxial compression test for a comparably prepared sample. The data from both tests are presented to demonstrate the amount and trend of shear modulus reduction that occurs at large shear strain levels (greater than 10^{-2}%).

3.4.3.4.5 EXCAVATION AND BACKFILL

Excavations up to 30 feet deep were required for establishing foundations of the Category I structures. Some non-Category I structures, such as the pump pits, required foundations at greater depths. Construction excavation slopes of one vertical to one horizontal (1:1) were used and maintained during construction. In the area where the fan house foundation was constructed with compacted fill adjacent to the deeper Sand Filter Building, the excavation slope was limited to approximately one vertical to x 1.5 horizontal to minimize the possibility of disturbance to the natural material. All foundations are constructed above the existing groundwater level, except for the DWPF low point pump pit and the Z-Area drain tank.

Up to 20 feet of compacted fill was placed during rough grading operations. The fill was obtained from onsite stockpiles or offsite sources of clayey sand similar to the materials in the upper 25 feet of S-Area. To minimize post-construction settlement, the compaction specification requirement as discussed in Subsection 3.4.3.4.7 for all fill placed, either during the rough grading or as structural backfill, was 95% of modified Proctor maximum dry density.

Natural site materials from ground surface level to a depth of 25 feet consisted primarily of fine to medium clayey sand and sand and some clay with typically greater than 20% fines. The water content of this fill material typically varied from 15 to 20%. Occasional sandy clay layers, 2 feet or thicker, were encountered in several borings.

Modified Proctor compaction tests (ASTM D1557, Method A) performed on S-Area clayey sands (Ref. 35) resulted in maximum densities ranging from 121 to 127 pcf, with associated optimum water contents ranging from 10 to 13%. The compaction curves are typically steeply sloping, indicating the density is highly sensitive to the moisture content. The highest water contents at which 95% of the maximum dry density (the required density) could be achieved ranged from 13 to 16%, up to 4% below natural water content of onsite materials. The water content of natural materials was adjusted during the construction fill operations to maintain it within ±3% of optimum to achieve the specified level of compaction. Where new

foundations for Category I structures are supported on backfill placed in local excavations, the backfill was restricted to a select material that could be readily compacted with smaller equipment.

The gradation requirement for clean granular select fill material was as follows:

Sieve Size	Percentage Passing by Weight
4 in.	100
No. 4	70 to 100
No. 40	0 to 70
No. 200	0 to 12*

* Based on percentage passing the No. sieve.

The fan house (292-S) is the only Category I structure supported on compacted fill which was placed after rough grading was completed. An open-cut excavation made for the adjacent Sand Filter Building (294-S) extended approximately 22 feet below rough grade. A one vertical to 1.5 horizontal (1:1.5) construction slope for the south side of the Sand Filter Building was made approximately 28 feet south of the fan house north wall. Therefore, the north wall was founded on select backfill compacted to 95% of modified Proctor maximum dry density.

3.4.3.4.6 GROUNDWATER CONDITIONS

Water-table elevations in the Barnwell Group in this region of SRS exhibit gradual fluctuations, as indicated by the piezometric levels shown in Figures 3.4-35 through 3.4-38. These levels are consistently at or below an elevation of 255 feet msl. Over a period of nearly 4 years, the Barnwell and the Santee piezometers exhibited gradual fluctuations of approximately 5 to 8 feet, with the peaks and troughs corresponding to periods of above- and below-average rainfall. The fluctuations in the Congaree and Ellenton Formations were smaller in magnitude, but had the same relations with respect to wet and dry periods. The highest extrapolated groundwater levels were at elevation 265 feet msl, which is approximately 15 feet below yard level of DWPF Category I buildings (Ref. 42).

Aquifer performance tests were conducted prior to construction using wells screened in the water-bearing sands of the Barnwell Group and the Santee Formation. These tests provided basic aquifer data required for design of dewatering systems. For the Barnwell Group, the transmissivity (T) was 3,140 gpd/feet; for the Santee Formation, the transmissivity was 660 gpd/feet. The permeability of the “tan clay” was approximately 8E-07 cm/sec for an assumed thickness of 10 feet.

Over the plant life, fluctuations in groundwater levels can be expected to occur as they have in the past. Runoff of rainwater will likely increase; therefore, a modest decline in groundwater levels could occur. Plant usage of groundwater will be approximately 170 gpm. This water will be withdrawn from Cretaceous sands and will have no significant effect on the aquifer (Subsections 3.4.2.2 and 3.4.3.5). In summary, construction of the DWPF plant will have no significant long-term effect on subsurface aquifers and their associated piezometric contours, gradients, or flow rates.

3.4.3.4.7 STATIC FOUNDATION BEHAVIOR

3.4.3.4.7.1 Bearing Capacity of Spread Footings

The ultimate bearing capacity of foundations was determined using the conventional Terzaghi method of analysis and material parameters based on the results of field and laboratory test data.

All facilities are supported on spread foundations are founded on either stratum S1 or compacted fill. The maximum allowable bearing capacity for both compacted fill and S1 materials is 3 tons/square feet (tsf). This bearing capacity is applicable for spread footings between 3 and 6 feet wide as well as for subgrades of roads and railroads. Footings less than 3 feet wide have reduced design bearing capacities equal to 1/3 x B x 3 tsf, where B is the footing width. Factors of safety against bearing capacity failure are at least 3.0.

3.4.3.4.7.2 Bearing Capacity of Mat Foundations

The mat foundations for the vitrification building, glass waste storage building #1, and sand filter building are founded 13 to 23 feet below final grade on stratum S1 materials consisting of medium compact to compact clayey sands. For these sandy materials, the ultimate bearing capacity of a mat is a function of the embedment depth, mat, and mat rigidity. Increasing any of these parameters increases the bearing capacity because a correspondingly larger material mass resists failure. The relative mat rigidity is a function of the mat thickness and the stiffness of the superstructure.

Allowable bearing capacities for foundations are summarized in Table 3.4-13. The bearing capacity of Category I structures were evaluated for two cases: Case 1 assumes that the structure acts as a completely rigid body, and Case 2 assumes an effective mat rigidity based on the mat thickness and column and wall spacings shown on preliminary structural drawings. In both cases, the allowable bearing capacities are based on a safety factor of 3.0 against ultimate shear failure and do not consider settlements.

For case 1, allowable bearing values are quite high at 17 to 20 tsf. In case 2, the relatively thin mat of the Sand Filter Building limits the allowable bearing capacity to 6 tsf. The allowable bearing values for the other structures increase with mat thickness from 10 tsf for the Glass Waste Storage Building #1 to 15 tsf for the Vitrification Building.

3.4.3.4.7.3 Material Parameters

Table 3.4-14 summarizes static design parameters used for undisturbed natural materials between the ground surface and foundation subgrade level, as well as parameters for compacted fill. For design purposes, the properties of natural soils and compacted fill are similar, except for a slightly higher fill unit weight. Because the fill and natural material parameters are similar, the design earth pressure coefficients, equivalent fluid pressures, and coefficient of vertical subgrade reaction are similar for both materials.

3.4.3.4.7.4 Settlement Analyses of Category I Structures

Static settlements for Category I structures were estimated using one-dimensional consolidation of the soil profile under applied loads (Ref. 28) and soil removal for the foundation excavation was considered as negative loading to determine the amount of post-excavation heave. The change in stress state due to structural loads, which was based on available preliminary drawings, was determined using a Boussinesq solution. A material property profile (Figures 3.4-44 through 3.4-47) representing average conditions was developed from geologic sections for each Category I structure. The average existing grade, post-rough-grading, and foundation excavation grade were based on the available rough-grading and structural plans. Average groundwater levels were assigned to each formation for computation of in situ effective stresses. Based on the available piezometric data, the average piezometric surfaces of the Barnwell Group, Santee Formation, and Congaree Formation are at elevations 245, 240, and 170 feet msl, respectively.

Material properties were assigned to each stratum based on an evaluation of the available S-Area laboratory test data and data from previous H-Area studies, since the subsurface conditions in H-Area are similar to those in S-Area. Table 3.4-9 lists the parameters used in the settlement analyses. Previous H-Area studies have established that clayey materials of the "Upland unit," the Barnwell Group, and the Santee Limestone are preconsolidated to stresses greater than those imposed by the DWPF structure. Settlement measurements of existing H-Area tank structures with foundation fill loads of the same order of magnitude (about 4,000 psf) as the DWPF foundation loads reasonably agree with the settlement estimates based on recompression of the soil profile. Therefore, recompression indices from S-Area tests have been used for analyses of all strata except stratum C2. Within Stratum C2, two of the six S-Area consolidation tests exhibited preconsolidation stresses less than or approximately equal to the existing effective overburden pressure. This indicated that virgin compression may have occurred within some portion of the silty clay layer. A conservative analysis was performed by assuming that one-half of the clay layer would experience virgin compression and the remaining one-half would experience recompression under the net stresses imposed by the structures.

The estimated total settlement for each Category I structure is the sum of the settlement and heave. Figure 3.4-48 shows the estimated heave and total settlements at several points within the glass waste storage building #1, sand filter, and fan house buildings. Figure 3.4-49 shows the estimated heave and total settlements at several points within the Vitrification Building.

The predicted post-construction settlement for the Vitrification Building ranged from 2.7 inches at the northwest corner to 4.7 inches at the center (Ref. 28). The anticipated maximum differential settlement was 2.0 inches over 40 feet. The total and differential settlements predicted for other Category I structures were somewhat less due to smaller stresses imposed by lighter structures. A construction and post-construction settlement monitoring program was conducted for the Vitrification Building at key foundation locations (Ref. 43). This program began in November 1984, the date of mat placement, and was terminated in April 1991 after it was determined that post-construction settlement had ceased. However, the program was re-activated in July, 1994. The cumulative total settlement through July, 1994 ranged from 2.6 to 2.9 inches in the northern section of the Vitrification Building, where the heaviest loads were applied, to 1.5 to 2.2 inches in the southern section (Ref. 31).

A summary of the foundation detail for each of the major structures is given below

- Glass Waste Storage Building #1 (250-S), (Figure 3.4-48)

  The Glass Waste Storage Building #1 is a mat-supported, reinforced-concrete box. The top of the vault area base slab is approximately at elevation 264.5 feet msl. The structure is bordered by the intake and exhaust stacks on the east and west sides, the latter also with tops of base slabs at elevation 264.5 feet msl. Wheel lanes for the shielded canister transporter (SCT) border the vault area on the north and south sides, with tops of base slabs at elevation 285.5 feet msl. Office and maintenance areas, with tops of base slabs at elevations 286.5 feet msl and 285 feet msl, respectively, are constructed adjacent to the south SCT wheel lane and the exhaust stack. The average stress release due to excavation in the vault and stack areas was about 1.5 tsf and the gross area load of the structure was estimated at 0.9 tsf. Therefore, the structure caused a net unloading of 0.6 tsf immediately below the base slab.

  The maximum estimated excavation heave at the center of the vault area was 0.7 inches, 0.3 inches in the exhaust stack area, and less than 0.2 inches in the SCT wheel lanes and maintenance and office areas. The estimated maximum total settlement of 0.6 inches was at the center of the exhaust stack and 0.3 inches at the center of the structure. At the sides, estimated foundation total settlements were 0.2 to 0.4 inches with the slightly greater settlement occurring beneath the raised canister transporter runway. The temporary loading caused by the loaded transporter were not to affect these estimates.

- Sand Filter Building (294-S), (Figure 3.4-48)

  The Sand Filter Building is a reinforced-concrete, mat-supported box. The top of base slab slopes downward to the north from elevation 259 feet msl to 257 feet msl. Adjacent rough grades averaged elevation 272 feet msl. The average excavation stress release was estimated at 1.1 tsf, while the average structural area dead load was estimated at 0.8 tsf. The structure caused a net unloading of 0.3 tsf at subgrade.

  The estimated maximum excavation heave of 0.7 inches was to occur at the center of the Sand Filter Building and the estimated heave at the sides and corner were 0.3 and

0.2 inches, respectively. Total estimated foundation settlements ranged from 0.4 inches at the center to 0.3 inches at the north inlet and south outlet tunnels to 0.2 inches beneath the corners. The maximum differential settlement was estimated at 0.2 inches over 100 feet.

- Fan House (292-S), (Figure 3.4-48)

  The fan house is a reinforced-concrete structure with the top of the base slab at elevation 276.5 feet msl. The average surrounding rough grades were at elevation 276 feet msl. All structural dead loads, with the exception of the isolated diesel generator pads, were supported on strip footings bearing at 3 tsf. The excavation stress release at subgrade averaged 0.1 tsf and the average building load was estimated at 1.2 tsf.

  The excavation heave was estimated as negligible due to the minor excavation stress release. The maximum estimated foundation settlement was 1.1 inches at the center of the interior strip footing. Estimated settlements at the sides varied from 0.7 to 0.9 inches and 0.6 inches at the center of the generator pads.

- Vitrification Building (221-S) (Figure 3.4-49)

  The Vitrification Building is supported by a 10-foot thick reinforced mat with the base slab top generally at elevation 280 feet msl and at elevation 270 feet msl in a depressed section near the north end of the structure (Figure 3.4-49). The existing ground surface averages elevation 276 feet msl. The average stress release due to excavation was 0.4 tsf at subgrade. Some of this release was due to rough grading, which removed up to 2 feet of material within the building limits. Placement of structural backfill to elevation 284 feet msl around the building was assumed to increase the surface loading adjacent to the structure from 0.85 tsf to 1.05 tsf.

  The estimated excavation heave varied from 0.7 inches at the center of the depressed section and 0.5 inches at the center of the structure to 0.2 inches at the northwest corner. Estimated foundation settlements ranged from a maximum of 4.4 inches at the center of the northern third of the building to a minimum of 2.0 inches at the southwest corner. The actual measured (1994) total settlements ranges from 1.5 to 2.9 inches. The maximum measured (1994) differential settlement along the long and short sides of the vitrification building are 1.1 and 0.5 inches, respectively. With the exception of the depressed section, differential settlements between the middle and sides range from 0.8 to 1.1 inches. The differential settlement between the center of the depressed area and the north side is 0.9 inches. The analysis assumed flexible foundations, but the stiffness of the mat foundation was to reduce the differential settlements. Actual measured and estimated settlements for this structure are shown in Figure 3.4-50 (see Ref. 31).

3.4.3.4.8 RESPONSE OF SOIL AND ROCK TO DYNAMIC LOADING

The seismicity of the site region is discussed in Subsection 3.4.3.2. Historical earthquake data are presented, as well as the criteria for establishing the design basis earthquake (DBE).

Subsurface field data and the results of laboratory testing are presented in Subsection 3.4.3.4.3. Dynamic material test data include results from cyclic triaxial, cyclic torsional, and resonant column tests. Subsection 3.4.3.5 includes descriptions and results of the seismic reflection survey and the cross-hole and down-hole seismic surveys.

These data have been used in the analysis of liquefaction and cyclic mobility potential below. To predict the response of foundations to dynamic loading related to either earthquakes, wind, or mechanical equipment, it is necessary to define the stiffness and damping parameters for the subgrade. Because these parameters vary with strain, it is also necessary to describe their strain dependence.

The results of cross-hole seismic surveys and resonant column tests on in situ materials have been used to establish a subgrade profile for the site that defines “low strain” shear moduli and the strain-dependent relationship for both moduli and damping ratios. In addition, results of resonant column tests on compacted samples were used to define dynamic parameters for these subsurface materials.

Figure 3.4-41 presents a simplified subgrade profile to a depth of about 300 feet and includes values of shear modulus for small strain (G_{max}) for each layer and representative values of total unit weight and Poisson's ratio. This profile was developed for use in the dynamic analysis of the seismic response of the subsurface materials and the structures.

The values of (G_{max}) are applicable to the free field condition (i.e., no influence from structural loads). Values of (G_{max}) at selected locations beneath the four Category I structures are summarized in Table 3.4-15. Between the foundations of these structures and elevation 260 feet msl, the distribution of the building weight in a horizontal plane results in a significant variation in (G_{max}) in the horizontal plane. An estimate of (G_{max}) for any point beneath the structure and above elevation 260 feet msl was made from the graph in Figure 3.4-51. The material profile shown in Figure 3.4-41 was used to evaluate the dynamic responses of the DWPF structures. The values of (G_{max}) for the in situ materials were modified to account for the confining stress imposed by the structure of interest.

Figure 3.4-51 shows the reduction in shear modulus (G/G_{max}) and the increase in damping (D) with increasing shear strain (g) for both in situ and compacted backfill materials. These curves were developed from resonant column tests for strains less than approximately 3×10^{-3}% and from cyclic torsional and static triaxial tests for larger strains. The laboratory data indicated that the relationship between G/G_{max} versus correlations of the in situ materials and the backfill materials was quite small. Hence, a single set of curves is used for both types. However, the difference in D versus for the two types was significant, and two curves are provided.

3.4.3.4.8.1 Liquefaction and Cyclic Mobility Potentials

Introduction

The DWPF site is underlain by thick sequences of variable silty and clayey sands interbedded with sandy and silty clays. The behavior of saturated sands subjected to the cyclic loading caused by earthquakes is an important issue in the siting and design of important facilities founded on such materials. For analyzing the potential effects of earthquake shaking, it is important to distinguish between two different phenomena; a liquefaction (flow failure) and cyclic mobility (Ref. 40, 44, 48).

Liquefaction

Liquefaction is a phenomenon wherein a mass of material loses most of its shear strength when subjected to undrained dynamic loading. In such a state, the soil flows like liquid until the shear stresses acting on the mass equal the reduced shear strength.

Liquefaction generally occurs in saturated sands but can also occur in very large masses of sand or silts that are dry and loose enough so that the air cannot escape from the voids fast enough to prevent undrained shear.

Liquefaction, as defined above, involves large unidirectional shear deformations; thus, one would expect the material to tend toward steady state of deformation during liquefaction failures. If the shear strength at the steady state is lower than the applied shear stress in the ground, then in principle, it is possible for liquefaction to occur. Conversely, if the steady-state shear strength is greater than the shear stress in the ground, then liquefaction cannot occur because the associated large, unidirectional deformations are not possible.

Cyclic Mobility

Cyclic mobility refers to the tendency of sand, even in a medium dense state, to exhibit significant shear strains when subjected to a strong vibratory disturbance. These cyclic shear strains are accompanied by changes in effective stress and/or void ratio, depending on the degree of saturation and drainage conditions.

During cyclic mobility of the soil, the softening is accompanied by high pore pressures, increasing cyclic deformation, and sometimes permanent deformations, but it does not lead to catastrophic loss in shear strength as with the case of liquefaction.

Thus, cyclic mobility represents a less severe phenomenon from liquefaction. This distinction is especially important with dense and very dense sand because liquefaction cannot occur for such materials, although, to a limited extent, cyclic mobility can occur.

Thus, for design purposes, the ability of a saturated sand to resist cyclic loading should be described by its potential to develop either liquefaction or cyclic mobility. An analysis of liquefaction and cyclic mobility was performed by (1) comparing the properties of the sand at DWPF site with actual sites that have exhibited some degree of liquefaction under seismic

excitation (Empirical Method) and (2) estimating the potential for liquefaction or cyclic mobility on the basis of computed static and earthquake stresses and results of undrained static and cyclic tests conducted in the laboratory (Analytical Method). Each is discussed in the following subsections.

3.4.3.4.8.2 Methods to Evaluate Liquefaction and Cyclic Mobility Potentials

Introduction

The methods used to evaluate the potential for liquefaction (flow failure)and cyclic mobility can be divided into two groups: empirical methods and analytical methods. Both methods of analysis have been applied to the materials at the DWPF site.

The use of several methods of analysis is necessary because no single method is considered completely reliable. Each method has certain inherent limitations as well as advantages and disadvantages when applied to a specific site. The conclusions from each approach must be examined with the results of the other methods to provide a more complete assessment of the potential for liquefaction or cyclic mobility.

The empirical methods relate the field performance of sand deposits in areas of known earthquakes to an in situ characteristic of the deposit. Field measurements of this in situ characteristic are then made at the new site to provide a basis for comparison with the observed performance at other sites. The data base associated with field observations of ground failures does not distinguish between occurrence of liquefaction versus cyclic mobility. Hence, the term ground failure will be used instead of liquefaction or cyclic mobility for analyses based on empirical methods.

Analytical methods to evaluate the potential for liquefaction or cyclic mobility are based on laboratory measurement of the static or dynamic properties of site-specific material samples. These properties are compared to the computed static stresses (liquefaction) of cyclic stresses or strains (cyclic mobility) imposed during the seismic event.

Empirical Method

Methods for evaluating the potential for seismically induced ground failure based on field data traditionally have centered on correlations between Standard Penetration Tests (SPT) and occurrences of ground failure.

The advantage of using these empirical methods to evaluate the potential for seismically induced ground failure is that the correlations are based on actual sites where an earthquake has occurred and the response of the subsurface materials has been observed. The primary limitation of these methods is that the correlations are based on SPTs and CPTs, which are relatively crude field index tests. Such tests cannot reflect correctly all the factors that influence the occurrence of seismically induced ground failure. Thus, there is a large area of uncertainty where both ground failure and no ground failure have been observed for sands with the same blowcounts (SPT) when subjected to similar earthquakes. An additional uncertainty in the empirical methods is that the data base associated with both the SPT and the

CPT correlations is based on observations of ground failure occurring in materials shallower than about 50 feet. At the DWPF site, consideration of ground failure is required to depths on the order of 80 feet.

The development of empirical correlations has been described previously by others (Ref. 57, 45). Recently, the database associated with SPT resistance was expanded (Ref. 47) and includes data provided by researchers in many countries, particularly those in the US., China, and Japan. Of particular interest are the data gathered following the Miyagiken-Oki earthquake in Japan in June 1978 (magnitude 7.4) (Ref. 48). In evaluating this data, Tokimatsu and Yoshimi grouped materials by D50 (the grain size at which 50% of the particles by weight are finer) into relatively clean sands (D50 >0.25 mm) and silty sands (D50 <0.10 mm). Based on this distinction, they demonstrated that silty sands were more resistant to ground failure than clean sands for the same blowcount. This distinction in defining clean versus silty sands is particularly relevant to the DWPF site, which is predominantly underlain by slightly silty or clayey sands to silty or clayey sands.

Seed and Idriss (Ref. 47), using a D50 of 0.15 mm rather than 0.10 mm to define the limit for silty sands and developed correlations for boundaries between seismically induced failures and nonfailures associated with each soil type. Subsequently, Tokimatsu and Yoshimi (Ref. 49) reanalyzed the same data on the basis of percentage of fines in the sand rather than D50. The soils were grouped into clean sands (<7% fines) and silty sands (10% fines). The importance of the fines content on ground failure potential was also investigated by Zhou (Ref. 50), who also concluded that ground failure potential was greatly influenced by the fines content. He developed correlations based on cone penetration resistance and fines content from field observations of seismically induced ground failures and nonfailures in China.

Applications of the above empirical methods based on SPTs and CPTs are presented later in this subsection.

Analytical Methods

The advantage of using analytical methods for liquefaction and cyclic mobility analyses is that the influence of specific factors on resistance to ground failure can be investigated using materials from the site. In particular, these two liquefaction phenomena can be evaluated independently. The primary limitations of analytical methods are the difficulty in obtaining representative undisturbed samples from the site and modeling earthquake conditions in the laboratory. Specific uncertainties involved in analytical methods are discussed in the following subsections.

Liquefaction

Liquefaction of loose (contractive) sands can occur when the driving shear stresses (building loads) are greater than the undrained steady-state shear strength of the sand deposit. The steady-state shear strength is the shear strength at large strains and corresponds to the condition of continuous deformation, with the shear stress needed to cause deformation at a given normal effective stresses remaining constant (Ref. 51).

For contractive sands, shear stresses can be applied under drained conditions (e.g., loads due to building construction) that are less than the peak, undrained shear strength of the sand but are greater than the undrained steady-state shear strength without any harmful consequences. However, under rapid loading, such as an earthquake, the material mass behaves in an undrained manner. As the resultant shear deformations occur, the available shear strength of the deposit tends to the undrained steady-state shear strength. If the driving shear stresses are greater than the undrained steady-state shear strength, liquefaction can occur. For level ground conditions liquefaction may result in a bearing capacity failure.

A dilative sand (a sand that is dense enough to increase in volume during drained shear or generate negative pore pressure during undrained shear) has an undrained steady-state shear strength that is greater than its drained shear strength. Hence, a dilative sand deposit that can support a building under static conditions may experience minor deformations during earthquake shaking, but when the earthquake motions cease, the deformations stop because the available undrained shear strength exceeds the applied shear stresses. Therefore, dense (dilative) sands are not subject to liquefaction like loose (contractive) sands.

The analysis for potential liquefaction involves two steps. First, the steady-state shear strength of the sand must be determined. If the sand is dilative, it will not experience a liquefaction. If the sand is contractive, liquefaction is possible if the driving stresses (building loads) are greater than the undrained steady-state shear strength of the deposit. The main uncertainty in this is the determination of the in situ steady-state shear strength of the as a function of in situ void ratio.

The analysis of liquefaction potential is presented later in this subsection.

Cyclic Mobility

The analytical method most commonly used to determine cyclic mobility is presented in Reference 33. This approach (stress method) compares the cyclic stresses required to cause cyclic mobility in laboratory undisturbed specimens to the estimated cyclic mobility in laboratory undisturbed specimens to the estimated cyclic stresses resulting from a dynamic load. The main uncertainty in this method relates to the differences between the in situ material and earthquake stresses and the laboratory test specimen and test procedures.

These differences include the following:

1. Sample disturbance
2. Boundary effects in the tests that lead to development of gross nonuniformities in the specimen
3. State of stress
4. Test system compliance
5. Multi-directional shaking
6. Number of equivalent stress cycles

The impact of each of these factors must be evaluated in order to interpret the laboratory data appropriately. However, given the present state-of-the-art, definitive assessment of these factors is not possible, and considerable judgment is required.

A second analytical method compares cyclic strains rather than stresses (Ref. 52). This approach (strain method) is based on the premise that for undrained cyclic loading of sand there is a predictable correlation between cyclic shear strain after a given number of cycles and excess pore water pressure and that there is a threshold shear strain below which no significant pore water pressure buildup can occur.

This method determines the predicted cyclic shear strain during an earthquake as a function of ground acceleration and material shear modulus (at the predicted cyclic strain level). This predicted shear strain level then is compared to a threshold shear strain below which no excess pore water pressure is generated; hence, no cyclic mobility can occur.

The above two analytical approaches are applied to the DWPF site later in this subsection.

3.4.3.4.8.3 Design Material Profile

Introduction

The design dynamic material profile based on the results of the subsurface exploration program and on laboratory tests, making use of all pertinent data, is shown on Figure 3.4-41. The groundwater elevation was established from piezometers installed during the site field exploration program. The field tests included classification and geophysical testing. Laboratory tests included classification and density determinations, resonant column tests, consolidated-undrained triaxial tests, cyclic triaxial tests, cyclic torsional tests, and membrane penetration tests. An accurate estimate of shear wave velocity as a function of depth was obtained from cross-hole geophysical measurements.

Disturbed samples (using a standard split-spoon barrel sampler) were recovered at several locations in the zones of interest. For these samples, SPT blowcount per foot of penetration was determined. Cone penetration testing was performed at locations adjacent to SPT borings.

Undisturbed samples were recovered using thin-walled tube samplers. These samples were used in the laboratory to measure the in situ density and to test the dynamic characteristics of the material strata. More specifically, resonant column tests were conducted on undisturbed, fine-grained materials and on either undisturbed or compacted, coarse-grained materials to obtain the relationships of shear modulus and damping to shear strain. In addition, cyclic triaxial and cyclic torsional tests were conducted to measure the pore pressure and strain responses of cohesionless materials due to dynamic loading. Static triaxial tests were used to determine whether the materials are contractive and hence subject to liquefaction.

Seismic Material Response Analysis

The seismic material response was determined using the SHAKE computer code (Ref. 53). This program establishes the earthquake-induced total shear stress and shear strains for use in both the empirical and analytical liquefaction and cyclic mobility analyses.

Values of the maximum shear modulus between the ground surface and a depth of 300 feet were determined from the cross-hole shear wave velocity measurements presented in Subsection 3.4.3.5. Below a depth of 300 feet and extending down to the bedrock level at a depth of about 1,050 feet, the value of the maximum shear modulus were determined using the relationship given in Ref. 54.

The groundwater level was assumed to be an elevation 245 feet msl, which corresponds to a depth of about 25 to 30 feet below ground surface (bgs). Actual groundwater levels ranged from 30 to 50 feet bgs during the monitoring period.

The idealized material profile used for the seismic material response analysis and the computed free-field material moduli are presented in Figure 3.4-41. The relationship between the shear modulus and damping ratio to shear strain is presented in Figure 3.4-51.

3.4.3.4.8.4 Selection of Strata Requiring Liquefaction and Cyclic Mobility Analyses

A screening process was used to determine what portion of the material profile was the most critical with respect to liquefaction and cyclic mobility potential. This process involved a statistical evaluation of SPT values along with the material index property data.

As part of the site characterization in a previous report the boring log data were combined into 11 groups as shown in Figure 3.4-52 (Ref. 55). The figure shows the location of borings and certain field tests in relation to other DWPF structures. Several boring groups are associated with individual structures (e.g., Group 4 includes borings near the Vitrification Building), while others incorporate boring data gathered during all field sampling programs.

Figure 3.4-53 shows that the trends in SPT resistance are remarkably similar for all boring groups. In group 4, for example, mean penetration resistance decreases from a value greater than 20 in the desiccated surficial materials of the "Upland unit" and the Tobacco Road Formation to less than 15 near elevation 240 feet msl. Resistance then increases to approximately 25 near elevation 215 feet msl then decreases to approximately 20 near elevation 200 feet msl. SPT N-values generally increase in the underlying Santee materials. Similar trends in mean SPT resistance may be observed among the boring groups. Because group 11, which includes the 87 borings used in the analysis, exhibits a pattern very similar to many individual groups (each comprising from 3 to 11 borings), the site appears reasonably homogeneous (based on SPT resistance) at any prescribed elevation.

The statistical analysis of the SPT data along with the material index properties serves to identify zones where liquefaction and cyclic mobility potential should be evaluated. Above elevation 250 feet msl the materials have mean SPT values generally in excess of 15 to 20 and

are predominantly clays or clayey sands. This zone is also characterized by relatively high mean shear wave velocities (in excess of 1,150 feet/sec) and high mean cone penetration resistance (in excess of 100 kg/cm^2). Hence, liquefaction or cyclic mobility need not be evaluated further in this zone.

From elevations 250 feet msl to 200 feet msl, the SPT data show that mean values are similar to or less than values above elevation 250, and the materials contain significantly less fines. Hence, this zone appears to be the most critical zone with respect to liquefaction and cyclic mobility potential.

At about elevation 200 feet msl, a tan clay "marker layer" exists in many borings is characteristic of the lower Dry Branch Formation. The Dry Branch Formation is generally characterized by mean SPT values ranging from 25 to 35. The materials range from slightly silty to clayey sands to clays. Some low SPT values were found below the tan clay which are generally associated with liquefaction zones in the Santee Formation. With respect to liquefaction or cyclic mobility potential, this stratum was considered less susceptible than the zone between elevation 200 feet msl and 250 feet msl for the following reasons:

- The corrected SPT values for this deposit are greater than for the stratum between elevations 200 feet msl and 250 feet msl.
- The earthquake shear stress ratio computed from the ground response analysis is smaller than the stress ratio in the critical zone between elevations 200 feet msl and 250 feet msl.
- The Santee Formation tends to have slightly higher fines content than the critical zone between elevations 200 feet msl and 250 feet msl.

Hence, it was concluded that the sediments most critical with respect to liquefaction and cyclic mobility are found in the zone between elevations 200 feet and 250 feet msl. Therefore, the remainder of the analyses presented herein relate to this material stratum.

The materials in this elevation zone consist of strata S1, S2a, and S2b described in the geologic sections. These strata are generally described as clayey, fine to coarse sand (S1), fine to medium sand with traces of silt (S2a), and fine to medium sand with traces of clay (S2b). The sand grains are generally subangular. The results of extensive grain-size and hydrometer analyses are shown in Figures 3.4-54 through 3.4-56. These data indicate that for materials with more than about 10% fines, most of the fines tend to be in the clay-size range rather than in the silt-size range. Sands that contain more than 20% fines have an average liquid limit of 34 and a plasticity index of 12.

Stratification of the materials tended to be in the range of 5 feet or more, although occasional clayey or silty lenses were observed on the order of less than an inch.

3.4.3.4.8.5 Earthquake Shear Stresses

Method of Analysis

For a postulated time history, the free-field, earthquake-induced shear stresses for the profile were estimated by using the SHAKE computer program (Ref. 58).

The analysis of earthquake shear stresses was performed based on three recorded accelerograms considered applicable to the DWPF site (Ref. 55, 43, 44). These three accelerograms listed in Table 3.4-16 were chosen because (1) they were all recorded over deep alluvial deposits, (2) they are related to earthquakes of moderate magnitude (6.6 to 7.1), and (3) horizontal ground-surface accelerations were reasonably large (0.202 g $<a_{max}<$0.348 g).

All three accelerograms were scaled to a peak horizontal ground-surface acceleration of 0.20 g, the same as the DBE. The accelerograms along with their corresponding response spectra for 5% damping are shown in Figure 3.4-57.

The duration of significant seismic motion for the site was determined to be approximately 16 sec. This duration envelops the requirements (strong motion of 16 sec) for deep cohesionless material sites (significant motion of 16 sec). To maintain additional conservatism, full 30-sec duration events were used (Ref. 30, 58, 59).

Shear stress time histories calculated for the postulated three earthquake events using the SHAKE program are shown as functions of depth in Figures 3.4-58 through 3.4-60. Although the peak shear stress varies greatly with depth, the peaks occur in all layers at about the same time. Peak shear stresses at various depths are also summarized for the three postulated accelerograms in Figure 3.4-61.

The above results were based on a profile of maximum shear wave velocity versus depth that was slightly different from the one adopted for final design (Figure 3.4-41) (Ref. 57). Hence, an additional SHAKE analysis was performed using the final material profile. Because the values of maximum shear modulus were only slightly changed, a re-analysis was performed using only the El Centro accelerogram, which was the most critical in the previous analyses.

3.4.3.4.8.6 Results: Empirical Methods

For the blowcount analysis, all of the SPT data from the 24 borings comprising boring groups 1, 2, and 4 were used. The SPT data were grouped by fines content into USCS groups A, B, and C, and the results are plotted in Figure 3.4-62. The solid points represent SPT values where the material classification data were confirmed by laboratory grain-size analyses. Solid points with a cross are samples that had more than 20% finer than 0.074 mm or, where a hydrometer analysis was performed, more than 15% finer than 0.005 mm. The open points represent SPT values that were grouped according to their visual USCS classification. Grain-size tests were performed on the samples with the lowest blowcounts, which are the most critical to the analysis. The lowest SPT values are generally associated with materials having

more than 10% fines and that a large percentage of the lowest SPT values are associated with clayey sands that are considered not susceptible to seismic-induced ground failure. The corresponding ground-failure criteria are also plotted in Figure 3.4-63 for groups A and C (Ref. 35). For group B, the ground-failure criterion was chosen as the average of the criteria for clean and silty sands.

The average blowcounts greatly exceed the failure criteria for the three USCS groups. There is a wide scatter in the blowcount data, and a small percentage of SPT values fall below the corresponding ground-failure criteria. These percentages are summarized below:

Elevation Zone	Percentage of SPT Values Below Ground Failure Criteria
240 to 250	0 (0 out of 43)
230 to 240	0 (0 out of 42)
220 to 230	16 (6 out of 38)
210 to 220	8 (3 out of 39)
200 to 210	3 (1 out of 33)

The blowcounts that fall below the ground-failure criteria lines occur randomly between elevations 200 feet msl and 230 feet msl and do not correspond to a vertically or horizontally continuous zone. During an earthquake, the weaker materials will be softer and will be subjected to lower than average dynamic stresses. Because the ground-failure criteria are upper limits of observed failures (Figures 3.4-63 and 3.4-64), even some of the lowest blowcounts may not necessarily correspond to a ground-failure condition. The zone with the largest percentage (16%) of low blowcounts occurs at a depth of 50 to 60 feet so that even if isolated pockets of material were to soften at that depth the effect on surface structures would be negligible. Thus, it is concluded that the blowcount analysis indicates that the potential for liquefaction and cyclic mobility is negligible for the earthquake analyzed.

The CPT analysis was based on a fewer number of borings than the SPT analysis. However, a continuous record of CPT versus depth was made in these borings, which provides a more complete assessment of the material resistance than is provided by the SPT test obtained at 5-feet intervals. The CPT analysis indicates that essentially all of the materials penetrated by the cone penetrometer exceed the ground failure criterion established by Zhou (Ref. 50). Thus, it is concluded that the CPT analysis indicates the potential for liquefaction for the earthquake analyzed is negligible.

3.4.3.4.8.7 Results: Analytical Methods

The slope of the steady-state line for the DWPF sands was estimated by plotting the undrained steady-state shear strength estimated in each of the tests (15 tests) as a function of void ratio. The average slope of the lines that encompass all of these data points was considered to be the slope of the steady-state line corresponding to each specific specimen. This slope was compared to steady-state lines for several sands and was considered to be a reasonable slope for this material (Ref. 35). The slope was used as the basis for correcting (decreasing) the steady-state shear strengths measured on the test specimens.

The assumed slope of the steady-state line and the corrected, undrained steady-state shear strengths derived from each of the 15 consolidated-undrained triaxial tests are summarized in Figure 3.4-65.

The driving shear stresses were computed for the Vitrification Building on the basis of a static building load of 7.0 ksf (3.4 kg/cm^2) using the computer program SSTAB1. During DBE, the distribution of stresses beneath the Vitrification Building change as the building accelerates. The maximum stresses computed for this case are based on a trapezoidal distribution of vertical stresses beneath the building varying from 2.1 ksf on one side of the building to 13.1 ksf (2.0 to 12.7 kg/cm^2) on the other side of the building.

The driving stresses imposed by the Vitrification Building during the static condition and during the safe shutdown earthquake are compared to the undrained steady-state shear strength of the deposit in Figure 3.4-65. This figure shows that for 13 of the 15 test specimens the applied static and dynamic shear stresses are less than the undrained steady-state shear strengths. The two test specimens with relatively low, steady-state shear strengths corresponds to two specimens of silty sand.

These data show that, in general, the steady-state shear strength of the deposit is significantly greater than the static and peak dynamic shear stresses that are applied by the Vitrification Building. Hence, for the earthquake analyzed, the building will not experience a bearing capacity failure. However, some limited zones of material as represented by the two tests on silty sand may be stressed to their steady-state shear strength, which will shift slightly higher stresses into the stronger materials.

Cyclic Mobility - Stress Method

For the cyclic mobility evaluation, materials between elevations 200 feet msl and 250 feet msl, were considered. The range of the average cyclic shear stress ratio produced by the earthquake analyzed is 0.13 to 0.15 for this same interval. Thus, the computed factor of safety against cyclic mobility is 2.1 to 2.5. The correction factors used for the evaluation were intended to represent the best state-of-the-art estimate, but the selection of these factors involves a considerable degree of judgment. However, any other correction factors that might reasonably be chosen would likely result in satisfactory factors of safety against cyclic mobility for the DWPF site.

Cyclic Mobility - Strain Method

A method for predicting pore water pressure buildup and cyclic mobility of sands during earthquakes has been developed (Ref. 40). This approach is based on the experimental finding that there is a correlation between cyclic shear strain and pore water pressure buildup of saturated sands that, at least for low strains, is independent of density and stress level and applies to many sands. These correlations indicate that there is a threshold cyclic shear strain, $\gamma_t \simeq 10^{-2}$%, below which there is no pore water pressure buildup in saturated sands.

Analysis requires in situ measurement of maximum shear modulus (G_{max}) laboratory measurement of G/G_{max} versus shear strains, the threshold cyclic shear strain, and the pore pressure-cyclic shear strain relationship.

The level of cyclic shear strain induced by the safe shutdown earthquake (γ_c) is computed as a function of the peak ground-surface acceleration and the shear modulus-shear strain relationship. This value is compared to the threshold cyclic shear strain to assess the potential for cyclic mobility.

Stress-controlled cyclic triaxial tests were performed in conjunction with the analysis (Figure 3.4-66). For six of the 19 tests performed, the cyclic stresses were small, producing cyclic strains that were essentially constant for the first 10 or more cycles.

The pore pressure ratios generated at the 10th cycle for these five tests are shown in Figure 3.4-67(a). This figure is a plot of the relationship between pore pressure ratio and cyclic shear strain prepared for tests on three different sands, using a variety of compaction procedures and different confining pressures. This plot demonstrates the existence of a threshold cyclic shear strain at about 10^{-2}% and the relative unsensitivity of the pore pressure versus cyclic shear strain plot to many test variables (Ref. 40).

Although the DWPF cyclic triaxial tests were not performed specifically for use in a cyclic strain analysis, the data in Figure 3.4-67(a) suggest that use of the Dobry curve is reasonable and possibly conservative for purposes of estimating the DWPF material behavior (Ref. 35).

Values of cyclic shear strains computed in the SHAKE analysis for the earthquakes analyzed are shown in Figure 3.4-67(b). For cyclic shear strains of this magnitude, the plot in Figure 3.4-67(a) suggests that the earthquakes will generate small pore pressures of 0 to 15% of the effective confining pressure. Cyclic load tests indicate that these pore pressures do not result in any measurable softening of the materials; thus, cyclic strains will remain very small, and will not affect the undrained shear strength of the materials.

3.4.3.4.8.8 <u>Summary of Liquefaction and Cyclic Mobility Analysis</u>

The potential for ground failure (liquefaction and/or cyclic mobility) at the DWPF site was evaluated using both empirical and analytical methods.

The analysis of ground failure using the SPT approach indicated that limited pockets of material do not meet established ground-failure criterion, but these were considered to be zones that are not laterally continuous and, hence, pose no hazard to the DWPF facilities.

An analysis based on CPT data indicated that adequate resistance to ground failure was encountered at all locations where CPT data was obtained. Because CPT data provide a continuous profile of resistance versus depth, the results of the CPT analysis confirm the conclusion made from the SPT data that low SPT values were random and that continuous layers of weak materials were not found.

Analytical methods were used to evaluate the potential for liquefaction and cyclic mobility independently. The analysis of liquefaction potential was based on the results of consolidated undrained triaxial tests. These tests demonstrated that, in general, the materials are not subject to liquefaction. A small percentage of tests (two out of 15) revealed that the steady-state strength of limited zones of material was about equal to the driving shear stresses. However, adequate resistance to the driving shear stresses will be developed in the stronger materials that represent the typical subsurface conditions.

The potential for the occurrence of cyclic mobility was evaluated by two methods. The analyses based on stress-controlled cyclic triaxial tests indicated that the factor of safety against the development of significant cyclic strains (5% peak to peak) was at least 2.1.

Some of the data measured in the stress-controlled cyclic triaxial tests were reanalyzed using the strain approach (Ref. 52). This analysis indicated that only limited pore pressures (on the order of 0 to 15% of the effective stress) are likely to develop during the safe shutdown earthquake. Pore pressures of this magnitude will result in very small cyclic strains and will not affect the undrained shear strength of the material.

Hence, all of the analyses performed for the DWPF site indicate that there is an adequate margin of safety against the occurrence of bearing capacity failure due to flow and cyclic mobility (the development of significant strains).

These findings are further supported by the qualitative assessment of worldwide ground failures. Youd and Perkins (Ref. 32) have correlated the occurrence of earthquake-induced ground failures with the geological origin of the materials involved. These data show that cohesionless deposits of pre-Pleistocene sand deposited in a coastal zone have a very low likelihood of being susceptible to earthquake-induced ground failure. In fact, ground failures in even the most susceptible type of material deposits (continental deposits in river channels, flood plains, deltas) are generally limited to deposits of the Pleistocene Epoch or more recent times. Youd and Perkins also pointed out that for water-table depths greater than about 33 feet, the likelihood of ground failure occurring is low. At the DWPF site, the groundwater level in the “Upland unit” and Tobacco Road Formation ranges from 30 to 50 feet below the ground surface (Ref. 60).

Thus, it is concluded that there is overwhelming evidence that the DWPF soils will not experience a significant liquefaction or deform excessively during the safe shutdown earthquake.

3.4.3.4.9 TECHNIQUES TO IMPROVE SUBSURFACE CONDITIONS

Because of the critical nature of DWPF and the uncertainty in the characterization data, Mueser recommended grouting of the Santee Formation underneath all Category I structures. Figure 3.4-68 summarizes the abandonment grouting data compiled during the subsurface investigation initiated by D'Appolonia (Ref. 28, 55, 60). This figure includes the grout take ratio (grout take divided by nominal borehole volume), grouted depth, borehole diameter, number of bags of cement, and the time charged to grouting. Grout takes were determined by assuming one bag of cement yielded 2.2 cubic feet of grout. This assumed average grout yield per cement bag was later confirmed by Girdler Exploration and Foundation Inc., the drilling subcontractor for D'Appolonia. The grout take ratios presented in Figure 3.4-68 are shown within the squares posted adjacent to the boring symbol.

In three of the four borings drilled at the location of the Glass Waste Storage building #1 (Bldg. 250-S), rod drops and/or calcareous materials were encountered (Ref. 60). In Boring No. 86L1P, a rod drop of 5 feet occurred between elevations 143 and 138 feet msl. Calcareous materials were noted on the field logs in Boring No. 83 and 84. Positive reaction to dilute HCl occurred with some samples from Boring No. 84 between elevations 162 and 126 feet msl. In Boring No. 62, the only boring drilled within the limits of the Sand Filter building (Bldg. S294), samples from elevations 164 to 139 feet msl, reacted positively to HCl. However, in Boring No. 66, located immediately north of the Sand Filter building, no rod drops or calcareous materials were noted. In Boring No. 159, located on the east wall of the Fan House (Bldg. S292), a rod drop of 4 feet and low SPT blow counts occurred and calcareous materials were noted by the field inspector. None of these indications of leached conditions were noted in the borings beneath the Vitrification Building (Bldg. S221). However, in Boring No. 24, located adjacent to the south side of the building, calcareous material was noted between elevations 163 and 158 feet msl (Ref. 60).

Mueser, after reviewing the field data, noted a paucity of notations regarding the loss of drilling fluid on the field logs (Ref. 60). Drawing on experience in F- and H-Areas, they concluded that a loss of drilling mud typically precedes a rod drop or a zone of unusually low penetration resistance. They also suggested for these zones that the amount of fluid loss is an indicator of the size or extent of the highly porous materials. Because of the similarity of the subsurface conditions in F-, H-, and S-Areas, Mueser also suggested that losses of circulation probably had occurred in conjunction with rod drops in S-Area. However, loss of drilling mud was noted by D'Appolonia for only one of the thirty-three borings which had indications of soft zones. Temporary loss of 90% circulation was noted in Boring No. 25 at an approximate elevation of 150 feet msl, immediately above a rod drop of 5 feet. Neither the quantity of lost mud, the depth, nor the time of circulation return was recorded for that boring.

The scarcity of notations of fluid losses on the field logs implied to Mueser that either no other mud losses had occurred or that mud losses had not been recorded. The latter

explanation was preferred by Mueser et al., because some borings were drilled without continuous inspection by D'Appolonia. D'Appolonia's field logs indicated that at least 10 borings were drilled between elevations 130 and 160 feet msl by the drillers without the presence of D'Appolonia field personnel (Ref. 60). Also, Mueser et al. commented that in their experience, very few drillers will note the loss of drilling mud unless specifically requested.

On the basis of the data presented in Figure 3.4-68, Mueser concluded that some soft zones or "voids" of limited lateral extent may exist within the area of Category I structures (Ref. 60). They concluded that although these indications are not sufficient by themselves to definitely conclude that extensive voids are present, or that the "voids" represent a severe threat to the performance of the structures, the general lack of notations on the field logs of mud loss during drilling was suspect and lead to a lack of confidence in the recorded information. This implied that perhaps other important occurrences (rod drops or calcareous materials) were unreported. Thus, a grouting program was implemented. Grout hole locations are shown on Figure 3.4-69 for the Vitrification Building, and Figure 3.4-70 for the Glass Waste Storage Building #1, Fan House and Sand Filter Buildings.

Drill rigs arrived at the site on March 7, 1984, and began drilling grout holes at the northern end of the Vitrification Building (S221) (Ref. 33). Drilling continued southward within the footprint of the Vitrification Building with grouting closely following the drilling operation. The grout holes for the remaining Category I structures were drilled starting at the Fan House (S292) and continued north to the Sand Filter (S294) and the Glass Waste Storage Building #1 (250-S). Also, four secondary grout holes were drilled and grouted in the Vitrification Building. In all, 39 grout holes were completed by March 30, 1984 (Ref. 33).

The grout holes were drilled with truck-mounted drill rigs using four inch nominal diameter tricone roller bits and drilling mud to maintain a stable borehole. During the contract period, the location of the Fan House was moved 10 feet to the south. Therefore, some grout holes in this area were drilled outside the building limits. Grout holes were generally advanced without sampling from the ground surface to elevation 180 feet msl. The boreholes were then advanced with split-spoon sampling at 5 feet intervals to a minimum elevation of 130 feet msl, or approximately 10 feet below the base of the calcareous materials. All split spoon samples were logged and classified by Mueser's resident engineer and tested for the presence of calcareous materials (Ref. 33).

The grout was batched one tank at a time. Each tank was calibrated so that grout quantities could be accurately recorded. A typical batch of grout was composed of one 94 lb. bag of Type I cement; eight, 5 gallon buckets of sand (calibrated for 0.67 cf. per bucket); one-third of a 50 lb. bag of bentonite, and 30 gal of water. The grout yield per batch was approximately 7 cf. The bentonite was first premixed with water in a 130 gal tub to yield sufficient bentonite-water slurry for 4.5 batches. When grouting could not begin on the same day a hole was drilled, the open hole was flushed prior to grouting with water to remove any heavy drilling mud and cuttings that had settled to the bottom. During the flushing operations and at the start of grouting, the grout pipe was positioned approximately 1 feet above the bottom of the

borehole. Before the grout was pumped, the levels of the grout mix within each tank were recorded (Ref. 33).

Generally, grout was pumped at an initial pressure of less than 5 psi, measured at the top of the grout pipe. When the pressure exceeded approximately 5 psi, pumping ceased and the grout take and depth of the bottom of the grout pipe were recorded. The grout pipe was then raised approximately 10 feet and grouting was restarted. Occasionally, a pressure of 20 psi was required to initiate grout flow, but once flow was obtained, the pressure was decreased to a maximum of 5 psi until the grout take ceased (Ref. 33).

The small grout take ratios (Figures 3.4-69 and 3.4-70) indicate that large leached zones do not exist underneath DWPF facilities in the Santee Formation. Grout take ratios in all holes, except Hole No. 2, varied from 0.9 to 2.7, with most of the ratios close to 1.3, indicating stable ground conditions. Grout take ratios were calculated by dividing the grout take by the theoretical or nominal volume of the borehole. The grout take ratio in Grout Hole No. 2 was 7.7, which appeared to be excessively high. Two secondary grout holes (Nos. 36 and 37) were installed adjacent to Grout Hole No. 2 (Figure 3.4-69) to explore the reasons for this relatively high grout take. The resulting grout take ratios in these secondary holes were approximately 1.0, indicating that a large pocket was not present. It was later hypothesized during a review of the records that the high grout take in Grout Hole No. 2 was probably due to inadvertent high grouting pressure which caused local fracturing or compressing of the soil mass (Ref. 33).

During drilling of the grout holes, isolated cases of rod drops, mud losses, and calcareous materials were encountered in the north end of the Vitrification Building and the Glass Waste Storage Building #1. These observations suggested the presence of thin layers of calcareous materials that had been leached in the past. However, no voids or continuous layers of loose soil with a fragile structure were encountered. At the Sand Filter building, calcareous material was encountered in six grout holes between elevations 131 and 163 feet msl in layers up to 12 feet thick. This material and the overlying soils were typically medium dense to dense, indicating significant leaching had not occurred (Ref. 33).

Calcareous material was also encountered in all five grout holes at the fan house between elevations 142 and 162 feet msl in layers up to 7 feet thick. Very loose materials, including two cases of rod drops, were encountered in the soils immediately overlying the calcareous material. This suggested some leaching of the calcareous material and possible raveling of the overlying soil into the leached zone. Like the sand filter building, the calcareous soil underneath the fan house is generally medium dense to dense. Significant settlement due to further leaching of this soil is not anticipated (Ref. 33).

3.4.3.4.10 CRITERIA AND DESIGN METHOD

Field and laboratory testing related to the DWPF was performed in accordance with the American Society for Testing and Materials and the American National Standards Institute standards. The field and laboratory investigations were covered by written quality control procedures and monitored by a quality assurance program. The results of this testing are

documented in Subsection 3.4.3.5. Analyses of settlement, bearing capacity, lateral earth pressures, and cyclic liquefaction potential were performed in accordance with currently accepted engineering principles and practices, as described in Subsection 3.4.3.5. Evaluation criteria are described in these subsections.

3.4.3.4.11 RECENT EVALUATIONS

The evaluations drawn from the previous geotechnical and geological investigations were reviewed in late 1994 with respect to current practice and knowledge at SRS (Ref. 31). This study was performed to determine the technical adequacy of past work and the need for additional investigations and/or analyses. This report included review of the past work that addressed seismic soil criteria as well as comparison of new data and results for nearby facilities which incorporated updated seismic criteria. The conclusions are as follows:

- The previous investigations performed were thorough and well-planned.
- Adequate characterization and analyses have been performed to assess the stability of the foundation soils.
- The subsurface conditions at DWPF are similar and consistent with those found at other facilities in H- and S-Areas.
- No design basis geologic nor geotechnical hazards that would adversely affect DWPF were identified.
- Post-construction settlement measurements at DWPF confirm the geotechnical parameters used in the settlement analysis as well as confirm the static stability of the subsurface soils.
- Previous and current liquefaction susceptibility analysis show that the soils beneath DWPF will not liquefy for the seismic events analyzed.
- Dynamic settlement analyses for the current site distant Design Basis Earthquake (DBE) indicate that the dynamic foundation settlement will be less than 0.5 inches.

Based on results of this review, no further geotechnical work involving field characterization, laboratory testing, or engineering analyses is required for DWPF. The continuation of the settlement monitoring program for the Vitrification Building at DWPF was recommended in the review report (Ref. 31).

The settlement monitoring program for the Vitrification Building is being implemented as part of the DWPF Structural Integrity Program, which addresses the specific locations of the settlement measurements as well as the frequency of the measurements.

3.5 NATURAL PHENOMENA THREATS

This section provides identification of specific natural phenomena events considered to be potential accident initiators. Three specific events were considered: floods, earthquakes and tornadoes.

3.5.1 FLOODS

All of the floods represented by site data in SRNS-IM-2013-00019, Site Information and Program Description (Ref. 3) were the result of excess precipitation runoff and the associated creek or stream flooding. It was concluded that flooding is not a credible hazard for DWPF because of S-Area being located on a relatively elevated region of SRS. The adjacent streams are in broad valleys and are more than 100 feet lower in elevation than the DWPF grade. For these reasons, Chapter 9 of the FSAR states that there are no credible radiological or chemical source terms associated with rain and floods.

For additional details, see Subsection 3.4.2.1.

3.5.2 EARTHQUAKES

Earthquakes are discussed in Subsection 3.4.3.2. The hazard and accident analysis related to the design basis earthquake (DBE) [synonymous to safe shutdown earthquake (SSE) in Chapter 3] is discussed in Chapter 9.

3.5.3 TORNADOES

Tornadoes are discussed in Subsection 3.4.1. The hazard and accident analysis related to high winds and tornadoes is included in Chapter 9.

3.6 EXTERNAL MAN-MADE THREATS

This section provides identification of specific external man-made phenomena associated with the site considered to be potential accident initiators, exclusive of sabotage and terrorism. The two man-made phenomena considered are transportation effects and missile and blast effects.

3.6.1 TRANSPORTATION

During the history of SRS operations, numerous transportation incidents have occurred on the site (as documented below). One single-engine plane landed on an onsite highway during a period of low ground traffic density (the pilot avoided highway vehicles). A single-engine plane crash landed on the entrance road to the railroad Classification Yard. A helicopter crashed on the site in April 1989 while applying fertilizer to the pine forest. A security patrol helicopter crash on the site in September 1985 did not cause any hazardous substance release. An Edgerton, Gremeshausen and Grier, Inc. (EG&G) survey helicopter landed in the burial ground area when its engine malfunctioned, and an amphibian plane landed at Par Pond when the pilot mistook it for Thurmond Lake (formerly Clarks Hill Reservoir). There have been no documented cases of transportation-related incidents in S-Area.

See SRNS-IM-2013-00019, Site Information and Program Description for a discussion of offsite and onsite roads/highways and SRS railroads as well as the location of airports and airspace within the general area of SRS (Ref. 3).

3.6.2 MISSILE AND BLAST EFFECTS

The hazard and accident analysis related to missiles and blast effects is included in Chapter 9.

3.7 NEARBY FACILITIES

The Vogtle Electric Generating Plant (VEGP), a two-unit nuclear power plant licensed by the NRC and located across the Savannah River from SRS, is the only nearby nuclear facility that would have the potential of affecting SRS operations due to an emergency situation. Other nearby nuclear facilities include:

- Chem Nuclear Systems Inc. (CNSI), a low level nuclear waste disposal facility, located near the eastern boundary of SRS.
- Transnuclear Inc. located in Aiken County, SC, a transporter of both HLW and LLW to various disposal facilities, and a provider of decontamination services.
- Carolina Metals Inc. located in Barnwell, SC, a processor of depleted uranium hexafluoride for the US Department of Defense (DOD).

Additionally, the Barnwell Nuclear Plant, which never operated, is located near the SRS eastern boundary. Originally built to chemically reprocess commercial reactor fuels, the plant never stored or handled spent irradiated nuclear fuel because of a federal policy to defer reprocessing.

There are five reactor facilities (i.e., K, R, C, P and L Reactors) located within a 10-mile radius of DWPF, all permanently shutdown. Nuclear fuel elements and target assemblies, previously irradiated in reactors, are processed in the F-and H-Canyon facilities, located in F and H-Areas respectively. Primary operations include dissolution followed by chemical and physical separation and purification of materials. Liquid radioactive wastes are stored in the F- and H-Area Tank Farms for future processing and disposal in the Defense Waste Processing Facility (S-Area) and the Saltstone Facility (Z-Area). There are approximately 35,000,000 gallons of liquid high level radioactive waste currently stored in underground tanks in these two areas.

H-Area also contains tritium facilities which extract tritium from irradiated reactor targets. These facilities have the potential to releases significant quantities of tritium. Risks to the safety of DWPF as a result of H-Area operations are minimal except for tritium releases.

The reactor material facilities are located approximately 6 miles from S-Area. The facility no longer processes aluminum, lithium, uranium, and other materials for SRS reactors and poses no risk to S-Area because of the distance between the two facilities.

The heavy water plant, located approximately 8 miles from S-Area, is no longer in operation and poses no undue risk to facilities in S-Area.

E-Area is located approximately 1 mile from DWPF. It is used for disposal of SRS solid radioactive waste and poses no undue risk to DWPF.

Z-Area, located adjacent to S-Area, processes and disposes of decontaminated salt solution supernates from F- and H-Area waste tanks and contaminants removed by the Effluent

Treatment Facility Project (ETP). The Saltstone process is considered a low hazard operation and thus poses no significant risk to DWPF.

For a discussion of the industries within a 5-mile radius of SRS, their addresses, employment size, and primary products or purposes, see SRNS-IM-2013-00019, Site Information and Program Description. SRNS-IM-2013-00019, Site Information and Program Description discusses the active military installations in SC and GA in relation to SRS (Ref. 3).

As discussed in SRNS-IM-2013-00019, Site Information and Program Description (Ref. 3), Bush Field in Augusta , GA and the Columbia Municipal Airport in Lexington County, SC, are the only two airports within 65 miles of SRS that provide scheduled air passenger services. Barnwell County Airport, a small, general aviation facility, is the closest airport to the SRS boundary.

3.8 VALIDITY OF EXISTING ENVIRONMENTAL ANALYSES

Site characteristic assumptions from this chapter and the SRNS-IM-2013-00019, Site Information and Program Description (Ref. 3) were included in the Final Supplemental Environmental Impact Statement (EIS) for DWPF, DOE/EIS-0082-S (Ref. 62). A supplemental EIS for the DWPF was issued in November 1994 to address design changes to the facility since issuance of the 1982 EIS (Ref. 61). Another supplemental EIS was issued in June 2001 to address alternatives for separating the high-activity and low-activity fractions of the HLW salt solution (Ref. 65). No significant discrepancies exist between the Supplemental EIS's and this chapter of the DWPF FSAR (Ref. 61, 62, 65).

3.9 REFERENCES

1. Nuclear Safety Management. Code of Federal Regulations, 10 CFR 830 Subpart B, Government Printing Office, Washington, DC, January 2001.

2. Preparation Guide for U.S. Department of Energy Nonreactor Nuclear Facility Safety Analysis Reports. DOE Standard DOE-STD-3009-94. U.S. Department of Energy, Washington, DC, Change Notice No. 3 March 2006.

3. Site Characteristics and Program Description. SRNS-IM-2013-00019, Rev. 1.

4. Environmental Dose Assessment. WSRC-IM-91-1, Rev. 2.

5. Design Basis Floods for Nuclear Power Plants. US Nuclear Regulatory Commission. Regulatory Guide 1.59, 1977.

6. Alvin W. Vogtle Electric Generating Plant, Unit 1 and Unit 2, Final Safety Analysis Report. Vol. 1-34 Georgia Power Company, 1987.

7. Schreiner, L.C. and Riedel, J.T Probable Maximum Precipitation Estimates, United States East of the 105th Meridian. Hydrometeorological Report No. 51, National Weather Service, NOAA, US. Department of Commerce, Washington, DC, 1978.

8. Hansen, E.M., Schreiner, L.C., and Miller, J.F. Application of Probable Maximum Precipitation Estimates, United States East of the 105th Meridian. Hydrometeorological Report No. 52, National Weather Service, NOAA, US. Department of Commerce, Washington, DC, 1982.

9. Design of Small Dams. Bureau of Reclamation. United States Government Printing Office, Washington, DC, 1987.

10. Horton, J. H. and Hawkins, R. H. Flow Path of Rain from the Soil Surface to the Water Table. Soil Science, Vol. 100, pp. 377-383, 1965.

11. Drawings W761584 through W761587 and W761595 through W761600.

12. Fetter, C. W. Applied Hydrogeology. 2nd Edition, Merrill Publishing Company, Columbus, OH, 1988.

13. Stage 1 Investigation: Aquifer Performance Tests, 200-S Area, Savannah River Plant, Aiken, SC , CORR 86-0060 D'Appolonia Consulting Engineers, Inc. DWPF, 1981.

14. Technical Data Summary for the Defense Waste Processing Facility, Stage 2. DPSTD-80-39-2, Du Pont (E. I. du Pont de Nemours and Co.). Savannah River Plant, Aiken, SC, 1981a.

15. Technical Data Summary for the Defense Waste Processing Facility, Sludge Plant. DPSTD-80-38-2, Du Pont (E. I. du Pont de Nemours and Co.). Savannah River Plant, Aiken SC, Rev. 2.

16. Standards for Radiation Protection. ERDA Manual, Chapter 0524. U.S. Energy Research and Development Administration, 1975.

17. Handbook of Chemistry and Physics. 61st Edition, CRC Press, Inc., Chemical Rubber Company. Boca Raton, FL, 1981.

18. Prout, W. E. Adsorption of Fission Products by Savannah River Plant Soil. DP-394, Atomic Energy Commission and Du Pont (E. I. du Pont de Nemours and Co.), Savannah River Plant, Aiken, SC, 1959.

19. Wiley, J. R. A Study of Methods for Removing Strontium, Plutonium, and Ruthenium from Savannah River Plant Waste Supernate. DP-1408, U.S. Energy Research and Development Administration and Du Pont (E. I. du Pont de Nemours and Co.), Savannah River Plant, Aiken, SC, 1976.

20. Freeze, R. A. and Cherry, J. A. Groundwater. Prentice-Hall, Inc., Englewood Cliffs, NJ, 1979.

21. Gupta, S. P. and Greenkorn, R. A. Determination of Dispersion and Nonlinear Adsorption Parameters for Flow in Porous Media. Water Resources Research Institute, Vol. 10, No. 4, pp. 839-846, 1974.

22. Exploration Software. Document ER-DW-89-1. Exploration Software, Athens, GA, 1989.

23. Mikol, S. C., Burckhalter, L. T., Todd, T. L., and Martin, D. K. U.S. Department of Energy, Savannah River Plant Environmental Report for 1987. Vol. II Figures and Data Tables. DPSU-88-30-1, Du Pont (E. I. du Pont de Nemours and Co.), Savannah River Plant, Health Protection Department, Aiken , SC, 1988.

24. Onishi, Y., Serve, R. J., Arnold, E. M., Cownen, C. E., and Thompson, F. L. Critical Review: Radionuclide Transport, Sediment Transport, and Water Quality Mathematical Modeling; and Radionuclide Adsorption/Desorption Mechanisms. Pacific Northwest Laboratory Report PNL-2901. NUREG 1 CR-1322, 1981.

25. Deleted.

26. Zeigler, C. C., Heath, E. M., Taus, L. B., Todd, J. L., and Tille, J. E. U.S. Department of Energy Savannah River Plant Environmental Report for 1986. Vol. II. Figures and Data Tables. DPSPU-87-30-1, Du Pont (E. I. du Pont de Nemours and Co.), Savannah River Plant, Health Protection Department, Aiken, SC, 1987.

27. Deleted.

28. Mueser, Rutledge, Johnston, and DeSimone, Geotechnical Report, Design and Construction, Defense Waste Processing Facility, 200-S-Area, Savannah River Plant. report prepared for Du Pont (E. I. du Pont de Nemours and Co.), Engineering Department, Louviers Building, Wilmington, Delaware, August 1984.

29. Stieve, A. L., et. al, Pen Branch Fault Program: Consolidated Report on the Seismic Reflection Surveys and the Shallow Drilling (U). WSRC-TR-91-0087, Rev. 0.

30. .Update of Seismic Design Criteria for the Savannah River Plant, Vol. I, An Executive Summary. DP-3699, URS/John A. Blume and Associates, Du Pont (E. I. du Pont de Nemours and Co.), Savannah River Plant, Aiken, SC, 1982.

31. Bartlett, S. F. Review of the Subsurface Soils and Foundation Conditions for the Defense Waste Processing Facility (U). WSRC-TR-95-0072, Rev. 0.

32. Youd, T. L., Perkins, D. M. Mapping Liquefaction Induced Ground Failure Potential. Journal of Geotechnical Engineering Division, American Society of Civil Engineers, Vol. 104, No GT4, April 1978.

33. Mueser, Rutledge, Johnston, and DeSimone. Foundation Grouting Program, Data Report, Defense Waste Processing Facility, Savannah River Plant, 200-S-Area, 4-9084. report prepared for Du Pont (E. I. du Pont de Nemours and Co.), Engineering Department, Louviers Building, Wilmington, Delaware, June 1984.

34. Bartlett, S. F., et. al. Geological Characterization in the Vicinity of the In-Tank Precipitation Facility (U). WSRC-TR-94-0373, Rev. 0.

35. Preliminary Safety Analysis, Defense Waste Processing Facility. DPST-82-675, Du Pont (E. I. du Pont de Nemours and Co.), Savannah River Plant, Aiken, SC, September 1982.

36. Seismic and Geologic Siting Criteria for Nuclear Power Plants. Appendix A to Part 100 of Title 10, Chapter 1, Code of Federal Regulations. US Nuclear Regulatory Commission. 1971.

37. Ladanyi, B. In Situ Determination of Undrained Stress-Strain Behavior of Sensitive Clays with the Pressuremeter. Canadian Geotechnical Journal, Vol. 9, No. 3, pp. 313-319, 1972.

38. Hardin, B. O. Shear Modulus and Damping by the Resonant Column. Special Procedures for Testing Soils and Rock for Engineering Purposes, American Society for Testing and Materials STP 479, pp. 516-529, 1970.

39. Hardin, B. O., Drnevich, V. P. Shear Modulus and Dynamic Damping in Soils: Design Equations and Curves. Journal of the Soil Mechanics and Foundations Division, ASCE, Vol. 98, No. SM7, pp. 667-692, 1972.

40. Casagrande, A. Liquefaction and Cyclic Deformation of Sands: A Critical Review. Harvard Soil Mechanics, Series No. 88, 1975.

41. Deleted.

42. Reichert, S. O. Summary Report on the Geology and Hydrology of the 100 and 200 Areas at Savannah River Plant for the Period 1961-1966. DPST-67-457, Rev. 0, Du Pont (E. I. du Pont de Nemours and Co.), Savannah River Plant, Aiken, SC.

43. Mueser, Rutledge, Johnston, and DeSimone, Progress Report #10, Vitrification Building Design Area S221, Settlement Monitoring Program, Defense Waste Processing Facility, Savannah River Site, 200-S-Area. July 1991.

44. Castro, G. Liquefaction and Cyclic Mobility of Saturated Sands. Journal of the Geotechnical Engineering Division, American Society of Civil Engineers, Vol. 101, No. GT6, pp. 551-569, 1975.

45. Seed, H. B. Soil Liquefaction and Cyclic Mobility Evaluation for Level Ground During Earthquakes. Journal of the Geotechnical Engineering Division, American Society of Civil Engineers, Vol. 105, No. GT2, 1979.

46. Deleted.

47. Seed, H. B. and Idriss, I. M. Evaluation of Liquefaction Potential of Sand Deposits Based on Observations of Performance in Previous Earthquakes. American Society of Civil Engineers National Convention, St. Louis, MO, 1981 Session on Site Testing to Evaluate Liquefaction Susceptibility, 1981.

48. Tokimatsu, K. and Yoshimi, Y. Field Correlation of Soil Liquefaction with SPT and Grain Size. International Conference on Recent Advances in Geotechnical Earthquake Engineering and Soil Dynamics, Vol. 1, St. Louis, MO, 1981.

49. Tokimatsu, K. and Yoshimi, Y. Predictions of Liquefaction and Cyclic Mobility of Sands. Seventeenth Japan National Conference on Soil Mechanics and Foundation Engineering, 1982.

50. Zhou, S. G. Influence of Fines on Evaluating Liquefaction of Sands by CPT. Proceedings, International Conference on Recent Advances in Geotechnical Earthquake Engineering and Soil Dynamic, Vol. 1, St. Louis, MO, 1981.

51. Poulus, S. J. The Steady State Deformation. Journal of the Geotechnical Engineering Division, American Society of Civil Engineers, Vol. 107, No. GT5, 1981.

52. Dobry, R., Ladd, R. S., Yokel, F. Y., Chung, R. M., and Powell, D. Prediction of Pore Water Pressure Buildup and Liquefaction of Sands During Earthquakes by the Cyclic Strain Method. National Bureau of Standards Building Science Series 138, 1982.

53. Schnabel, P. B., Lysmer, L., and Seed, H. B. SHAKE, A Computer Program for Earthquake Response Analysis of Horizontally Layered Sites. Earthquake Engineering Research Center, EERC 72-12, University of California, Berkeley, CA, 1972.

54. Seed, H. B. and Idriss, I. M. A Simplified Procedure for Evaluating Soil Liquefaction Potential. Earthquake Engineering Research Center Report, EERC 70-9, University of California, Berkeley, CA, 1970.

55. Balance of Plant Geotechnical Report, Defense Waste Processing Facility, 200-S-Area, Savannah River Plant. D'Appolonia Consulting Engineers, Inc., 1982a.

56. Deleted.

57. Stability of Subsurface Materials. Draft Section 3.6.4, D'Appolonia Consulting Engineers, Inc. Defense Waste Processing Facility Preliminary Safety Analysis Report, 1982c.

58. Bolt, B. A. Duration of Strong Ground Motions. Fifth World Conference on Earthquake Engineering, Rome, 1973.

59. Trifunac, M. D. and Brady, A. G. A Study on the Duration of Strong Earthquake Ground Motion. Bulletin of the Seismological Society of America, Vol. 65, No. 3, 1975.

60. Mueser, Rutledge, Johnston, and DeSimone. Letter in Correspondence File from Elmer A. Richards to Fred Herzog Regarding Presence of Voids, Defense Waste Processing Facility, Savannah River Plant, 200-S-Area, July 1983.

61. Final Supplemental Environmental Impact Statement, Defense Waste Processing Facility, Savannah River Site, Aiken, SC. DOE/EIS-0082-S, US Department of Energy, Savannah River Site, Aiken, SC, November 1994.

62. Final Environmental Impact Statement, Defense Waste Processing Facility, Savannah River Plant, Aiken, SC. DOE/EIS-0082, U. S. Department of Energy, Savannah River Plant, Aiken, SC, 1982.

63. Standards/Requirements Identification Document (S/RID). SRR-RP-2009-00558-000.

64. Compliance Assurance Manual. 8B.

65. Final Supplemental Environmental Impact Statement, Salt Processing Alternatives. DOE/EIS-0082-S2, US Department of Energy, Savannah River Site, Aiken, SC, June 2001.

66. Glass Waste Storage Building #2 Geotechnical Baseline and Evaluation Report (U). K-ESR-S-00006, Rev. 2.

67. Glass Waste Storage Building #2 – 251-S, System Design Description, Structure & Services (CS-05) (U). G-SYD-S-00077, Rev. 3.

3.10 TABLES

Table 3.4-1 Elevations of Piezometers Used in the Preliminary Investigation at the DWPF Site

Well	Ground Elevation (ft msl)	Screen Zone Elevation (ft msl)	Zone Monitored
BH 2	259.3	(46.2-48.7)[a]	4
BH 3	276.0	154.5-152.0	6
BH 4	283.7	97.7-95.2	5
BH 6	276.9	180.4-177.9	6
BH 6B	276.7	233.2-230.7	7c
BH 8	271.6	45.1-42.6	5
BH 9	273.2	(22.3-24.8) [a]	4
BH 13	304.8	0.3-(2.2) [a]	4
BH 14	285.4	247.9-245.4	7c
BH 15	267.4	101.9-99.4	5
BH 17A	284.0	220.5-218.0	7c
BH 20A	283.0	(30.0-33.0) [a]	4
BH 21A	278.0	84.0-78.0	5
BH 23A	288.4	241.4-238.4	7c
BH 48B	283.4	164.4-161.4	6
BH 50A	282.9	(24.1-27.1) [a]	4
BH 62A	268.9	153.1-150.9	6
BH 64A	275.9	46.4-43.4	5
BH 69A	284.7	85.7-82.7	5
BH 75A	271.0	224.0-221.0	7c
BH 82	264.3	202.8-200.3	7c
BH 86	267.1	(41.4-43.9) [a]	4
BH 98A	276.6	147.6-144.6	6
HC 9A	269.3	123.8	5
HC 9B	269.3	174.7	6
HC 13B	291.3	193.3	6
HC 13C	291.3	207.1	7c
HC 16A	262.6	118.1	5
HC 16B	262.6	183.6	7c
RSS 1	293.4	~217	7c
RSS 2	276.9	~201	7c
RSS 3	264.2	~198	6
RSS 4	289.1	~238	7c
RSS 5	292.7	~215	7c

[a] Numbers in parenthesis indicate feet below msl.
Reference 22: Exploration Software (1989)

Table 3.4-2 Results of Ground-Water Monitoring for the DWPF Site

Well SBG 1

SRS Grid	N 74619.4	Screen Zone Elev.	218.4 - 188.4 ft
Coordinates	E 63749.1	Screen Zone Depth	42.0 - 72.0 ft
		Drill Depth	72.0 ft
Latitude	33.294822°N	Casting Elevation	262.4 ft
Longitude	81.643880°W	Casting Material PVC	

Parameter	Units	03/26/86	05/29/86	08/25/86	10/07/86
Sampling Method		Pump	Pump	Pump	Pump
Water table	Meters	72.5	72.4	72.3	72.3
Elevation	Feet	237.7	237.4	237.1	237.3
pH	pH	4.1	4.3	4.5	4.7
Conductivity	µmho/cm	30	36	45	47
Arsenic	mg/L	<0.002	-	<0.001	<0.002
Barium	mg/L	0.013	-	0.013	0.013
Beryllium	mg/L	-	-	-	-
Cadmium	mg/L	<0.002	-	<0.002	<0.002
Chloride	mg/L	4.0	-	3.4	4.0
Chromium	mg/L	>0.004	-	<0.004	<0.004
Copper	mg/L	-	-	-	-
Cyanide	mg/L	-	-	-	-
Fluoride	mg/L	<0.10	-	0.40	<0.10
Iron	mg/L	0.028	-	0.012	0.020
Lead	mg/L	0.021	-	0.028	0.014
Manganese	mg/L	0.018	-	0.020	0.020
Mercury	mg/L	0.0006	-	0.0007	0.0010
Nickel	mg/L	-	-	-	-
Selenium	mg/L	<0.002	-	<0.002	<0.002
Silver	mg/L	<0.0020	-	<0.0020	<0.0020
Sodium	mg/L	4.28	-	4.86	4.45
Zinc	mg/L	-	-	-	-
NO_3 (as N)	mg/L	2.12	-	2.22	2.23
SO_4	mg/L	<5.0	-	<5.0	<3.0
Phenols	mg/L	<0.002	-	<0.002	<0.002
Tot. org. carbon	mg/L	<1.000	-	<1.000	<2.000
Tot. org. halogen	mg/L	0.005	-	0.006	<0.005
Carbon tet.	mg/L	-	-	-	-
Chloroform	mg/L	-	-	-	-
Tetrachloroethene	mg/L	-	-	-	-
Trichloroethene	mg/L	-	-	-	-
1.1.1-TCE	mg/L	-	-	-	-
Gross alpha	pCi/L	<2.0	-	2.3	1.4
Nonvol. beta	pCi/L	<3.0	-	1.7	1.6
Total radium	pCi/L	<1.0	-	1.0	1.2

Table 3.4-2 Results of Ground-Water Monitoring for the DWPF Site (Continued)

Well SBG 1					
SRS Grid	N 74619.4	Screen Zone Elev.		218.4-188.4 ft	
Coordinates	E 63749.1	Screen Zone Depth		42.0 - 72.0 ft	
		Drill Depth		72.0 ft	
Latitude	33.294822°N	Casting Elevation		262.4 ft	
Longitude	81.643880°W	Casting Material PVC			
Parameter	Units	01/20/87	04/30/87	08/12/86	10/22/87
Sampling Method		Pump	Pump	Pump	Pump
Water elevation	Meters	72.4	73	73	72.8
pH	pH	4.0	4.7	5.0	4.8
Conductivity	µmho/cm	54	43	39	41
TDS	mg/L	26	-	-	-
Arsenic	mg/L	<0.002	-	-	-
Barium	mg/L	0.015	-	-	-
Beryllium	mg/L	-	-	-	-
Cadmium	mg/L	<0.002	-	-	-
Calcium	mg/L	0.843	-	-	-
Chloride	mg/L	3.7	-	-	-
Chromium	mg/L	<0.004	-	-	-
Copper	mg/L	-	-	-	-
Cyanide	mg/L	-	-	-	-
Fluoride	mg/L	<0.10	-	-	
Iron	mg/L	0.014	-	-	-
Lead	mg/L	0.006	-	0.006	-
Magnesium	mg/L	0.695	-	-	-
Manganese	mg/L	0.020	-	-	-
Mercury	mg/L	0.0006	-	0.0006	-
Nickel	mg/L	-	-	-	-
Potassium	mg/L	0.445	-	-	-
Selenium	mg/L	<0.002	-	-	-
Silica	mg/L	3.85	-	-	-
Silver	mg/L	<0.0020	-	-	-
Sodium	mg/L	4.43	-	-	-
Total phosphate	mg/L	0.020	-	-	-
Zinc	mg/L	-	-	-	-
NO_3 (as N)	mg/L	2.50	-	-	-
SO_4	mg/L	<3.0	-	-	-
Phenols	mg/L	<0.002	-	-	-
Tot. org. carbon	mg/L	<1.000	-	<1.000	-
Tot. org. halogen	mg/L	<0.005	-	0.015	-
Carbon tet.	mg/L	-	-	-	-
Chloroform	mg/L	-	-	-	-
Tetrachloroethene	mg/L	-	-	-	-
Trichloroethene	mg/L	-	-	-	-
1.1.1-TCE	mg/L	-	-	-	-
Gross alpha	pCi/L	<3.0	-	-	-
Nonvol. beta	pCi/L	2.5	-	-	-
Total radium	pCi/L	1.0	-	-	-
Tritium	pCi/mL	22.5	-	23.2	-

Table 3.4-2 Results of Ground-Water Monitoring for the DWPF Site (Continued)

Well SBG 2

SRS Grid	N 74570.2	Screen Zone Elev.	234.0-204.0 ft
Coordinates	E 64939.6	Screen Zone Depth	54.0 - 84.0 ft
		Drill Depth	84.0 ft
Latitude	33.296655°N	Casting Elevation	290.0 ft
Longitude	81.640649°W	Casting Material PVC	

Parameter	Units	03/26/86	05/29/86	09/09/86	10/07/86
Sampling Method		Pump	Pump	Pump	Pump
Water table	Meters	72.6	72.5	72.3	72.4
Elevation	Feet	238.1	237.9	237.1	237.4
pH	pH	4.5	4.9	4.6	4.7
Conductivity	µmho/cm	12	15	22	23
Arsenic	mg/L	<0.002	-	<0.001	<0.002
Barium	mg/L	0.005	-	0.004	0.004
Beryllium	mg/L	-	-	-	-
Cadmium	mg/L	<0.002	-	<0.002	<0.002
Chloride	mg/L	2.3	-	2.8	2.3
Chromium	mg/L	<0.004	-	<0.004	<0.004
Copper	mg/L	-	-	-	-
Cyanide	mg/L	-	-	-	-
Fluoride	mg/L	<0.10	-	0.10	<0.10
Iron	mg/L	0.015	-	0.014	0.018
Lead	mg/L	0.018	-	1.018	0.016
Manganese	mg/L	0.021	-	0.020	0.021
Mercury	mg/L	<0.0002	-	<0.0002	<0.0002
Nickel	mg/L	-	-	-	-
Selenium	mg/L	<0.002	-	<0.002	<0.002
Silver	mg/L	<0.0020	-	<0.0020	<0.0020
Sodium	mg/L	0.83	-	1.39	1.00
Zinc	mg/L	-	-	-	-
NO_3 (as N)	mg/L	0.85	-	0.78	0.85
SO_4	mg/L	<5.0	-	<3.0	<3.0
Phenols	mg/L	<0.002	-	<0.002	<0.002
Tot. org. carbon	mg/L	<1.000	-	<1.000	<1.000
Tot. org. halogen	mg/L	<0.005	-	<0.005	0.005
Carbon tet.	mg/L	-	-	-	-
Chloroform	mg/L	-	-	-	-
Tetrachloroethene	mg/L	-	-	-	-
Trichloroethene	mg/L	-	-	-	-
1.1.1-TCE	mg/L	-	-	-	-
Gross alpha	pCi/L	<2.0	-	<3.0	<3.0
Nonvol. beta	pCi/L	<3.0	-	1.9	<2.0
Total radium	pCi/L	<1.0	-	<1.0	<1.0

Table 3.4-2 Results of Ground-Water Monitoring for the DWPF Site (Continued)

Well SBG 2					
SRS Grid	N 74570.2	Screen Zone Elev.		234.0-204.0 ft	
Coordinates	E 64939.6	Screen Zone Depth		54.0 - 84.0 ft	
		Drill Depth		84.0 ft	
Latitude	33.296655°N	Casting Elevation		290.0 ft	
Longitude	81.640649°W	Casting Material PVC			
Parameter	Units	01/20/87	04/30/87	07/29/87	10/05/87
Sampling Method		Pump	Pump	Pump	Pump
Water Table	Meters	72.3	72.8	72	73.1
pH	pH	4.0	4.8	5.0	5.1
Conductivity	µmho/cm	30	21	22	20
TDS	mg/L	44	-	-	-
Arsenic	mg/L	<0.002	-	-	-
Barium	mg/L	0.005	-	-	-
Beryllium	mg/L	-	-	-	-
Cadmium	mg/L	<0.002	-	-	-
Calcium	mg/L	0.629	-	-	-
Chloride	mg/L	2.5	-	-	-
Chromium	mg/L	<0.004	-	-	-
Copper	mg/L	-	-	-	-
Cyanide	mg/L	-	-	-	-
Fluoride	mg/L	<0.10	-	-	-
Iron	mg/L	0.013	-	-	
Lead	mg/L	0.020	-	0.012	-
Magnesium	mg/L	0.492	-	-	-
Manganese	mg/L	0.020	-	-	-
Mercury	mg/L	<0.0002	-	<0.0002	-
Nickel	mg/L	-	-	-	-
Potassium	mg/L	0.299	-	-	-
Selenium	mg/L	<0.002	-	-	-
Silica	mg/L	3.33	-	-	-
Silver	mg/L	<0.0020	-	-	
Sodium	mg/L	1.08	-	-	
Total phosphate	mg/L	0.020	-	-	-
Zinc	mg/L	-	-	-	-
NO_3 (as N)	mg/L	0.82	-	-	-
SO_4	mg/L	<3.0	-	-	-
Phenols	mg/L	<0.002	-	-	-
Tot. org. carbon	mg/L	<1.000	-	<1.000	-
Tot. org. halogen	mg/L	<0.005	-	<0.005	-
Carbon tet.	mg/L	-	-	-	
Chloroform	mg/L	-	-	-	-
Tetrachloroethene	mg/L	-	-	-	-
Trichloroethene	mg/L	-	-	-	-
1.1.1-TCE	mg/L	-	-	-	-
Gross alpha	pCi/L	<3.0	-		-
Nonvol. beta	pCi/L	2.7	-	-	-
Total radium	pCi/L	<1.0	-	-	-
Tritium	pCi/mL	14.9	-	16.4	-

Table 3.4-2 Results of Ground-Water Monitoring for the DWPF Site (Continued)

Well SBG 3			
SRS Grid	N 73699.9	Screen Zone Elev.	234.6-204.6 ft
Coordinates	E 65265.6	Screen Zone Depth	50.0 - 80.0 ft
		Drill Depth	80.0 ft
Latitude	33.295262°N	Casting Elevation	286.6 ft
Longitude	81.638100°W	Casting Material PVC	

Parameter	Units	03/26/86	05/29/86	08/09/86	10/07/86
Sampling Method		Pump	Pump	Pump	Pump
Water table	Meters	72.6	72.5	72.3	72
Elevation	Feet	238.3	237.7	237.2	236.2
pH	pH	4.1	4.9	4.5	5.0
Conductivity	µmho/cm	12	13	20	21
Arsenic	mg/L	<0.002	-	<0.001	<0.002
Barium	mg/L	0.005	-	<0.004	<0.004
Beryllium	mg/L	-	-	-	-
Cadmium	mg/L	<0.002	-	0.002	<0.002
Chloride	mg/L	2.9	-	5.7	1.7
Chromium	mg/L	<0.004	-	<0.004	<0.004
Copper	mg/L	-	-	-	-
Cyanide	mg/L	-	-	-	-
Fluoride	mg/L	<0.10	-	0.10	<0.10
Iron	mg/L	0.016	-	0.008	0.018
Lead	mg/L	0.015	-	0.012	0.010
Manganese	mg/L	0.018	-	0.019	0.018
Mercury	mg/L	<0.0002	-	<0.0002	<0.0003
Nickel	mg/L	-	-	-	-
Selenium	mg/L	<0.002	-	<0.002	<0.002
Silver	mg/L	<0.0020	-	<0.0020	<0.0020
Sodium	mg/L	1.08	-	1.43	1.17
Zinc	mg/L	-	-	-	-
NO_3 (as N)	mg/L	0.50	-	0.56	0.57
SO_4	mg/L	<5.0	-	<3.0	<3.0
Phenols	mg/L	<0.002	-	<0.002	<0.002
Tot. org. carbon	mg/L	<1.000	-	<1.000	<1.000
Tot. org. halogen	mg/L	0.006	-	<0.005	<0.005
Carbon tet.	mg/L	-	-	-	-
Chloroform	mg/L	-	-	-	-
Tetrachloroethene	mg/L	-	-	-	-
Trichloroethene	mg/L	-	-	-	-
1.1.1-TCE	mg/L	-	-	-	-
Gross alpha	pCi/L	<2.0	-	<3.0	<3.0
Nonvol. beta	pCi/L	<3.0	-	1.9	<2.0
Total radium	pCi/L	<1.0	-	<1.0	<1.0

Table 3.4-2 Results of Ground-Water Monitoring for the DWPF Site (Continued)

Well SBG 3					
SRS Grid Coordinates	N 73699.9 E 65265.6	Screen Zone Elev. Screen Zone Depth Drill Depth		234.6-204.6 ft 50.0 - 80.0 ft 80.0 ft	
Latitude	33.295262°N	Casting Elevation		286.6 ft	
Longitude	81.638100°W	Casting Material PVC			
Parameter	Units	01/20/87	04/30/87	07/29/87	10/05/87
Sampling Method		Pump	Pump	Pump	Pump
Water elevation	Meters	72.3	72.8	72.8	73
pH	pH	4.1	4.3	5.1	5.2
Conductivity	µmho/cm	30	20	28	18
TDS	mg/L	52	-	-	-
Arsenic	mg/L	<0.002	-	-	-
Barium	mg/L	0.005	-	-	-
Beryllium	mg/L	-	-	-	-
Cadmium	mg/L	<0.002	-	-	-
Calcium	mg/L	0.507	-	-	-
Chloride	mg/L	2.3	-	-	-
Chromium	mg/L	<0.004	-	-	-
Copper	mg/L	-	-	-	-
Cyanide	mg/L	-	-	-	-
Fluoride	mg/L	<0.10	-	-	-
Iron	mg/L	0.014	-	-	-
Lead	mg/L	0.012	-	0.012	-
Magnesium	mg/L	0.327	-	-	-
Manganese	mg/L	0.017	-	-	-
Mercury	mg/L	<0.0002	-	<0.0002	-
Nickel	mg/L	-	-	-	-
Potassium	mg/L	0.231	-	-	-
Selenium	mg/L	<0.002	-	-	-
Silica	mg/L	2.81	-	-	-
Silver	mg/L	<0.0020	-	-	-
Sodium	mg/L	1.13	-	-	-
Total phosphate	mg/L	0.030	-	-	-
Zinc	mg/L	-	-	-	-
NO_3 (as N)	mg/L	0.60	-	-	-
SO_4	mg/L	<3.0	-	-	-
Phenols	mg/L	<0.002	-	-	-
Tot. org. carbon	mg/L	<1.000	-	<1.000	-
Tot. org. halogen	mg/L	<0.005	-	0.005	-
Carbon tet.	mg/L	-	-	-	-
Chloroform	mg/L	-	-	-	-
Tetrachloroethene	mg/L	-	-	-	-
Trichloroethene	mg/L	-	-	-	-
1.1.1-TCE	mg/L	-	-	-	-
Gross alpha	pCi/L	<3.0	-	-	-
Nonvol. beta	pCi/L	<2.0	-	-	-
Total radium	pCi/L	<1.0	-	-	-
Tritium	pCi/mL	16.5	-	16.1	-

Table 3.4-2 Results of Ground-Water Monitoring for the DWPF Site (Continued)

Well SBG 4					
SRS Grid	N 72399.8	Screen Zone Elev.		213.1-183.1 ft	
Coordinates	E 65010.2	Screen Zone Depth		58.0 - 88.0 ft	
		Drill Depth		88.8 ft	
Latitude	33.291968°N	Casting Elevation		273.1 ft	
Longitude	81.636248°W	Casting Material PVC			
Parameter	Units	03/26/86	05/29/86	08/25/86	10/07/86
Sampling Method		Pump	Pump	Pump	Pump
Water table	Meters	73.5	73.2	73.1	72.8
Elevation	Feet	241.2	240	239.8	239
pH	pH	4.3	5.0	4.6	4.9
Conductivity	µmho/cm	21	24	32	33
Arsenic	mg/L	<0.002	-	<0.001	<0.002
Barium	mg/L	0.009	-	0.009	0.008
Beryllium	mg/L	-	-	-	-
Cadmium	mg/L	<0.002	-	<0.002	<0.002
Chloride	mg/L	2.9	-	2.8	2.8
Chromium	mg/L	<0.004	-	<0.004	<0.004
Copper	mg/L	-	-	-	-
Cyanide	mg/L	-	-	-	-
Fluoride	mg/L	<0.10	-	0.41	<0.10
Iron	mg/L	0.017	-	0.012	0.010
Lead	mg/L	0.020	-	0.062	0.034
Manganese	mg/L	0.014	-	0.010	0.009
Mercury	mg/L	<0.0002	-	<0.0002	<0.0002
Nickel	mg/L	-	-	-	-
Selenium	mg/L	<0.002	-	<0.002	<0.002
Silver	mg/L	<0.0020	-	<0.0020	<0.0020
Sodium	mg/L	2.04	-	2.63	1.99
Zinc	mg/L	-	-	-	-
NO_3 (as N)	mg/L	1.40	-	1.43	1.35
SO_4	mg/L	<5.0	-	<5.0	<3.0
Phenols	mg/L	<0.002	-	<0.002	<0.002
Tot. org. carbon	mg/L	<1.000	-	<1.000	<1.000
Tot. org. halogen	mg/L	0.032	-	0.034	0.032
Carbon tet.	mg/L	-	-	-	-
Chloroform	mg/L	-	-	-	-
Tetrachloroethene	mg/L	-	-	-	-
Trichloroethene	mg/L	-	-	-	-
1.1.1-TCE	mg/L	-	-	-	-
Gross alpha	pCi/L	<2.0	-	2.4	1.5
Nonvol. beta	pCi/L	<3.0	-	7.7	7.3
Total radium	pCi/L	<1.0	-	1.2	1.1

Table 3.4-2 Results of Ground-Water Monitoring for the DWPF Site (Continued)

Well SBG 4					
SRS Grid	N 72399.8	Screen Zone Elev.		213.1-183.1 ft	
Coordinates	E 65010.2	Screen Zone Depth		58.0 - 88.0 ft	
		Drill Depth		88.8 ft	
Latitude	33.291968°N	Casting Elevation		273.1 ft	
Longitude	81.636248°W	Casting Material PVC			
Parameter	Units	01/20/87	04/30/87	07/29/87	10/05/87
Sampling Method		Pump	Pump	Pump	Pump
Water table	Meters	73.3	73.5	73.5	73.6
pH	pH	3.8	4.8	5.5	5.0
Conductivity	µmho/cm	36	31	30	28
TDS	mg/L	34	-	-	-
Arsenic	mg/L	<0.002	-	-	-
Barium	mg/L	0.010	-	-	-
Beryllium	mg/L	-	-	-	-
Cadmium	mg/L	<0.002	-	-	-
Calcium	mg/L	0.674	-	-	-
Chloride	mg/L	2.1	-	-	-
Chromium	mg/L	<0.004	-	-	-
Copper	mg/L	-	-	-	-
Cyanide	mg/L	-	-	-	-
Fluoride	mg/L	<0.10	-	-	-
Iron	mg/L	0.014	-	-	
Lead	mg/L	0.020	-	0.014	-
Magnesium	mg/L	0.539	-	-	-
Manganese	mg/L	0.007	-	-	-
Mercury	mg/L	<0.0002	-	<0.0002	-
Nickel	mg/L	-	-	-	-
Potassium	mg/L	0.286	-	-	-
Selenium	mg/L	<0.002	-	-	-
Silica	mg/L	3.12	-	-	-
Silver	mg/L	<0.0020	-	-	
Sodium	mg/L	1.88	-	-	
Total phosphate	mg/L	<0.020	-	-	-
Zinc	mg/L	-	-	-	-
NO_3 (as N)	mg/L	1.40	-	-	-
SO_4	mg/L	<3.0	-	-	-
Phenols	mg/L	<0.002	-	-	-
Tot. org. carbon	mg/L	<1.000	-	<1.000	-
Tot. org. halogen	mg/L	<0.033	-	0.039	-
Carbon tet.	mg/L	-	-	<0.005	
Chloroform	mg/L	-	-	<0.005	-
Tetrachloroethene	mg/L	-	-	0.005	-
Trichloroethene	mg/L	-	-	0.111	-
1.1.1-TCE	mg/L	-	-	<0.005	-
Gross alpha	pCi/L	3.2	-		-
Nonvol. beta	pCi/L	10.4	-	-	-
Total radium	pCi/L	<1.0	-	-	-
Tritium	pCi/mL	9.67	-	10.7	-

Table 3.4-2 Results of Ground-Water Monitoring for the DWPF Site (Continued)

Well SBG 5					
SRS Grid	N 72208.3	Screen Zone Depth		66.9-60.8 meters	
Coordinates	E 64499.0	Top of casing elevation		86.71 meters	
Latitude	33.290712°N	Casting Material PVC			
Longitude	81.637223°W				
Parameter	Units	03/16/87	05/02/87	08/12/87	11/11/87
Sampling Method		Pump	Pump	Pump	Pump
Water elevation	Meters	75.8	76	76	75.8
pH	pH	7.3	7.1	7.0	7.0
Conductivity	µmho/cm	92	75	63	58
TDS	mg/L	54	56	40	64
Arsenic	mg/L	<0.002	<0.002	<0.002	<0.002
Barium	mg/L	0.015	0.013	0.012	0.014
Beryllium	mg/L	-	-	-	-
Cadmium	mg/L	<0.002	<0.002	<0.002	<0.002
Calcium	mg/L	13.5	9.38	5.21	10.5
Chloride	mg/L	2.9	1.7	2.7	2.7
Chromium	mg/L	<0.004	<0.004	<0.004	<0.004
Copper	mg/L	-	-	-	-
Cyanide	mg/L	-	-	-	-
Fluoride	mg/L	0.17	0.39	<0.10	<0.10
Iron	mg/L	0.019	0.071	0.008	0.058
Lead	mg/L	<0.006	<0.006	<0.006	<0.006
Magnesium	mg/L	0.258	0.283	0.280	-
Manganese	mg/L	0.006	0.010	0.008	0.010
Mercury	mg/L	<0.0002	<0.0002	<0.0002	<0.0002
Nickel	mg/L	-	-	-	-
Potassium	mg/L	1.51	0.920	0.787	0.856
Selenium	mg/L	<0.002	<0.002	<0.002	<0.002
Silica	mg/L	2.93	3.60	3.15	-
Silver	mg/L	<0.0020	<0.0020	<0.0020	0.0030
Sodium	mg/L	3.55	3.10	2.60	2.53
Total phosphate	mg/L	0.030	0.030	0.030	<0.020
Zinc	mg/L	-	-	-	-
NO_3 (as N)	mg/L	0.68	0.45	0.93	1.05
SO_4	mg/L	<5.0	2.5	<5.0	<5.0
Phenols	mg/L	<0.002	<0.005	<0.005	<0.049
Tot. org. carbon	mg/L	<1.000	<1.000	<1.000	33.2
Tot. org. halogen	mg/L	0.015	0.009	0.016	<0.018
Carbon tet.	mg/L	-	-	-	-
Chloroform	mg/L	-	-	-	-
Chloroform	mg/L	-	-	-	-
Tetrachloroethene	mg/L	-	-	-	-
Trichloroethene	mg/L	-	-	-	-
1.1.1-TCE	mg/L	-	-	-	-
Gross alpha	pCi/L	<3.0	<3.0	<3.0	-
Nonvol. beta	pCi/L	3.0	<2.0	2.0	-
Total radium	pCi/L	0.9	1.0	0.8	-
Tritium	pCi/mL	3.85	0.10	4.30	5.40

Table 3.4-2 Results of Ground-Water Monitoring for the DWPF Site (Continued)

Well SBG 6

SRS Grid Coordinates	N 73599.3	Screen Zone Elev.	240.7-210.7 ft
	E 63860.0	Screen Zone Depth	39.0 - 69.0 ft
		Drill Depth	69.0 ft
Latitude	33.292746°N	Casting Elevation	281.7 ft
Longitude	81.641607°W	Casting Material PVC	

Parameter	Units	03/26/86	05/29/86	08/25/86	10/07/86
Sampling Method		Pump	Pump	Pump	Pump
Water table	Meters	74.4	74.2	74.1	74
elevation	Feet	244.2	243.4	243	242.9
pH	pH	4.2	4.7	4.7	4.8
Conductivity	µmho/cm	25	28	40	39
Arsenic	mg/L	<0.002	-	0.003	<0.002
Barium	mg/L	0.011	-	0.011	0.011
Beryllium	mg/L	-	-	-	-
Cadmium	mg/L	<0.002	-	<0.002	<0.002
Chloride	mg/L	4.6	-	3.4	3.34
Chromium	mg/L	<0.004	-	<0.004	<0.004
Copper	mg/L	-	-	-	-
Cyanide	mg/L	-	-	-	-
Fluoride	mg/L	<0.10	-	0.10	<0.10
Iron	mg/L	0.020	-	0.014	0.097
Lead	mg/L	0.021	-	0.039	0.027
Manganese	mg/L	0.017	-	0.014	0.014
Mercury	mg/L	<0.0002	-	<0.0002	<0.0002
Nickel	mg/L	-	-	-	-
Selenium	mg/L	<0.002	-	<0.002	<0.002
Silver	mg/L	<0.0020	-	<0.0020	<0.0020
Sodium	mg/L	3.25	-	4.60	3.78
Zinc	mg/L	-	-	-	-
NO_3 (as N)	mg/L	1.65	-	1.70	1.64
SO_4	mg/L	<5.0	-	<5.0	<3.0
Phenols	mg/L	<0.002	-	<0.002	<0.002
Tot. org. carbon	mg/L	<1.000	-	1.000	<1.000
Tot. org. halogen	mg/L	<0.006	-	<0.005	0.005
Carbon tet.	mg/L	-	-	-	
Chloroform	mg/L	-	-	-	-
Tetrachloroethene	mg/L	-	-	-	-
Trichloroethene	mg/L	-	-	-	-
1.1.1-TCE	mg/L	-	-	-	-
Gross alpha	pCi/L	<2.0	-	1.1	1.0
Nonvol. beta	pCi/L	<3.0	-	1.8	<2.0
Total radium	pCi/L	<1.0	-	<1.0	1.0

Table 3.4-2 Results of Ground-Water Monitoring for the DWPF Site (Continued)

Well SBG 6					
SRS Grid Coordinates	N 73599.3	Screen Zone Elev.		240.7-210.7 ft	
	E 63860.0	Screen Zone Depth		39.0 - 69.0 ft	
		Drill Depth		69.0 ft	
Latitude	33.292746°N	Casting Elevation		281.7 ft	
Longitude	81.641607°W	Casting Material PVC			
Parameter	Units	02/07/87	04/30/87	07/29/87	10/05/87
Sampling Method		Pump	Pump	Pump	Pump
Water elevation	Meters	74.3	74.7	74.7	74.8
pH	pH	4.7	4.9	5.5	5.2
Conductivity	µmho/cm	45	35	35	34
TDS	mg/L	22	-	-	-
Arsenic	mg/L	<0.002	-	-	-
Barium	mg/L	0.012	-	-	-
Beryllium	mg/L	-	-	-	-
Cadmium	mg/L	<0.002	-	-	-
Calcium	mg/L	0.680	-	-	-
Chloride	mg/L	3.7	-	-	-
Chromium	mg/L	<0.004	-	-	-
Copper	mg/L	-	-	-	-
Cyanide	mg/L	-	-	-	-
Fluoride	mg/L	<0.10	-	-	-
Iron	mg/L	0.006	-	-	-
Lead	mg/L	0.024	-	0.017	-
Magnesium	mg/L	0.480	-	-	-
Manganese	mg/L	0.012	-	-	-
Mercury	mg/L	<0.0002	-	<0.0002	-
Nickel	mg/L	-	-	-	-
Potassium	mg/L	0.437	-	-	-
Selenium	mg/L	<0.002	-	-	-
Silica	mg/L	3.34	-	-	-
Silver	mg/L	<0.0020	-	-	-
Sodium	mg/L	4.14	-	-	-
Total phosphate	mg/L	0.030	-	-	-
Zinc	mg/L	-	-	-	-
NO_3 (as N)	mg/L	1.75	-	-	-
SO_4	mg/L	<3.0	-	-	-
Phenols	mg/L	<0.002	-	-	-
Tot. org. carbon	mg/L	<1.000	-	1.40	-
Tot. org. halogen	mg/L	0.005	-	<0.005	-
Carbon tet.	mg/L	-	-	-	-
Chloroform	mg/L	-	-	-	-
Tetrachloroethene	mg/L	-	-	-	-
Trichloroethene	mg/L	-	-	-	-
1.1.1-TCE	mg/L	-	-	-	-
Gross alpha	pCi/L	<3.0	-	-	
Nonvol. beta	pCi/L	1.6	-	-	-
Total radium	pCi/L	1.3	-	-	-
Tritium	pCi/mL	12.2	-	12.8	-

Reference 23, Mikol et al. (1988): Reference 26, Zeigler et al. (1987)

Table 3.4-3 Flow Velocities and Travel Times of Ground Water Along Flow Path

Flow Path Segment	Segment Length (ft)	Head Change (ft)	Head Gradient (ft/ft)	Segment Velocity (ft/yr)	Travel Time (yr)
A	320	2	0.0063	117	2.7
B	260	5	0.019	352	0.7
C	220	5	0.023	427	0.5
D	140	5	0.036	668	0.2
E	750	18	0.024	445	1.7
Total					5.8

Note: K (hydraulic conductivity) = 12.7 ft/day
ε (effective porosity) = 0.25

Table 3.4-4 Radionuclide Concentrations at Postulated Leak and at Groundwater Outcrop

Isotope	Initial Conc. at Leak: Sludge (Ci/gal)	Initial Conc. at Leak: Supernate (Ci/gal)	$t_{1/2}$ [a] (yr)	Exposure Conc. Guide (Ci/gal)	Conc. after 7.4 yr of decay (Ci/gal)	K_d [b]	Concentration Reduced by Ion Exchange (Ci/gal)	Concentration Reduced by Dispersion (Ci/gal)
^{3}H	-	3.2×10^{-4}	12.3	1.1×10^{-5}	2.1×10^{-4}	0	2.1×10^{-4}	7.6×10^{-10}
^{60}Co	2.9×10^{-1}	-	5.3	1.1×10^{-7}	1.1×10^{-1}	1000	[c]	[c]
^{59}Ni	2.4×10^{-3}	-	8×10^{4}	ND [d]	2.4×10^{-3}	ND	2.4×10^{-3}	8.6×10^{-9}
^{63}Ni	3.0×10^{-1}	-	9.2×10^{1}	ND	2.8×10^{-1}	ND	2.8×10^{-1}	1.0×10^{-6}
^{79}Se	2.3×10^{-4}	-	6.5×10^{4}	1.1×10^{-8}	2.3×10^{-4}	ND	2.3×10^{-4}	8.3×10^{-10}
^{87}Rb	1.6×10^{-8}	-	5×10^{11}	3.8×10^{-7}	1.6×10^{-8}	ND	1.6×10^{-8}	5.8×10^{-14}
^{90}Sr	5.2×10^{1}	-	28.1	1.1×10^{-9}	4.3×10^{1}	6 (2)	1.3×10^{-2}	4.7×10^{-8}
^{90}Y	5.3×10^{1}	-	7.3×10^{-3}	7.6×10^{-8}	[c]	ND	[c]	[c]
^{93}Zr	1.9×10^{-3}	-	1.5×10^{6}	3.0×10^{6}	1.9×10^{-3}	10^{4} (1)	1.5×10^{-3}	5.4×10^{-9}
^{95}Zr	1.7×10^{-5}	-	1.8×10^{-1}	2.3×10^{-7}	[c]	10^{4} (1)	[c]	[c]
^{94}Nb	9.4×10^{-7}	-	2.0×10^{4}	ND	9.4×10^{-7}	ND	9.4×10^{7}	3.4×10^{-12}
^{95}Nb	3.7×10^{-5}	-	9.6×10^{-2}	3.8×10^{-8}	ND	ND	[c]	-
^{99}Tc	4.3×10^{-3}	-	2.1×10^{5}	1.1×10^{-6}	4.3×10^{-3}	0 (1)	4.3×10^{-3}	1.5×10^{-8}
^{106}Ru	2.7	-	1.0	3.8×10^{-8}	1.5×10^{-2}	100 (2)	[c]	[c]
^{106}Rh	2.6	-	9.5×10^{-7}	ND	[c]	ND	[c]	[c]
^{107}Pd	1.6×10^{-5}	-	$\sim 7 \times 10^{6}$	1.1×10^{-8}	1.6×10^{-5}	ND	1.6×10^{-5}	5.8×10^{-11}
^{110m}Ag	2.2×10^{-2}	-	6.9×10^{-1}	ND	1.2×10^{-5}	ND	1.2×10^{-5}	4.3×10^{-11}
^{113}Cd	6.5×10^{-17}	-	$>1 \times 10^{15}$	ND	[c]	ND	[c]	[c]
^{121m}Sn	5.1×10^{-5}	-	7.6×10^{1}	1.1×10^{-8}	4.8×10^{-5}	ND	4.8×10^{-5}	1.7×10^{-10}
^{123}Sn	4.6×10^{-4}	-	8.0×10^{-5}	1.1×10^{-8}	[c]	ND	[c]	[c]
^{126}Sn	2.6×10^{-4}	-	$\sim 1 \times 10^{5}$	1.1×10^{-8}	2.6×10^{-4}	ND	2.6×10^{-4}	9.4×10^{-10}
^{125}Sb	1.4	-	2.7	7.6×10^{-8}	2.1×10^{-1}	1000 (1)	[c]	[c]
^{126}Sb	3.6×10^{-6}	-	3.4×10^{-2}	ND	[c]	1000 (1)	[c]	[c]
^{126m}Sb	2.6×10^{-5}	-	3.6×10^{-5}	ND	[c]	1000 (1)	[c]	[c]
^{125m}Te	3.4×10^{-1}	-	1.6×10^{-1}	7.6×10^{-7}	2.6×10^{-15}	ND	2.6×10^{-15}	[c]
^{127}Te	1.5×10^{4}	-	1.1×10^{-3}	ND	[c]	ND	[c]	[c]
^{127m}Te	1.5×10^{-4}	-	3.0×10^{-1}	2.3×10^{-7}	4.5×10^{-12}	ND	4.5×10^{-12}	[c]
^{129}I	1.2×10^{-5}	-	1.7×10^{7}	2.3×10^{-10}	1.2×10^{-5}	ND	1.2×10^{-5}	4.3×10^{-11}
^{134}Cs	3.0×10^{-1}	-	2.1	3.4×10^{-8}	2.4×10^{-2}	60 (2)	[c]	[c]
^{135}Cs	-	5.8×10^{-6}	3×10^{6}	3.8×10^{-7}	5.3×10^{-6}	60 (2)	5.8×10^{-6}	2.1×10^{-11}
^{137}Cs	2.9	-	30.2	7.6×10^{-8}	2.4	60 (2)	[c]	[c]
^{137m}Ba	2.7	-	4.9×10^{-6}	ND	[c]	[c]	[c]	[c]
^{142}Ce	1.6×10^{-8}	-	$>1 \times 10^{16}$	ND	1.6×10^{-8}	1000 (1)	1.6×10^{-8}	5.8×10^{-14}
^{144}Ce	1.7×10^{1}	-	7.8×10^{-1}	3.8×10^{-8}	2.2×10^{-3}	1000 (1)	[c]	[c]
^{144}Pr	1.7×10^{1}	-	3.3×10^{-5}	ND	[c]	1000 (1)	[c]	[c]
^{144}Pr	2.0×10^{-1}	-	3.2×10^{-5}	ND	[c]	1000 (1)	[c]	[c]
^{144}Nd	8.3×10^{-13}	-	$\sim 5 \times 10^{15}$	2.7×10^{-7}	8.3×10^{-13}	1000 (1)	[c]	[c]
^{147}Pm	4.2×10^{1}	-	2.5	7.6×10^{-7}	5.3	1000 (1)	[c]	[c]
^{147}Sm	3.4×10^{-9}	-	1.1×10^{11}	2.3×10^{-7}	3.4×10^{-9}	1000 (1)	3.4×10^{-9}	1.2×10^{-14}

[a] Half-life of isotopic
[b] Distribution coefficient [reference in parentheses: (1) Ref. 24, Onishi (1981), (2) Ref. 18, Prout (1959)]
[c] Concentration is less than 10^{-15} Ci/gal
[d] ND = data not available

Table 3.4-4 Radionuclide Concentrations at Postulated Leak and at Groundwater Outcrop (Continued)

Isotope	Initial Conc. at Leak: Sludge (Ci/gal)	Initial Conc. at Leak: Supernate (Ci/gal)	$t_{1/2}$ [a] (yr)	Exposure Conc. Guide (Ci/gal)	Conc. after 7.4 yr of decay (Ci/gal)	K_d [b]	Concentration Reduced by Ion Exchange (Ci/gal)	Concentration Reduced by Dispersion (Ci/gal)
^{148}Sm	9.8×10^{-15}	-	1.2×10^{13}	ND	9.8×10^{-15}	1000 (1)	9.8×10^{-15}	[c]
^{149}Sm	3.0×10^{-15}	-	$\sim 4 \times 10^{-14}$	ND	3.0×10^{-15}	1000 (1)	3.0×10^{-15}	[c]
^{151}Sm	4.2×10^{-1}	-	9.3×10^{1}	1.5×10^{-6}	4.0×10^{-1}	1000 (1)	[c]	[c]
^{152}Eu	6.4×10^{-3}	-	1.3×10^{1}	3.0×10^{-7}	4.6×10^{-3}	1000 (1)	[c]	[c]
^{154}Eu	1.1	-	1.6×10^{1}	7.6×10^{-8}	8.0×10^{-1}	1000 (1)	[c]	[c]
^{155}Eu	8.2×10^{-1}	-	1.8	7.6×10^{-7}	4.6×10^{-2}	1000 (1)	[c]	[c]
^{160}Tb	1.9×10^{-9}	-	2.0×10^{-1}	1.1×10^{-8}	[c]	1000 (1)	[c]	[c]
^{208}Ti	1.8×10^{-6}	-	5.9×10^{-6}	ND	[c]	ND	[c]	[c]
^{232}U	1.5×10^{-4}	-	73.6	1.1×10^{-7}	1.4×10^{-4}	100 (1)	[c]	[c]
^{233}U	1.7×10^{-8}	-	1.6×10^{5}	1.1×10^{-7}	1.7×10^{-8}	100 (1)	1.7×10^{-8}	6.1×10^{-14}
^{234}U	4.6×10^{-4}	-	2.5×10^{5}	1.1×10^{-7}	4.6×10^{-4}	100 (1)	4.6×10^{-4}	1.7×10^{-9}
^{235}U	1.5×10^{-6}	-	7.1×10^{8}	1.1×10^{-7}	1.5×10^{-6}	100 (1)	1.5×10^{-6}	5.4×10^{-12}
^{236}U	3.3×10^{-5}	-	2.4×10^{7}	1.1×10^{-7}	3.3×10^{-5}	100 (1)	3.3×10^{-5}	1.2×10^{-10}
^{238}U	8.5×10^{-6}	-	4.5×10^{9}	1.1×10^{-7}	8.5×10^{-6}	100 (1)	8.5×10^{-6}	3.1×10^{-11}
^{236}Np	3.0×10^{-11}	-	2.5×10^{-3}	1.1×10^{-8}	[c]	0 (1)	[c]	[c]
^{237}Np	1.5×10^{-5}	-	2.1×10^{6}	1.1×10^{-8}	1.5×10^{-5}	0 (1)	1.5×10^{-5}	5.4×10^{-11}
^{236}Pu	1.1×10^{-4}	-	2.9	1.1×10^{-6}	1.8×10^{-5}	20 (2)	[c]	[c]
^{238}Pu	1.3	-	8.6×10^{1}	1.9×10^{-8}	1.2	20 (2)	1.6×10^{-4}	5.8×10^{-10}
^{239}Pu	1.2×10^{-2}	-	24.4×10^{3}	1.9×10^{-8}	1.2×10^{-2}	20 (2)	1.2×10^{-2}	4.3×10^{-8}
^{240}Pu	7.7×10^{-3}	-	65.8×10^{2}	1.9×10^{-8}	7.7×10^{-3}	20 (2)	6.8×10^{-3}	2.4×10^{-8}
^{241}Pu	1.5	-	13.2	7.6×10^{-7}	1.0	20 (2)	[c]	[c]
^{242}Pu	1.1×10^{-5}	-	3.8×10^{5}	1.9×10^{-8}	1.1×10^{-5}	20 (2)	1.1×10^{-5}	4.0×10^{-11}
^{241}Am	1.9×10^{-2}	-	45.8×10^{1}	1.5×10^{-8}	1.9×10^{-2}	10^{4} (2)	[c]	[c]
^{242}Am	2.5×10^{-5}	-	1.8×10^{-3}	3.8×10^{-7}	[c]	10^{4} (2)	[c]	[c]
^{242m}Am	2.5×10^{-5}	-	15.2×10^{1}	1.5×10^{-8}	2.4×10^{-5}	10^{4} (2)	[c]	[c]
^{243}Am	9.9×10^{-6}	-	7.4×10^{3}	1.5×10^{-8}	9.9×10^{-6}	10^{4} (2)	[c]	[c]
^{242}Cm	6.0×10^{-5}	-	4.5×10^{-1}	7.6×10^{-8}	5.8×10^{-10}	ND	5.8×10^{-10}	2.1×10^{-15}
^{243}Cm	9.5×10^{-6}	-	3.2×10^{1}	1.9×10^{-8}	8.1×10^{-6}	ND	8.1×10^{-6}	3.7×10^{-11}
^{244}Cm	2.8×10^{-4}	-	17.6	2.7×10^{-8}	2.1×10^{-4}	ND	2.1×10^{-4}	9.7×10^{-10}
^{245}Cm	1.1×10^{-8}	-	9.3×10^{3}	1.5×10^{-8}	1.1×10^{-8}	ND	$1\ 1 \times 10^{-8}$	5.1×10^{-14}
^{246}Cm	9.1×10^{-10}	-	5.5×10^{3}	1.5×10^{-8}	9.1×10^{-10}	ND	9.1×10^{-10}	3.3×10^{-15}
^{247}Cm	1.1×10^{-15}	-	1.6×10^{7}	1.5×10^{-8}	1.1×10^{-15}	ND	1.1×10^{-15}	[c]
^{248}Cm	1.2×10^{-15}	-	4.7×10^{5}	1.5×10^{-8}	1.2×10^{-15}	ND	1.2×10^{-15}	[c]
^{51}Cr	1.5×10^{-19}	-	7.6×10^{-2}	7.6×10^{-6}	[c]	0 (1)	[c]	[c]
^{89}Sr	9.1×10^{-8}	-	1.4×10^{-1}	1.1×10^{-9}	[c]	6 (2)	[c]	[c]
^{91}Y	1.7×10^{-6}	-	1.6×10^{-1}	1.1×10^{-7}	[c]	ND	[c]	[c]
^{95m}Nb	2.2×10^{-7}	-	1.0×10^{-2}	ND	[c]	ND	[c]	[c]
^{103}Ru	2.0×10^{-11}	-	1.1×10^{-1}	3.8×10^{-8}	[c]	100 (2)	[c]	[c]
^{103m}Rh	2.0×10^{-11}	-	1.1×10^{-4}	ND	[c]	ND	[c]	[c]
^{115m}Cd	1.6×10^{-12}	-	1.2×10^{-1}	ND	[c]	ND	[c]	[c]
^{124}Sb	1.2×10^{-10}	-	1.7×10^{-1}	7.6×10^{-8}	[c]	1000 (1)	[c]	[c]

[a] Half-life of isotopic
[b] Distribution coefficient [reference in parentheses: (1) Ref. 24, Onishi (1981), (2) Ref. 18 Prout (1959)]
[c] Concentration is less than 10^{-15} Ci/gal
[d] ND = data not available

Table 3.4-4 Radionuclide Concentrations at Postulated Leak and at Groundwater Outcrop (Continued)

Isotope	Initial Conc. at Leak: Sludge (Ci/gal)	Initial Conc. at Leak: Supernate (Ci/gal)	$t_{1/2}$ [a] (yr)	Exposure Conc. Guide (Ci/gal)	Conc. after 7.4 yr of decay (Ci/gal)	K_d [b]	Concentration Reduced: by Ion Exchange (Ci/gal)	Concentration Reduced: by Dispersion (Ci/gal)
^{141}Ce	6.2×10^{-14}	-	9.0×10^{-2}	3.8×10^{-8}	[c]	1000 (1)	[c]	[c]
^{129}Te	3.8×10^{-15}	-	1.3×10^{-4}	ND	[c]	ND	[c]	[c]
^{129m}Te	5.9×10^{-15}	-	9.3×10^{-2}	ND	[c]	ND	[c]	[c]
^{148}Pm	1.2×10^{-13}	-	1.5×10^{-2}	ND	[c]	1000 (1)	[c]	[c]
^{148m}Pm	1.7×10^{-12}	-	1.2×10^{1}	ND	[c]	1000 (1)	[c]	[c]
^{237}Pu	7.8×10^{-15}	-	1.3×10^{-1}	ND	[c]	20 (2)	[c]	[c]

[a] Half-life of isotopic
[b] Distribution coefficient [reference in parentheses: (1) Ref. 24, Onishi (1981), (2) Ref. 18, Prout (1959)]
[c] Concentration is less than 10^{-15} Ci/gal
[d] ND = data not available

Table 3.4-5 Sedimentary Stratigraphy at the DWPF Site Based on Subsurface Exploration

Stratum - **old nomenclature** (new nomenclature)	Soil Designation	Stratum Thickness (ft)	Stratum Elevation Range (ft, msl)	Geologic Soil Characterization
Hawthorne Formation (Altamaha Fm. - also Upland Unit)	S1	0 +	surficial unit above 275 ±	poorly sorted, sandy with frequent lenses of gravel, pebbly sand; and oxidized, massive clay.
Barnwell Formation (Tobacco Road Fm., Irwinton Sand Mbr., Tan Clay Mbr.)	S2a S2b	80 ±	275 to 195	interbedded, clayey sand and sand with thin layers and lenses of clay or silt.
Undifferentiated (Tan Clay Mbr. - included above)	C2	5 to 20	215 to 195	stiff, silty clay.
McBean Formation (Tinker Fm. and Santee Limestone)	S3a S3b S3c	70	195 ± to 125 ±	alternating layers of sand, some clay and sand with trace clay or silt; discontinuous calcareous sand in lower strata.
Undifferentiated (Green Clay)	M1	10 ±	140 to 130	discontinuous, compact silt.
Congaree Formation (same)	S4	100 ±	125 to 30	continuous, dense sand and silty sand.
Ellenton Formation	----	----	----	dense, sandy to clayey silt with some silty sand.

Table 3.4-6 Summary of Borehole Groutings

Boring Number	Grouted Depth, ft	Borehole Diameter, in.	Volume of Borehole, ft^3	Amount of Cement Used Bags	Calculated Grout Take[b]= 2.12 x E, ft^3	Grout Take Ratio, F/D
1[c]	301.5	5	41	NA		
2P[d]	301.0	8	79	150	318	4.0
3P	115.5	6	22	110	233	10.6
4P	177.9	6	33	105	223	6.7
5[c]	301.5	5	41	700	1484	36
6P	91.5	6	17	28	59	3.5
7[c]	301.5	5	41	103	218	5.3
8P	210.5	8	55	NA		
9P	290.5	8	76	NA		
10	300.8	5	41	71	151	3.7
11	300.4	5[e]	41	NA		
12[c]	300.8	5[e]	41	74	157	3.8
13P	300.5	8	79	208	441	5.6
14	301.5	5	41	NA		
15P[c]	158.5	5	30	NA		
16	300.5	6[e]	59	NA		
17	101.5	4[e]	9	8	17	1.9
18	150.9	4[e]	13	55	117	9.0
20AP	306.5	8	80	130	276	3.4
21P	200.0	8	68	65	138	2.0
21BP	200.0	6[e]	39	18	38	1.0
22	191.2	6[e]	38	25	53	1.4
23	190.5	6[e]	37	58	123	3.3
24	301.5	4	26	46	98	3.8
25	180.2	4[e]	16	54	114	7.1
29	190.3	4[e]	17	20	42	2.5
30	126.5	4	11	8	17	1.5
31	190.6	4[e]	17	55	117	6.9
32	180.1	4[e]	16	15	32	2.0
33	180.3	6[e]	35	26	55	1.6
34	126.5	4[e]	11	30	64	5.8
35	111.5	4[e]	10	25	53	5.3
37	180.2	4	16	15	32	2.0
38	301.0	8	95	153	324	3.4
39	180.3	4[e]	16	20	42	2.6
41	190.3	4[e]	17	25	53	3.1
42	190.3	4[e]	17	60	127	7.5
43	125.1	4[e]	11	NA		
44	111.5	6[e]	22	16	34	1.5
45	190.9	4[e]	17	24	51	3.0
46	151.5	4[e]	13	11	23	1.8
47	190.8	4	17	52	110	6.5
48	301.5	6	59	90	191	3.2

Table 3.4-6 Summary of Borehole Groutings (Continued)

Boring Number	Grouted Depth, ft	Borehole Diameter, in.	Volume of Borehole, ft^3	Amount of Cement Used Bags	Calculated Grout Take[b]= 2.12 x E, ft^3	Grout Take Ratio, F/D
49[c]	200.3	6[e]	39	122	259	6.6
50[c]	301.5	6[e]	59	NA		
51	126.5	4[e]	11	8	17	1.5
53	126.5	4	11	7	15	1.4
54	200.5	4[e]	18	18	38	2.1
55	180.3	6[e]	35	60	127	3.6
56	180.4	4[e]	16	52	110	6.9
57	190.8	4[e]	17	32	68	4.0
58	190.3	4[e]	17	20	42	2.5
62	200.8	4[e]	17	18	38	2.2
62AP	107.0	6	20	19	40	2.0
63[c]	301.5	6	59	57	121	2.0
64[c]	201.5	8	70	NA		
66	200.8	4[e]	17	13	28	1.6
67	126.5	4	11	25	53	4.8
68	126.5	4	11	NA		
69	180.5	6	35	NA		
70	126.5	4[e]	11	8	17	1.5
72	301.5	4[e]	26	NA		
73[c]	200.8	6	39	NA		
74[c]	101.5	6[e]	20	20	42	2.0
75[c]	99.5	6[e]	20	20	42	2.0
77	180.5	4[e]	16	17	36	2.3
78	180.4	4[e]	16	22	47	2.9
80	180.4	4	16	28	59	3.7
81	180.5	4	16	45	95	5.9
83	150.5	4	13	26	55	4.2
84	151.3	4[e]	13	11	23	1.8
85	150.2	4	13	30	64	4.9
86L1	150.9	10	72	94	199	2.8
86L1A	300.0	10	144	85	180	1.3
86L2	300.9	10	144	90	191	1.3
87	76.5	4[e]	7	12	25	3.6
89	180.5	4[e]	16	NA		
90P	301.5	6[e]	59	45	95	1.6
90L2P	301.5	6[2]	59	45	95	1.6
92	180.4	4[2]	16	25	53	3.3
93	76.5	4[2]	7	4	8	1.1
96	76.5	4[2]	7	6	13	1.9
98	180.3	4[2]	16	NA		
101[c]	76.5	4[2]	7	4	8	1.1

Table 3.4-6 Summary of Borehole Groutings (Continued)

Boring Number	Grouted Depth, ft	Borehole Diameter, in.	Volume of Borehole, ft^3	Amount of Cement Used Bags	Calculated Grout Take[b]= 2.12 x E, ft^3	Grout Take Ratio, F/D
158	126.5	4[2]	11	8	17	1.5
159	201.5	4[2]	18	15	32	1.8
160	150.9	4	13	25	53	4.1

[a] Summary includes only borings extending into McBean Formation

[b] Calculated grout take is based on the typical neat cement grout mix used to grout boreholes.

[c] Boring is outside of limits shown on Figure 3.4-20.

[d] Where a piezometer was installed, the "Volume of Borehole" is the volume of the annular space between the riser pipe borehole.

[e] Diameter of borehole is not denoted on field log and has been assumed based on type of boring.

Note: NA = not available

Table 3.4-7 Summary of Borings with Indications of Voids or Leached Zones[a]

Boring Number	Approximate Elevation of Rod Drops	Approximate Elevation of Loose Zones Noted During Drilling	Approximate Elevation of Blow Count	Low Blow Counts Observed During Drilling, in.	Approximate Elevation of Loss of Drilling Fluid	Approximate Elevation of Samples with Reaction to HCL[b]	Approximate Elevation of Calcareous Notes on Field Logs	Grout Take Ratio
3P	None noted	None noted	170	3/18	None noted	/	None noted	10.6
4P	None noted	None noted	-	-	None noted	/	None noted	6.7
6P	None noted	199 to 190	-	-	None noted	/	None noted	3.5
8P	None noted	None noted	-	-	None noted	/	162 to 156	Not
13P	None noted	None noted	-	-	None noted	/	160 to 145	5.6
18	None noted	None noted	151 to 145	0/18	None noted	/	None noted	9.0
20	164 to 162	None noted	-	-	None noted	/	None noted	3.4
21P	None noted	None noted	172	0/12	None noted	None	None noted	2.0
23	145 to 141	None noted	147	0/18	None noted	/	None noted	3.3
24	153 to 145[c]	None noted	-	-	None noted	None	163 to 158	3.8
25	167 to 163	None noted	169	8/12	150	/	None noted	7.1
	148 to 143		149	8/12				
31	None noted	175 to 140	170 to 164	0/18	None noted	/	None noted	6.9
			149	0/18				
32	None noted	None noted	168	5/12	None noted	/	None noted	2.0
34	None noted	None noted	-	-	None noted	/	None noted	5.8
37	None noted	None noted	183	4/12	None noted	/	None noted	2.0
38	None noted	190 to 170	-	-	None noted	/	None noted	3.4
		148 to 140						
42	None noted	None noted	-	-	None noted	/	None noted	7.5
47	None noted	None noted	147	0/18	None noted	/	145	6.5
48P	None noted	None noted	157	4/12	None noted	/	153	3.2
			149	0/18				
54	None noted	None noted	-	-	None noted	/	161 to 151	2.1
56	None noted	141 to 135	136	2.18	None noted	/	None noted	6.9
62	None noted	None noted	-	-	None noted	16 139	164 to 123	2.2

Table 3.4-7 Summary of Borings with Indications of Voids or Leached Zones[a] (Continued)

Boring Number	Approximate Elevation of Rod Drops	Approximate Elevation of Loose Zones Noted During Drilling	Approximate Elevation of Blow Count	Low Blow Counts Observed During Drilling, in.	Approximate Elevation of Loss of Drilling Fluid	Approximate Elevation of Samples with Reaction to HCL[b]	Approximate Elevation of Calcareous Notes on Field Logs	Grout Take Ratio
64	None noted	None noted	152 to 145	0/18	None noted	/	163 to 158	Not
72	None noted	None noted	149	0/18	None noted	/	145	Not
80	None noted	None noted	141	7/12	None noted	/	None noted	3.7
81	None noted	None noted	-	-	None noted	/	None noted	5.9
83	None noted	None noted	164	7/12	None noted	None	160 to 158	4.2
84	None noted	None noted	-	-	None noted	162 to 157 135 to 126	135 to 129	1.8
86L1	143 to 138	None noted	-	-	None noted	None	None noted	2.8
86L2	168 to 162[c]	None noted	-	-	None noted	/	None noted	1.3
89	None noted	None noted	-	-	None noted	/	153	Not
92	None noted	None noted	144 to 138	0/18	None noted	/	None noted	3.3
159	169 to 165	None noted	174 158	4/12 6/12	None noted	/	155 to 150	1.8

a All elevations are in feet.

b / indicates samples were not available to MRJD for testing with dilute HCL.

c Field log notes that driller dropped rocks in noted interval.

Table 3.4-8 Summary of Static and Dynamic Laboratory Testing Program[a]

Static Triaxial Test CU[b]	Consolidated Test Undisturbed Silts and Clays	Sands		Compacted Sands	Compaction Test	Resonant Column Test	Cyclic Triaxial Test	Cyclic Torsional Test
(3)BH-3, ST-2 16 4' - 17 3'	(1)BH-6, ST-4 136 5' - 139 5'	(1)BH-8612, ST-1 145 0' - 147 5'	(1)BH-86L2, ST-18 41 6' - 41 9'	(95%M)Sample 2 40 0' - 50 0'	(5)Sample 1 30 0' - 40 0'	(3)BH-38, ST-2 51 5' - 54 5'	(3)BH-38, ST-2 51 5' - 54 5'	(3)BH-81, ST-3 56 5' - 58 5'
(3)BH-3, ST-5 83 9' - 84 8'	(1)BH-6, ST-6 221 3' - 221 6'	(1)BH-10, ST-2 40 0' - 42 5'	(1)BH-86L2, ST-19 43 4' - 43 8'	(M) Sample 2 40 0' - 50 0'	(M)Sample 1 30 0' - 40 0'	(3)BH-38, ST-3 71 5' - 53 5'	(3)BH-47, ST-1 31 5' - 33 5'	(1)BH-90, ST-1 37 0' - 39 0'
(3)BH-6, ST-5 141 9' - 142 8'	(1)BH-6A, ST-3 72 0' - 75 0'	(1)BH-20, ST-1 52 6'	(1)BH-86L2, ST-23 50 7' - 50 9'	(M)Blend 1 BH-24 10 0' - 20 0'	(M)Sample 2 40 0' - 50 0'	(3)BH-38, ST-5 91 0' - 94 0 '	(3)BH-38, ST-2 71 5' - 53 5'	(1)BH-9012, ST-2 50 2' - 54 0'
(3)BH-6A, ST-2 56 9' - 57 8'	(1)BH-7, ST-1 85 0' - 88 0'	(2)BH-38, ST-2 52 1' - 52 3'	(1)BH-86L2, ST-24 53 6' - 53 7'	(M)Blend 2 BH-24 20 0' - 30 0'	(M)Sample 3 50 0' - 60 0'	(3)BH-47, ST-1 31 5' - 33 5'	(3)BH-47, ST-3 51 5' - 53 5'	(1-M)Blend 4 BH-24 40 0' - 50 0'
(3)BH- 8, ST-14 145 9' - 146 8'	(1)BH-10, ST-6 81 5' - 84 5'	(2)BH-38, ST-5 91 7' - 91 9'	(1)BH-86L2, ST-46 109 6' - 109 8'	(M)Blend 3 BH-24 30 0' - 40 0'	(M)Blend 1 BH-24 10 0' - 20 0'	(3)BH-47, ST-2 46 5' - 48 5'	(3)BH-55, ST-3 56 5' - 58 5'	
(3)BH-10, ST-2 40 8' - 41 8'	(1)BH-20, 0-2 114 6'	(2)BH-38, P-1 246 5' - 246 7'	(3)BH-86L2, ST-49 115 6' - 115 8'	(M)Blend 4 BH-24 40 0' - 50 0'	(M)Blend 2 BH-24 20 0' - 30 0'	(3)BH-55, ST-3 56 5' - 58 5'	(3)BH-81, ST-2 46 5' - 48 5'	
(3)BH-10, ST-5 72 9' - 74 3'	(1)BH-47, ST-5 76 5' - 78 5'	(1)BH-47, ST-4 56 5	(1)BH-86L2, ST-51 119 6' - 119 8'	(M)Blend 5 BH-24 50 0' - 60 0'	(M)Blend 3 BH-24 30 0' - 40 0'	(3)BH-81, ST-2 46 5' - 48 5'		
(3)BH-38, ST-1 36 8' - 37 8'	(1)BH-55, ST-* 141 6' - 144 2'	(1)BH-47, ST-6 91 7'	(1)BH-86L2, ST-52 121 5' - 121 7'	(M)Blend 6 BH-24 60 0' - 68 0'	(M)Blend 4 BH-24 40 0' - 50 0'	(3-M)BH-22, ST-1 57 0' - 59 0'		
(3)BH-38, ST-6 108 4' - 109 4'	(1)BH-90, ST-4 68 0'	(1)BH-55, ST-6 125 7'	(1)BH-86L2, ST-53 124 7' - 125 0'		(M)Blend 5 BH-24 50 0 - 60 0'	(4-M)BH-55, ST-1 26 5 - 28 5		
(3)BH-47, ST-4 56 8' - 57 8'		(1)BH-63, P-1 47 0' - 50 0'	(1)BH-86L2, ST-58 137 2' - 137 5'		(M)Blend 6 BH-24 60.0 - 68.0	(4-M)BH-90, ST-2 46 5' - 48 5'		

Table 3.4-8 Summary of Static and Dynamic Laboratory Testing Program[a] (Continued)

Static Triaxial Test CU[b]	Consolidated Test Undisturbed Silts and Clays	Sands		Compacted Sands	Compaction Test	Resonant Column Test	Cyclic Triaxial Test	Cyclic Torsional Test
(3)BH-47, ST-6		(1)BH-63, ST-2	(1)BH-88612, P-1		(M)Blend 6			
91 9’ - 92 9’		122 0’ - 125 0’	142 1’ - 142 3’		BH-24			
					57 0’ - 59 0’			
(3)BH-63, PT		(1)BH-8612, ST-	(1)BH-8612, P-2		(M)BH-55,			
48 6’ - 49 2’		10	144 6’ - 144 9’		ST-1			
		25 2’ - 25 4’			26 5’ - 28 5’			
(3)BH-8612,		(1)BH-8612, ST-	(1)BH-90, ST-1		(M)BH-90,			
ST-17 38 3’ -		11	38 7		ST-2			
39 4’		27 5’ - 27 8’			46 5’ - 48 5’			
(3)BH-63, ST-2		(1)BH-8612, ST-	(1)BH-90, ST-5					
121 0’ - 124 2’		13	83 2					
		31 6’ - 31 8’						
(3)BH-9012,		(1)BH-8612, ST-	(1)BH-90, P-1					
ST-1		15	199 5					
35 4’ - 36 4’		35 6’ - 35 8’						
(3)BH-90, ST-3								
51 8’ - 52 8’								
(3-95%M)Blend 4								
BH-24								
40 0’ - 50 0’								
(3-100%M)Blend								
4								
BH-24								
40 0’ - 50 0’								

a Table indicates boring, sample number, and depth. Numbers in parentheses indicate number of tests conducted on a particular sample. Letters in parentheses for compaction tests indicate whether a standard Proctor (S) or modified Proctor (M) test was performed.

b CU denotes consolidated-undrained test with pore pressure measurements.

Table 3.4-9 Summary of Generalized Static Soil Properties

Stratum	Unit Weight, pcf	Average Water Content, %	Effective Shear Friction Angle, ~ϕ	Strength Properties Cohesion, c psf	Consolidation Parameters Compression Index, C_c	Swelling Index, C_c	Initial Void Ratio, e_o
S1	130	21	34	0		0.009	0.56
S2a	128	22	34	0		0.008	0.59
S2b	128	22	34	0		0.009	0.59
C2	106	53	31	0	0.85	0.070	1.4
53A	127	23	34	0		0.009	0.62
(Elev. 180-200)							
53a	121	30	34	0		0.015	0.80
(Elev. 130-180)							
53b	126	24	34	0		0.009	0.64
53c	125	25	34	0		0.009	0.67
M1	120	31	34	0		Considered	
S4	125	25	40	0		Considered	
						Imcompressible	

Table 3.4-10 Summary of CU Triaxial Test Results

Boring, Sample, and Depth	Soil Description	ϕ, degrees	**c**, ksf
BH-3, ST-2 16.4’ - 17.3’	Very stiff sandy silt	29.5	0.5
BH-3, ST-5 83.9’ - 84.8’	Stiff sandy silt	34.4	0
BH-6, ST-5 141.9’ - 142.8’	Dense silty fine to medium sand	38.8	0
BH-6A, ST-2 56.9’ - 57.8’	Medium dense clayey fine to medium sand	33.9	0
BH-8, ST-14 145.9’ - 146.8’	Dense to very dense silty fine to medium sand	37.0	0
BH-10, ST-2 40.8’ - 41.8’	Medium dense clayey fine to medium sand	32.2	0.2
BH-10, ST-5 72.9’ - 74.3’	Medium dense clayey fine to medium sand	33.9	0
BH-24, Blend 4 40.0’ - 50.0’	Compacted fine to medium sand, trace to some clay[a]	35.3	0
BH-24, Blend 4 40.0’ - 50.0’	Compacted fine to medium sand, trace to some clay[b]	39.6	0
BH-38, ST-1 36.8’ - 37.8’	Loose to medium dense fine to medium sand, some silt and clay	33.7	0
BH-38, ST-6 1088.4’ - 109.4’	Very loose to loose fine to medium sand, trace to clay	25.6	0
BH-47, ST-4 56.8’ - 57.8’	Loose fine to medium sand, trace of silt to silty fine to medium sand	29.5	0
BH-47, ST-6 91.9’ - 92.9’	Loose to medium dense clayey fine to medium sand	31.7	0
BH-63, P-1 48.6’ - 49.2’	Loose fine to coarse clayey sand	35.7	0
BH-63, ST-2 122.9’ - 124.2’	Medium dense fine to medium clayey sand	33.7	0
BH-86L2, ST-17 38.3’ - 39.4’	Loose fine to medium sand, some clay	30.6	0
BH-90L2, ST-1 35.4’ - 36.4’	Medium dense fine to medium sand, trace of clay	32.6	0
BH-90, ST-3 51.8’ - 52.8’	Loose to medium dense fine to medium sand, trace of clay and mica	34.1	0

[a] Compacted to 95% modified Proctor effort at optimum water content.
[b] Compacted to 100% modified Proctor effort at optimum water content.

Table 3.4-11 Summary of Consolidation Test Results for Silts and Clays

Boring, Sample and Depth	Soil Description	Compression Index, C_c	Recompression Index, C_{cr}	Void Ratio, e_o
BH-6, ST-4 136.5’ - 139.5’	Very stiff sandy silt	0.22	0.02	0.794
BH-6, ST-6 221.3’ - 221.6’	Very stiff to hard silt	0.14	0.03	0.587
BH-6A, ST-3 72.0’ - 75.0’	Soft clay, trace of sand	0.76	0.07	1.281
BH-7, ST-1 85.0’ - 88.0’	Medium stiff clay	1.07	0.12	1.474
BH-10, ST-6 81.5’ - 84.5’	Medium stiff clayey silt	0.69	0.07	0.985
BH-20, 0-2 114.6’	Stiff to very stiff clayey silt	0.28	0.01	1.007
BH-47, ST-5 76.5’ - 78.5’	Stiff sandy clay	1.83	0.11	1.553
BH-55, ST-8 143.6’ - 144.2’	Very stiff sandy clay	0.12	0.03	0.589
BH-90, ST-4 68.0’	Medium stiff silty clay	0.91	0.05	1.983

Table 3.4-12 Laboratory Determination of Shear Moduli of Backfill at Large Strains

Type of Test	Shear Strain, γ %	Shear Modulus G, psi
Torsional shear	1.7×10^{-2}	14,100
Torsional shear	6.2×10^{-2}	7,700
Triaxial compression	9.3×10^{-1}	2,500
Triaxial compression	2.9	1,900

Note: BH-24, 40-50 ft, blend 4, $\underline{\sigma}_o = 1$ kg/cm^2.

Table 3.4-13 Allowable Bearing Capacities of Mat Foundations for Category I Structures[a]

Structure	Mat Dimensions, ft	Embedment, ft	Assumed Mat Thickness, ft	Allowable Bearing Capacity (tsf) Case 1[b]	Case 2[c]
Vitrification Building (S-221)	117 x 360	13	10	20	15
Glass Waste Storage Building #1 (S-250)	90 x 202	23	3.5	17	10
Sand Filter Building (S-294)	160 x 190	19	2.0	20	6

[a] allowable bearing capacities relate to ultimate shear failure and do not consider settlements. The subsoils will respond elastically to applied loading less that these allowable values. Actual bearing values for these structures should be selected based on tolerated estimated settlements.

[b] Case 1 assumes that mat foundations are completely rigid.

[c] Case 2 assumes a relative foundation rigidity based on mat thickness.

Table 3.4-14 Soil Design Parameters

Parameter	Stratum S1 Natural Soils	Compacted Fill [a,b]
Allowable bearing capacity (for spread footing and design of roads and railroads	3 tsf	3 tsf
Effective unit weights		
Above water table	127 pcf	130 pcf
Below water table[d]	68 pcf	71 pcf
Angle of internal friction (ϕ)	34°	34°
Earth pressure coefficients [e,f]		
Coefficient of active earth pressure (K_A)	0.28	0.28
Coefficient of earth pressure at rest (K_O)	0.44	0.44
Coefficient of passive earth pressure (K_P)	3.50	3.50
Equivalent fluid pressure[g]		
Flexible walls: Above water table	36 psf/ft	36 psf/ft
Below water table	82 psf/ft	82 psf/ft
Rigid Walls: Above water table	60 psf/ft	60 psf/ft
Below water table	95 psf/ft	95 psf/ft
Coefficient of vertical subgrade reaction (k_S)	200 pci	200 pci
Excavation slopes (maximum)	1 vert. ON 1 horiz. (1:1)	1:1
Permanent slopes (maximum)	1 vert. ON 1 horiz. (1:2)	1:2
Frost penetration	5 in.	5 in.

a Minimum compacted fill density shall be 95% of ASTM D1557 (modified Proctor).
b Compacted fills are limited to onsite sandy soils or SRS designated borrow area sandy soils free of rubble and organic material, and with a maximum of 50% by dry weight passing the No. 200 sieve.
c For footing widths (B) of less than 3 ft allowable bearing pressure is 1/3 x 8 x 3 tsf.
d Design water levels
Average water table - elevation 245
Maximum water table - elevation 265
e The lateral pressure due to a surcharge loading over a large area adjacent to the permanent wall = surcharge load x K_0.
f Major compaction equipment should be kept at least 10 ft from permanent wall.
g Structural walls restrained at the top and bottom are "rigid". Walls restrained at the bottom and free at the top are "flexible."

Table 3.4-15 Summary of G_{max} Values for Category I Structures

Zone	ElevationRange, ft	Unit Weight kcf	Poisson's Ratio	Maximum Shear Modulus, tsf									
				Free Vitrification			Sand Filter		Fan House			GWSB #1	
				Field Center Wall	SW Corner Center		Mid N		Center	NE Corner	Center	Mid N Wall	Center of Exhaust
1	Backfill[a]	0. 0.130	0.35	(a)	(b)	(c)	(d)	(e)	(f)	(g)	(h)	(i)	(j)
2	[b]-260	0.127	0.35	6,700	c	c			c	c	c	3,000 c	c
3	260[d]-245	0.127	0.35	5,200	7,400	5,800	4,900	5,200	6,500	5,700	6,600	7,800	9,200
4	245-235	0.129	0.49	4,400	6,000	4,900	4,200	4,300	5,100	4,700	5,100	5,600	6,100
5	235-200	0.129	0.49	3,600	4,700	4,100	3,500	3,500	4,100	3,900	4,100	4,400	4,700
6	200-175	0.125	0.48	4,300	5,000	4,500	4,200	4,300	4,600	4,500	4,700	4,900	5,000
7	175-135	0.125	0.48	5,200	5,600	5,400	5,100	5,200	5,300	5,300	5,500	5,500	5,600
8	135-30	0.125	0.48	9,300	9,700	9,500	9,200	9,300	9.400	9.400	9.700	9.800	9,800
9	30- -30	0.125	0.48	11,800	11,800	11,800	11,800	11,800	11,800	11,800	11,800	11,800	11,800

a Elevation range for backfill under walls of Glass Waste Storage Building #1 = 280 to 267.

b Elevation corresponds to bottom of foundation as follows:

Column	a	b, c	f, g	h, j	
Elevation	275	270	271	261	267

c Between the bottom of the foundation and elevation 260, G_{max} must be computed.

d For columns d and e, this elevation should be 254.

Table 3.4-16 Strong Motion Accelerograms Used for Analysis of Liquefaction Potential

Earthquake	Richter Magnitude, M	Instrument Location	Site Geology	Epicentral Distance, km	Peak Horizontal Acceleration, g
El Centro May 18, 1940	6.7	Imperial Valley Irrigation District 32.79N, 115.55W	Alluvium deeper than 1,000 ft	58	0.348
San Fernando February 9, 1971	6.6	CIT Millikan Library 34.14N, 118.13W	Approx. 1,000 ft of alluvium	38	0.202
Seattle, WA April 13, 1949	7.1	Olympia Highway Test Laboratory 47.03N, 122.90	Deep alluvium	21	0.280

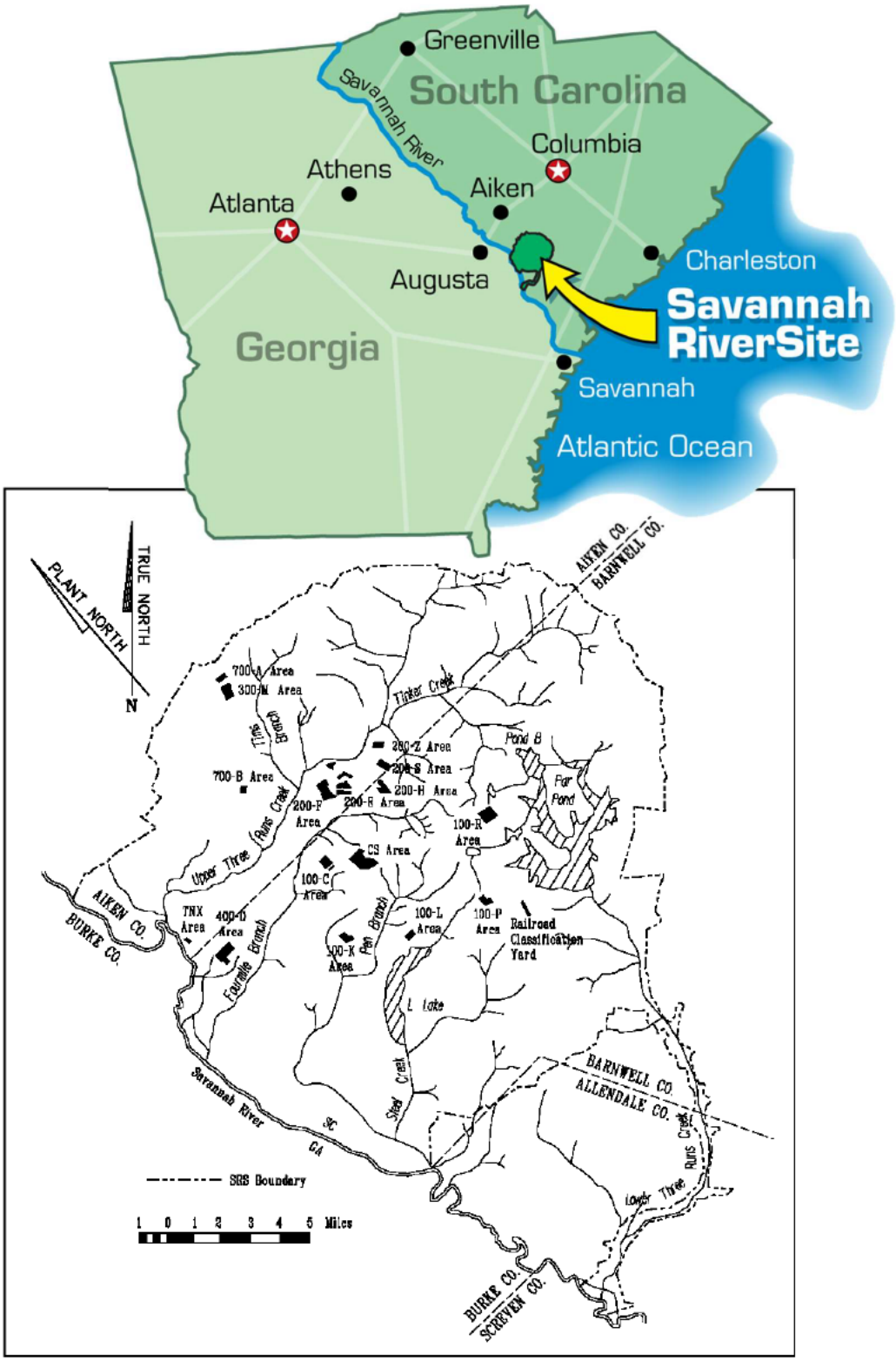

Figure 3.3-1 Savannah River Site Map

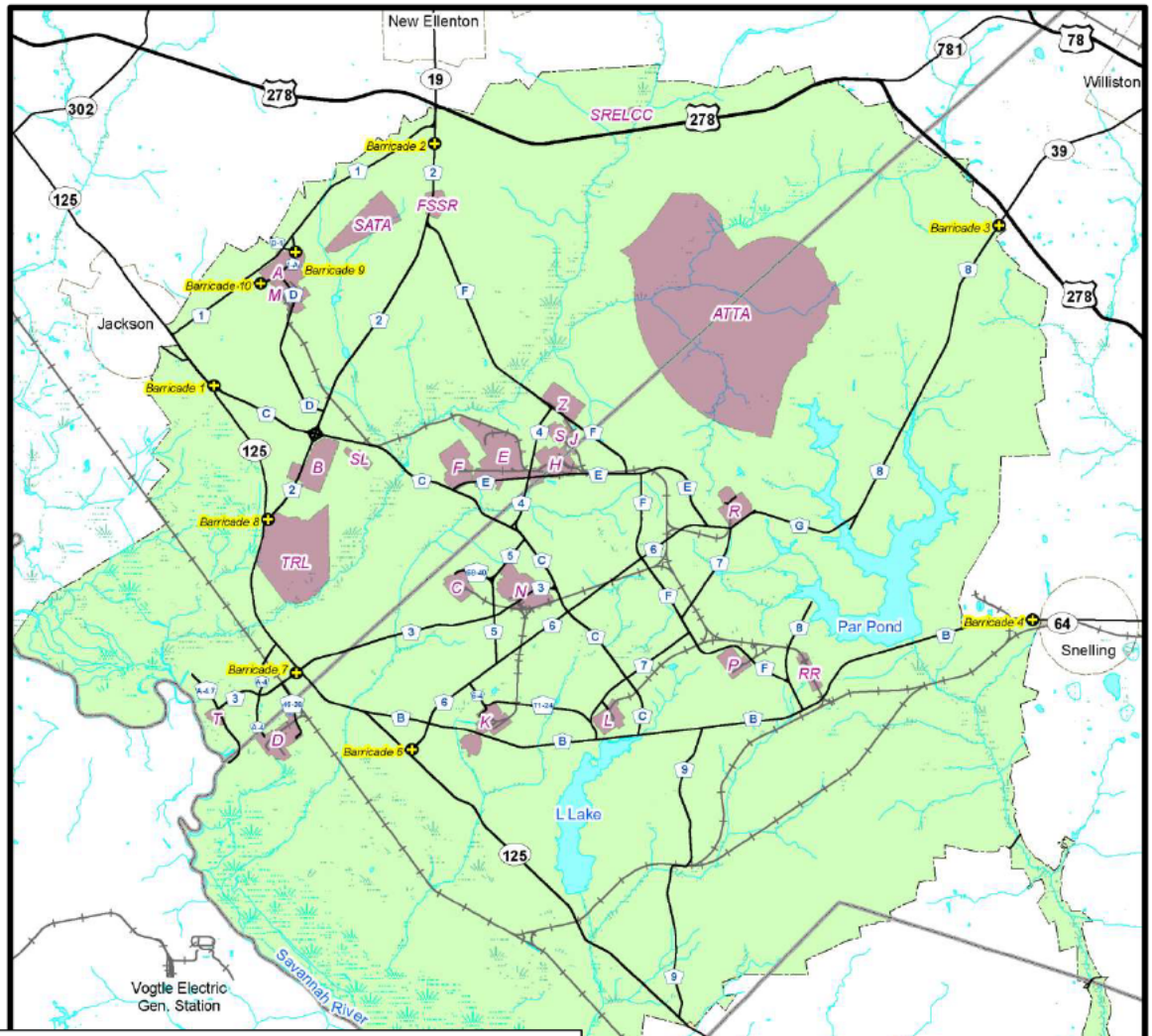

Legend	
A-Area	SRNL
B-Area	Administration
C-Area	C-Reactor
D-Area	Heavy Water Purification
E-Area	Burial Grounds
F-Area	F-Canyon, F-Tank Farm
H-Area	H-Canyon, H-Tank Farm, Tritium Facility
J-Area	Salt Waste Processing Facility
K-Area	K-Reactor
L-Area	L-Reactor
N-Area	Central Shops
P-Area	P-Reactor
Q-Area	Carolina Barbeque
R-Area	R-Reactor
S-Area	Defense Waste Processing Facility
Z-Area	Saltstone Production Facility

Figure 3.3-2 SRS Map Showing Key Facilities

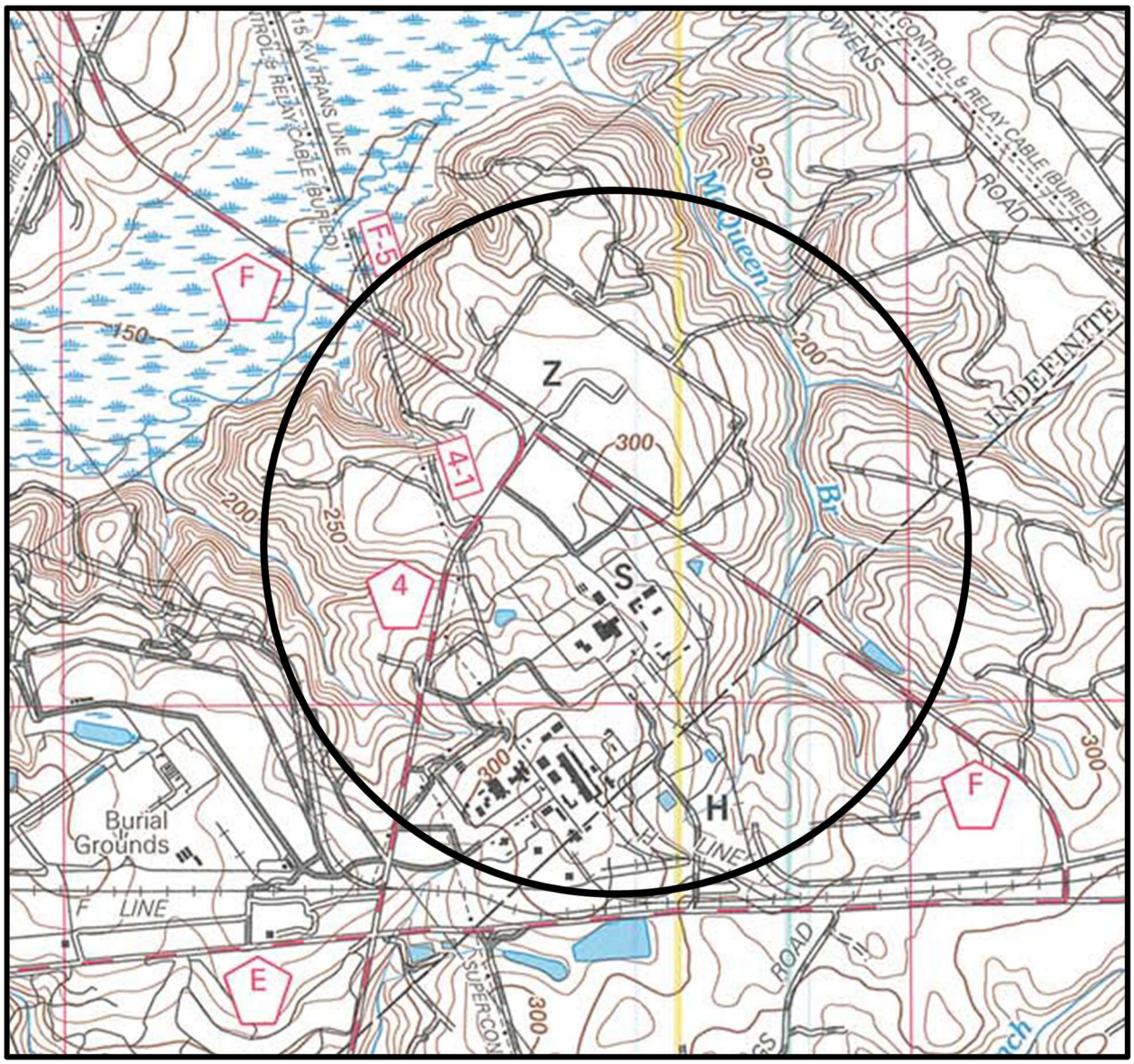

Contour Interval – 10 ft, 1-mile Radius, Scale 1:48 000
Source: FOREST SERVICE MAP: Constructed in 2004 by digital methods at the Geospatial Service and Technology Center, Salt Lake City, Utah, from FS Cartogrpahic Feature Files and quadrangle maps. Field review provided by the Southern Region.

Figure 3.4-1 Streams, Watersheds, and Topography of the DWPF Site Area

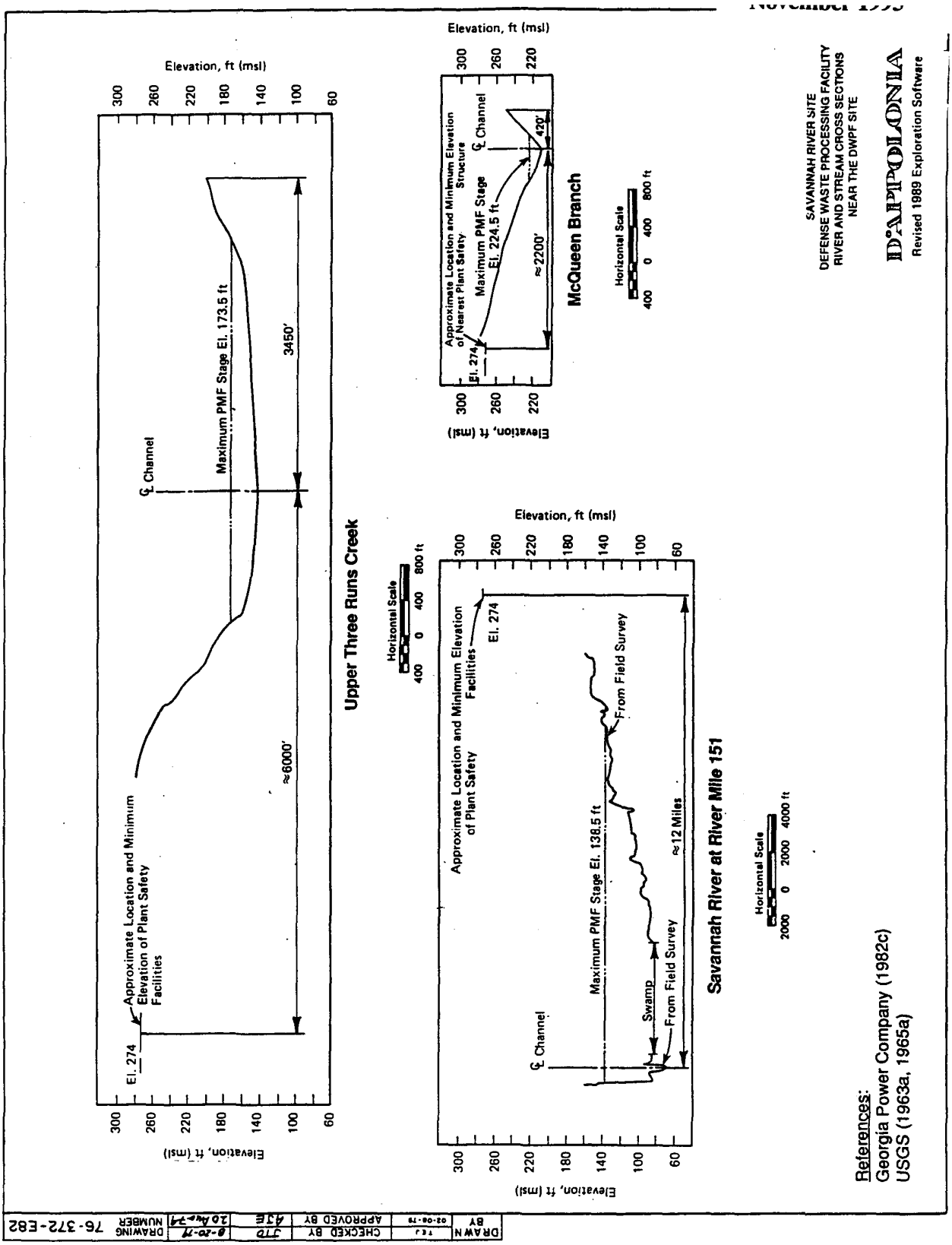

Figure 3.4-2 River and Stream Cross Sections Near the DWPF Site

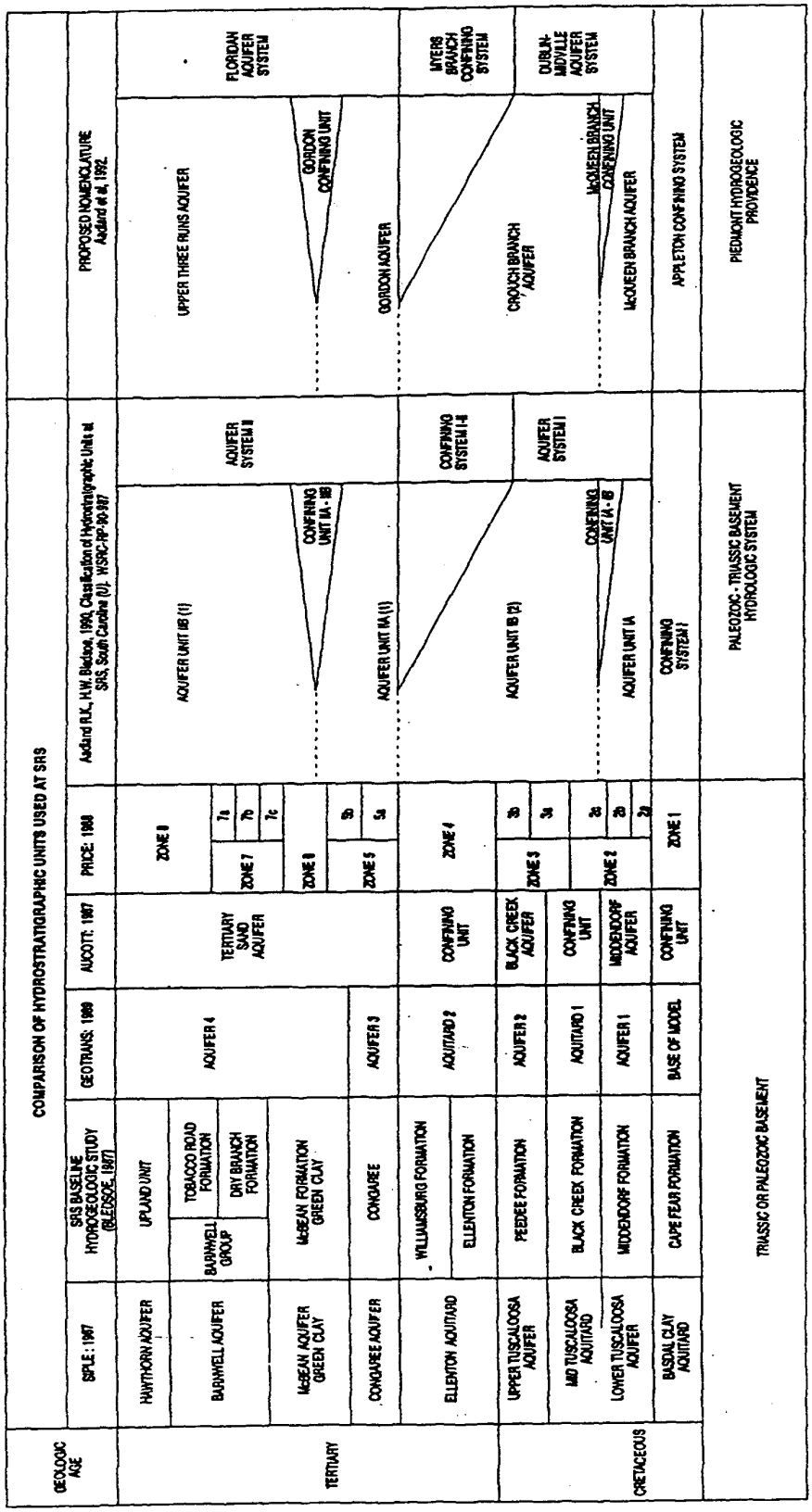

Note
(1) Located within the different units can be individual zones of relatively higher or lower permeability
(2) Hydrostratigraphic boundaries do not necessarily coincide with stratigraphic boundaries

Figure 3.4-3 Hydrostratographic Nomenclature

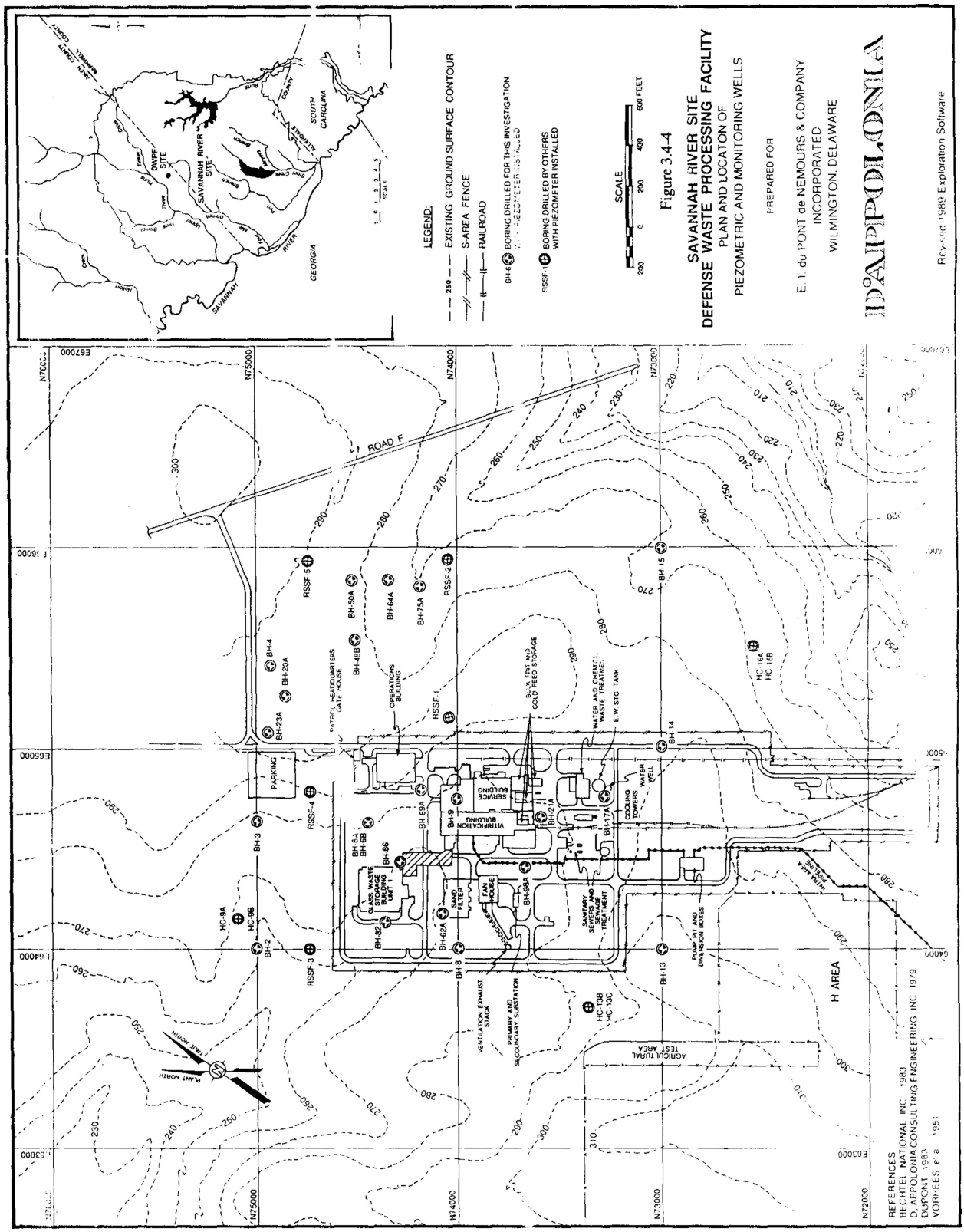

Figure 3.4-4 Plan View for Piezometric and Monitoring Wells

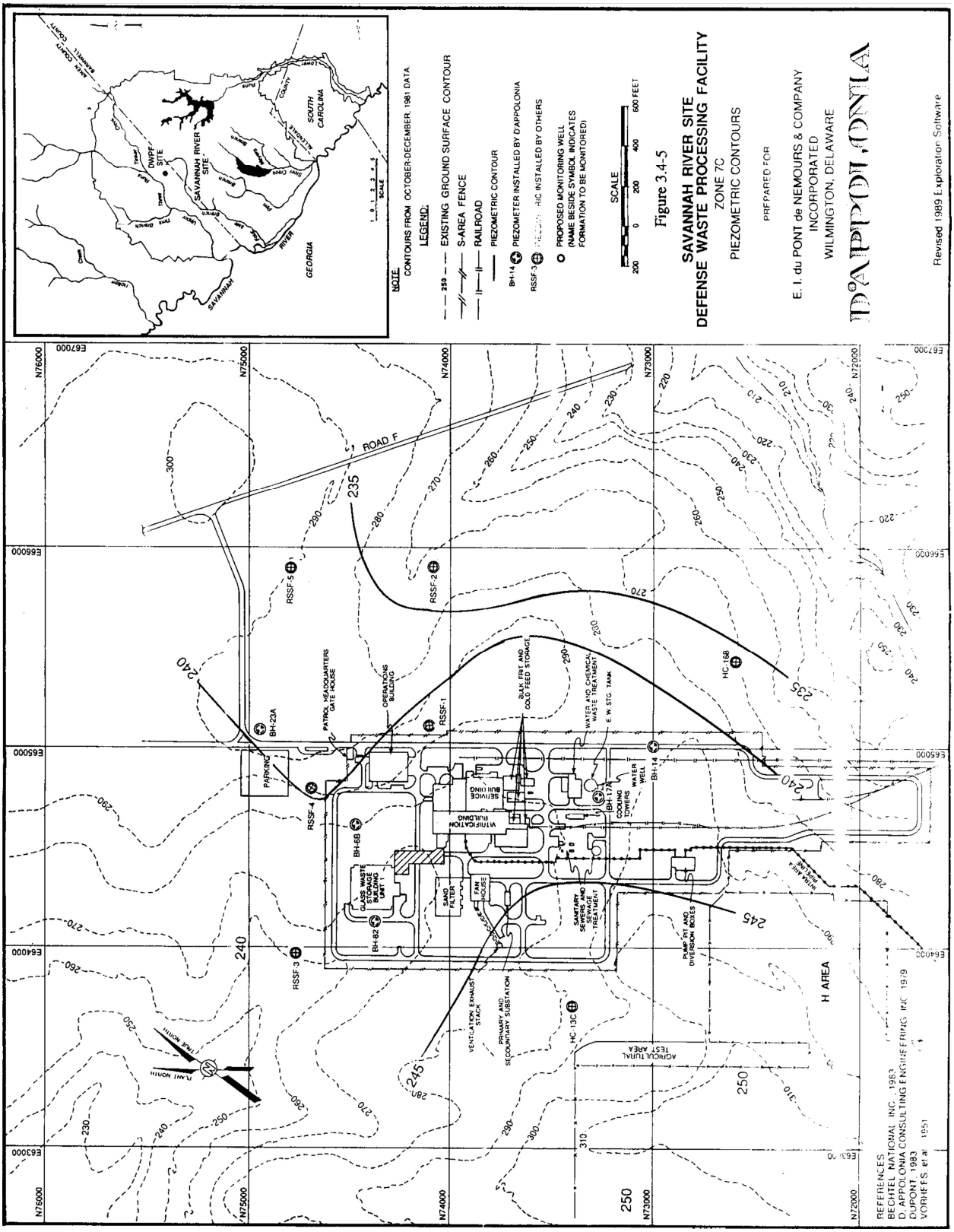

Figure 3.4-5 Zone 7c, Piezometric Contours

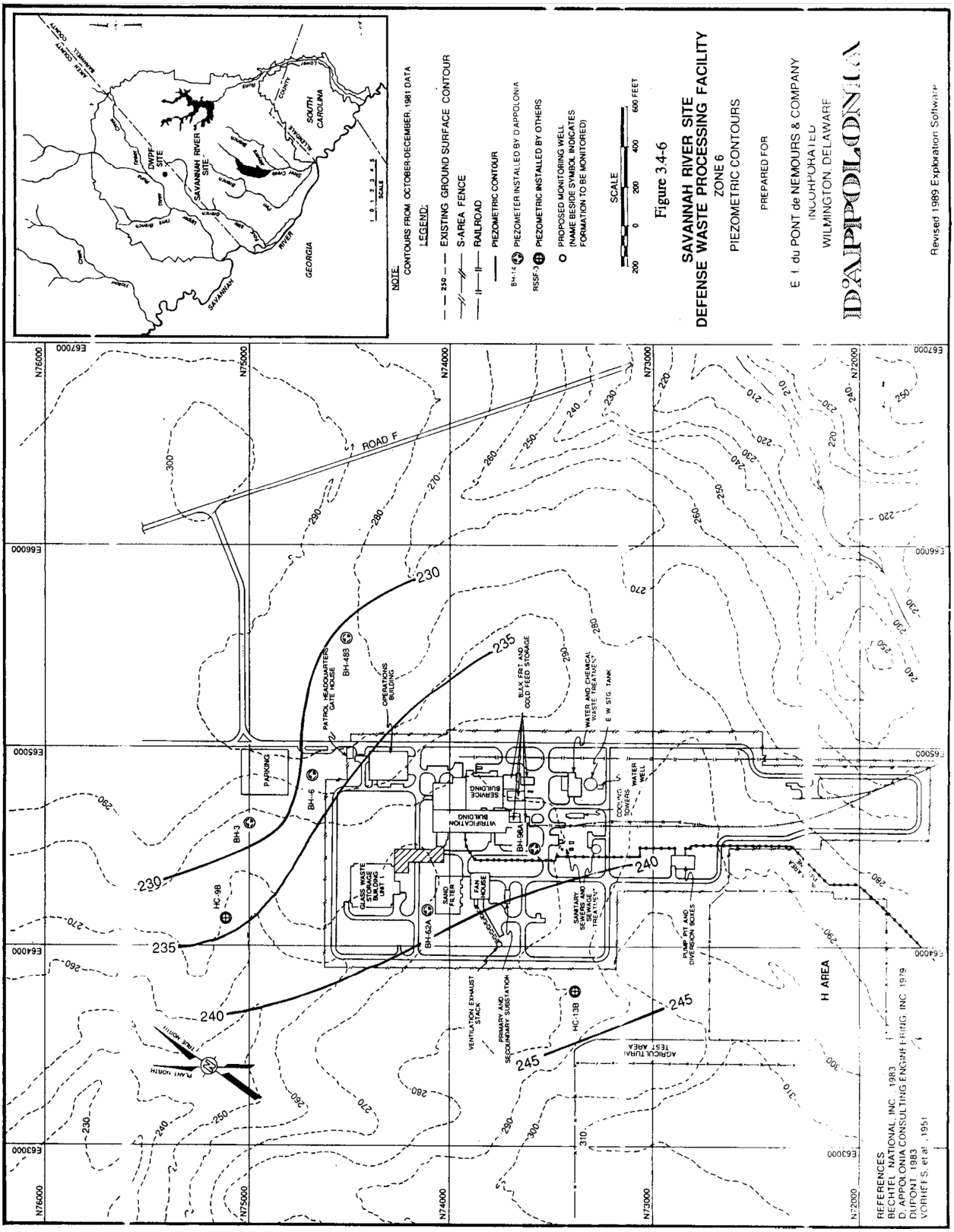

Figure 3.4-6 Zone 6, Piezometric Contours

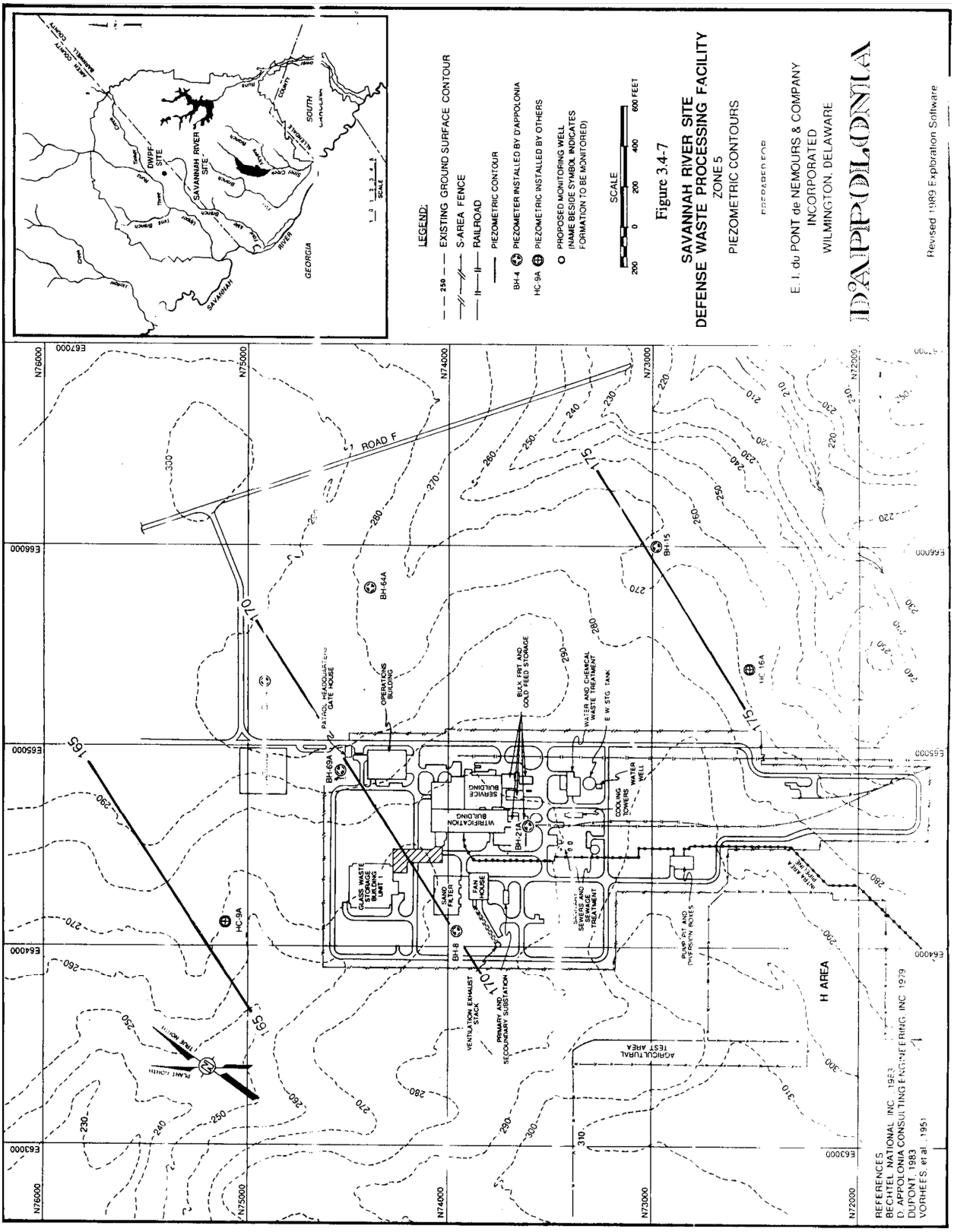

Figure 3.4-7 Zone 5, Piezometric Contours

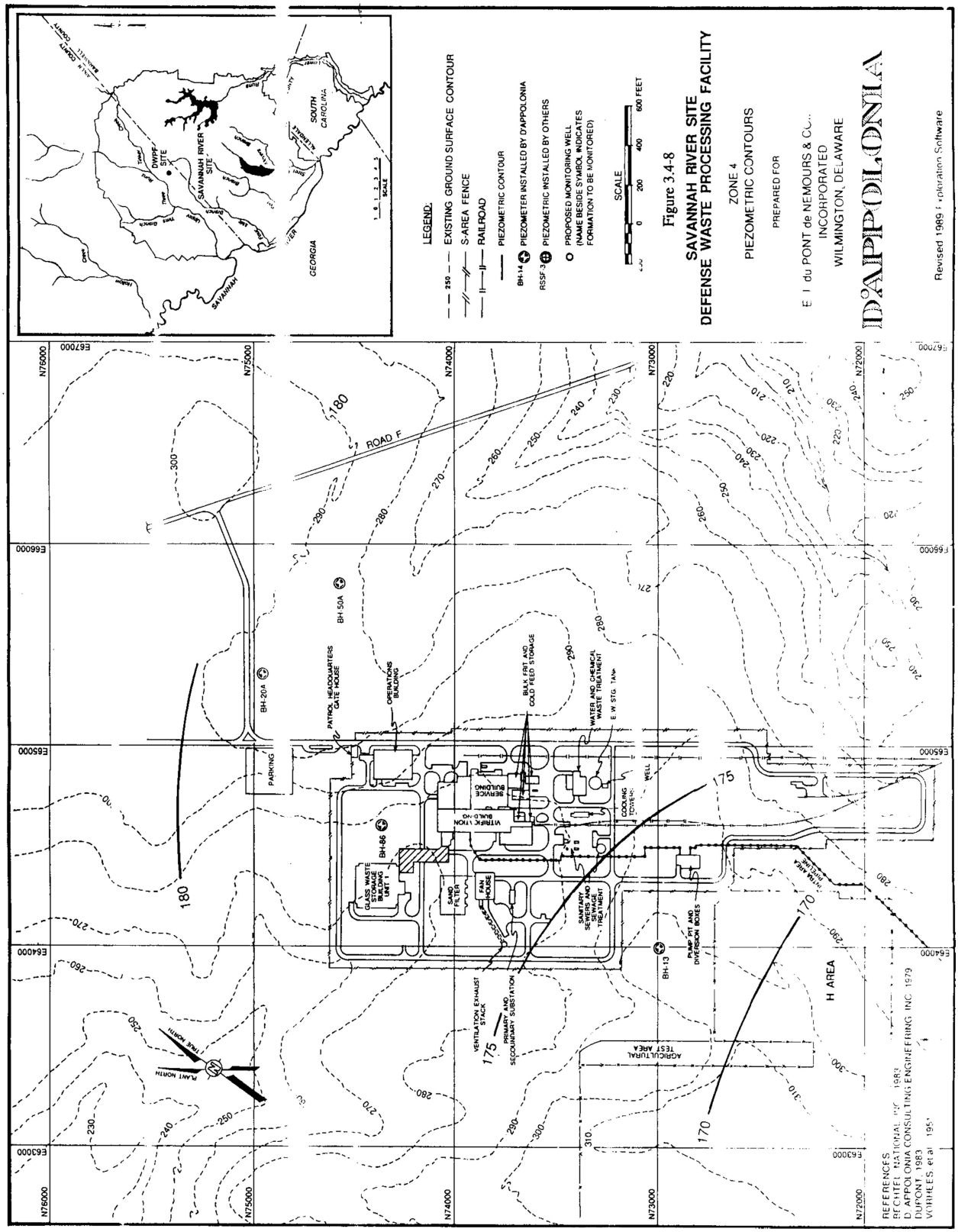

Figure 3.4-8 Zone 4, Piezometric Contours

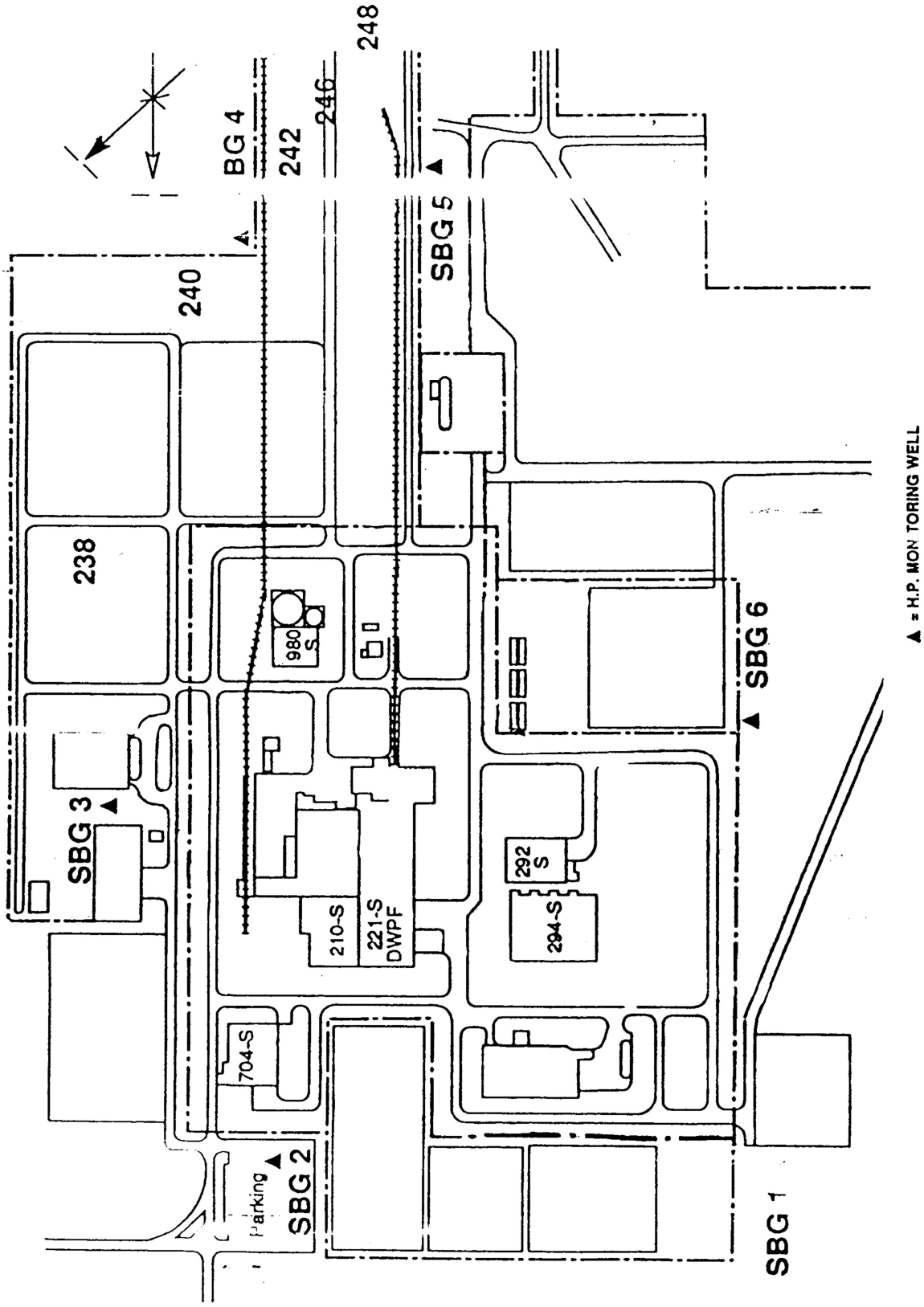

Figure 3.4-9 SBG Well Locations

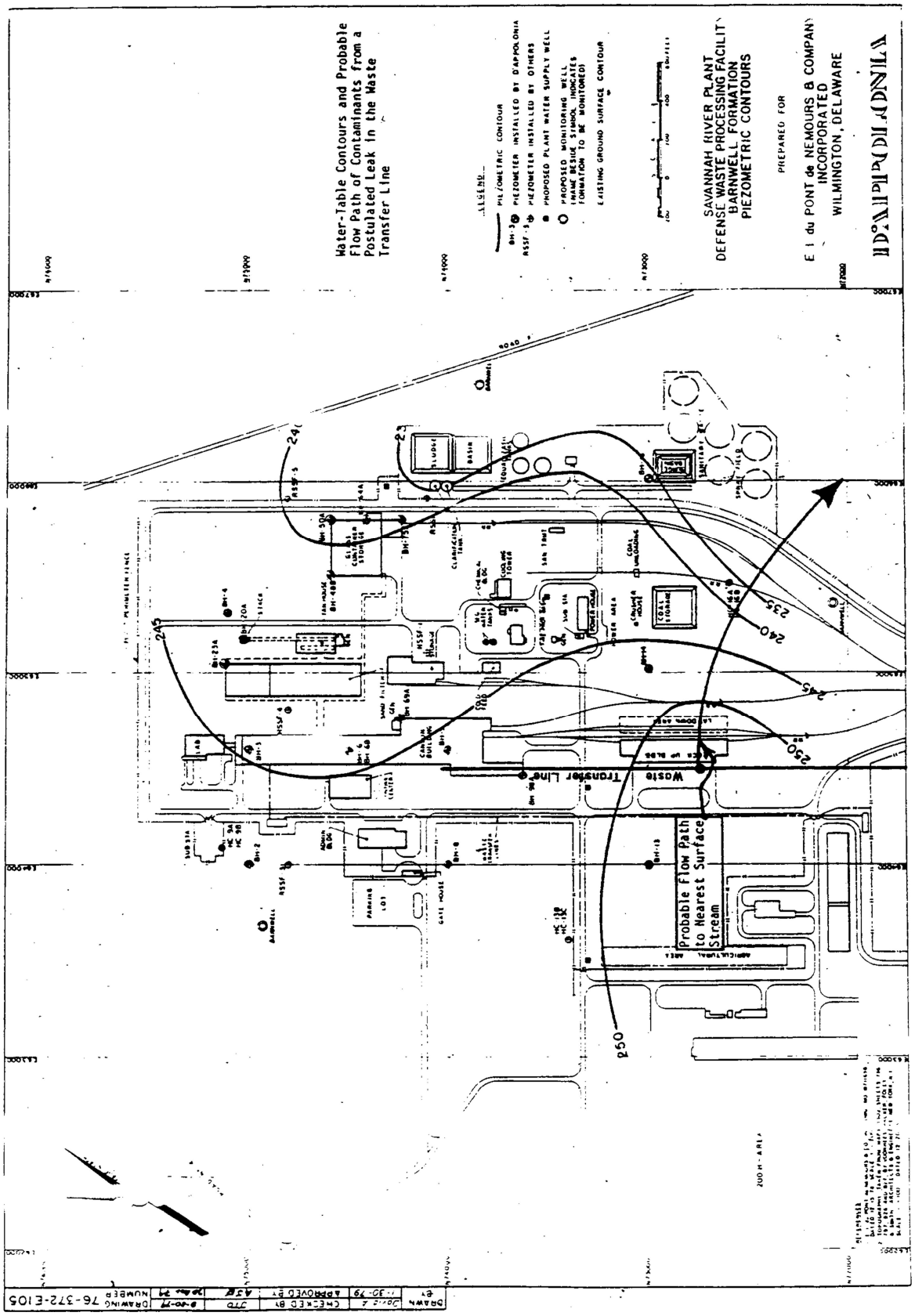

Figure 3.4-10 Flow Path

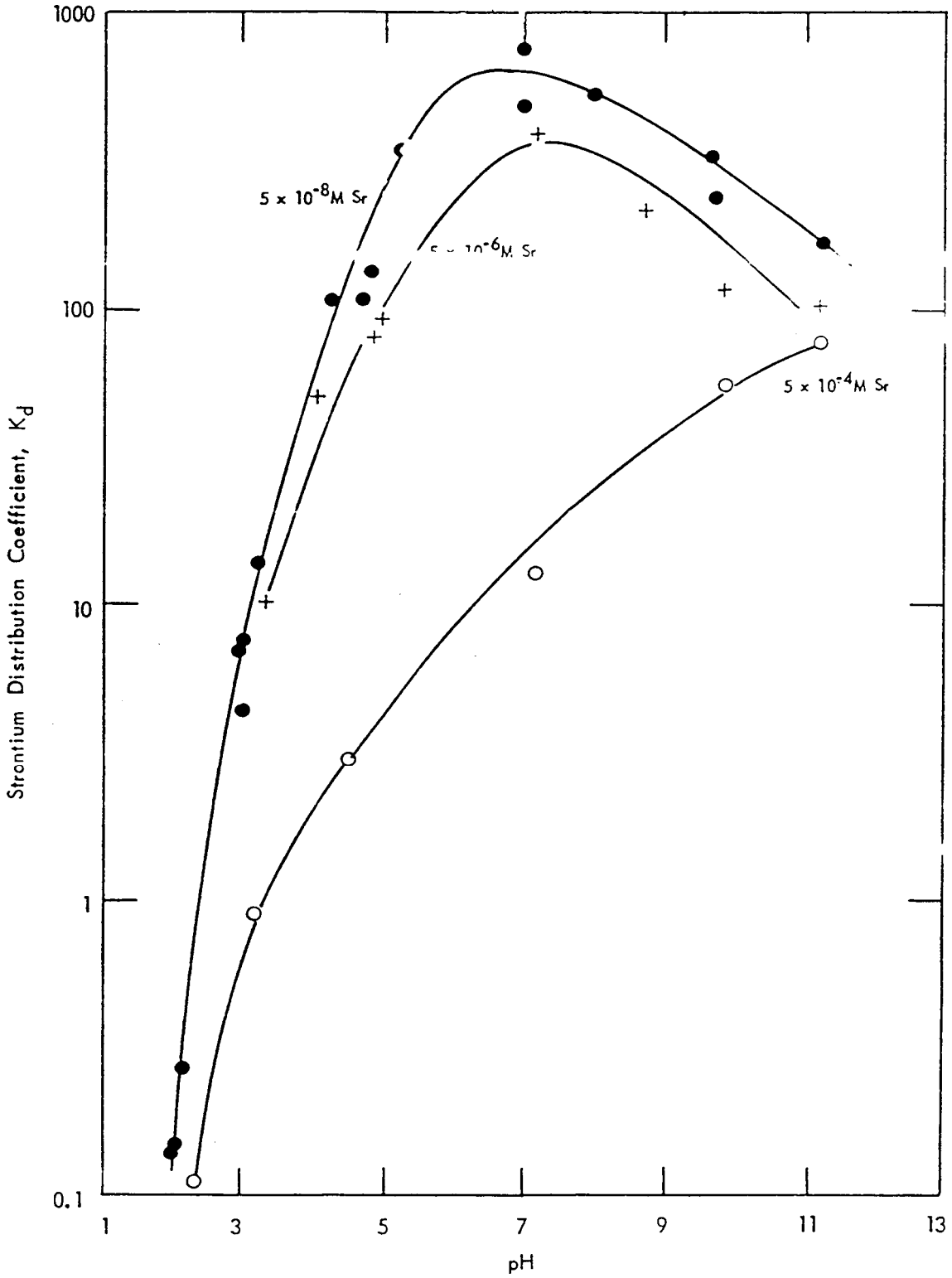

Figure 3.4-11 Strontium K_d

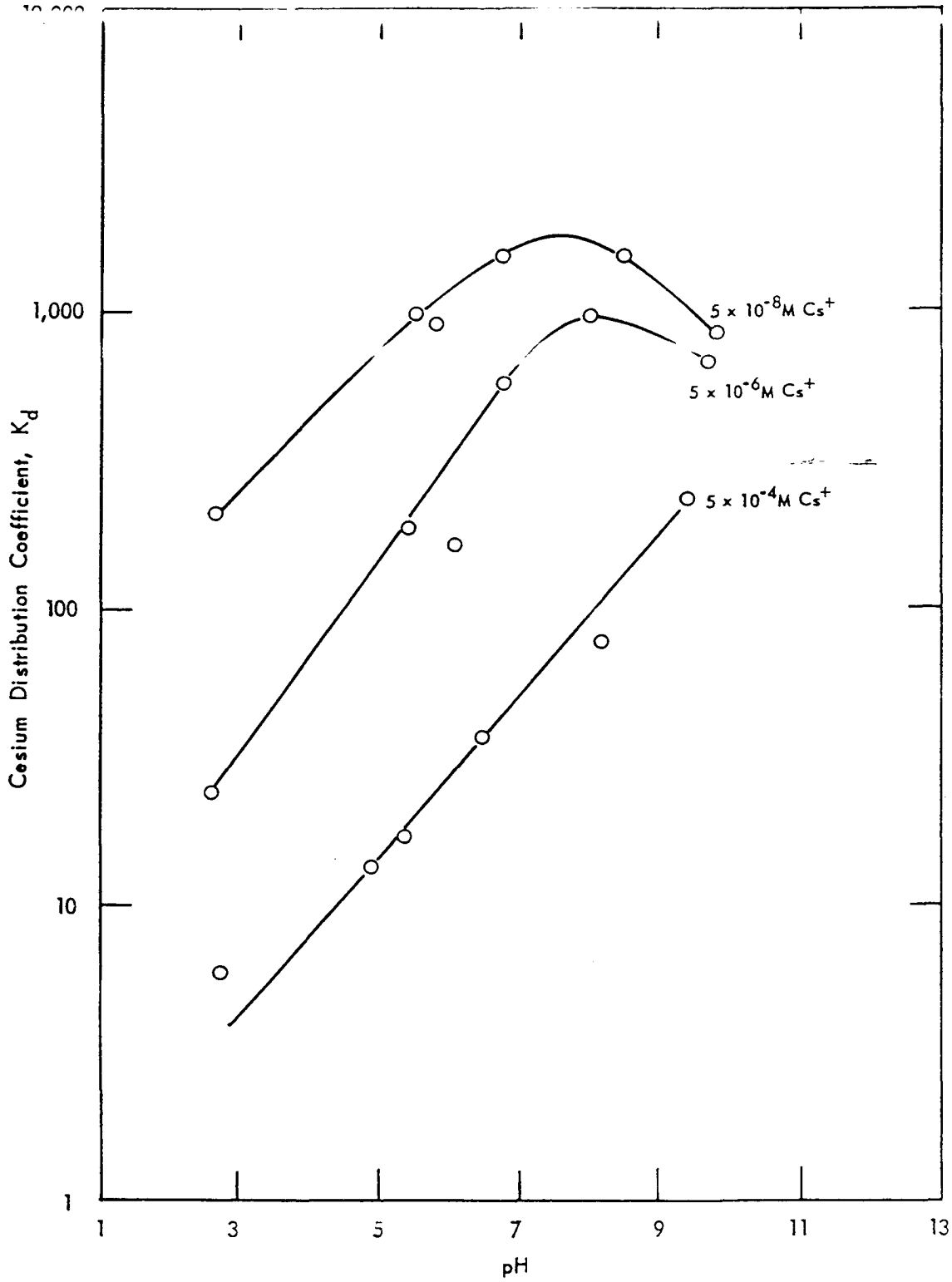

Figure 3.4-12 Cesium K_d

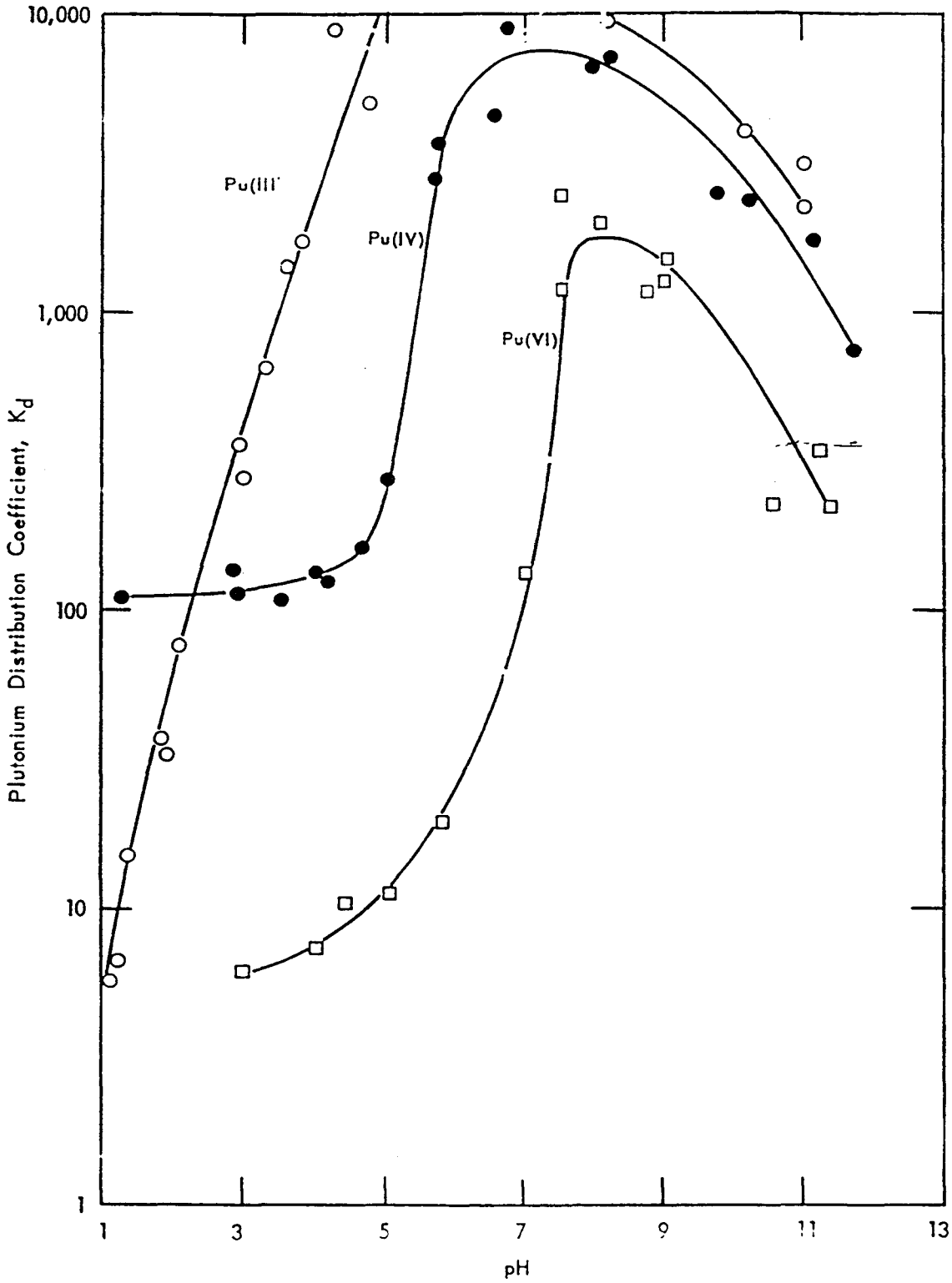

Figure 3.4-13 Plutonium K_d

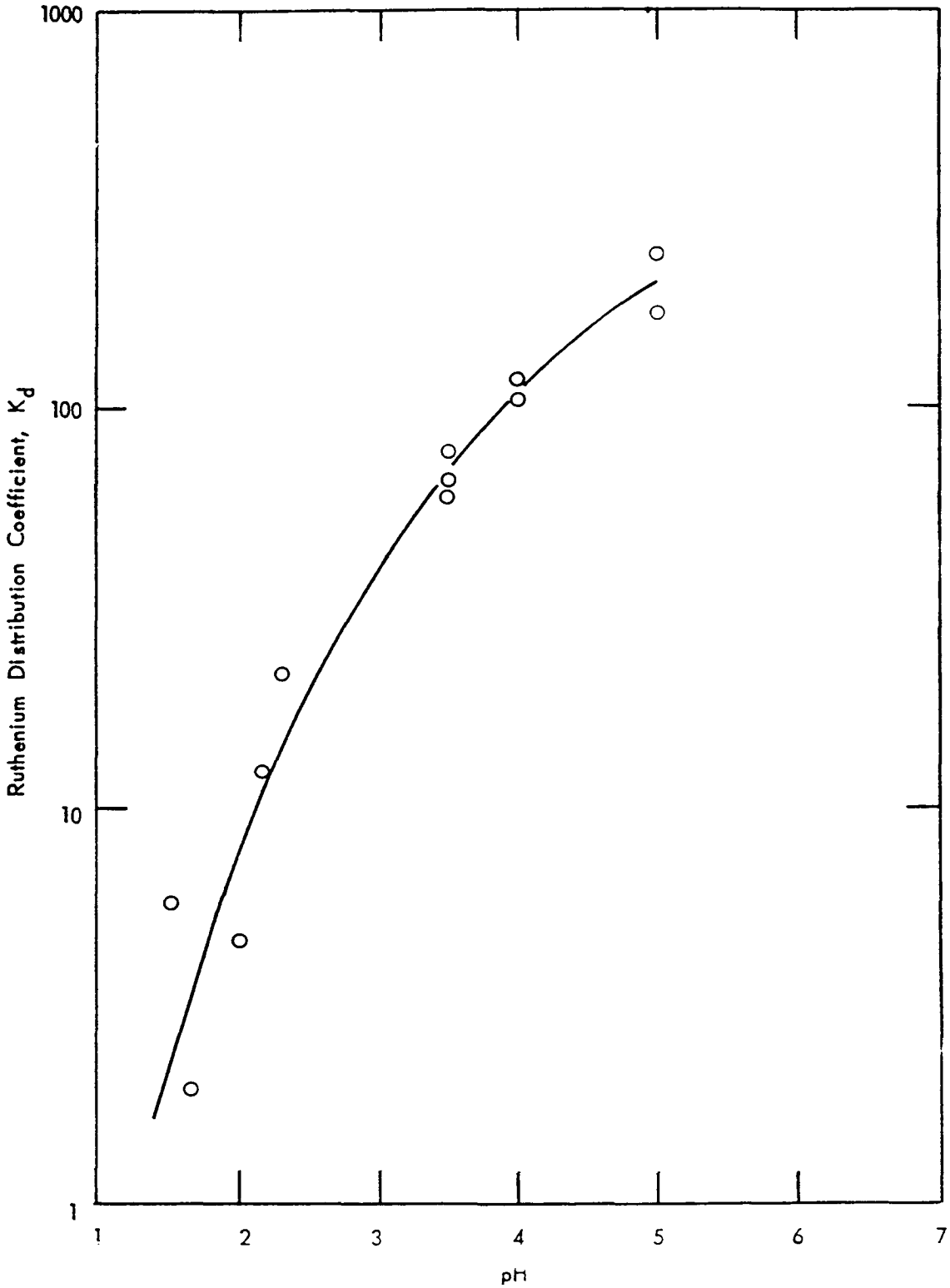

Figure 3.4-14 Ruthenium K_d

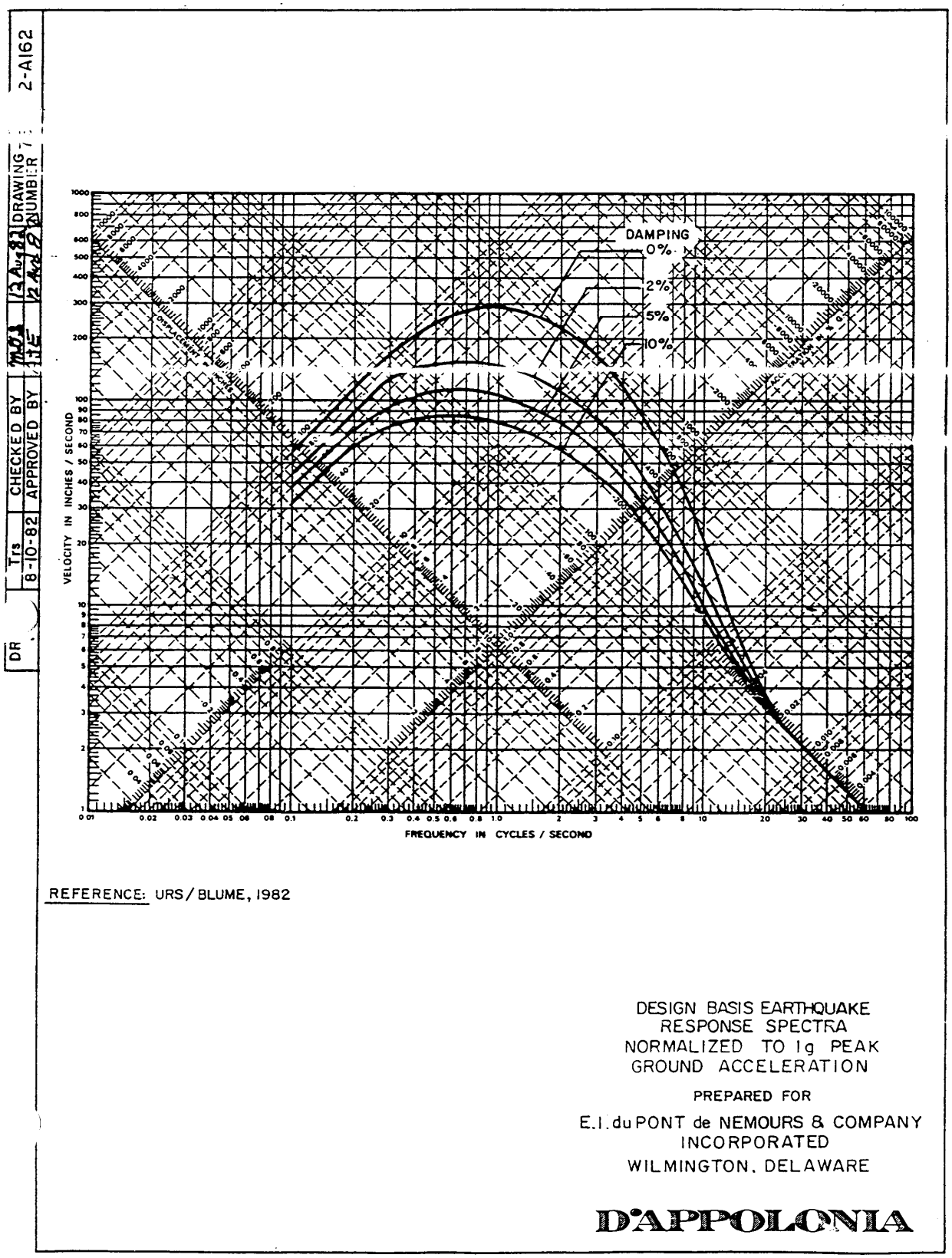

Figure 3.4-15 Response Spectra

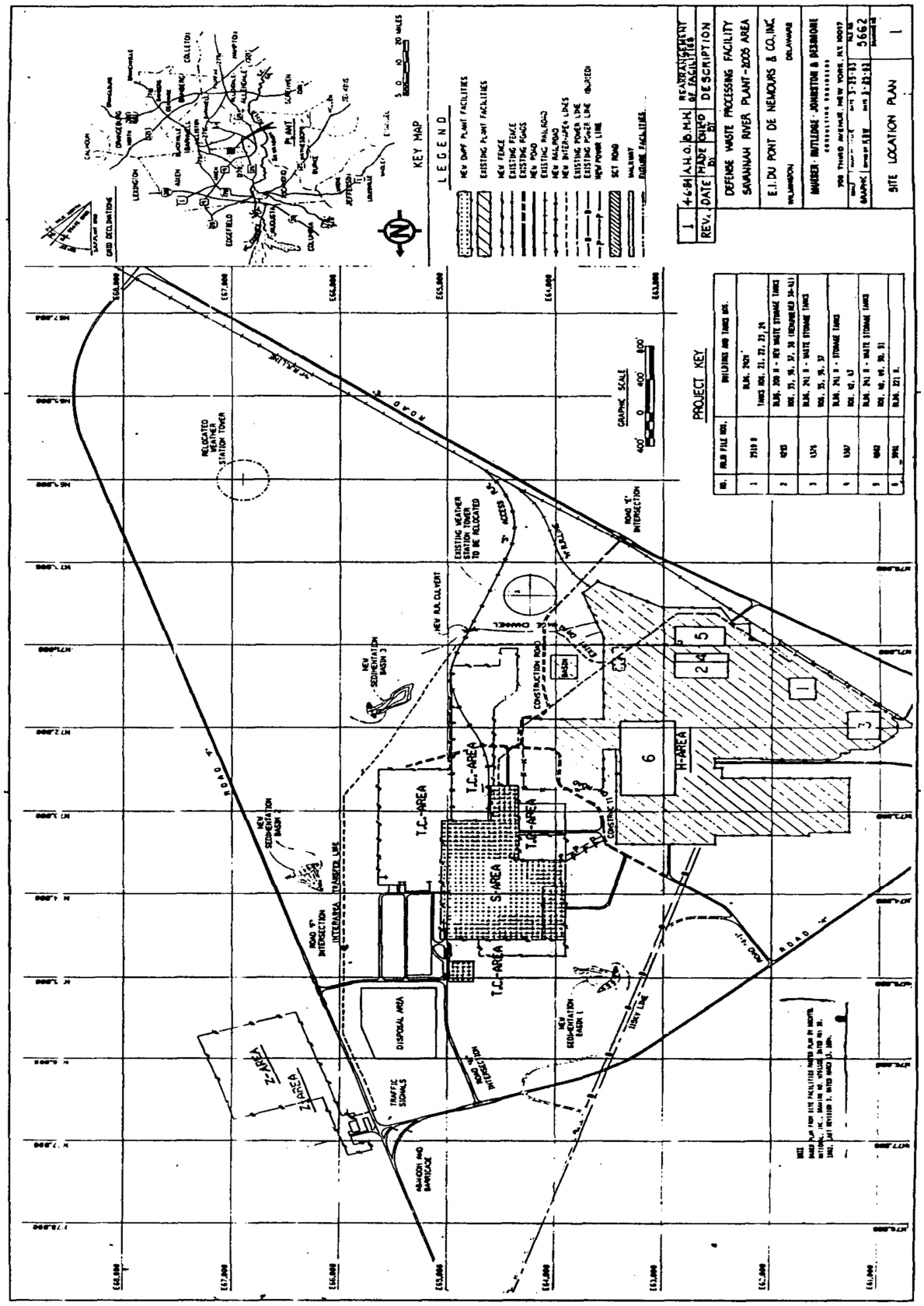

Figure 3.4-16 Site Location Plan

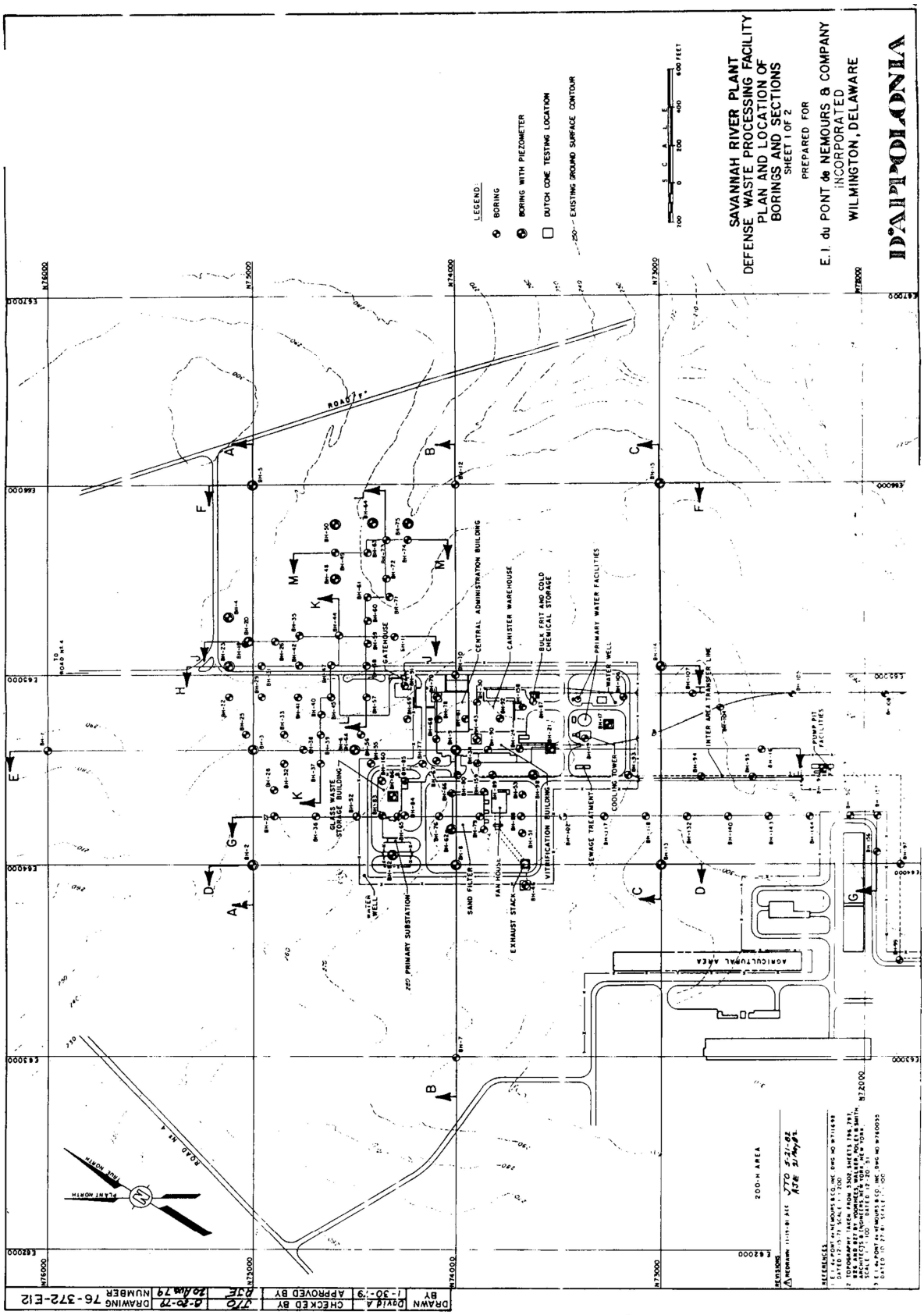

Figure 3.4-17 Plan View of Borings

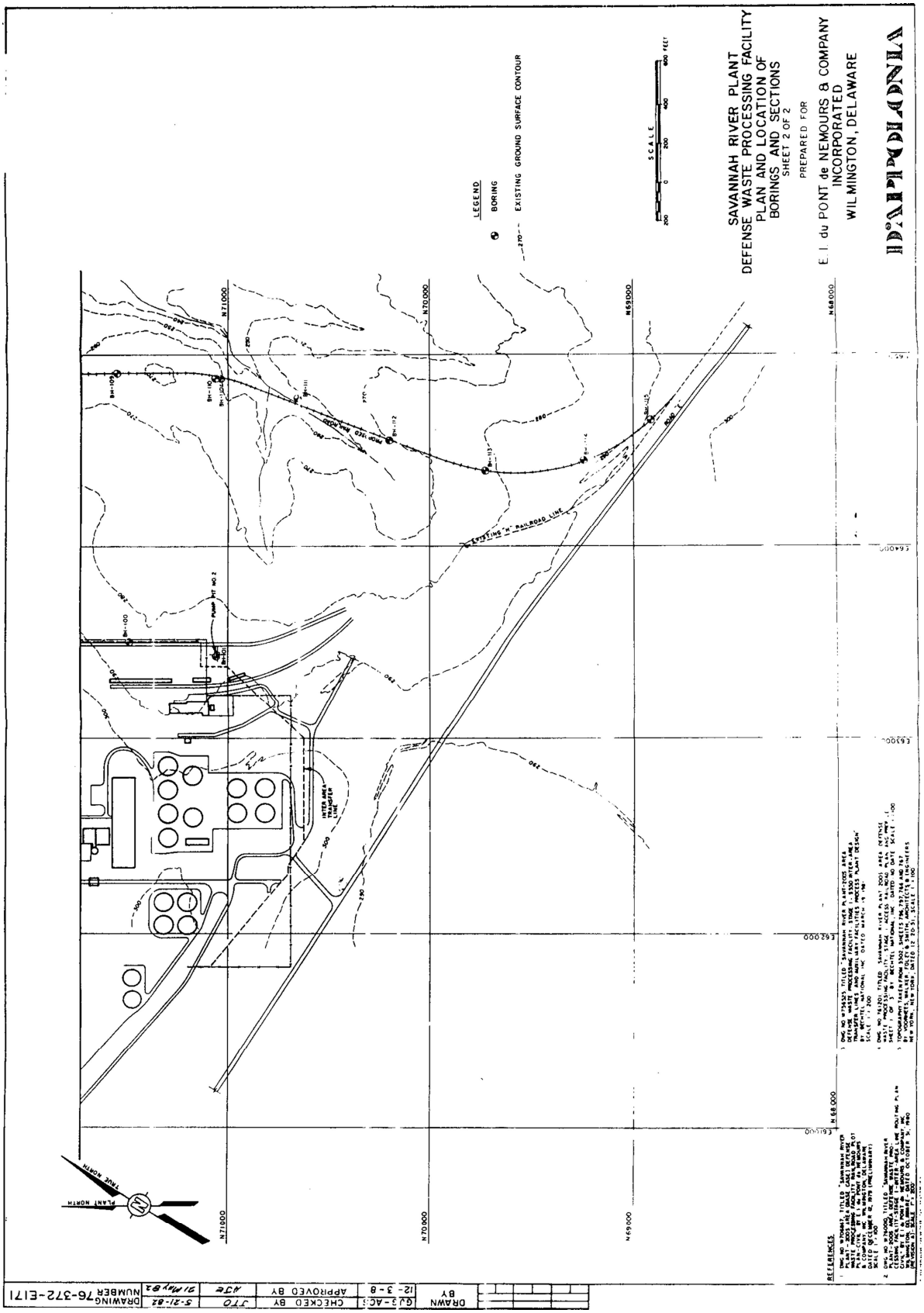

Figure 3.4-18 Plan View of Borings

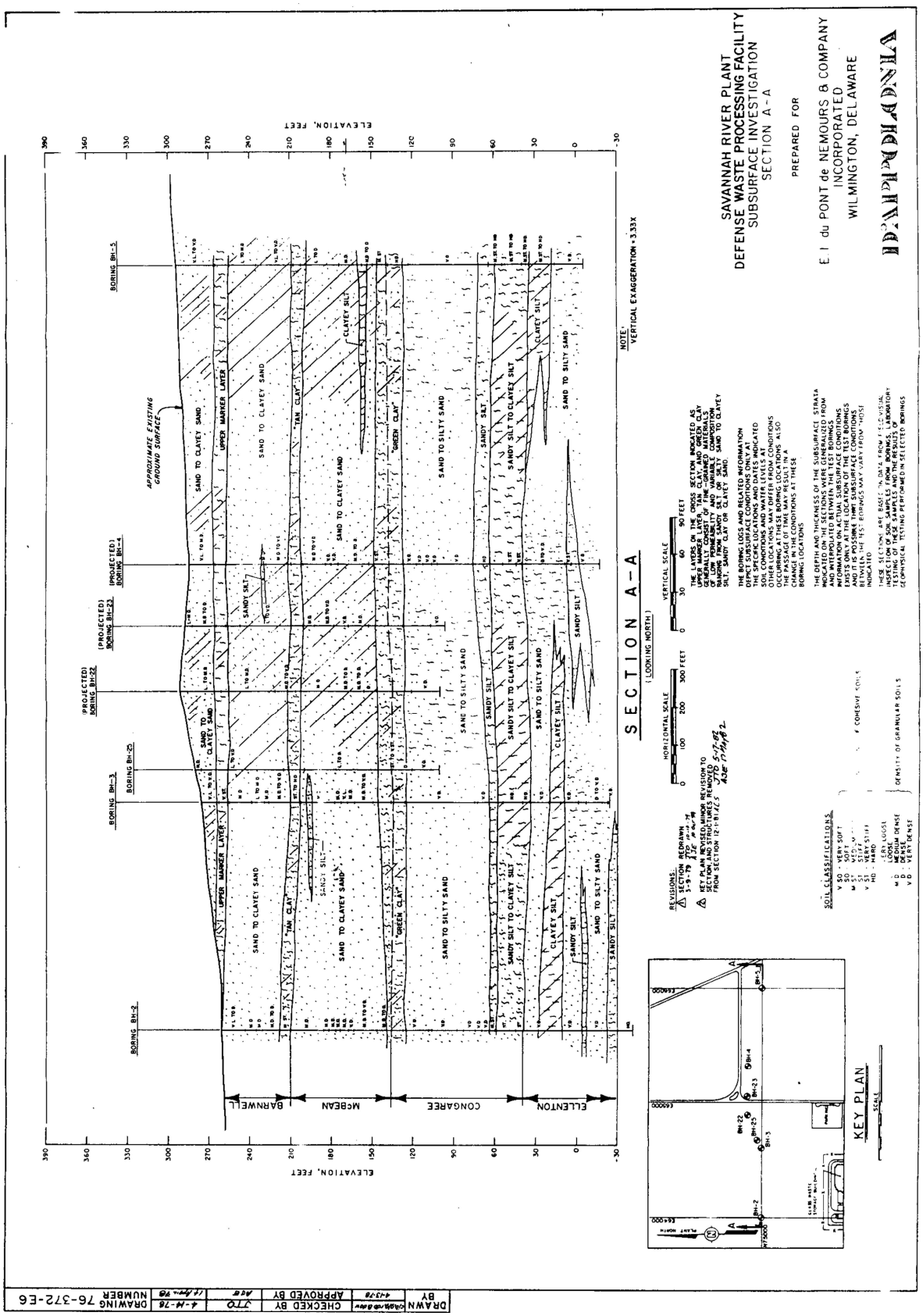

Figure 3.4-19 D'Appolonia Section AA

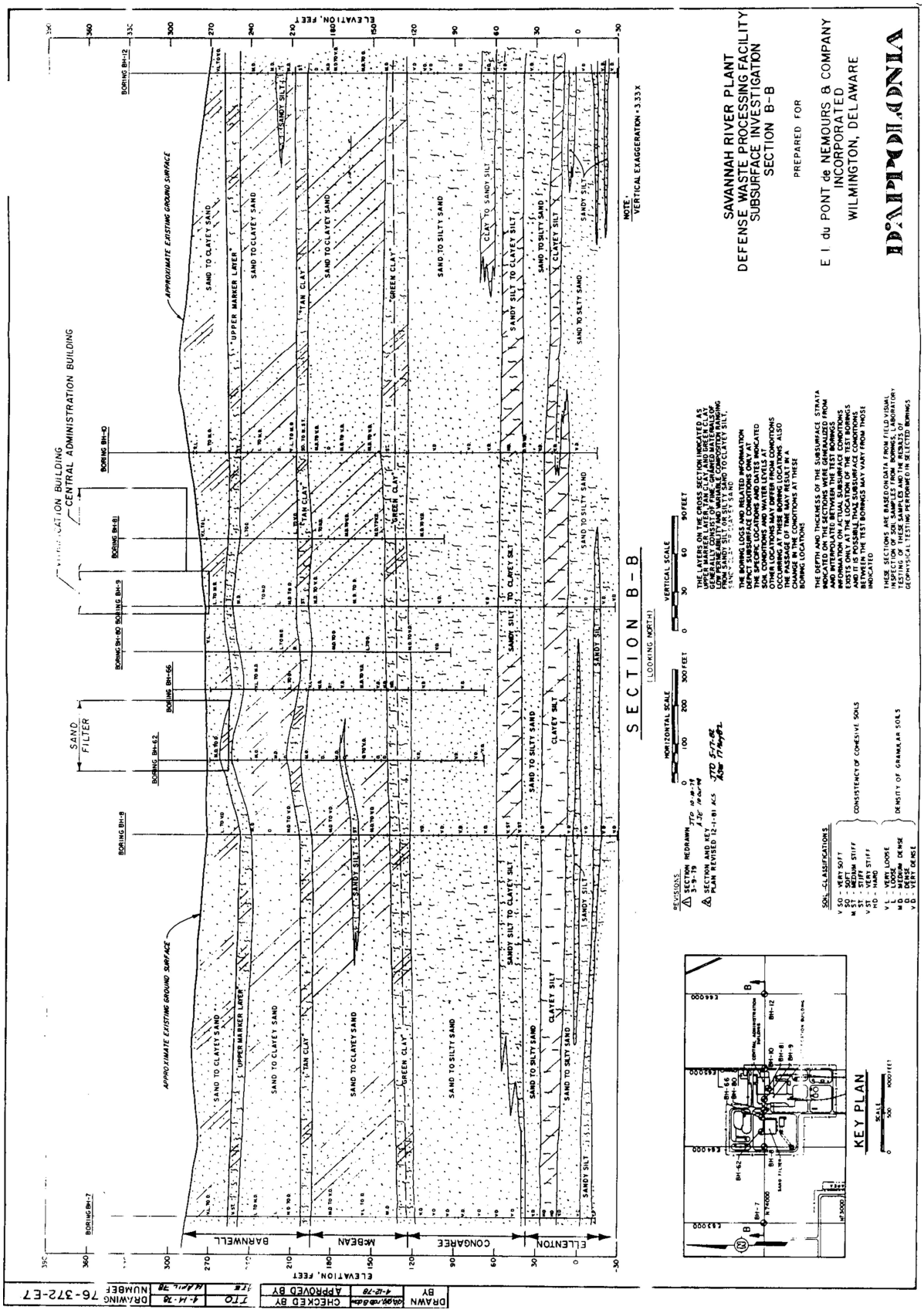

Figure 3.4-20 D'Appolonia Section BB

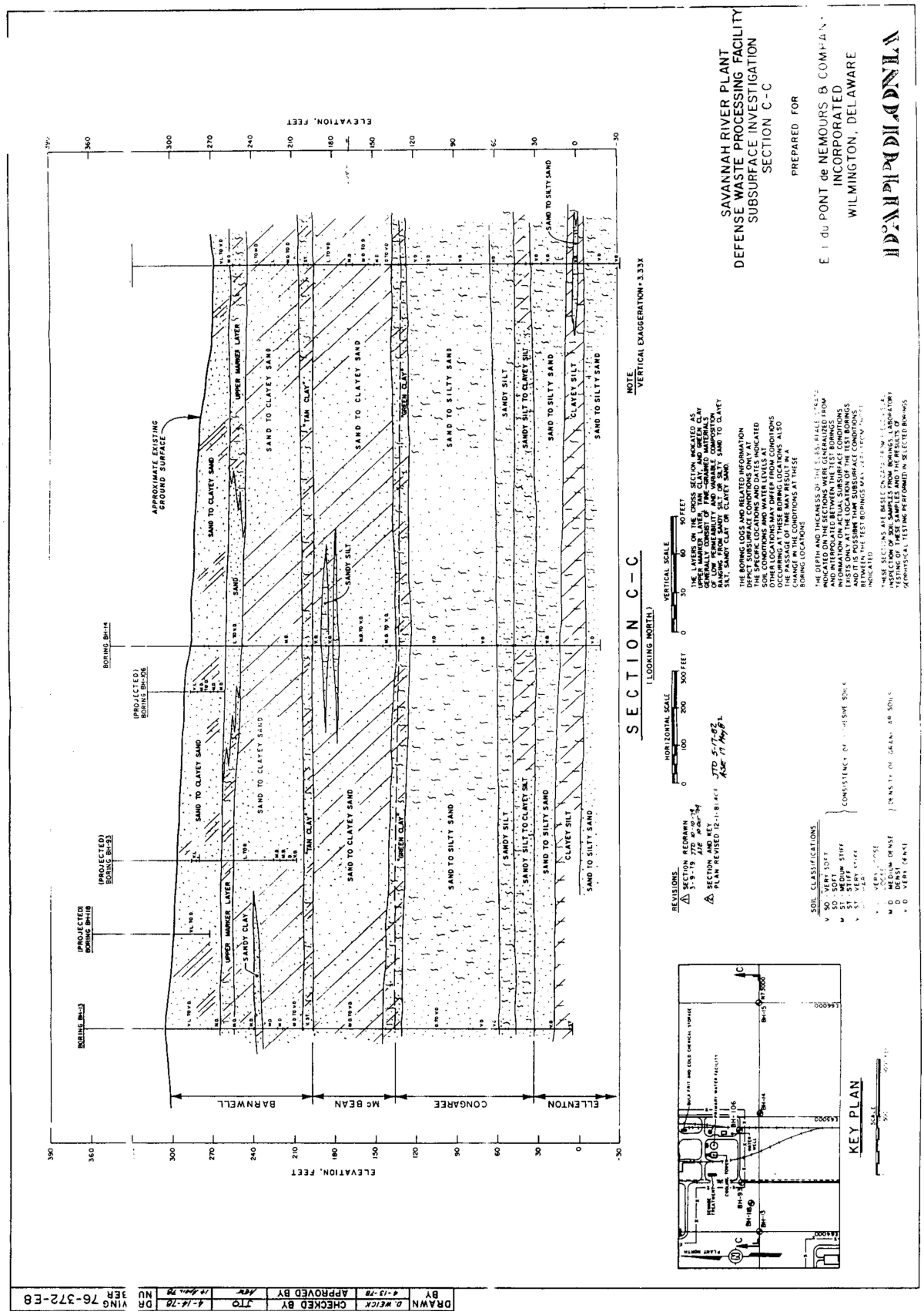

Figure 3.4-21 D'Appolonia Section CC

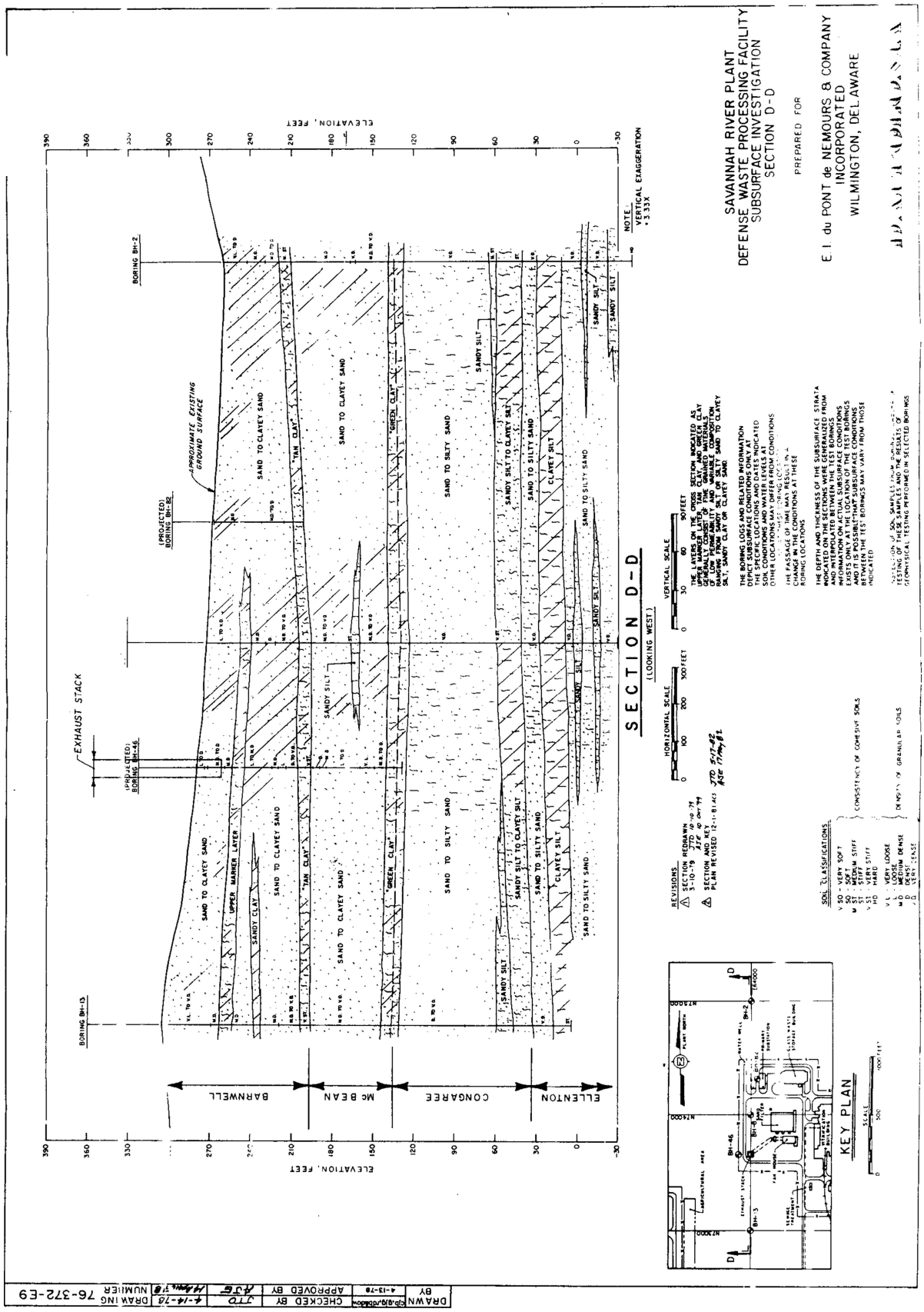

Figure 3.4-22 D'Appolonia Section DD

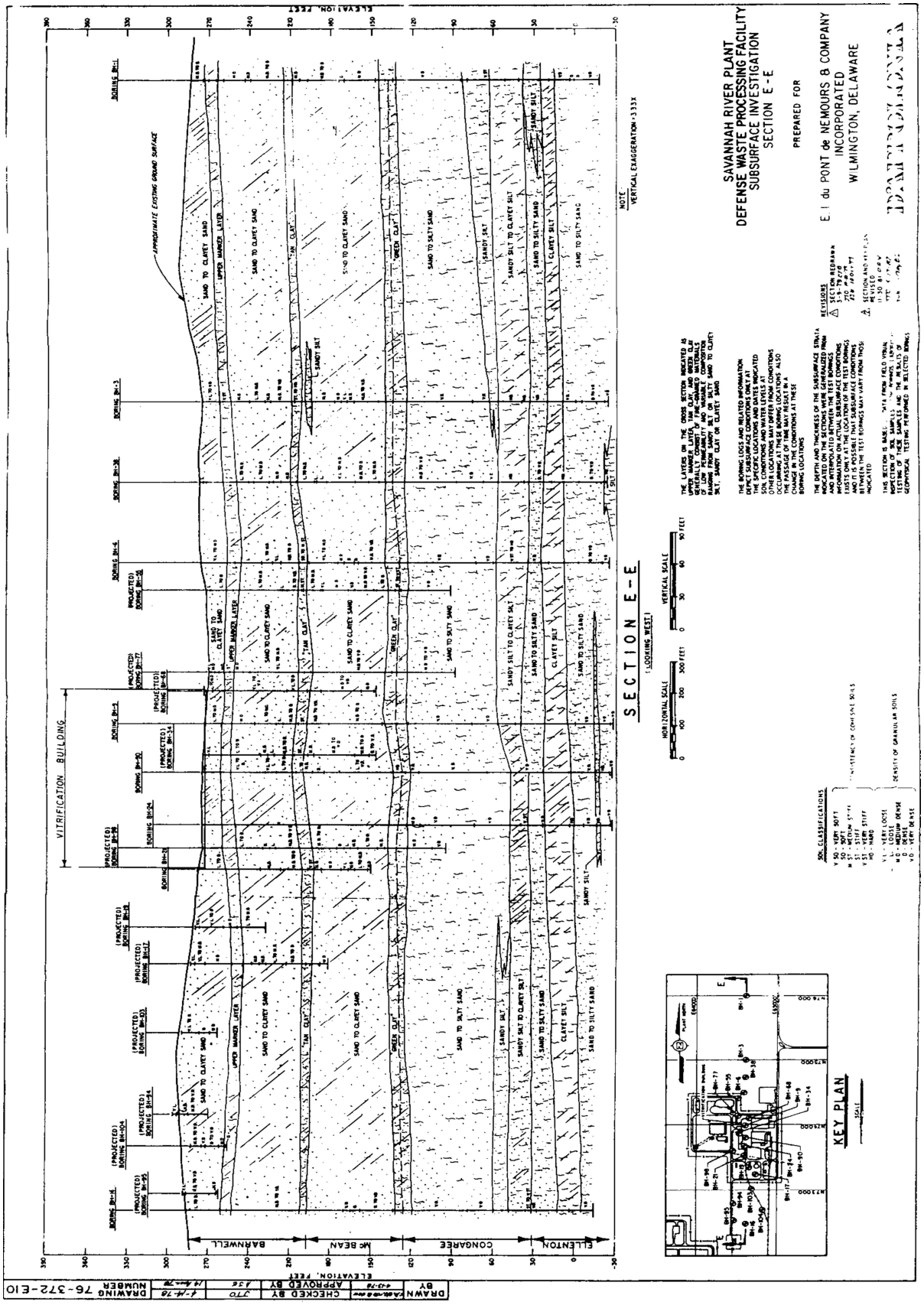

Figure 3.4-23 D'Appolonia Section EE

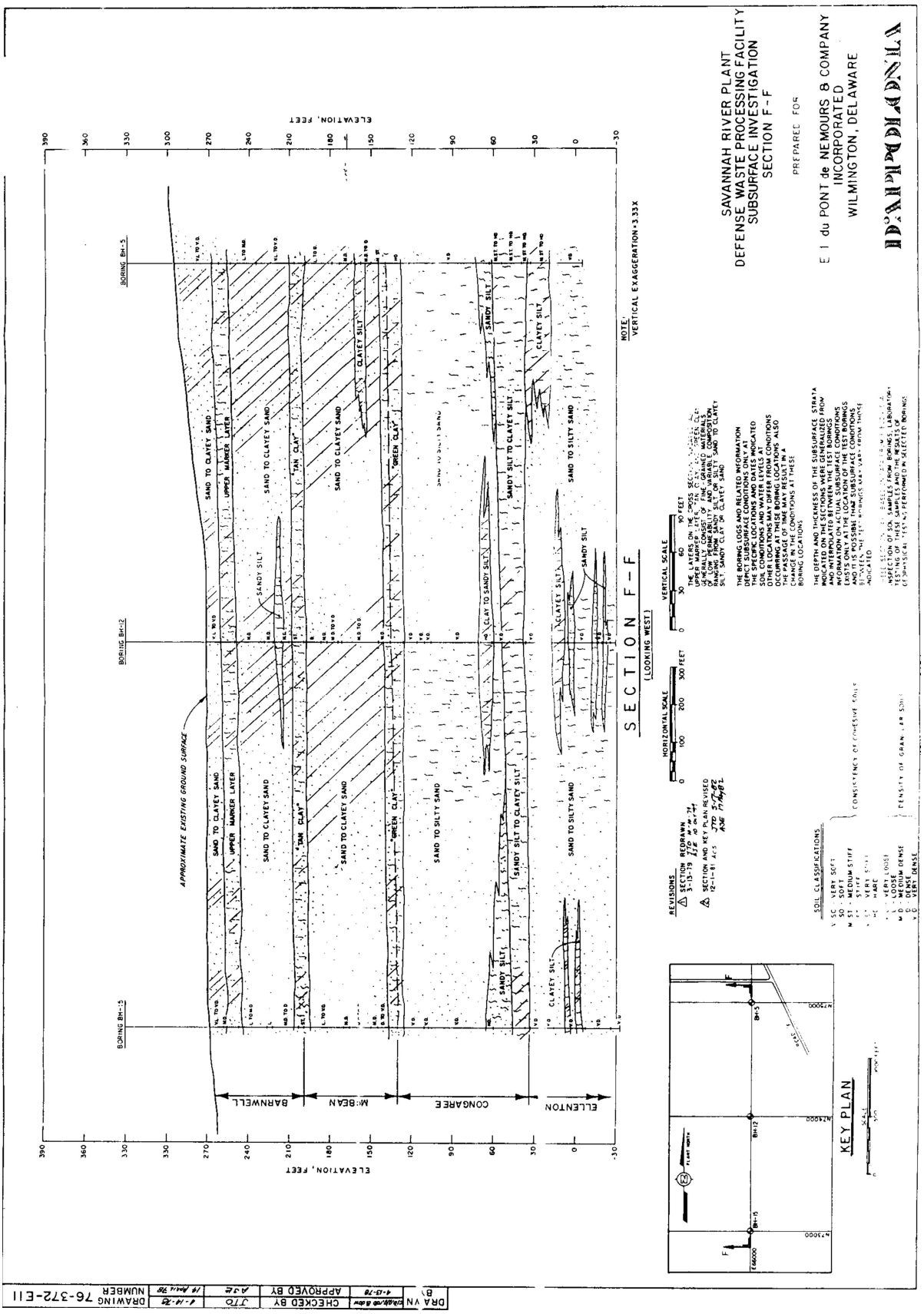

Figure 3.4-24 D'Appolonia Section FF

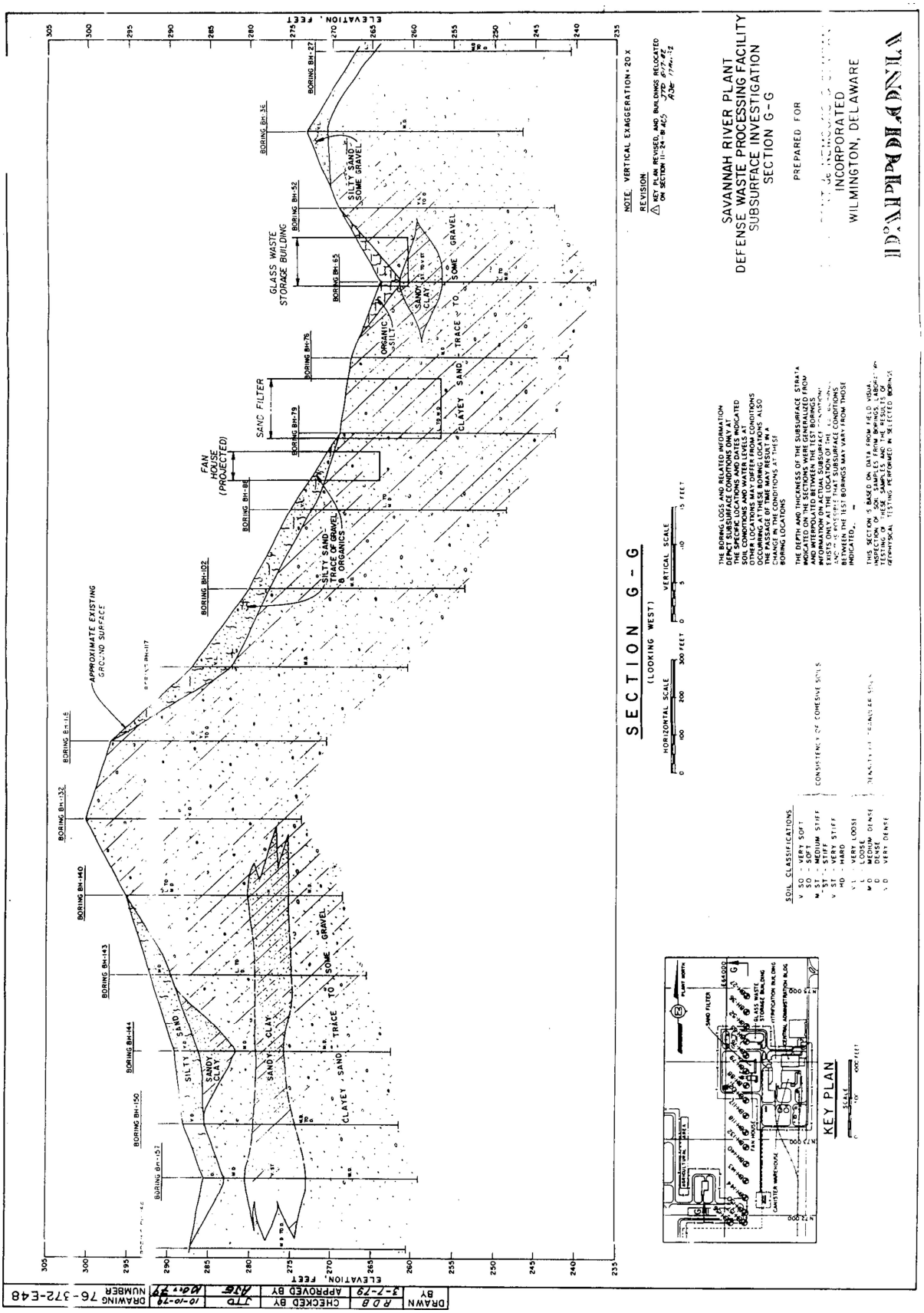

Figure 3.4-25 D'Appolonia Section GG

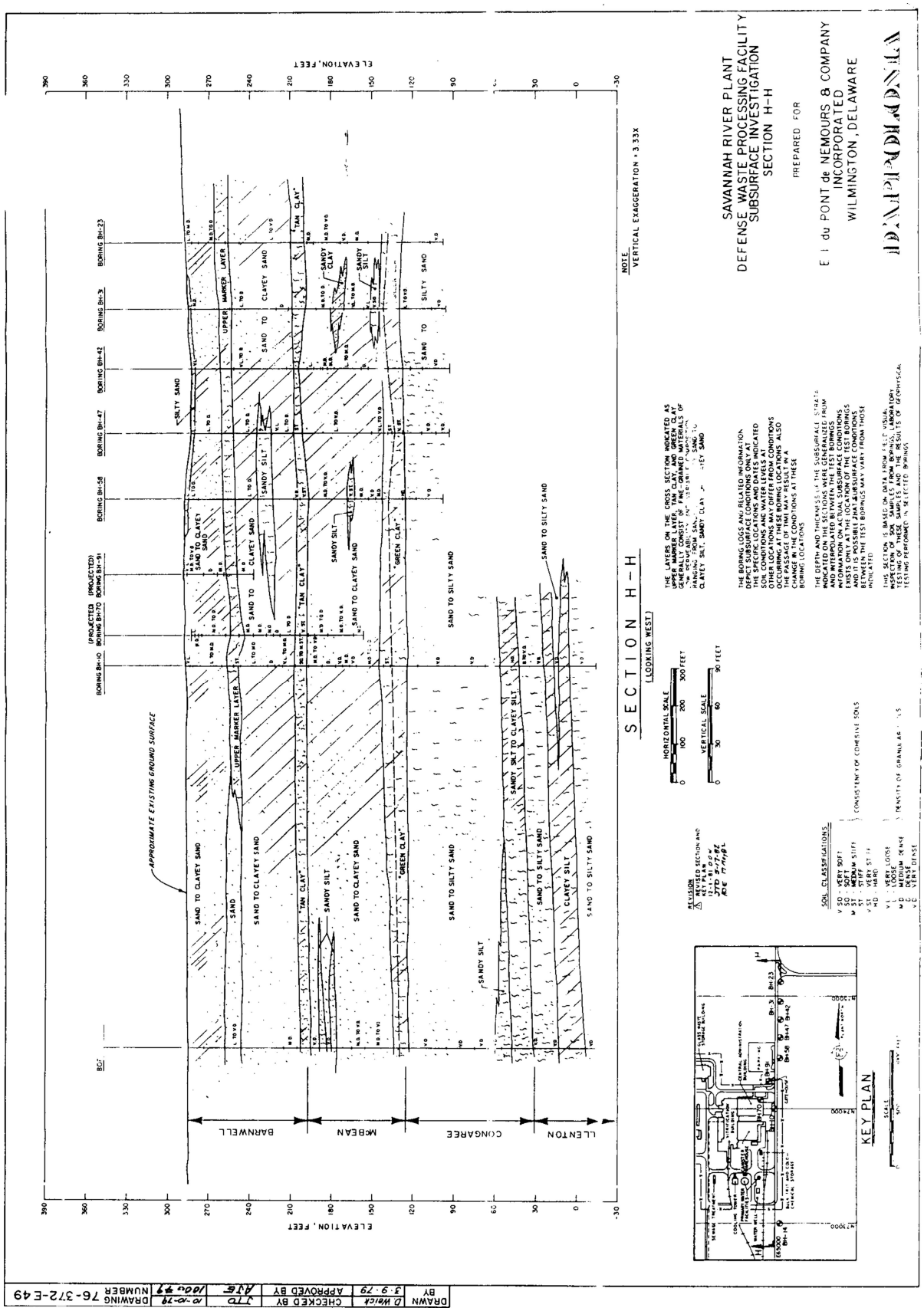

Figure 3.4-26 D'Appolonia Section HH

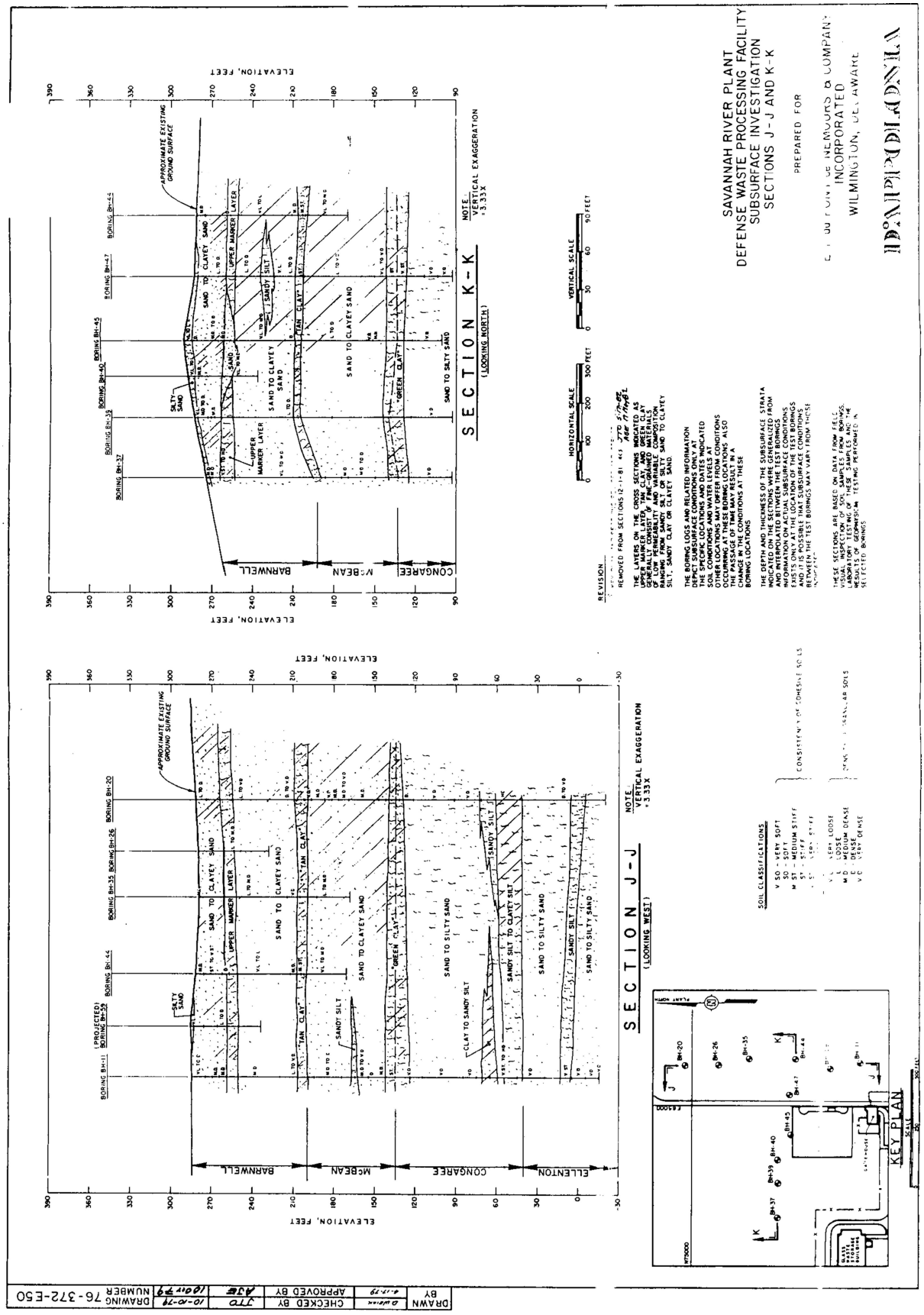

Figure 3.4-27 D'Appolonia Section JJ and KK

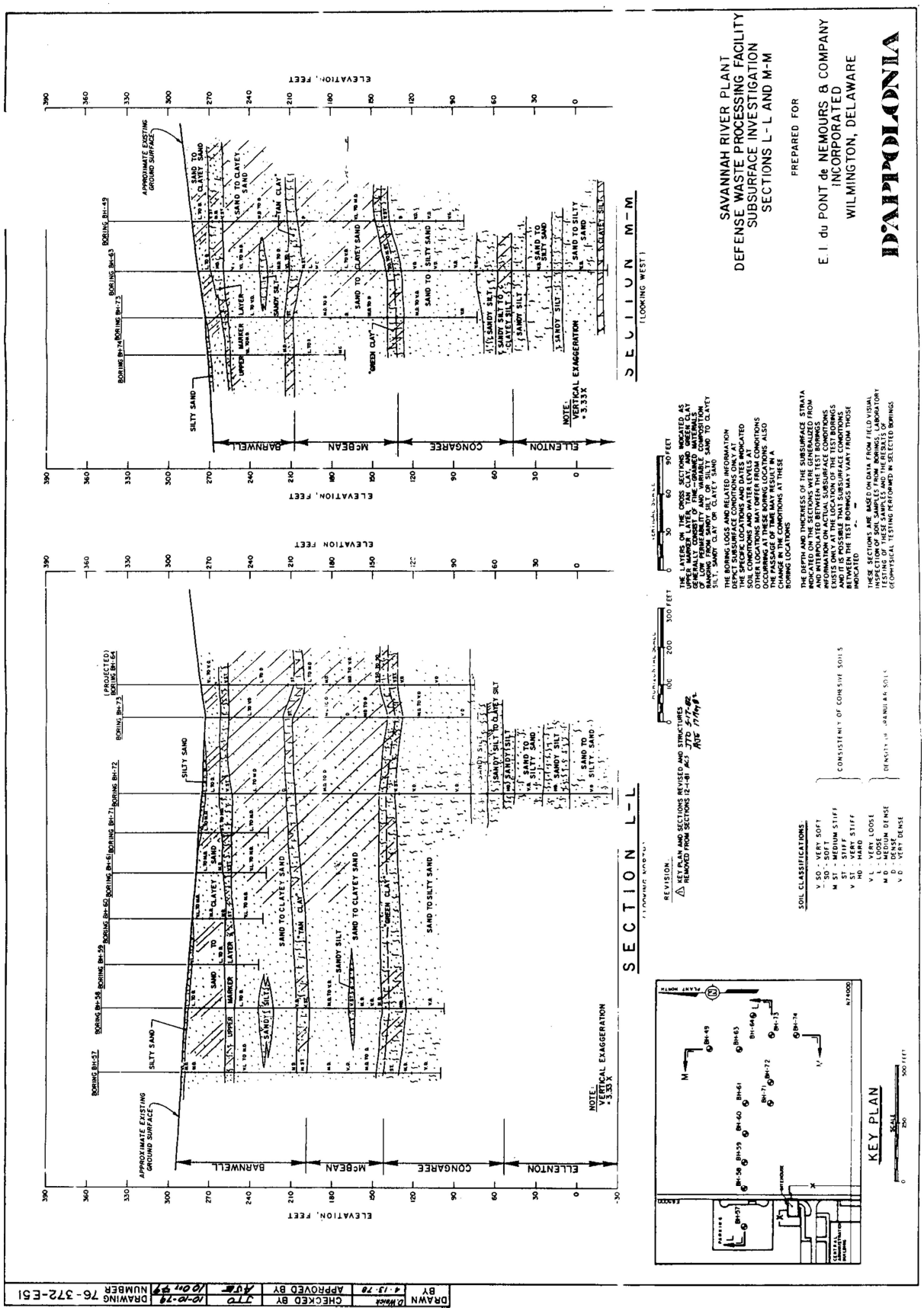

Figure 3.4-28 D'Appolonia Section LL and MM

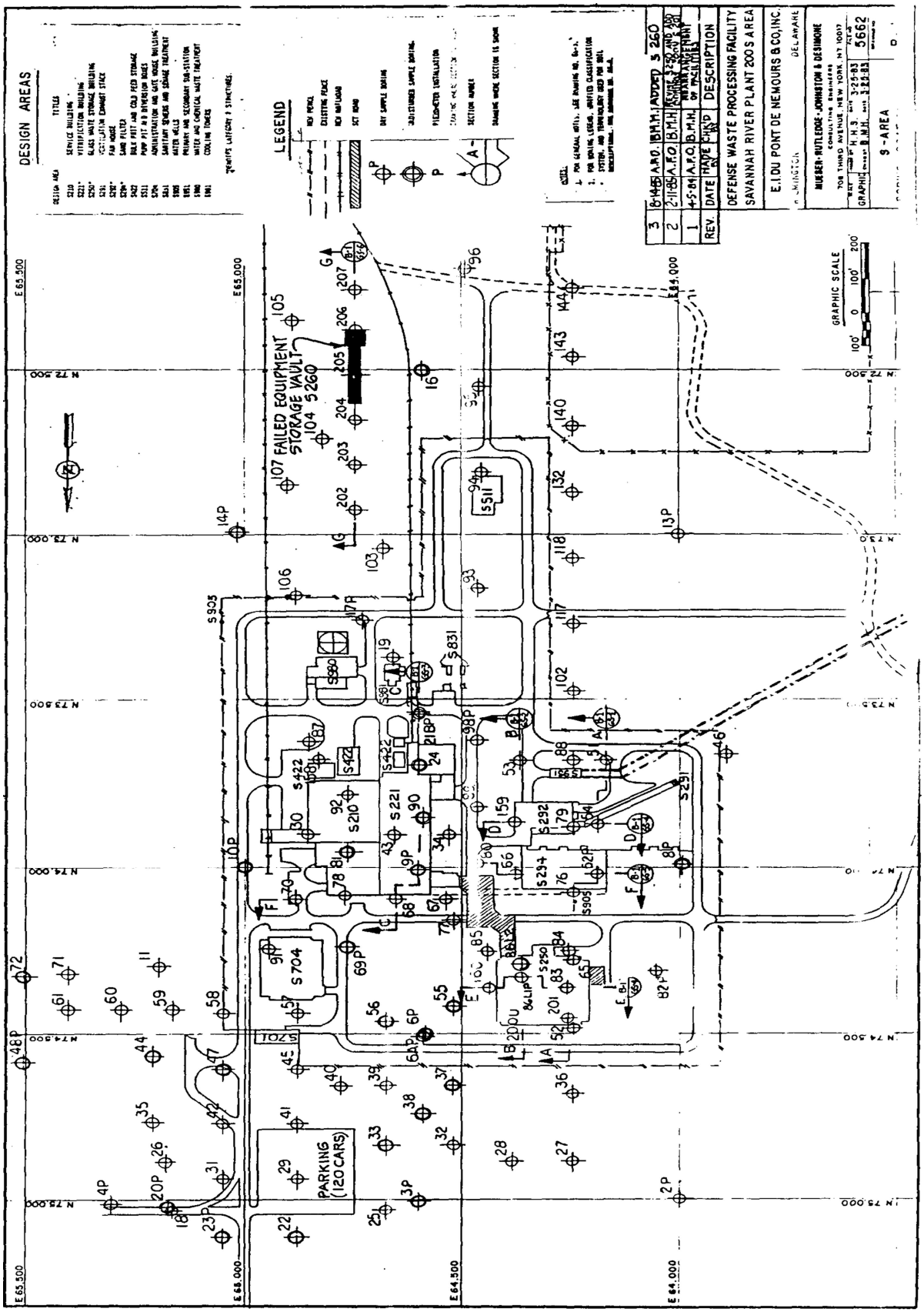

Figure 3.4-29 DWPF Boring Location Plan

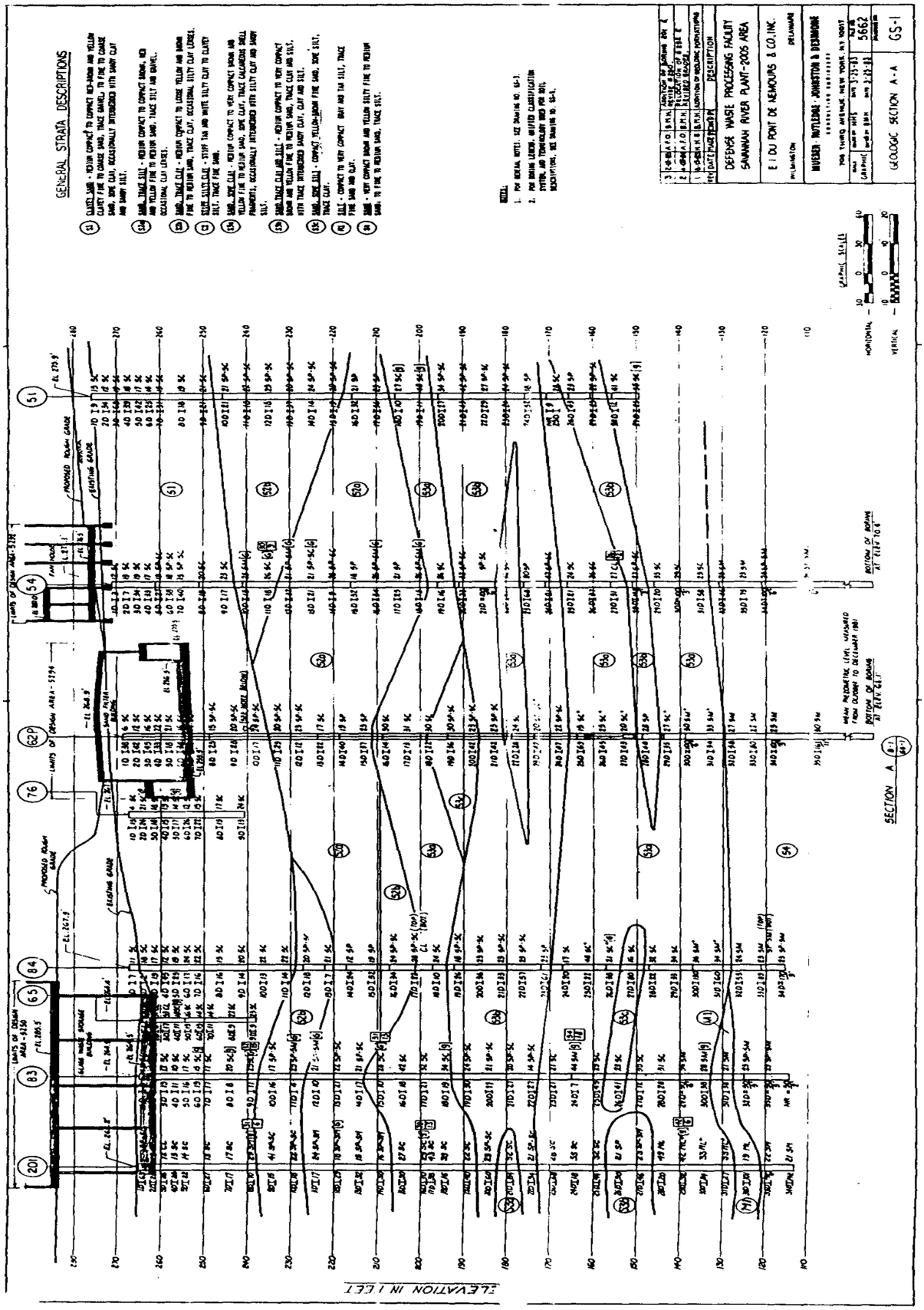

Figure 3.4-30 Mueser Section AA

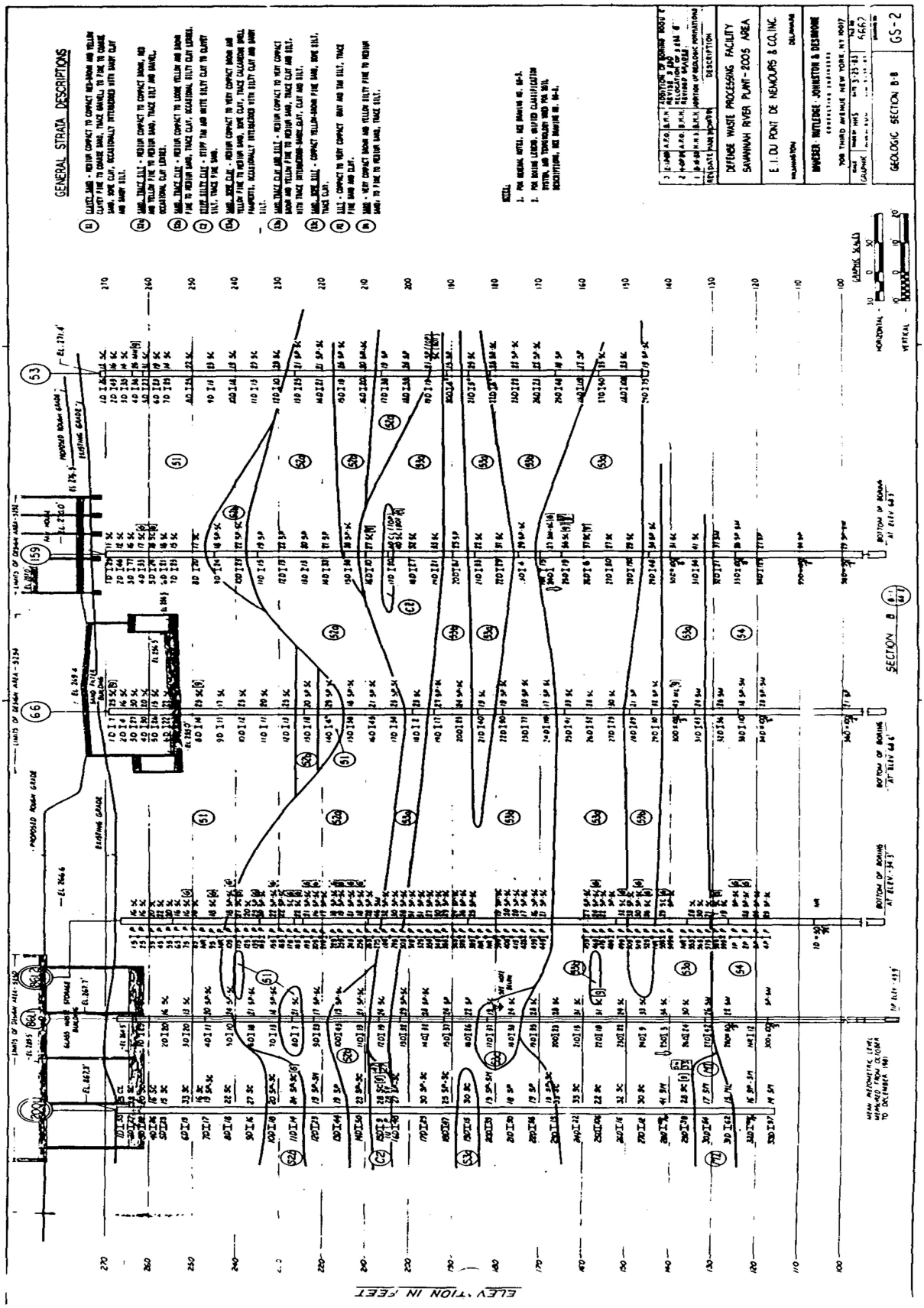

Figure 3.4-31 Mueser Section BB

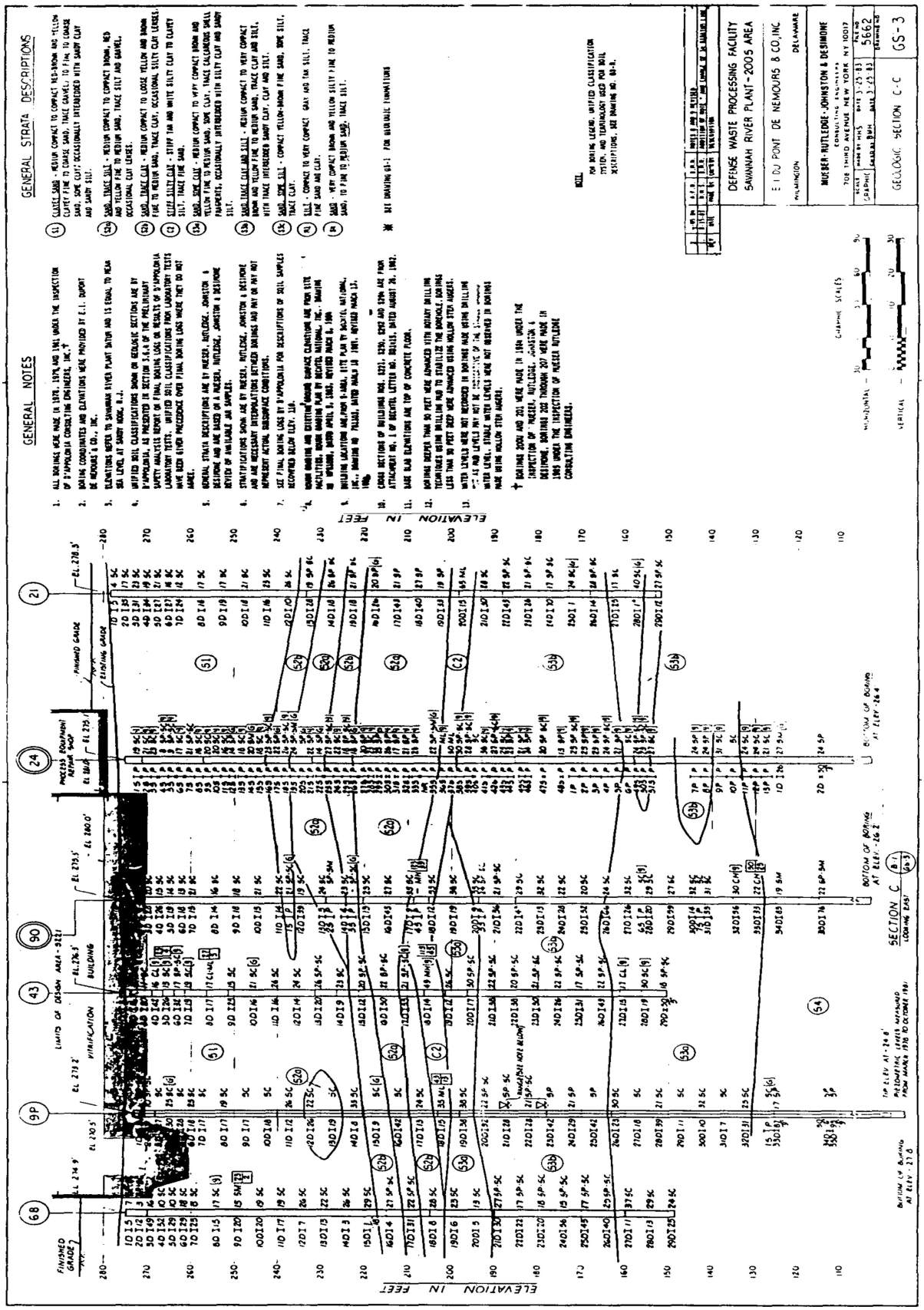

Figure 3.4-32 Mueser Section CC

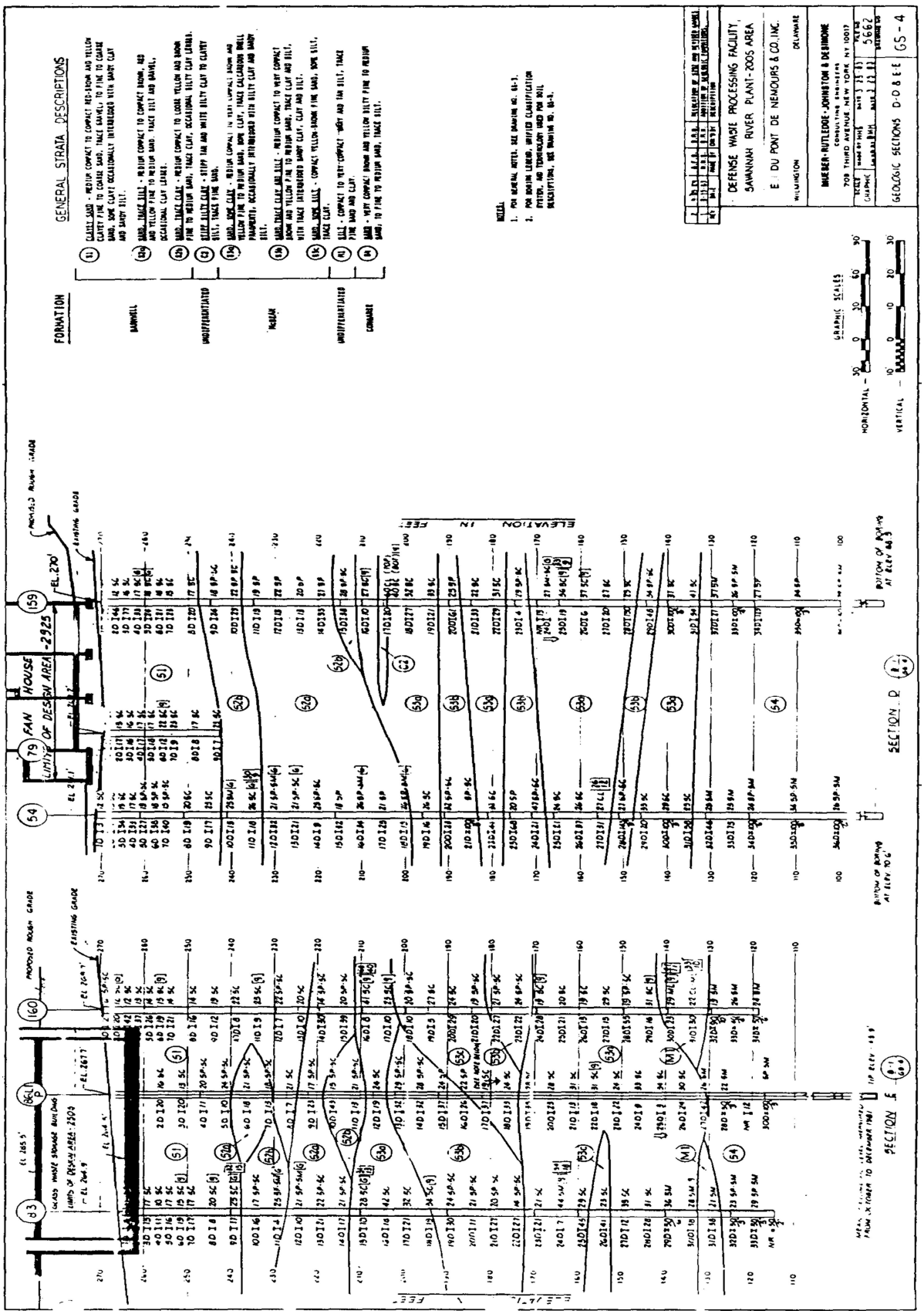

Figure 3.4-33 Mueser Section DD and EE

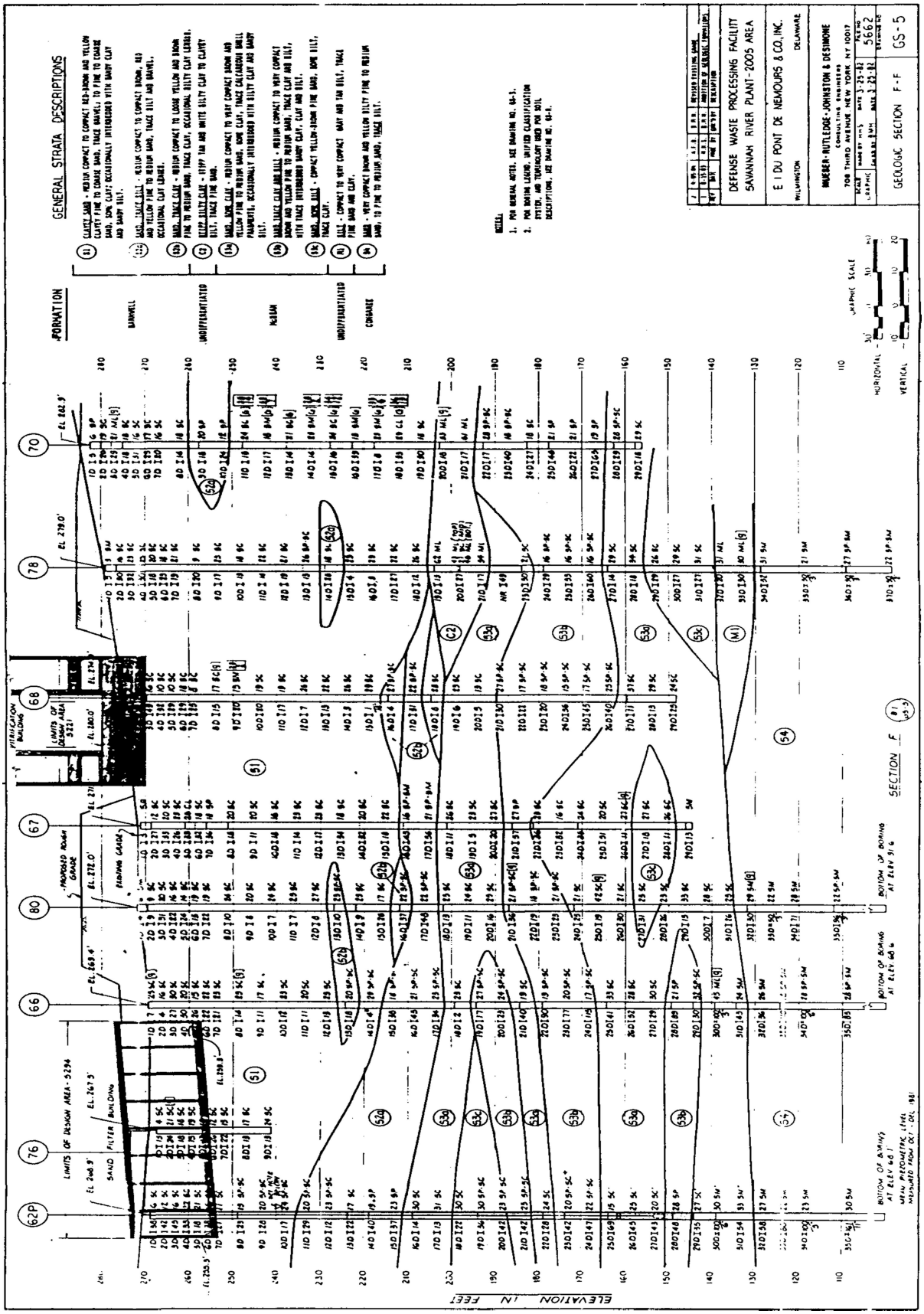

Figure 3.4-34 Mueser Section FF

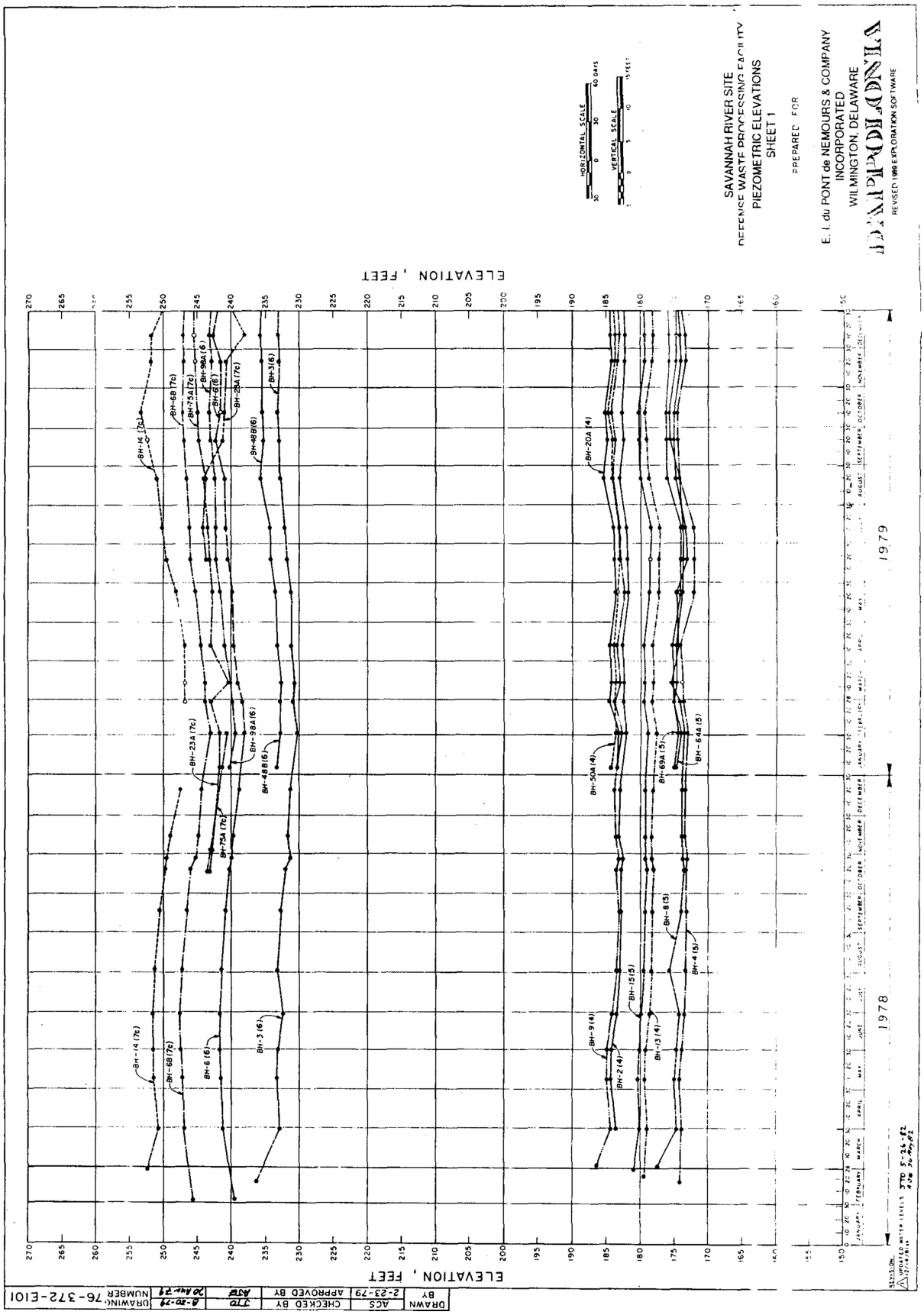

Figure 3.4-35 Piezometric Heads

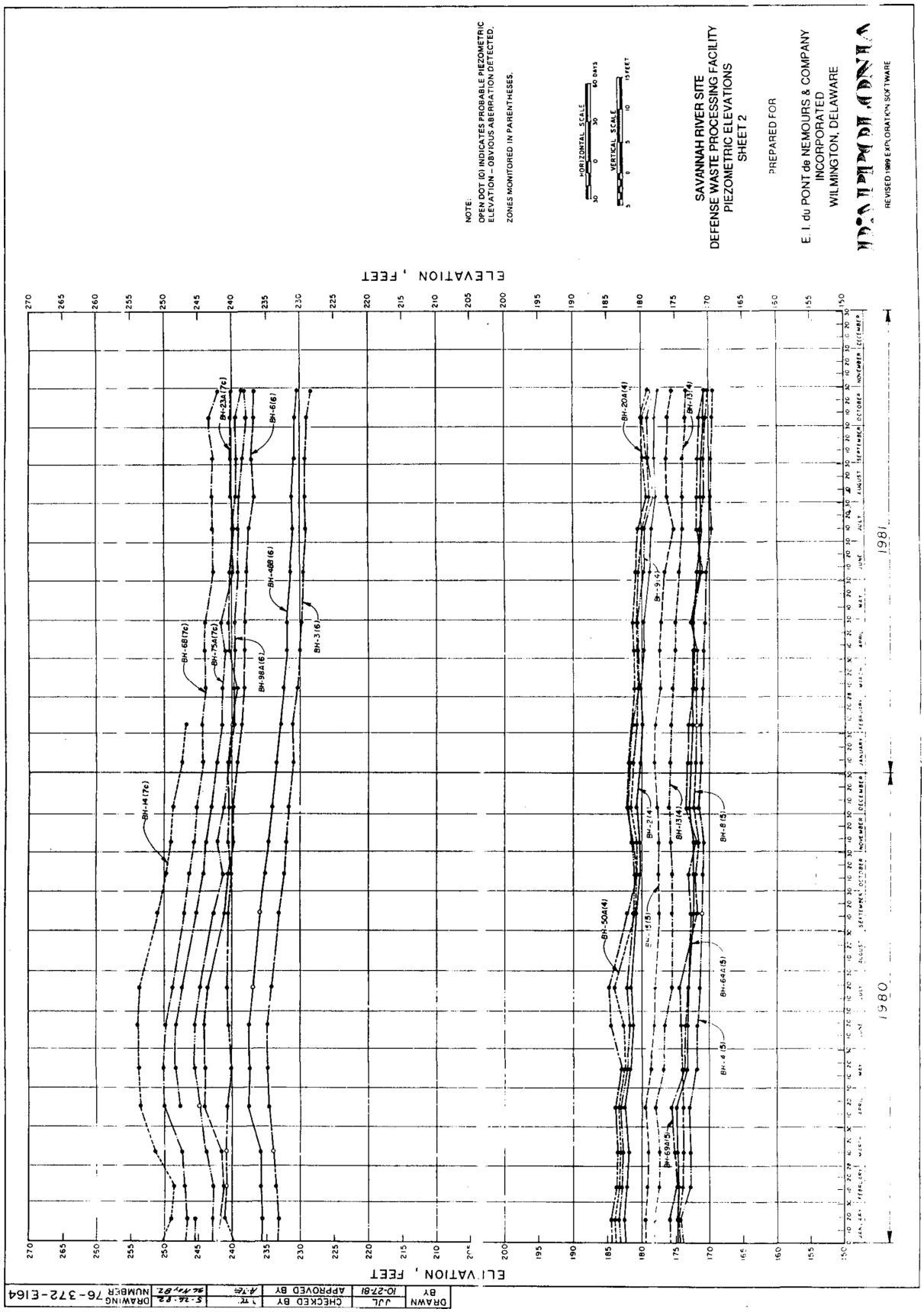

Figure 3.4-36 Piezometric Heads

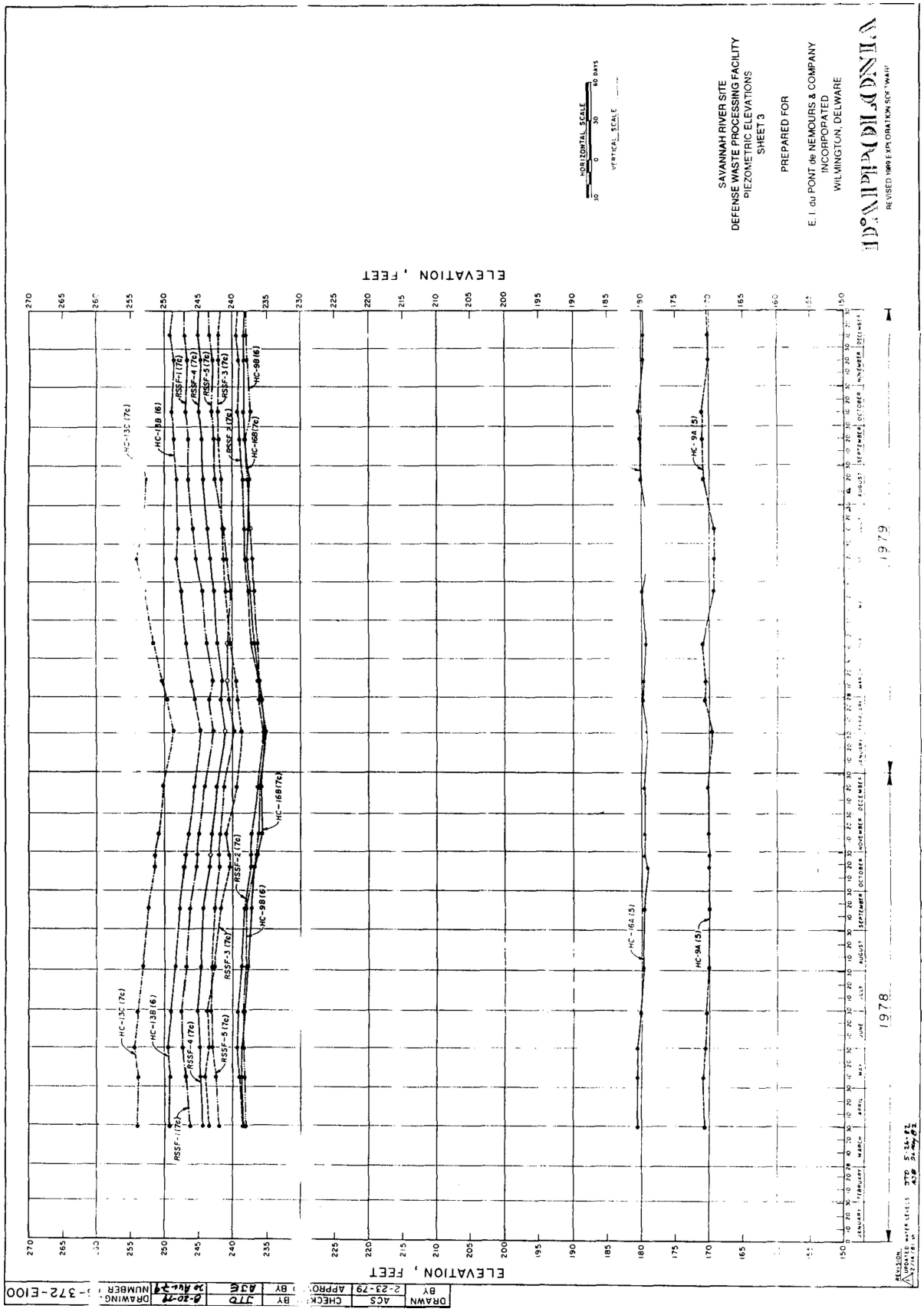

Figure 3.4-37 Piezometric Heads

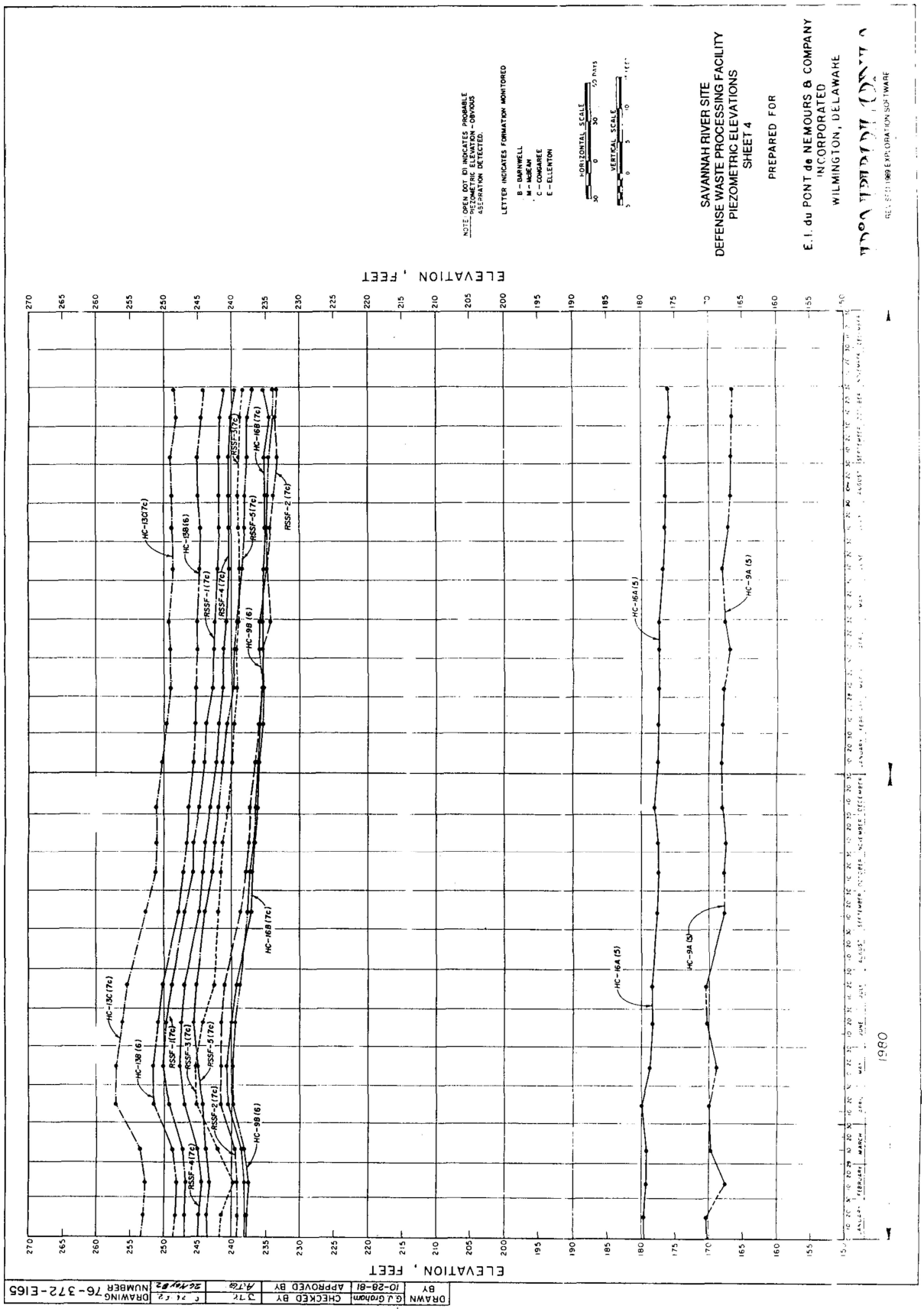

Figure 3.4-38 Piezometric Heads

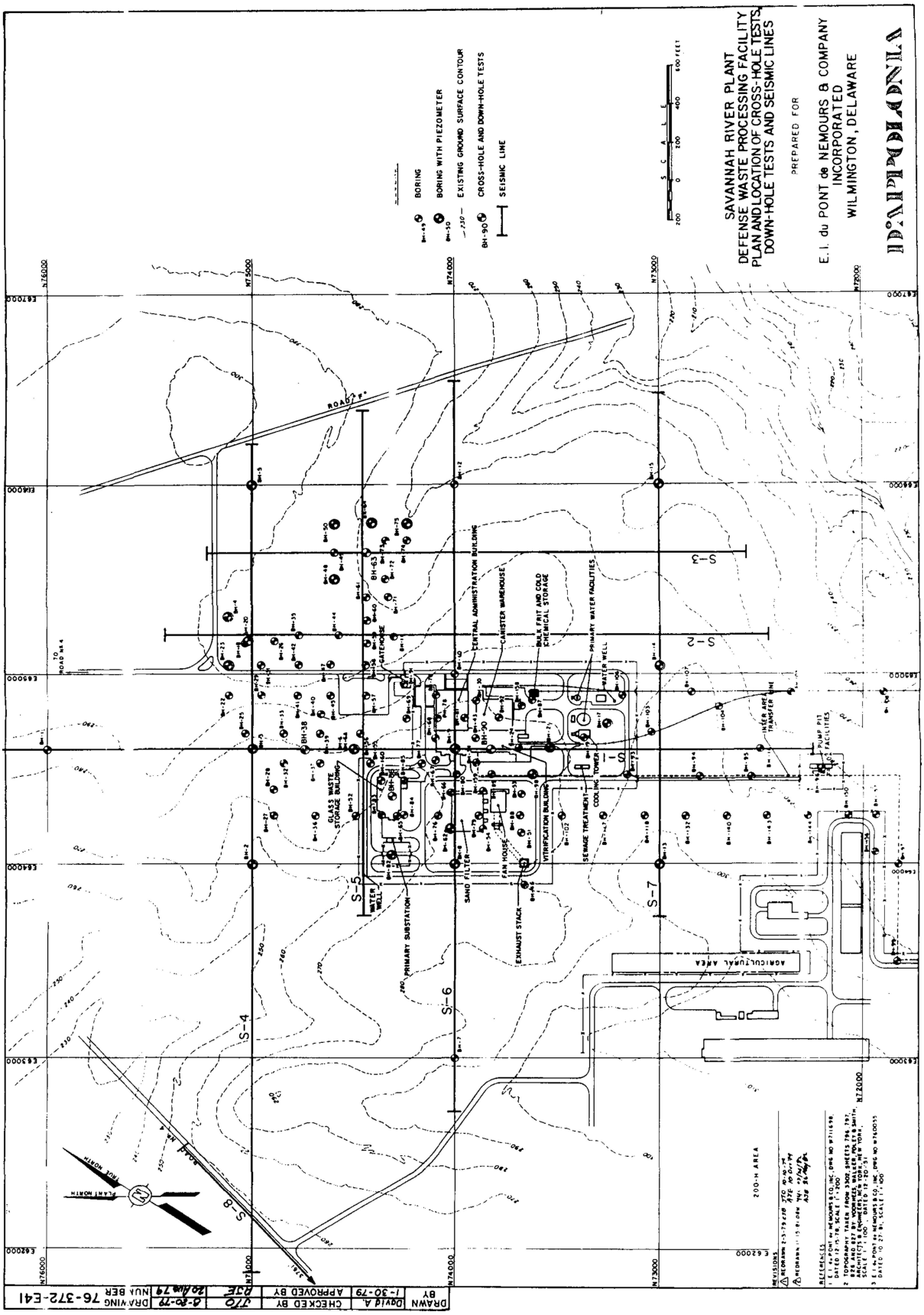

Figure 3.4-39 Plan View of Crosshole Tests, Downhole Tests and Seismic Lines

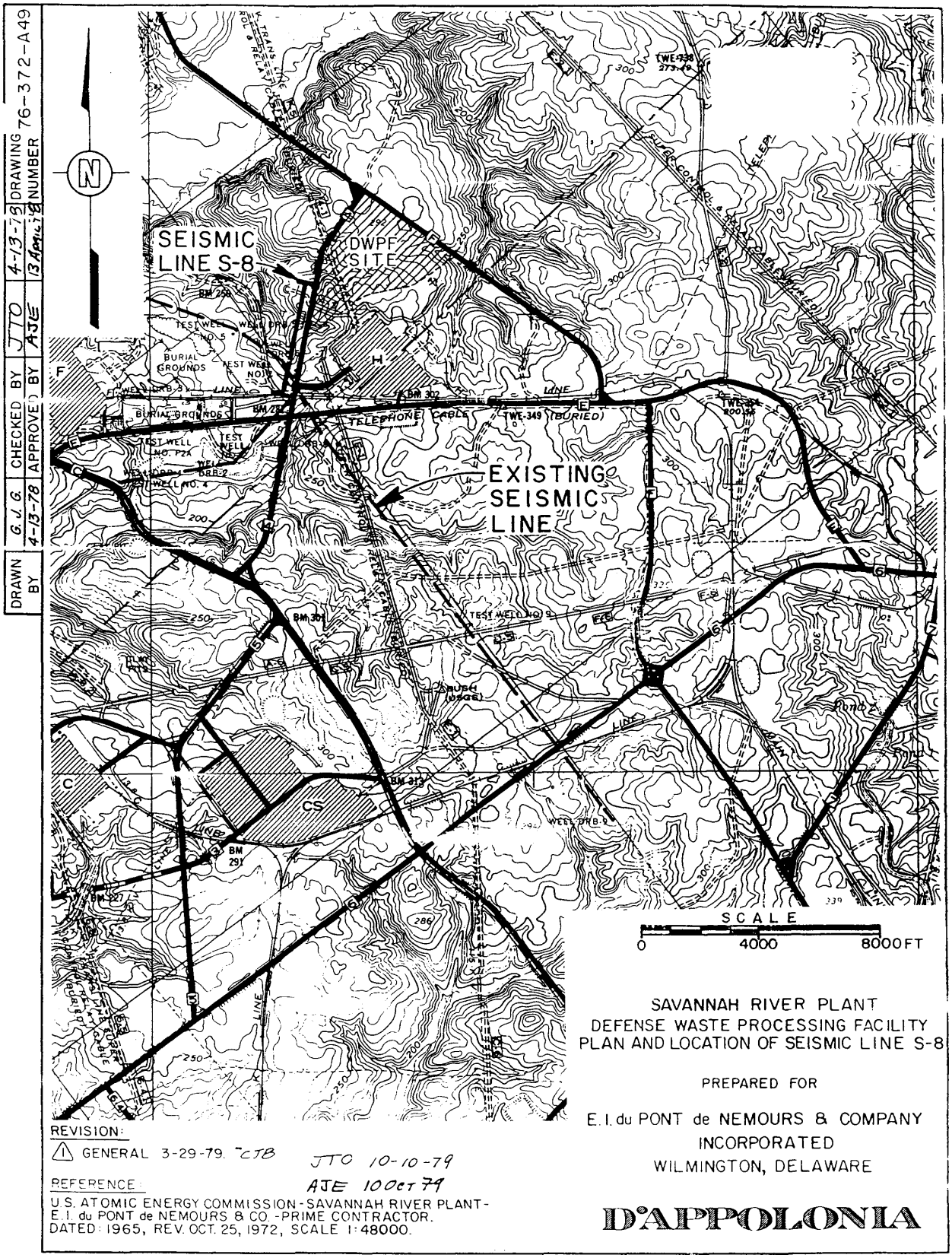

Figure 3.4-40 Seismic Line S-8

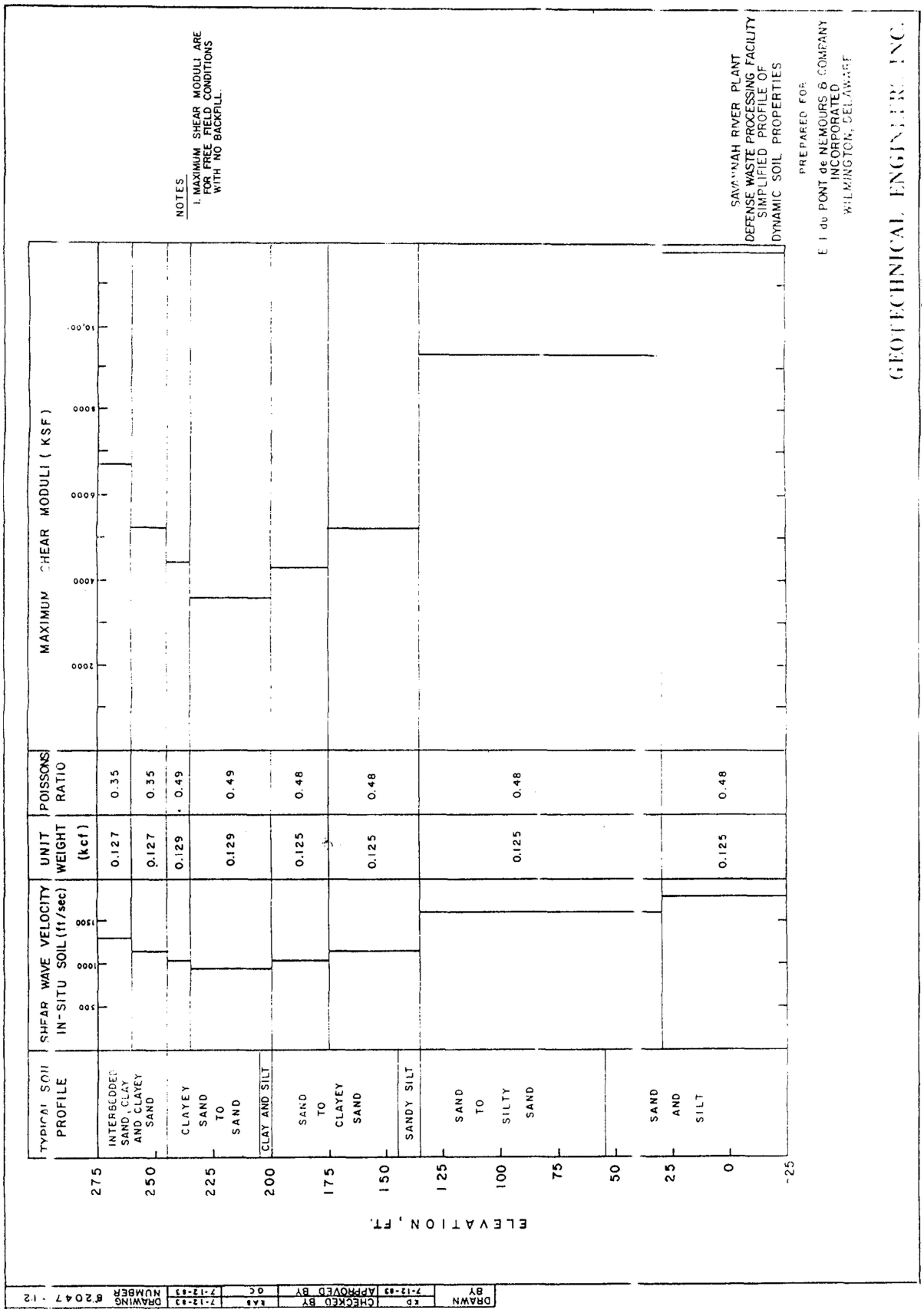

Figure 3.4-41 Simplified Dynamic Soil Properties

COMPARISON OF SHALLOW STRATIGRAPHY NOMENCLATURE

OLD NOMENCLATURE	NEW NOMENCLATURE	STRATUM ON SOIL LOGS
HAWTHORNE FM	ALTAMAHA FM (UPLAND UNIT)	S1
BARNWELL FM	TOBACCO ROAD FM	S2a or S2b
	DRY BRANCH FM: IRWINTON SAND MEMBER	
UNDIFFERENTIATED	DRY BRANCH FM: TAN CLAY MEMBER	C2
MCBEAN FM	TINKER FM	S3a, S3b or S3c
	SANTEE LIMESTONE	
UNDIFFERENTIATED	GREEN CLAY (INFORMAL)	M1
CONGAREE FM	CONGAREE FM	S4

Figure 3.4-42 Stratigraphic Nomenclature

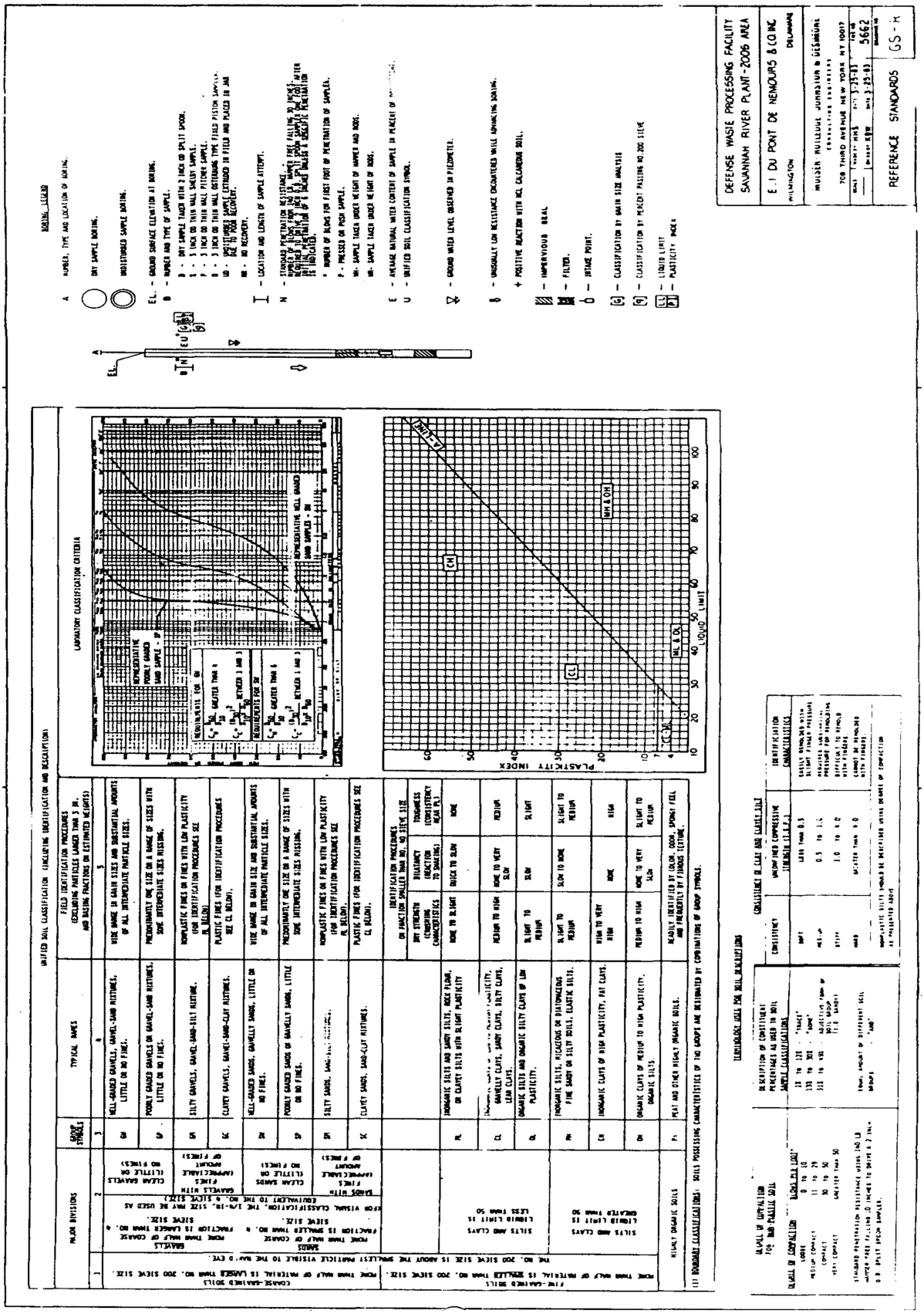

Figure 3.4-43 Reference Standards

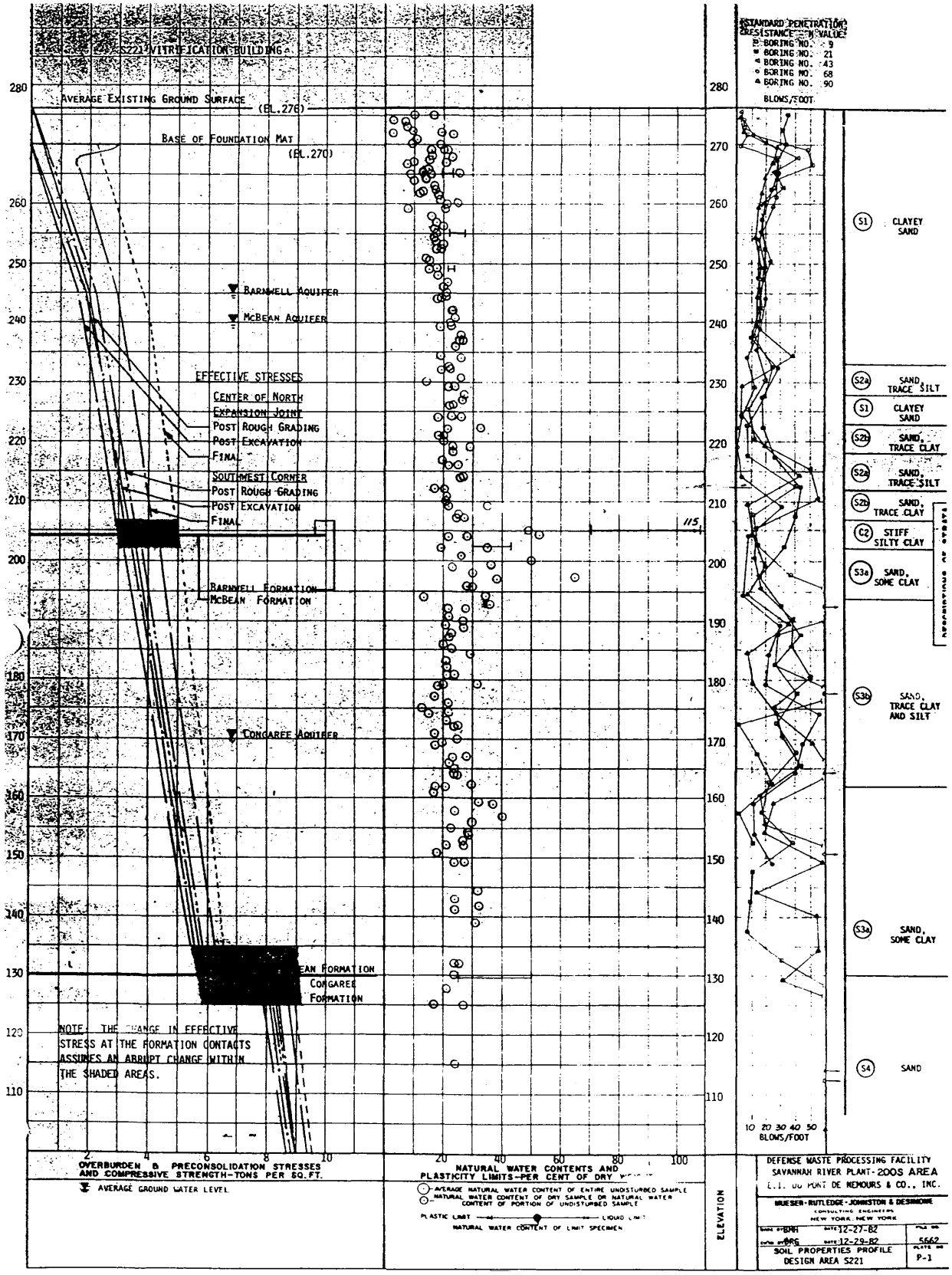

Figure 3.4-44 Soil Properties Profile

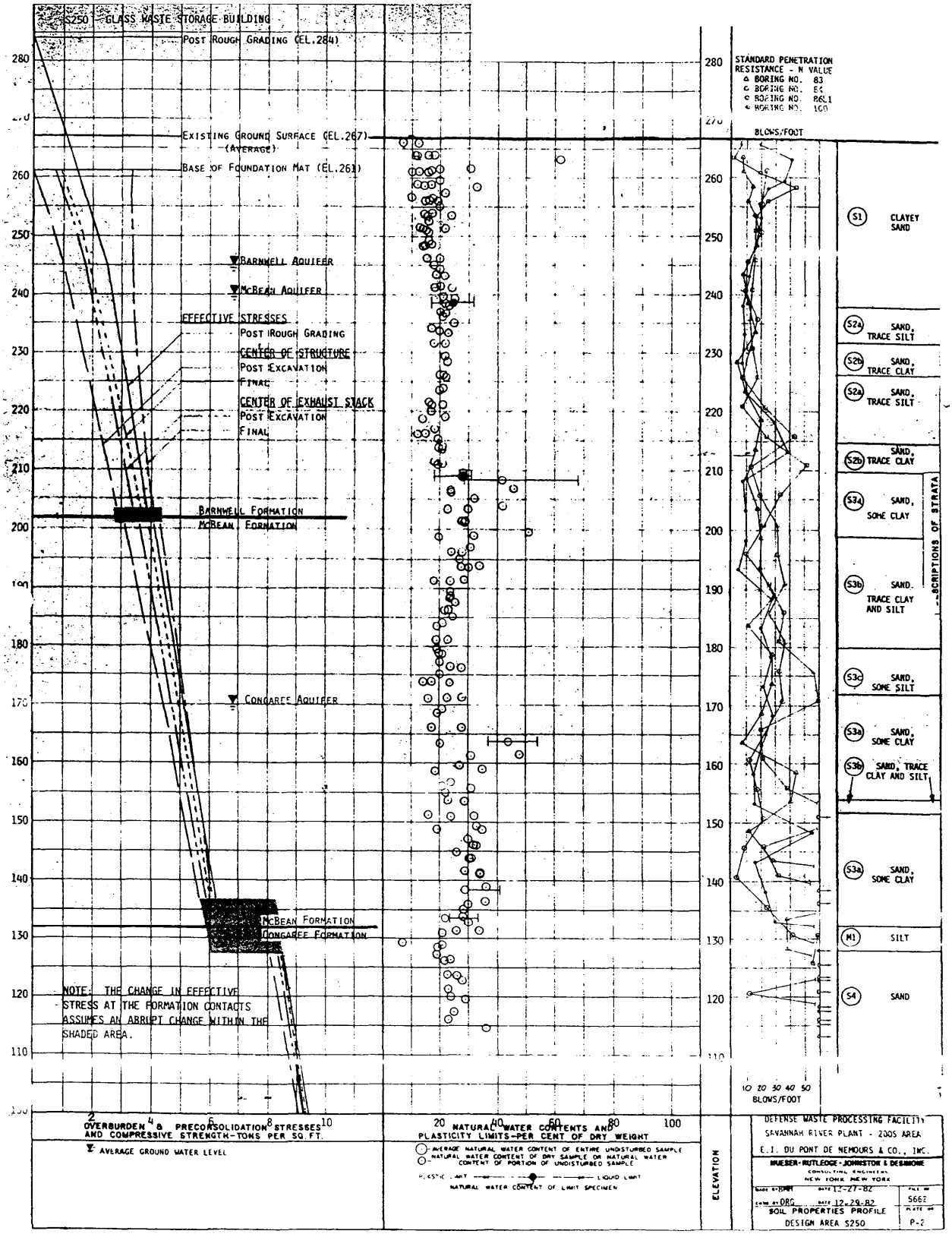

Figure 3.4-45 Soil Properties Profile

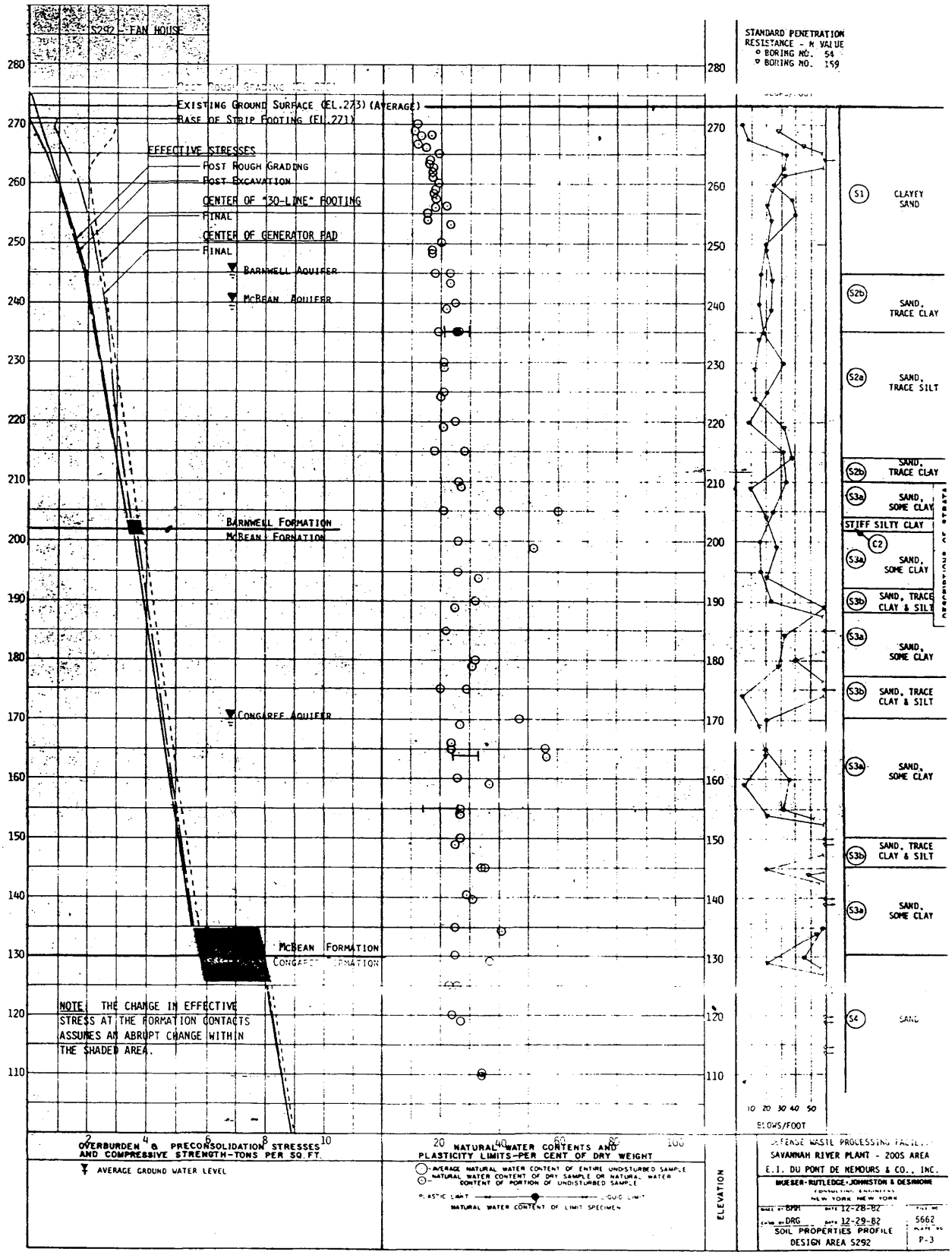

Figure 3.4-46 Soil Properties Profile

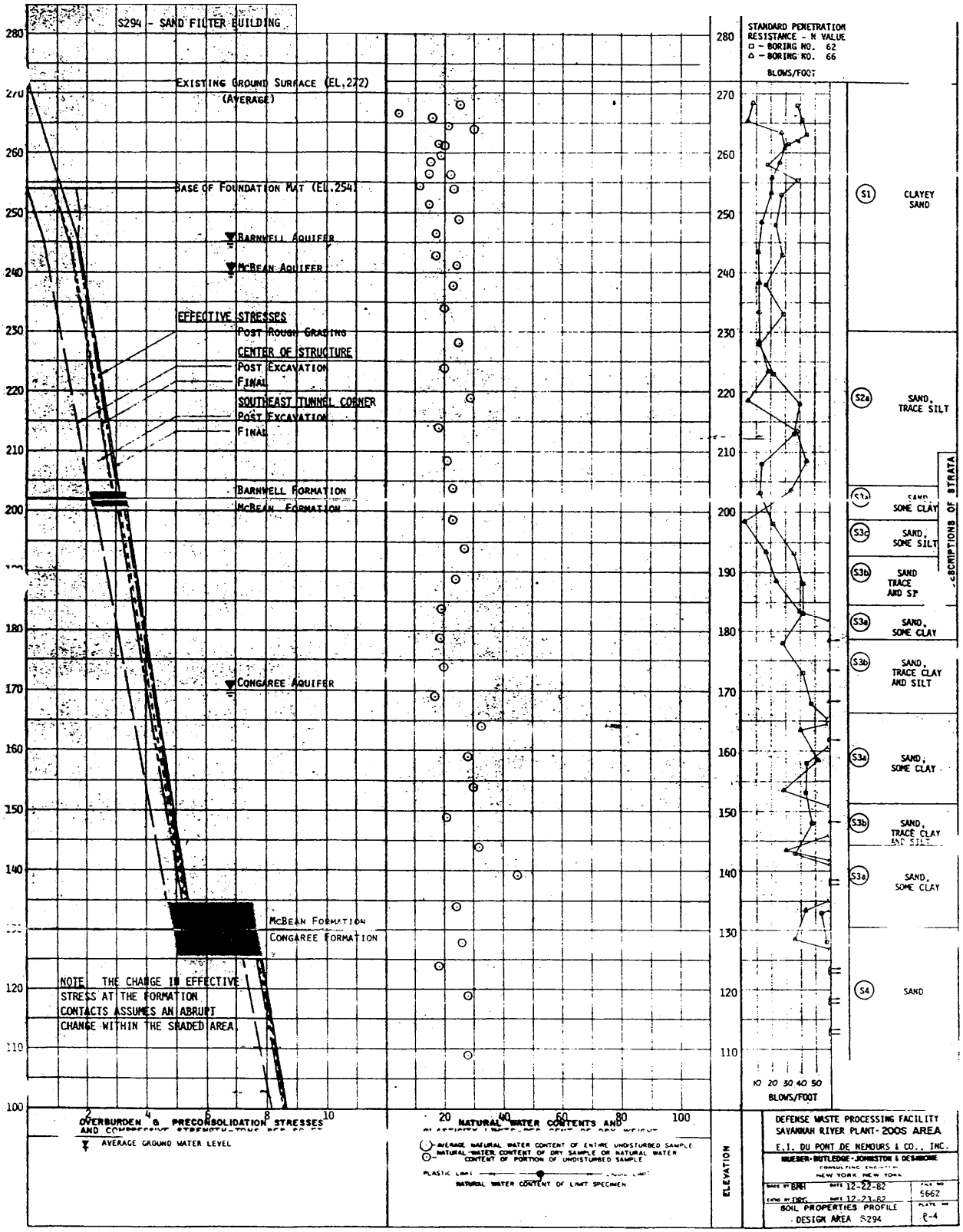

Figure 3.4-47 Soil Properties Profile

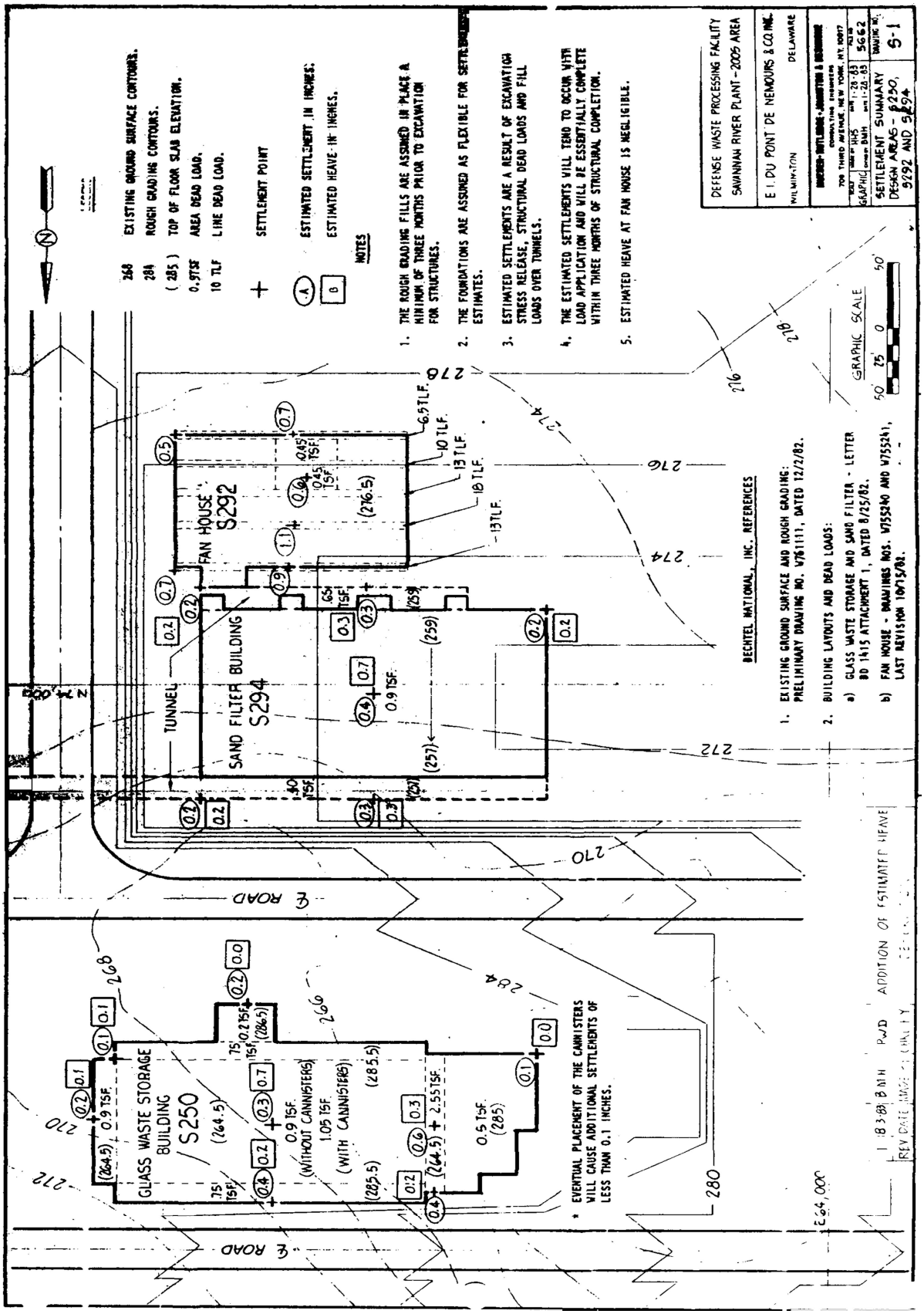

Figure 3.4-48 Settlement Summary for S250, S292, and S294

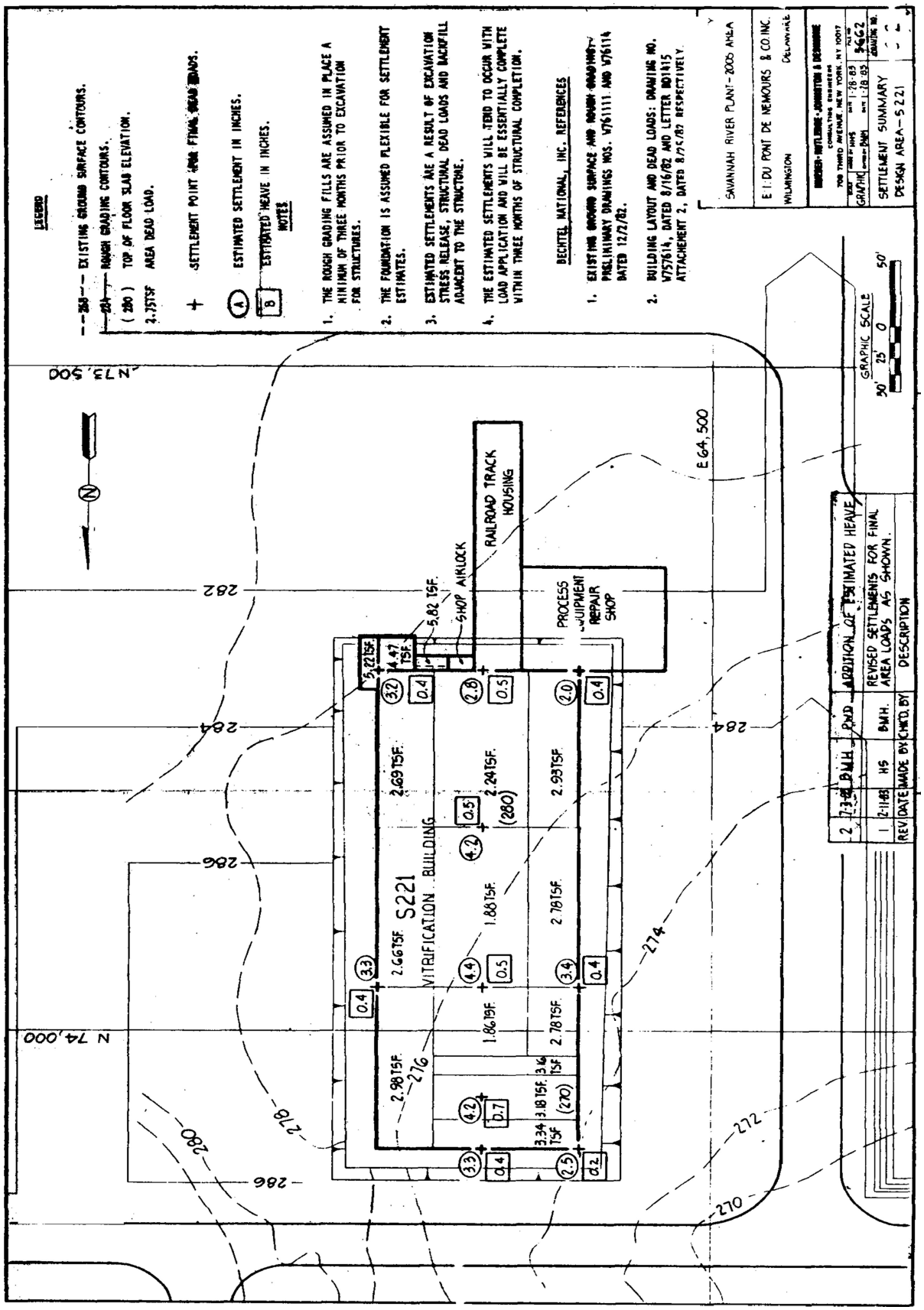

Figure 3.4-49 Settlement Summary for S221

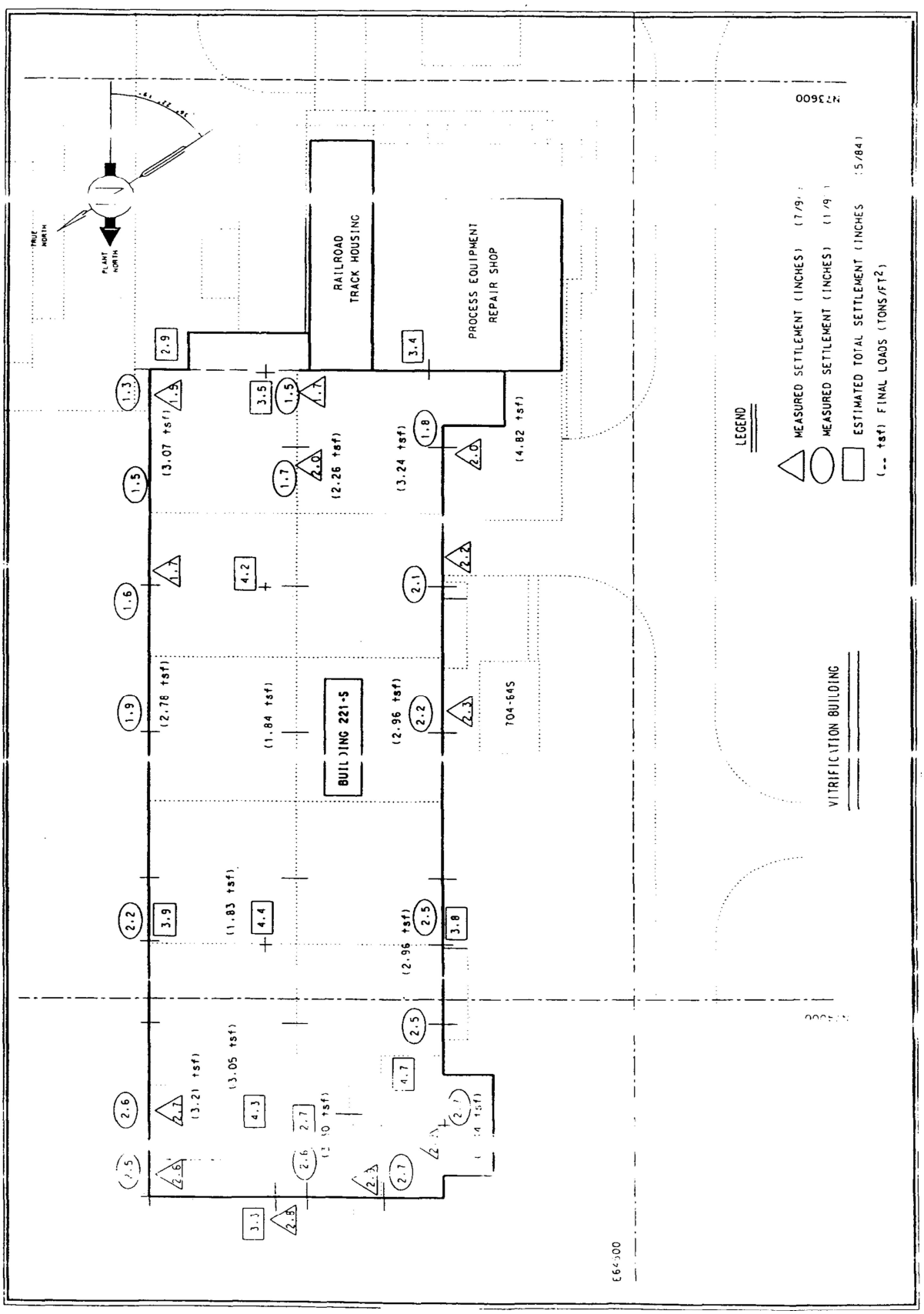

Plan View of Vitrification Building with Estimated and Actual Settlements

Figure 3.4-50 Estimated and Actual Settlements for Vitrification Building

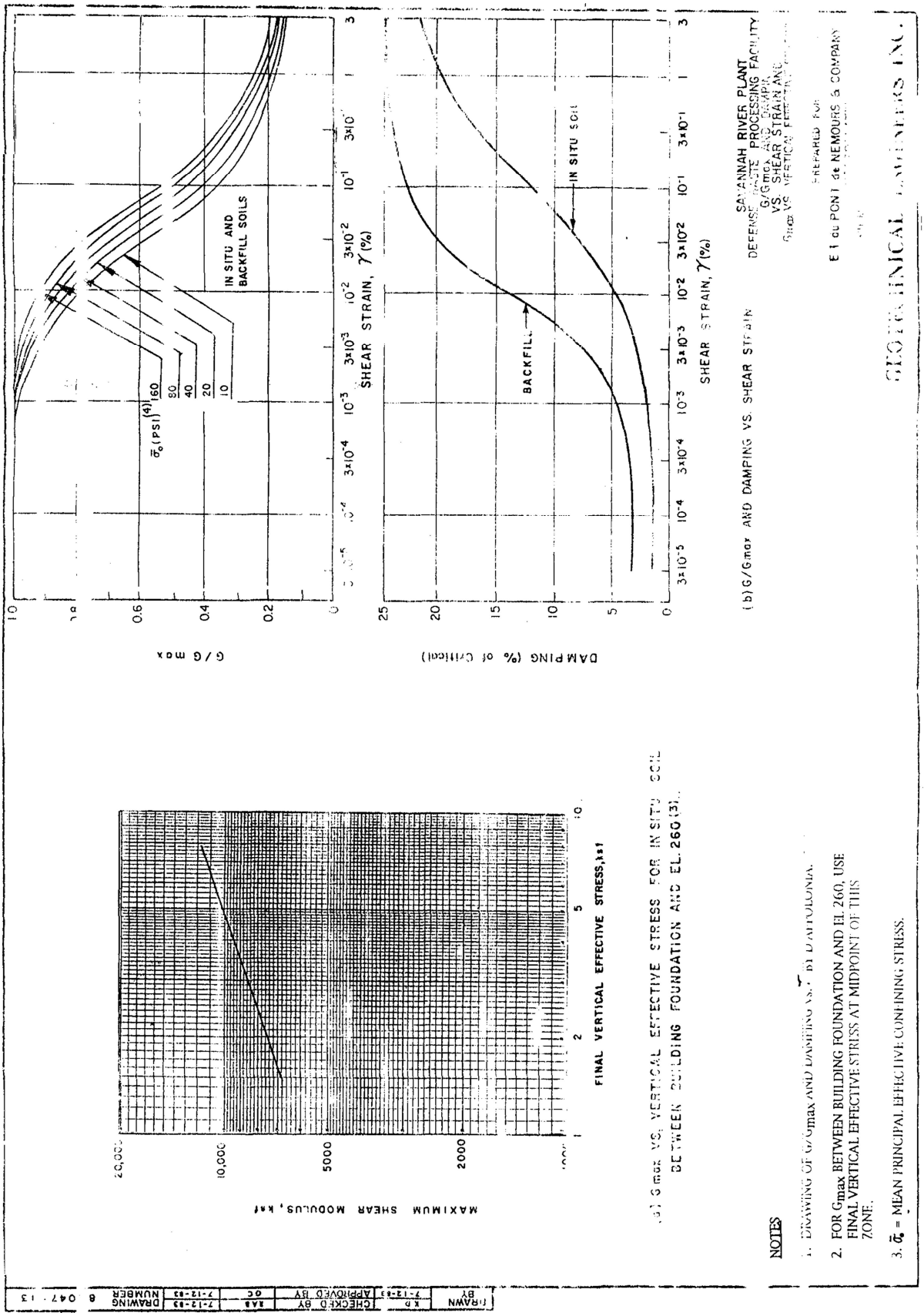

Figure 3.4-51 G/Gmax and Damping versus Shear Strength

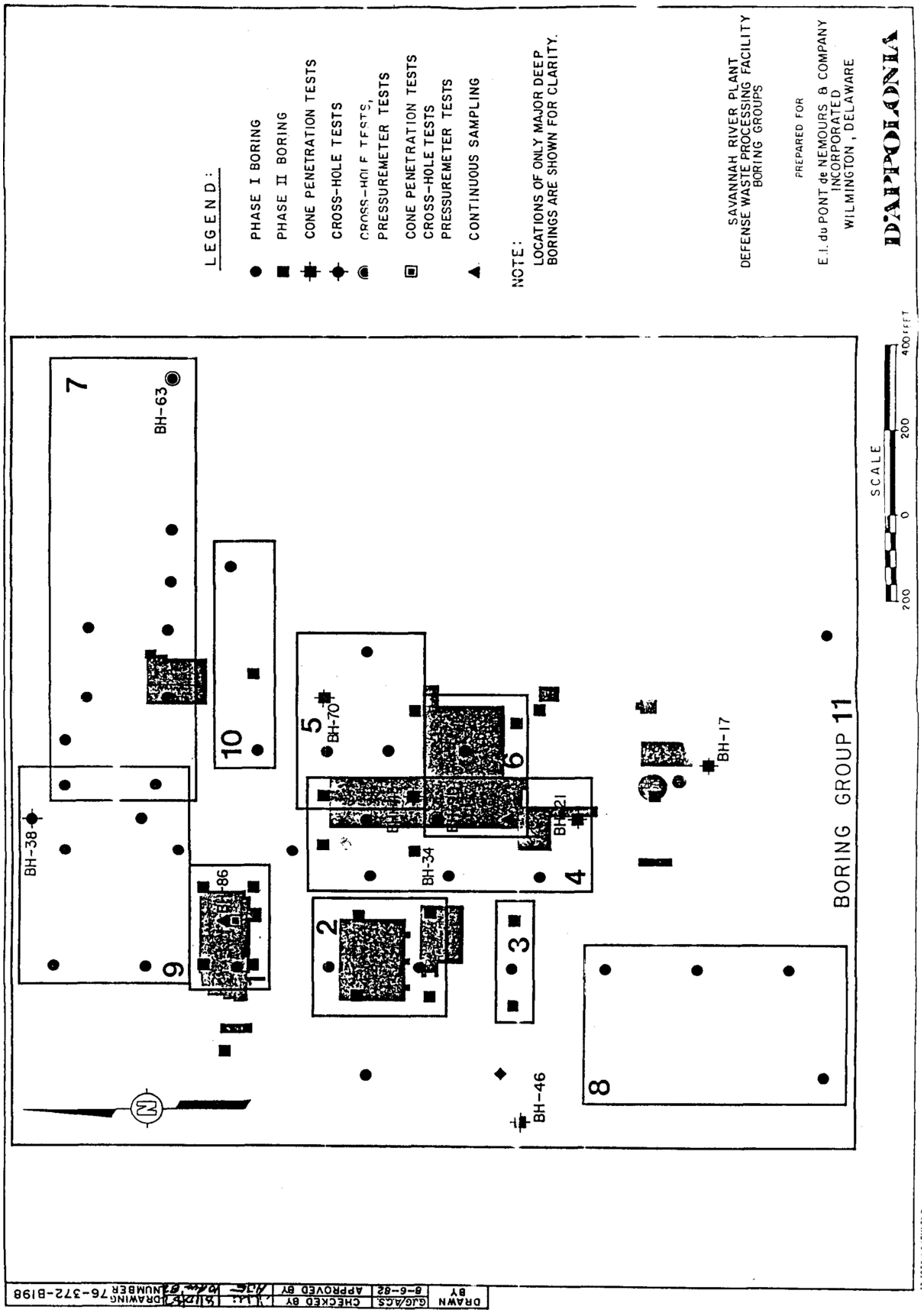

Figure 3.4-52 Boring Groups

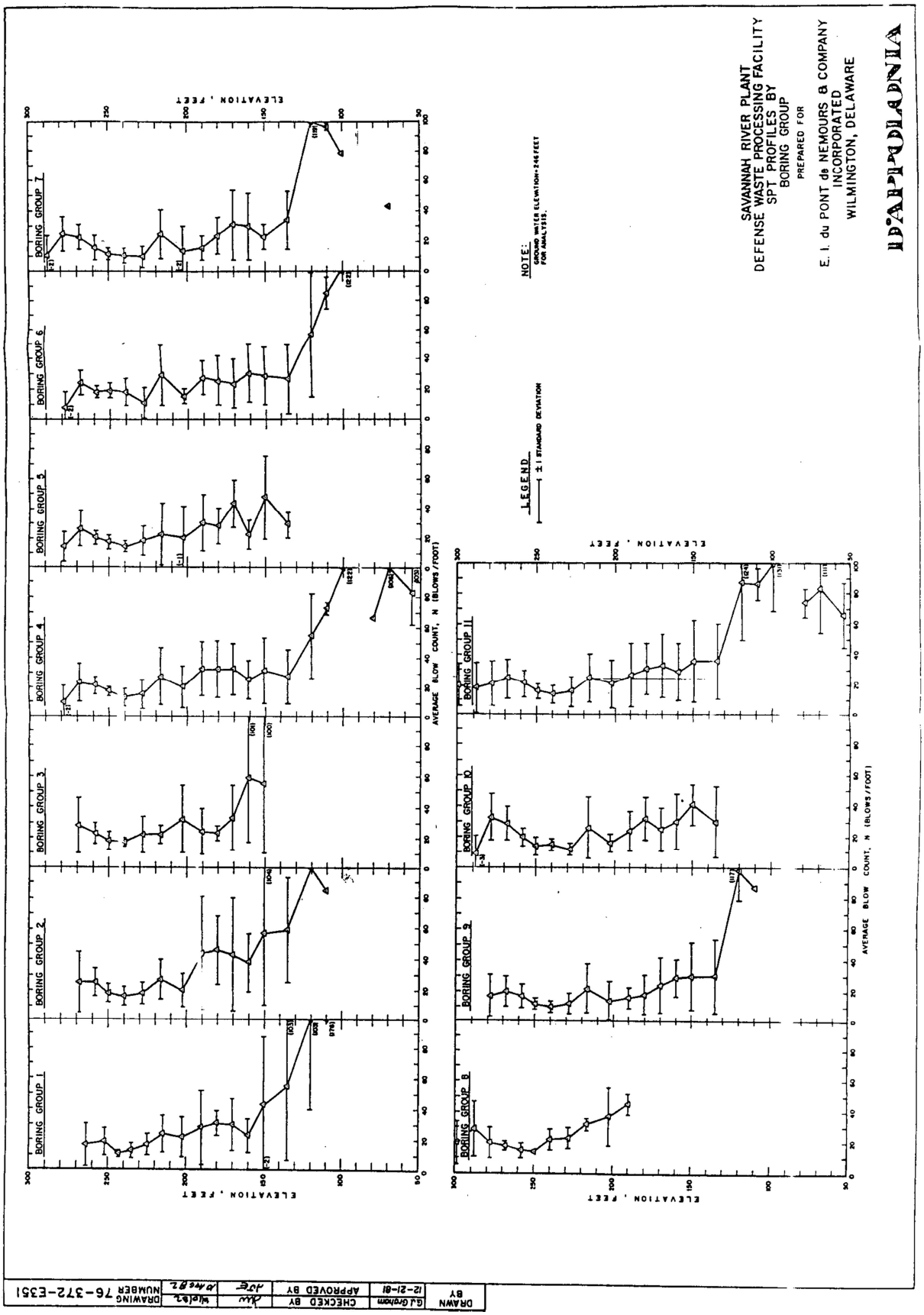

Figure 3.4-53 SPT Profiles

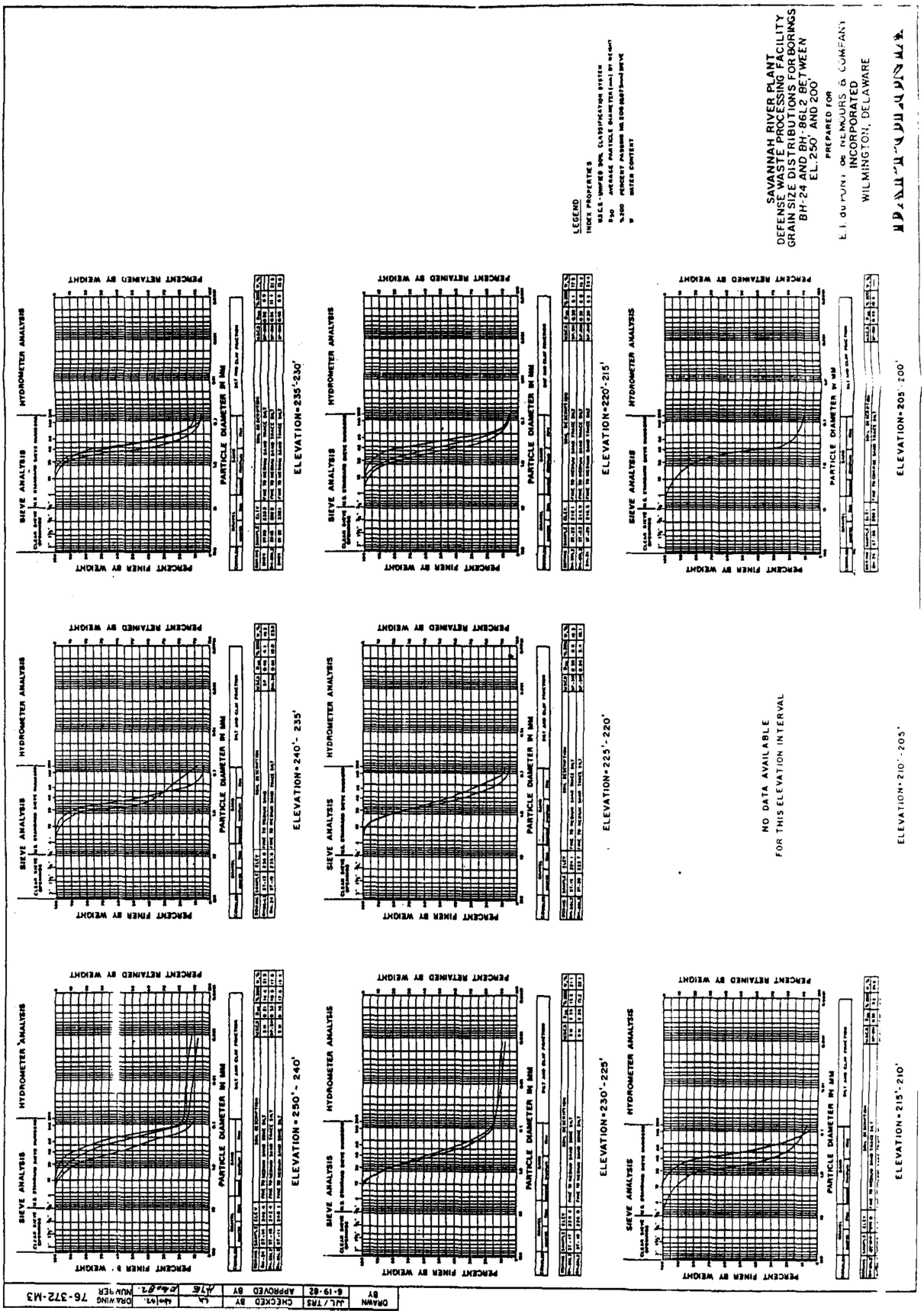

Figure 3.4-54 Grain Size Distribution

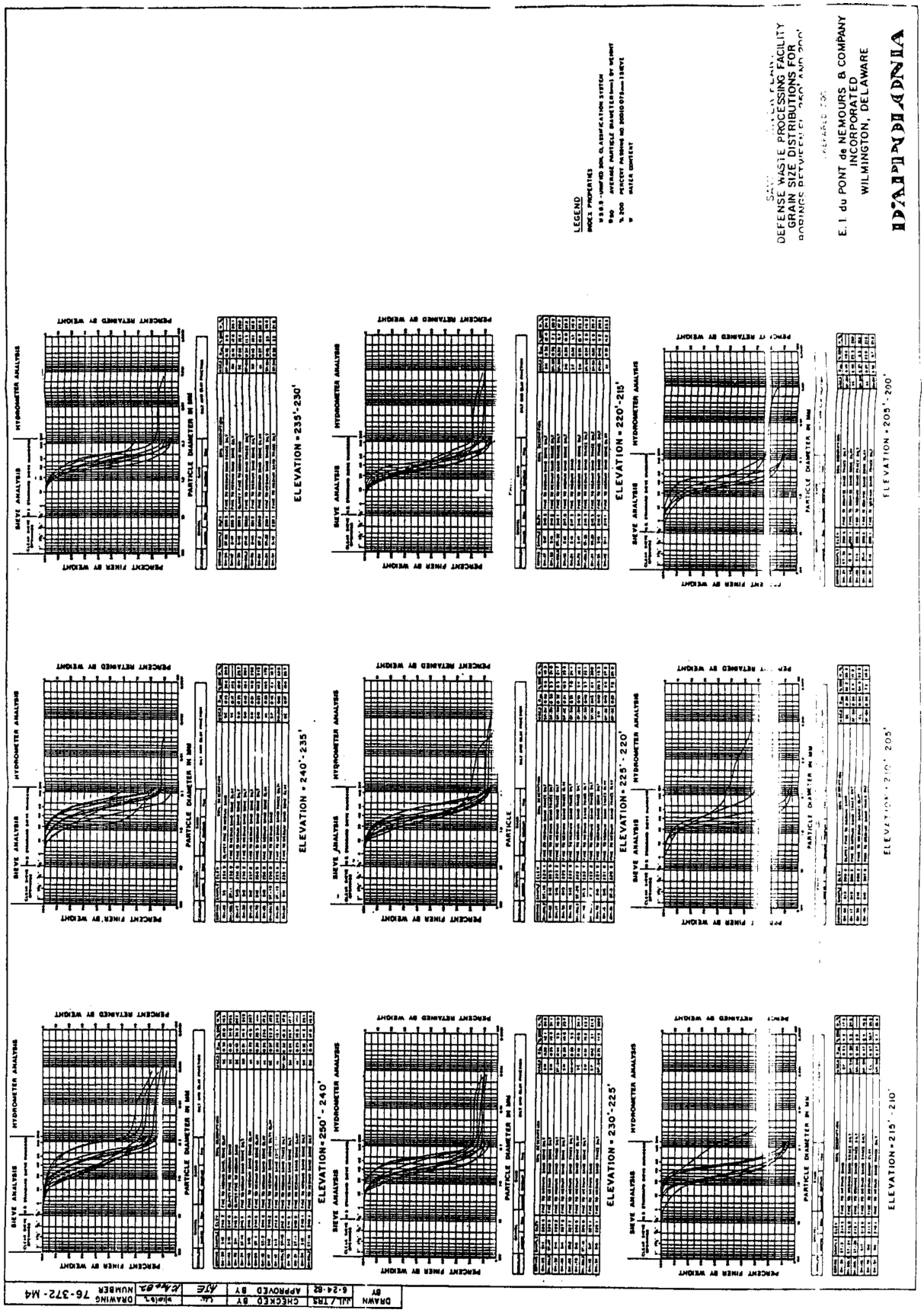

Figure 3.4-55 Grain Size Distribution

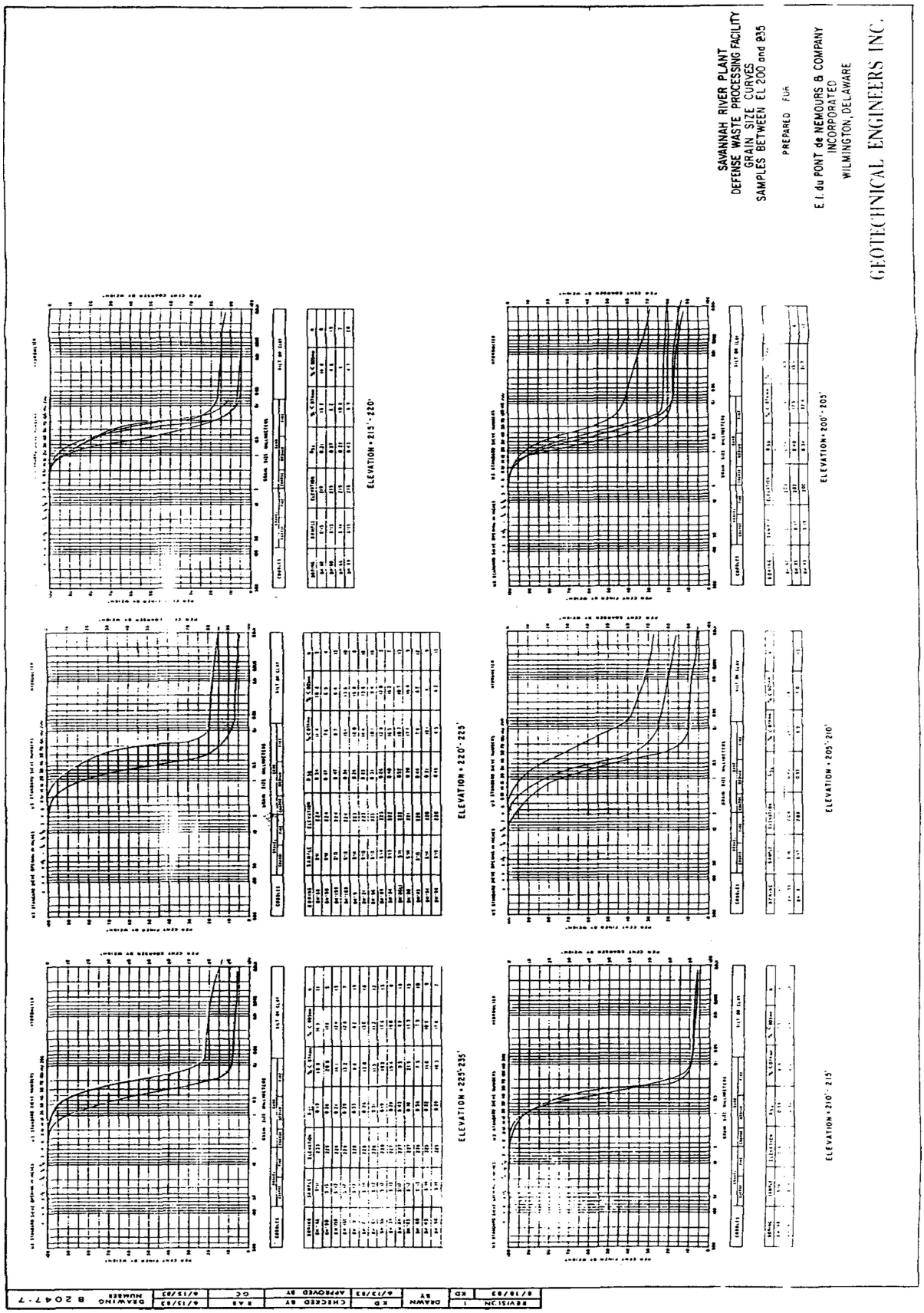

Figure 3.4-56 Grain Size Distribution

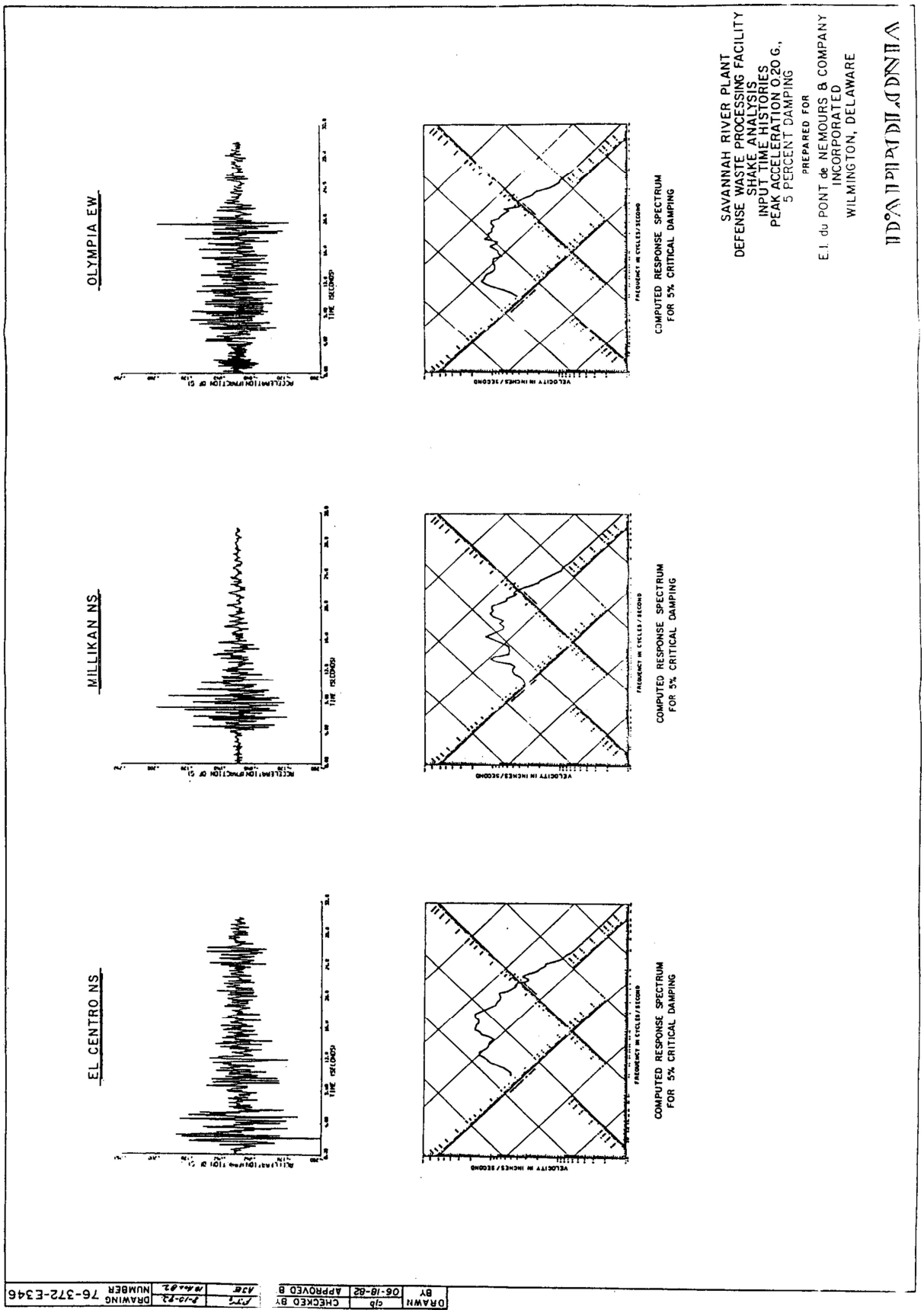

Figure 3.4-57 SHAKE Analysis Input Time Histories

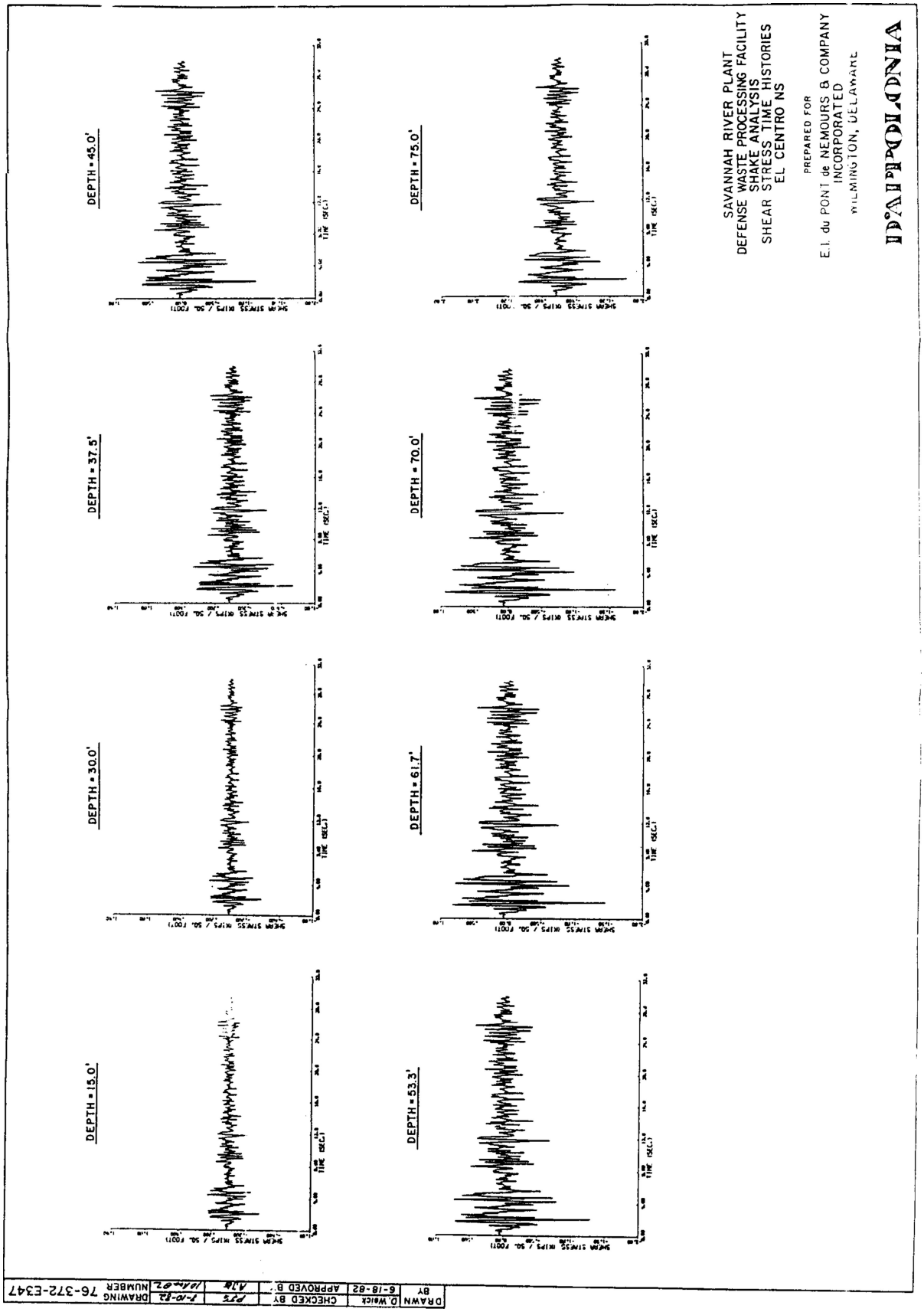

Figure 3.4-58 SHAKE Analysis Input Time Histories

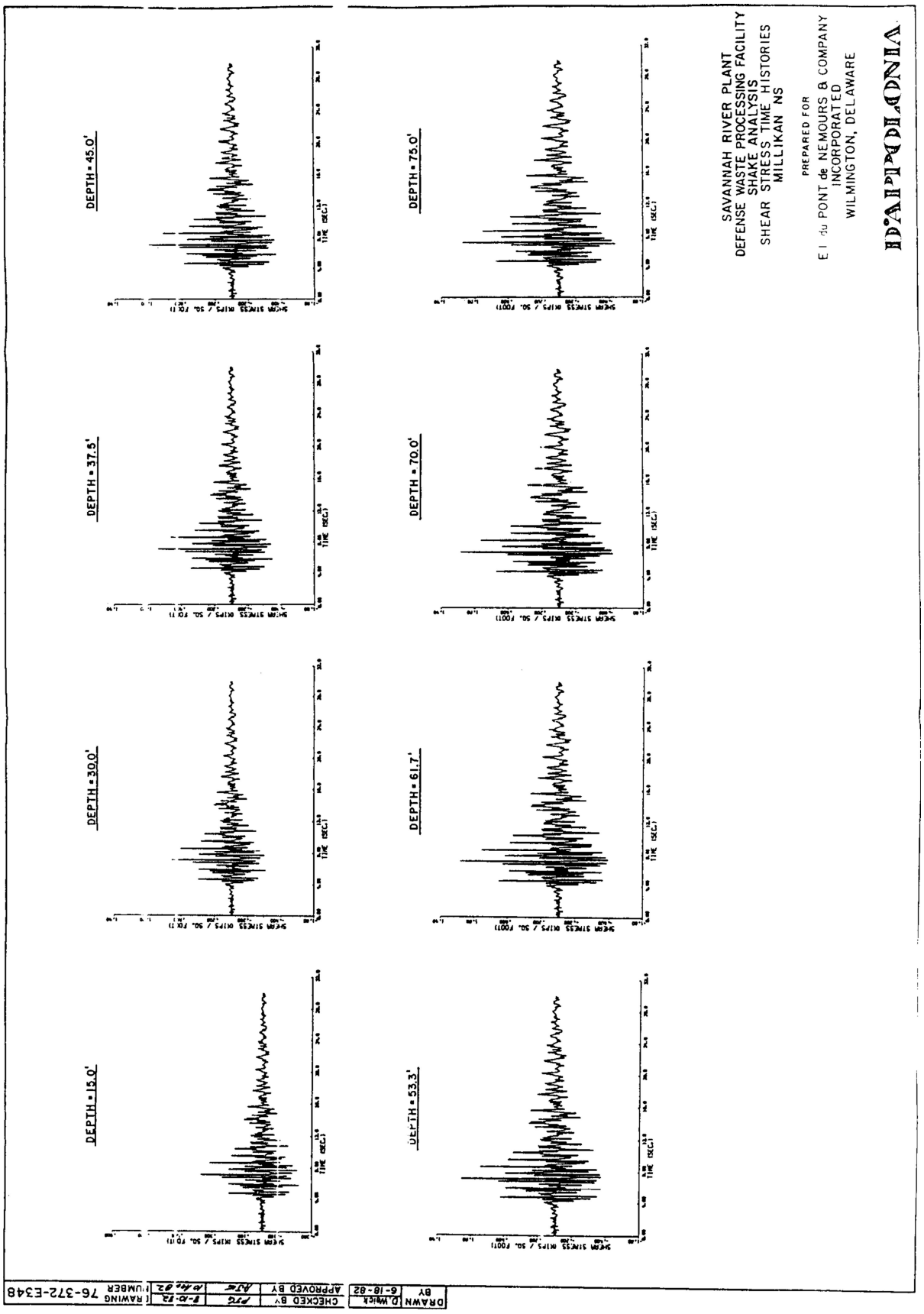

Figure 3.4-59 SHAKE Analysis Input Time Histories

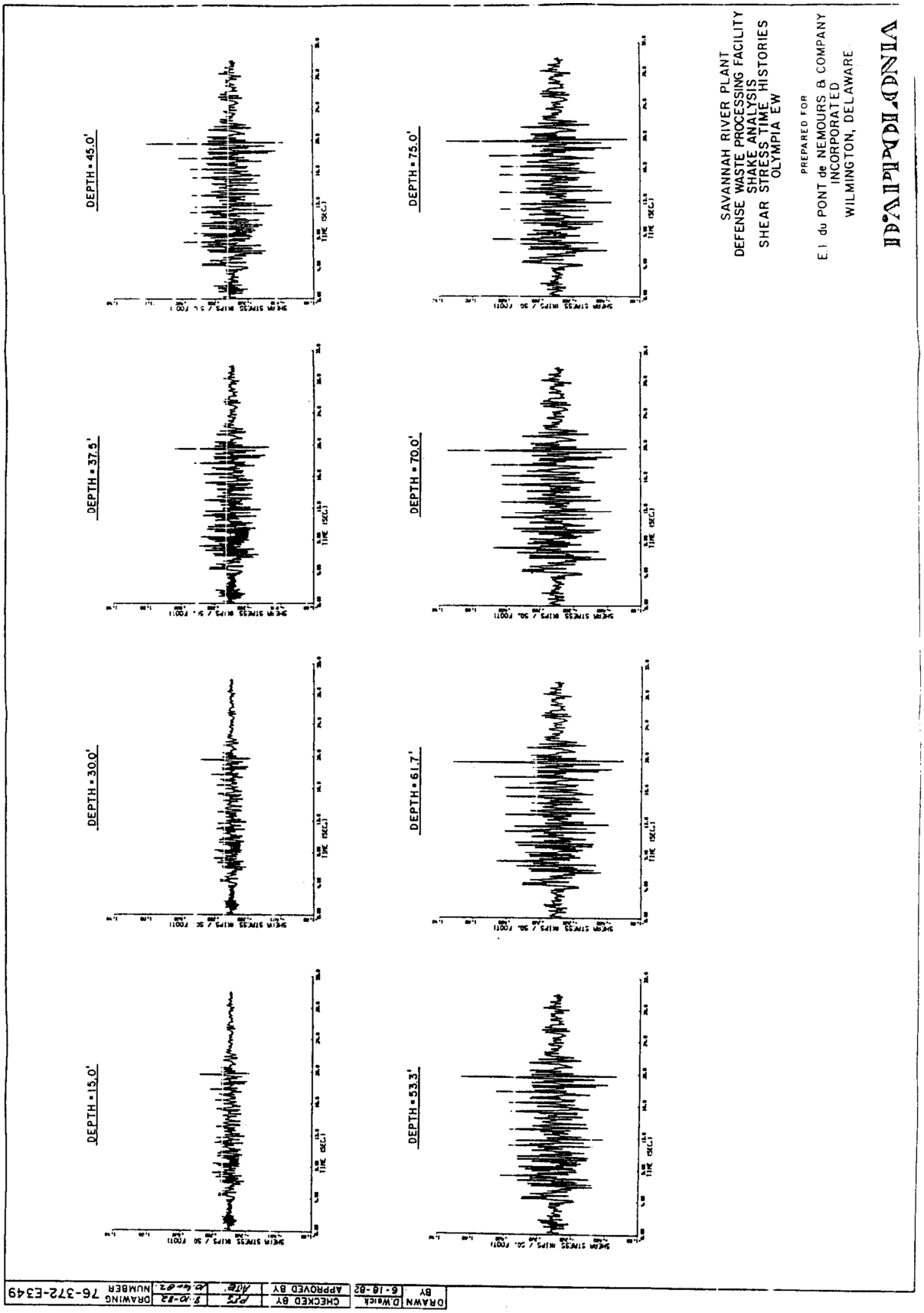

Figure 3.4-60 SHAKE Analysis Input Time Histories

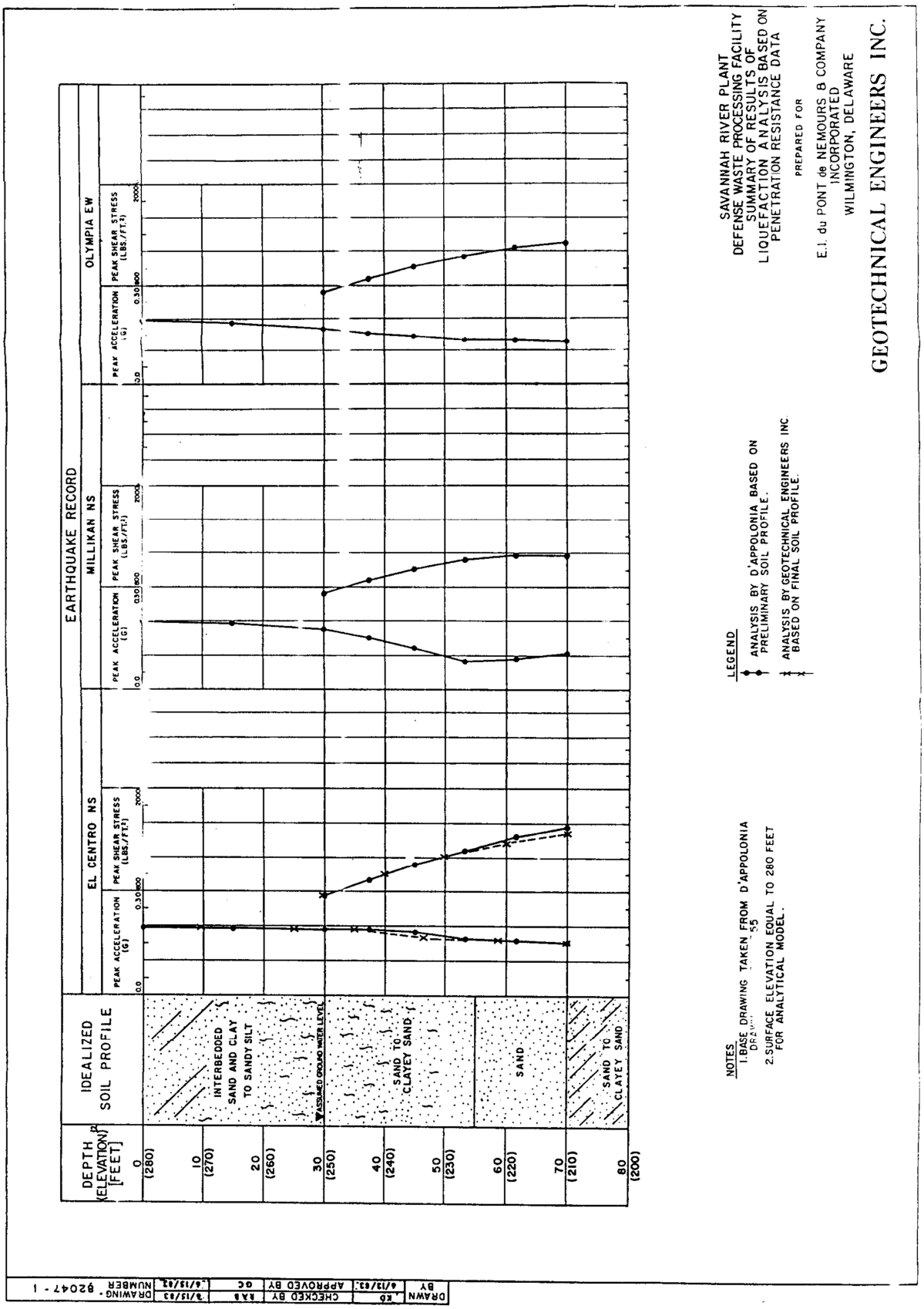

Figure 3.4-61 Summary Liquefaction Analysis

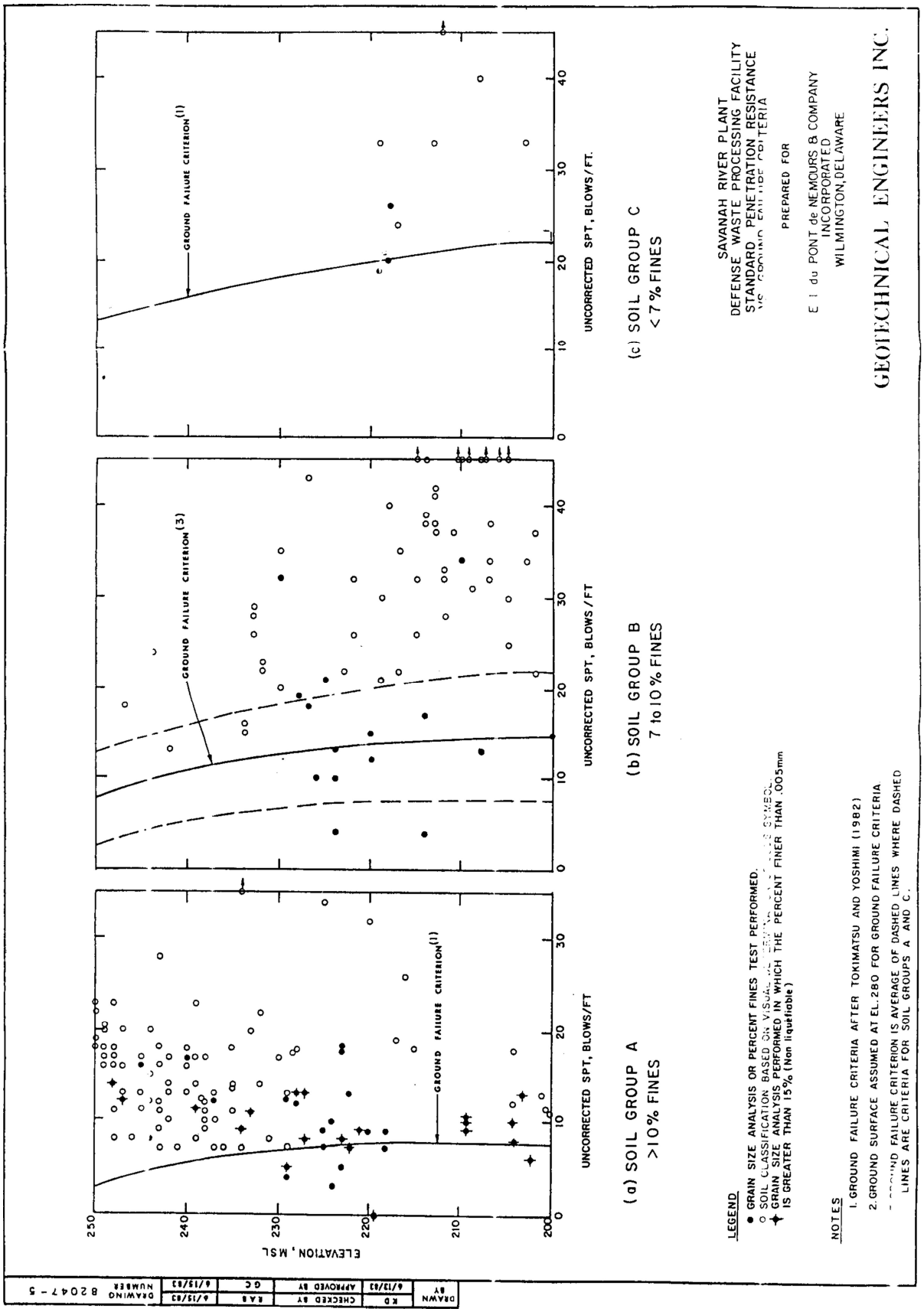

Figure 3.4-62 Standard Penetration Resistance Versus Ground Failure

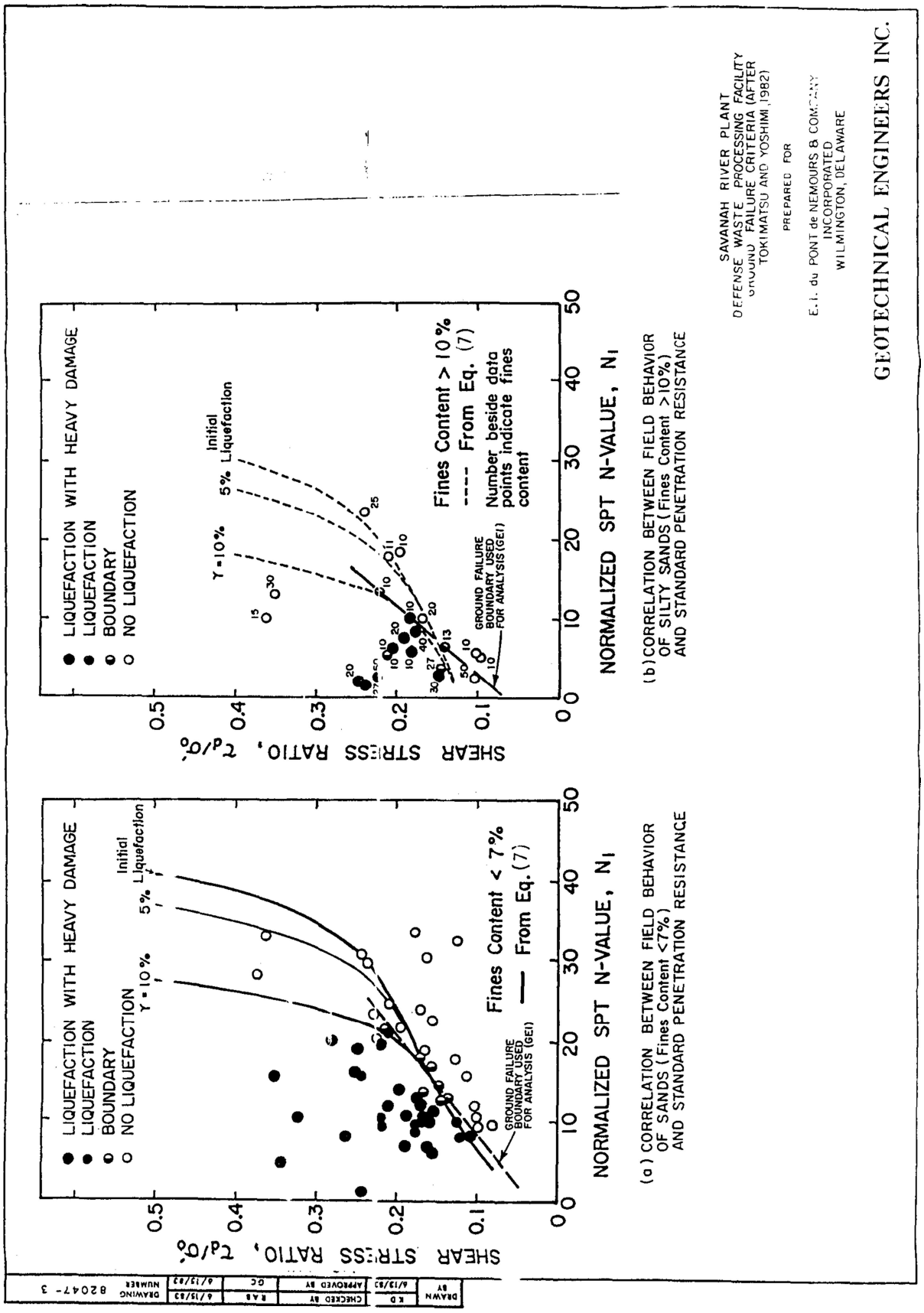

Figure 3.4-63 Ground Failure Criteria

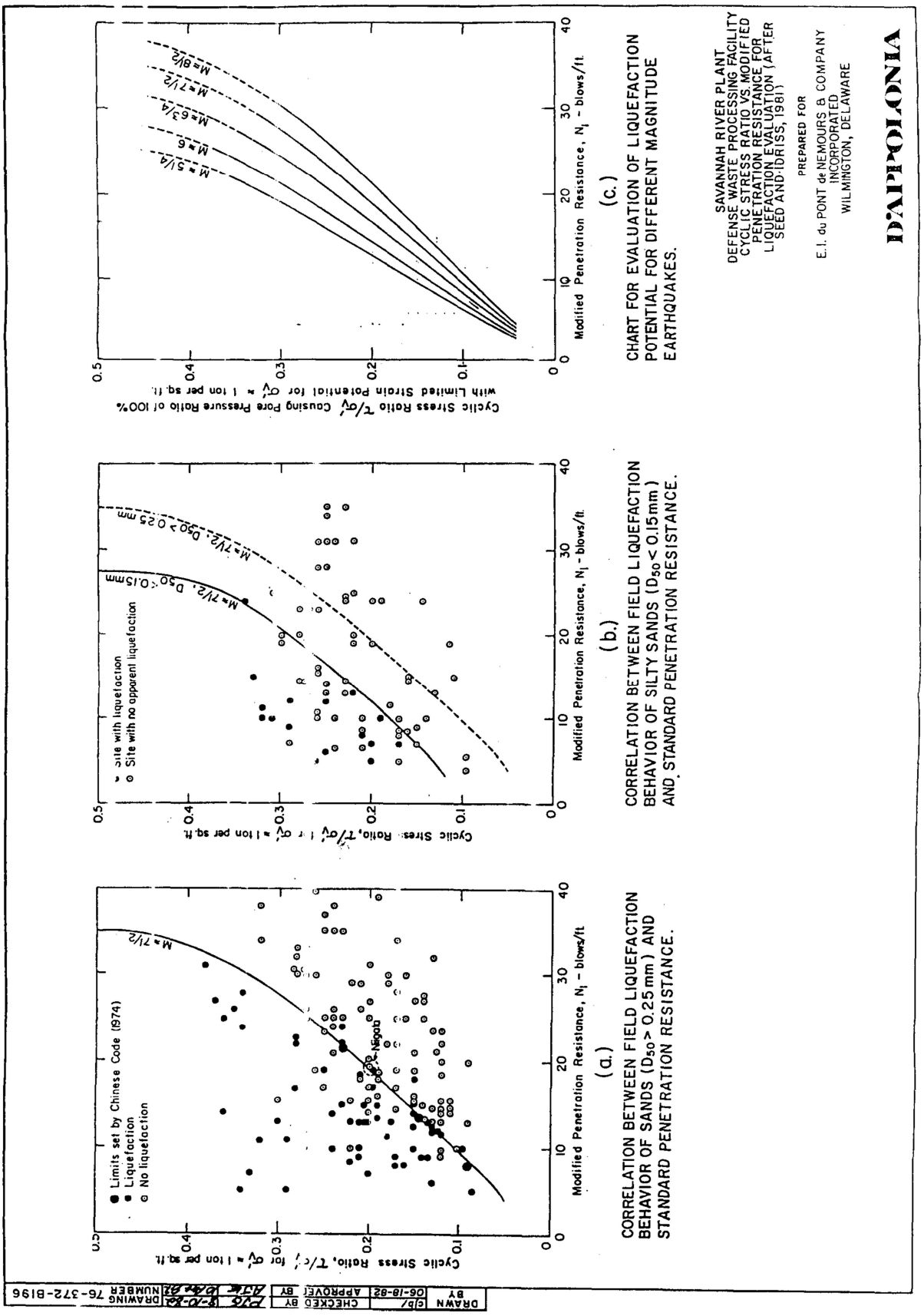

Figure 3.4-64 Cyclic Stress Ration Versus Modified Penetration Resistance

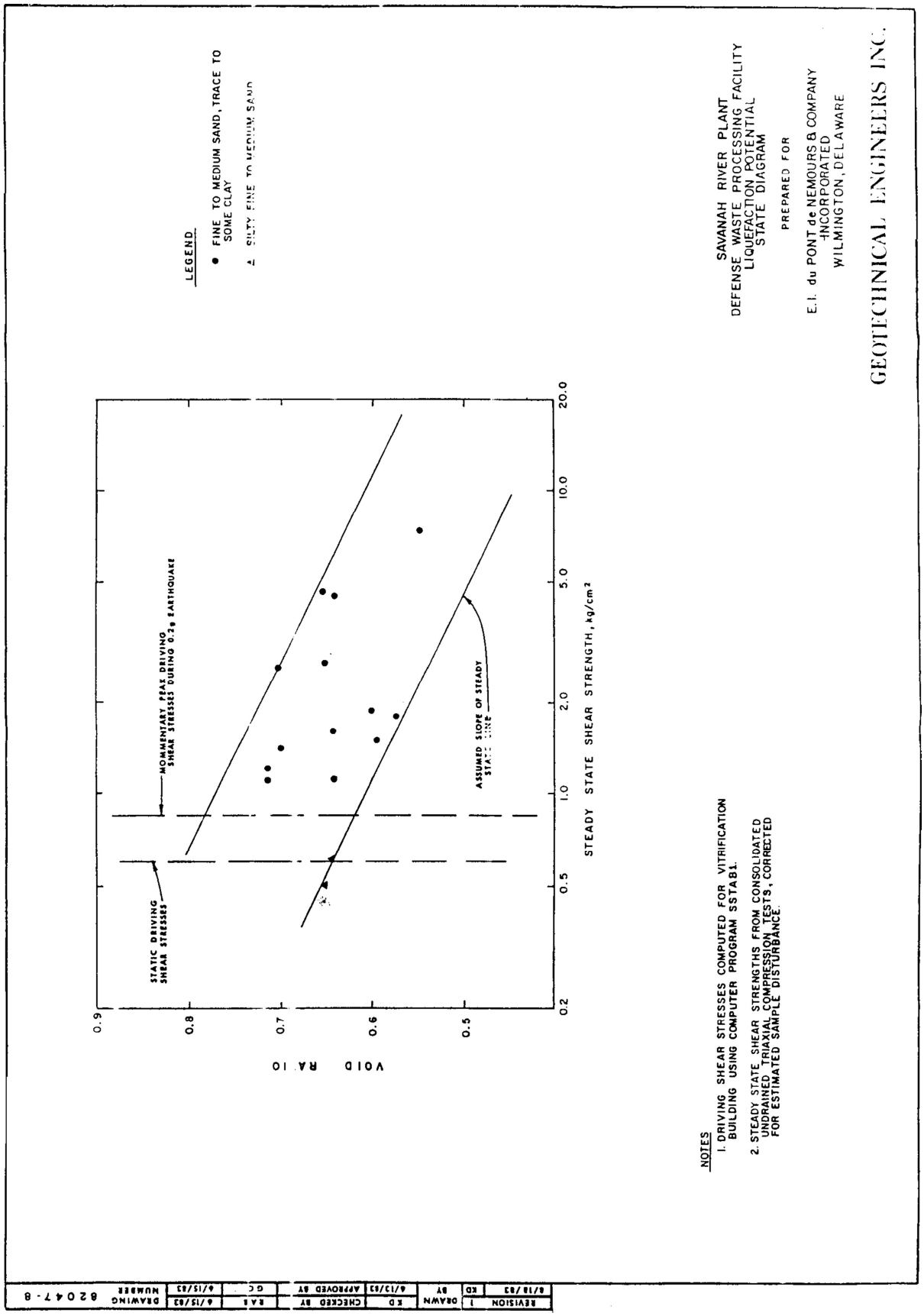

Figure 3.4-65 Liquefaction Potential State Diagram

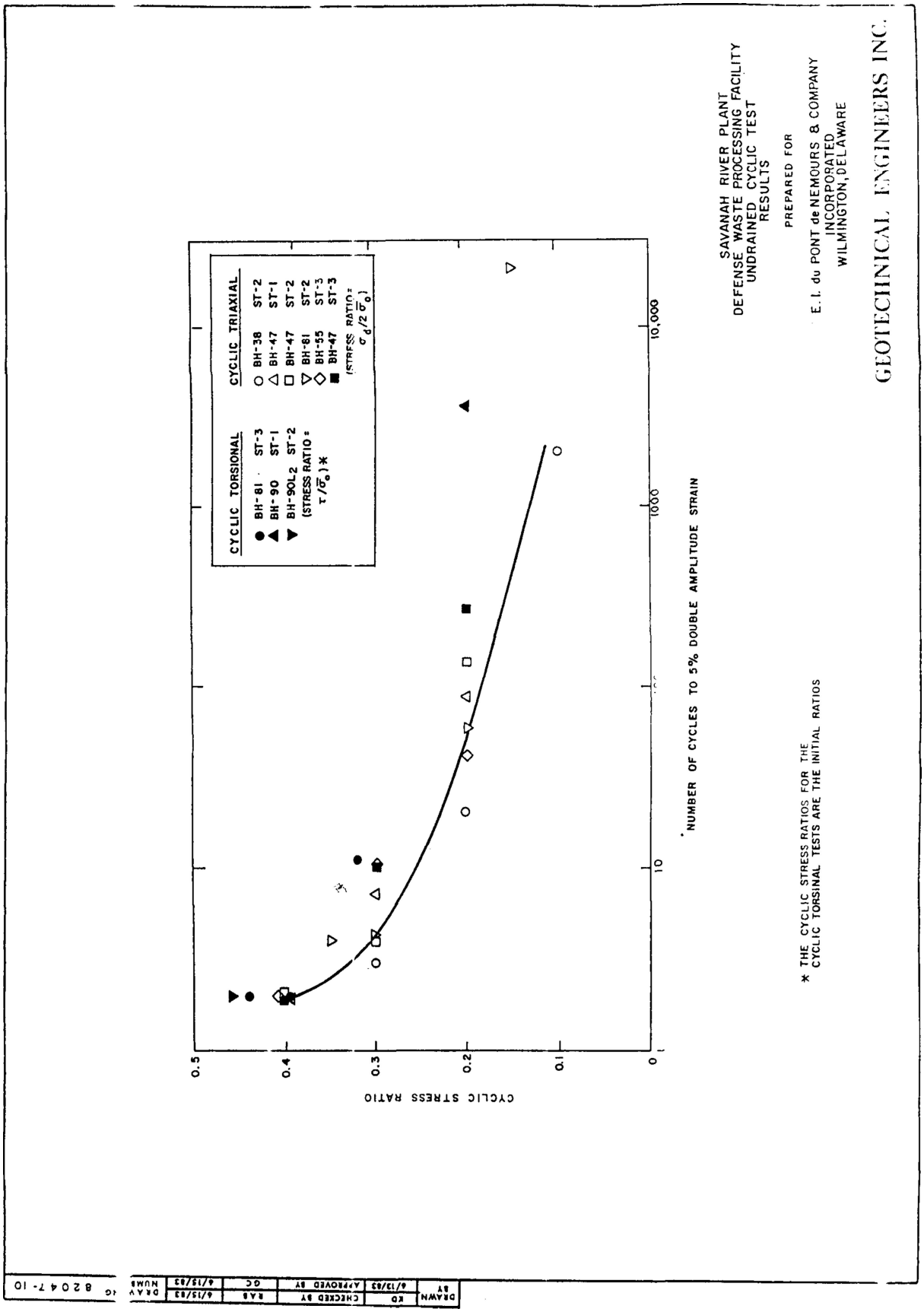

Figure 3.4-66 Undrained Cyclic Test Results

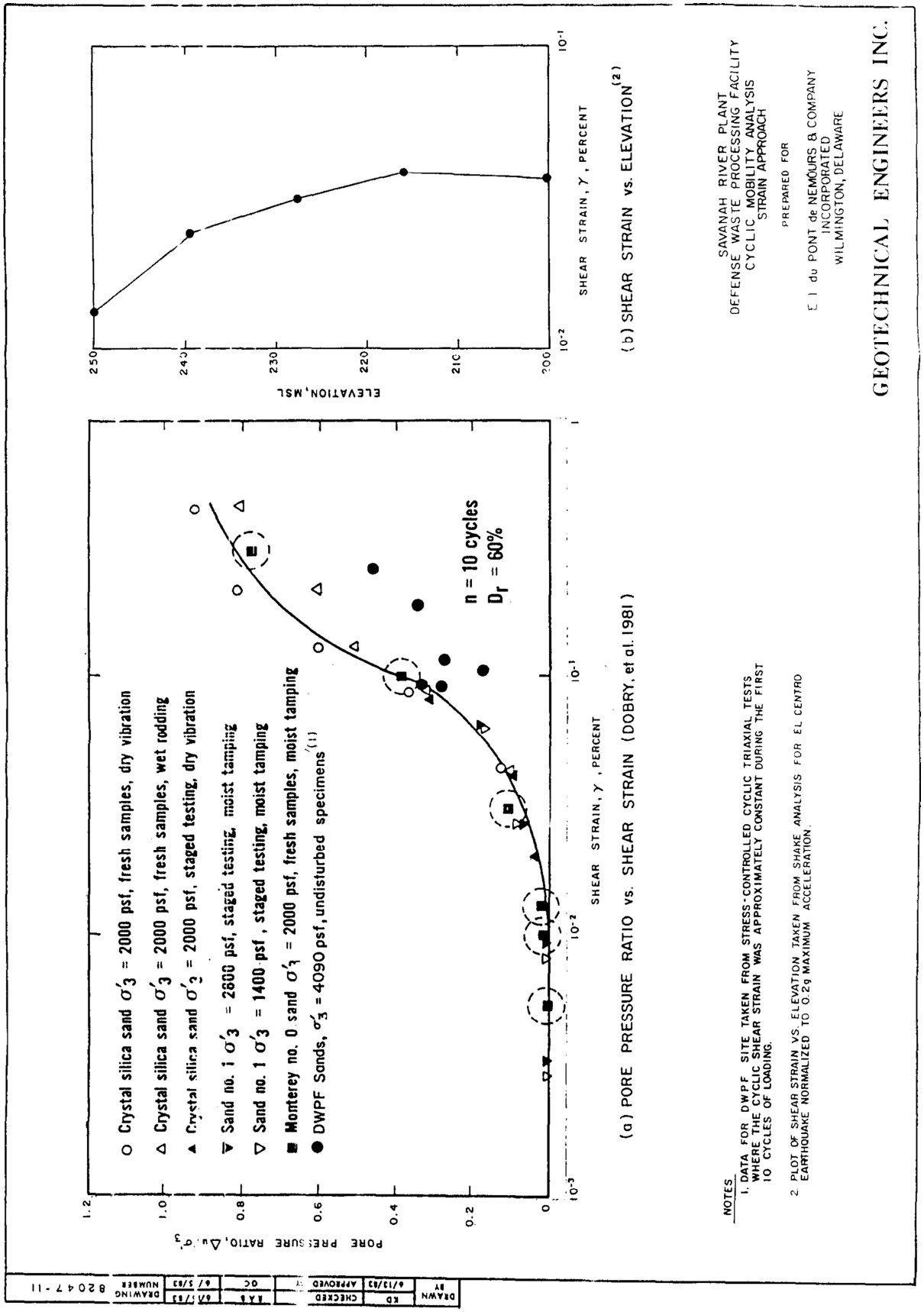

Figure 3.4-67 Cyclic Mobility Analysis

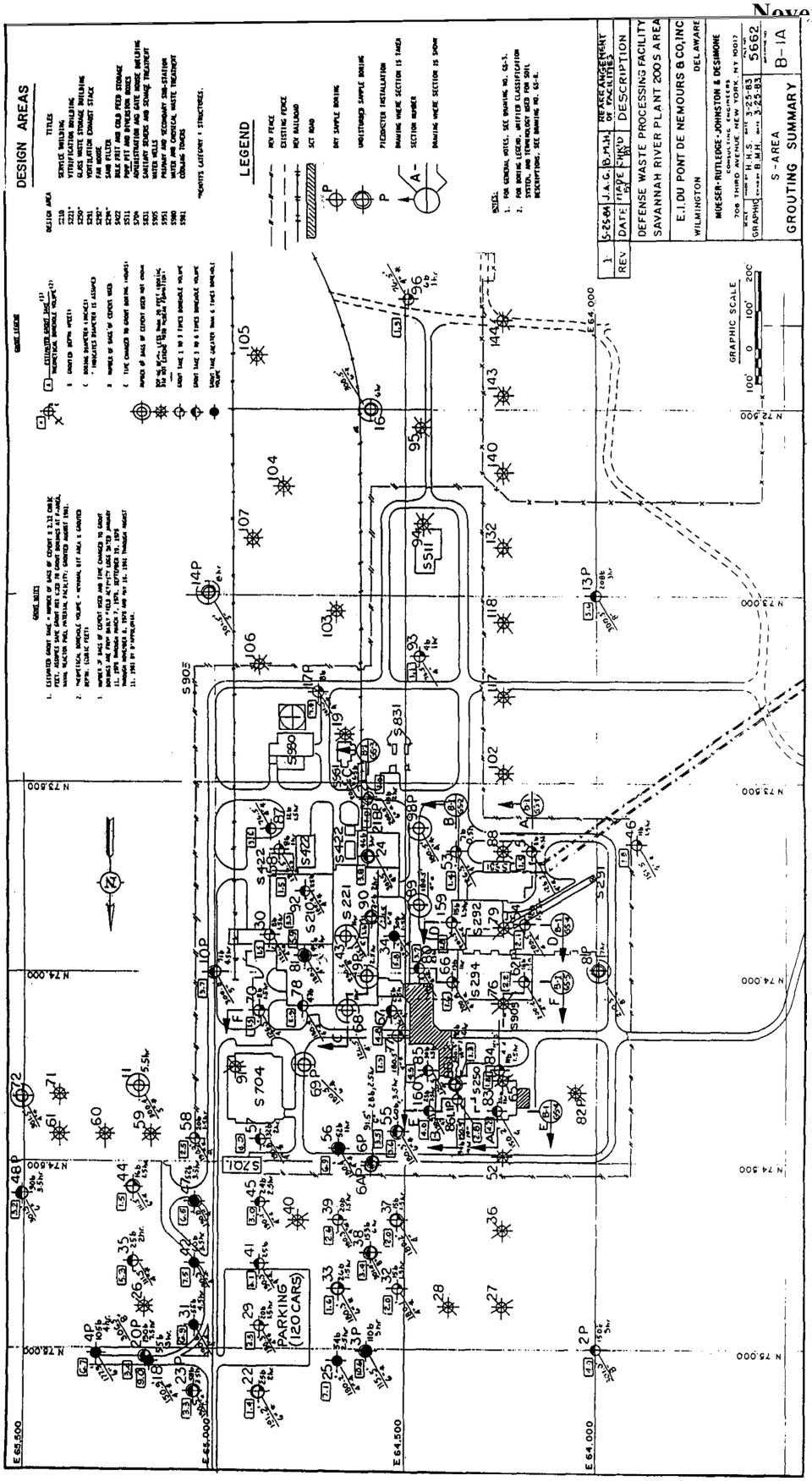

Figure 3.4-68 Grouting Summary

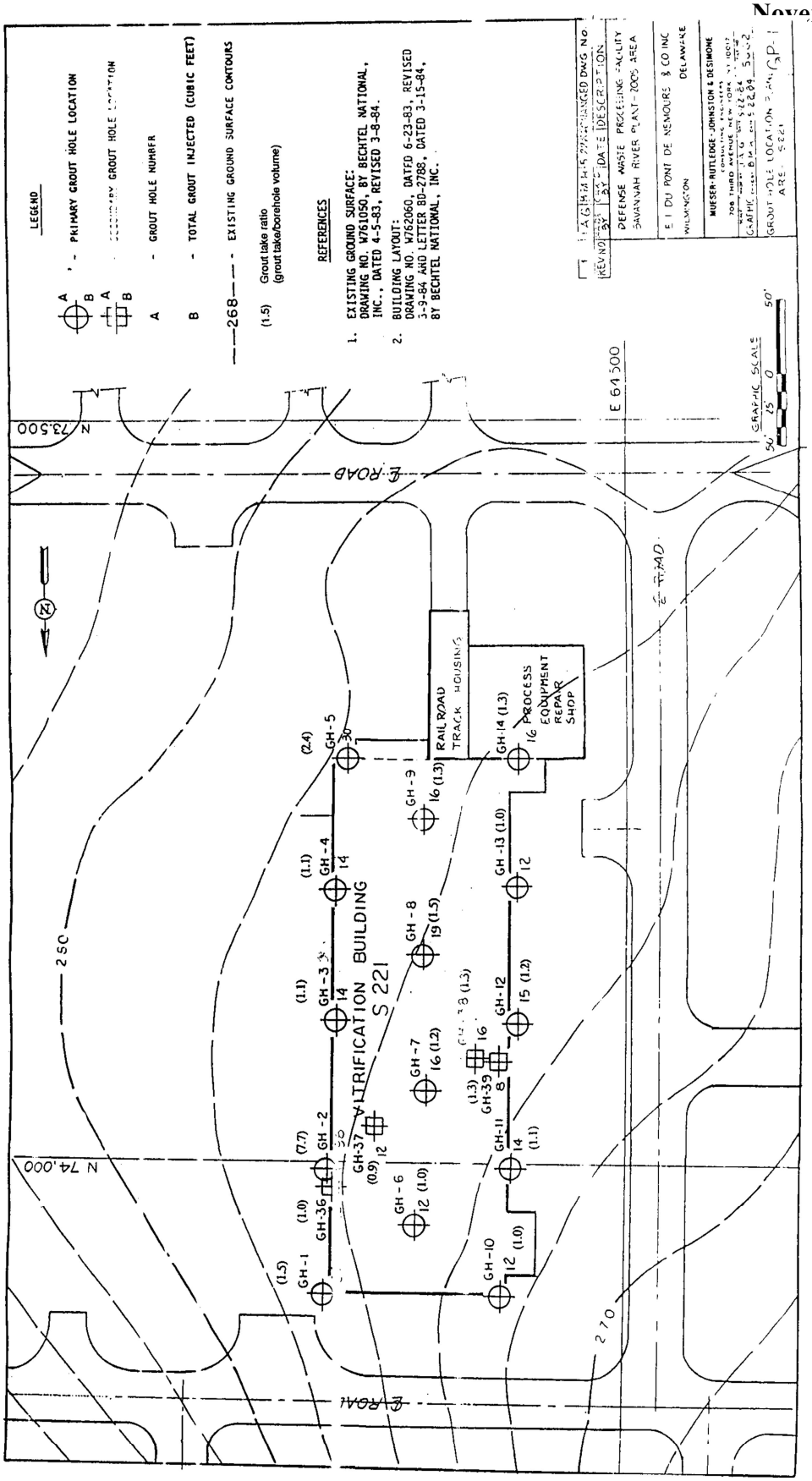

Figure 3.4-69 Grout Hole Location Plan for S221

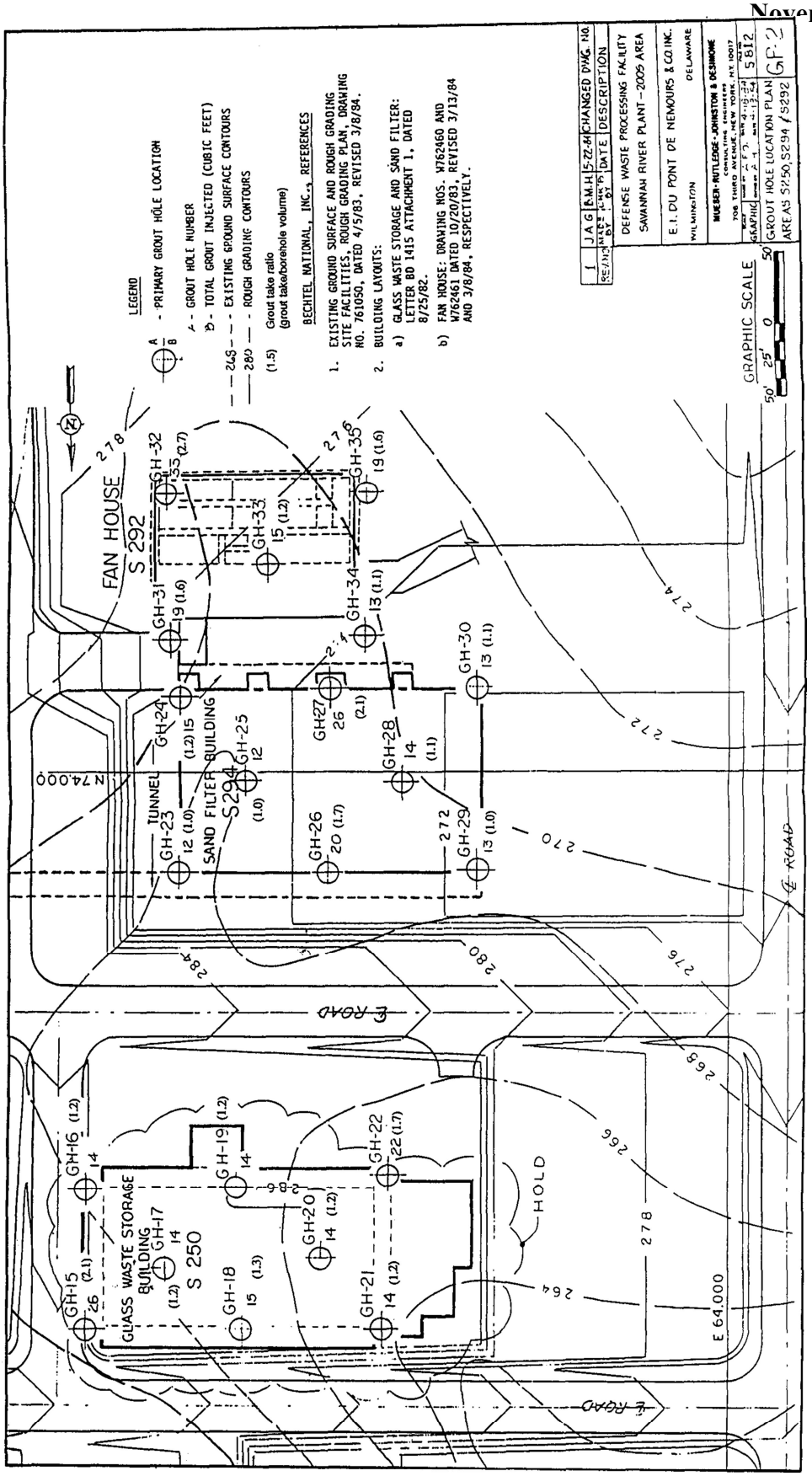

Figure 3.4-70 Grout Hole Location Plan for S250, S294 and S292